THE UNIVERSITY *of* EDINBURGH

BLOCK BY BLOCK: DEVELOPMENTS IN NMR METHODOLOGY

By

George Peat

A thesis presented for the degree of

Doctor of Philosophy

THE UNIVERSITY *of* EDINBURGH

Department of Chemistry

University of Edinburgh

Scotland

August 2023

Declaration

The Declaration states:

- That the thesis has been composed by myself, and
- Either that the work is my own, or, for work conducted as a member of a research group, that I have made a substantial contribution to the work, such contribution being clearly indicated, or
- That the work has not been submitted for any other degree or professional qualification except as specified, and
- That any included publications are my own work, except where indicated throughout the thesis and summarised and clearly identified on the declarations page of the thesis.

Signed: George Peat

Date: August 2023

Chapter 3 contains information published in the article:

C. L. Dickson, G. Peat, M. Rosetto, M. E. Halse, and D. Uhrín, *Chem. Commun.*, 2022, **36**, 5534-5537

Chapter 4 contains information published in the article:

G. Peat, P. J. Boaler, C. L. Dickson, G. C. Lloyd-Jones, and D. Uhrín, *Nat Commun*., 2023, **14**, 4410

Abstract

Due to its high information content and a non-destructive nature, NMR is a versatile and widely used analytical technique. A large variety of different NMR experiments exist, each providing specific information about the system being studied. Over the years a number of building blocks of NMR experiments have been designed, with new still appearing. When combined they can address issues such as spectral complexity, low sample concentrations or signal overlap. This thesis presents work in which several NMR building blocks have been modified and combined creatively to enhance their performance and to produce new, powerful NMR experiments.

The first building block to be utilised is DISPEL (Destruction of Interfering Satellites by Perfect Echo Low-pass filtration),[1] a pulse sequence element that suppresses one-bond ^{13}C satellites in 1D ^{1}H spectra. So far it has been utilised to declutter spectra and identify low concentration impurities in samples. In our work, the DISPEL pulse sequence has been combined with a 2D TOCSY experiment to enable the removal of one-bond ^{13}C satellites in 2D correlation spectra. Through comparisons of four DISPEL-TOCSY spectra that can be obtained by varying when the DISPEL elements are active, it was possible to obtain information about site-specific ^{13}C enrichment within molecules. This work has been applied to a sample of partially ^{13}C-labeled amino acids obtained by a digest of *E. coli* proteins prepared by using ^{13}C-labeled glucose as the carbon source. The DISPEL pulse sequence has also been combined with the JRES experiment aiding the identification of individual peaks and their multiplicity. This work widens the potential of NMR in studies of metabolic pathways.

The second building block explored is the SHARPER (Sensitive, Homogeneous And Resolved PEaks in Real time)[2] acquisition technique. This “pure-shift” method removes all heteronuclear and homonuclear couplings from a single signal, reducing the peak to a single singlet with a greatly increased signal to noise ratio, in part due to its inherent capability to compensate for magnetic field inhomogeneity. The original SHARPER pulse sequence was adapted for use on benchtop spectrometers accounting for varying levels of spectrometer hardware and sample requirements. Although equally applicable to high field instruments, this work is particularly beneficial to lower sensitivity, lower magnetic field homogeneity benchtop systems, e. g. for the purpose of reaction monitoring.

By shortening the spin-echo intervals and using non-selective pulses, the SHARPER pulse sequence was modified to remove chemical shift dispersion of all, or a selected group of ^{1}H resonances. This produced a possibility of collapsing an entire spectrum into a single intense and narrow signal that can act as a reporter of molecular properties of studied compounds.

This modification was used to design a SHARPER-DOSY (Diffusion-Ordered SpectroscopY) pulse sequence for the measurement of diffusion coefficients of pure compounds. When applied to small and medium size molecules, the sensitivity of this experiment is 10 to 100-fold higher than that of the original DOSY experiment. It was demonstrated that using cryogenically cooled probes on high-field NMR spectrometers, μM sample concentrations, prepared using as little as 1 μg of a compound, can yield a diffusion coefficient in several minutes.

Finally, SHARPER has been combined with a chemical-shift-selective-filter (CSSF), a technique that enables selective excitation of a single multiplet from a heavily overlapped spectral region, with chemical shift differences as small as 1-2 Hz. The CSSF building block was combined with the DOSY experiment to produce a CSSF-SHARPER-DOSY experiment that enables the determination of diffusion coefficients from highly overlapped spectra.

Lay summary

Nuclear magnetic resonance (NMR) spectroscopy is a powerful and widely used analytical technique that provides a large amount of information about molecules and chemical systems in a non-destructive manner. This is achieved by recording signals from atomic nuclei in the presence of an external magnetic field yielding spectra that contain a number of peaks. However, it is not always easy to interpret such spectra due to factors such as low sample concentrations, complex peak structures caused by nuclei interacting with each other or peak overlap arising from a large number of signals. These issues can be avoided by incorporating specific building blocks creating more complex NMR experiments. Such building blocks can be combined to obtain spectra more efficiently, or to highlight specific information. In this thesis we used several building blocks to produce new NMR experiments that can address specific challenges and make NMR a more efficient tool for biologists and chemists.

One such challenge is the impact of the ^{13}C isotope on the appearance of spectra of ^{1}H nuclei. As ^{13}C nuclei interact with ^{1}H nuclei while the more abundant ^{12}C nuclei don't, they produce additional peaks which complicate the final spectrum. Even though these signals have low intensity corresponding to 1% of ^{13}C in natural abundance samples, they can be sizable in samples prepared from ^{13}C-enriched sources, e.g., in metabolomics studies. A previously designed experiment termed DISPEL can be used to remove all signals arising from ^{13}CH protons. In our work the DISPEL building block was combined with a common NMR experiment called TOtal Correlation SpectroscopY (TOCSY), which provides two-dimensional spectra that shows interactions between different nuclei, to remove the ^{13}CH peaks from these spectra. Through manipulation of the resulting spectra, and variation in the position of the DISPEL block within the experiment, it was possible to produce spectra only containing peaks originating from ^{13}CH protons or a combination of both ^{13}CH and ^{12}CH. These peaks can then be used to estimate the ratio of ^{13}C to ^{12}C in specific positions in a molecule. Such information is important for metabolomic studies.

Another challenge for NMR is that peaks are often split into several lines, which greatly lowers their height and reduces the sensitivity of the technique. A building block called SHARPER removes such splittings by collapsing multiplets into a single 'sharp' peak while maintain the total area of the peak. In this thesis the SHARPER building block

was first transferred from traditional but very large and expensive high field NMR spectrometers, to a newer and much smaller benchtop NMR spectrometers which, as the name suggests, fit on a lab bench. This increases the range of systems the SHARPER technique can be used on and opens a possibility for it to be used for reaction monitoring within a fume hood.

The SHARPER block was also implemented into Diffusion Ordered SpectroscopY (DOSY), which determines how fast a molecule is moving in solution – a property that is related to its size. For this type of experiment, signals of individual protons of a molecule can be collapsed into a single peak, which enables the measurement at very low concentrations. This approach is not possible for mixtures, where multiple signals from different compounds overlap. Nevertheless, when combined with another NMR building block – the highly selective Chemical Shift Selective Filter (CSSF), which can select a single peak of interest from a heavily overlapped group, a multiplet from one molecule can be isolated at the time and its signal collapsed by the SHARPER module. This method can therefore be used to determine the diffusion coefficient of molecules in mixtures with higher efficiency and accuracy even when severe signal overlap is present.

Acknowledgments

Firstly, I need to thank my supervisor Dušan Uhrín for all the guidance and instruction over the past four years. It is a project that has continuously evolved due to both problems and revelations, and it is thanks to your steady support that it has become the success it is today.

I also must thank everyone who has helped along the way, Juraj Bella and Lorna Murray for keeping the spectrometers running smoothly despite the huge numbers of error messages I managed to trigger. Thank you to Scott Kennedy and the Falcon project for trusting me with your benchtop spectrometer, Meghan Halse and Mattheus Rossetto for teaching me how to use it and Craig Eccles for the advice on how to (safely) push it to its limits.

To my fellow residents of 14B. Thanks Claire, Patrick, Richard, Eleanor, Marc and Alan for providing a great atmosphere to work in while always being ready for a chat or a trip to SRUC or Mary Bruck. Thanks to Ezra, Sam, and Dana for greatly expanding my knowledge of Edinburgh restaurants and the constant supply of holiday sweets, and thanks to Justinas for being an excellent and responsible conference buddy/travel agent.

Outside of Joseph Black a huge thank you needs to be said to everyone in the EUHWC who has put up with my insane walk suggestions and terrible chat over many weekends. There are too many of you to list here but rest assured my time here wouldn't have been the same without you, although my car would be in considerably better condition. I will remember fondly the many weekends spent struggling up steep heather banks, wandering around featureless plateaus or clinging on for dear life on a slightly questionable scrambling route.

Thank you as well to everyone from Durham who has supported me along the way. Jacob, Ollie, Sam, and Harrison for the lockdown Jackbox sessions and quiz nights, everyone who trekked all the way to Barnard Castle each August for the annual reunion and Griff for always being ready to provide kind words of encouragement.

To Angus and Sally thank you for the continued support and many attempts to visit each other in our respective locations. I believe the hand in date of this thesis means I

have won our competition although there is always a chance for someone else to take the victory.

To my family, Mum, Dad and Alice thank you for all the support and interest in what I’m researching despite not fully understanding all of it. Thanks to all at the farm for looking after me and always having an extra space at dinner. Finally thank you to Granny Bat for paving the way in science, Edinburgh, and the hills.

Table of Contents

Acronyms 4

List of Figures 6

List of Tables 11

1 Introduction 12
- 1.1 What is NMR? 12
- 1.2 Theory of NMR 12
- 1.3 How a spectrum is obtained 15
- 1.4 The NMR spectrum 17
- 1.5 Benchtop spectroscopy 20
- 1.6 Building blocks of NMR experiments 21
  - 1.6.1 Pulse and acquire experiment. 21
  - 1.6.2 Spin echo 22
  - 1.6.3 Spin echo and coupled systems 23
  - 1.6.4 Spin echo for T_2 measurements 25
  - 1.6.5 Perfect echo 26
- 1.7 2D NMR 28
  - 1.7.1 COSY 30
  - 1.7.2 TOCSY 30
  - 1.7.3 DOSY 31
  - 1.7.4 *J*-RES 33
- 1.8 Decoupling 34

2 Aims and objectives 36

3 DISPEL 38
- 3.1 Declaration 38
- 3.2 Introduction to DISPEL 38
- 3.3 1D interleaving. 45
- 3.4 2D ^{1}H-^{1}H TOCSY 47
  - 3.4.1 ^{13}C enrichment estimation 53
  - 3.4.2 Application to metabolite samples 64
- 3.5 *J*-RES-DISPEL 67
- 3.6 Experimental details 70

4 Benchtop SHARPER 72
- 4.1 Declaration 72
- 4.2 Introduction to SHARPER 72
  - 4.2.1 Pure shift reaction monitoring 72
  - 4.2.2 Non-selective or ‘hard’ SHARPER 73
  - 4.2.3 *Sel*-SHARPER 76
- 4.3 Why take SHARPER to benchtop? 78
- 4.4 SHARPER without PFGs 79
- 4.5 Practicalities of SHARPER on benchtop NMR spectrometers 87
  - 4.5.1 Shaped pulses 87

4.5.2 Power calibration 88
4.5.3 Gradient pulses 94
4.6 Application to model compounds 97
4.6.1 Fluorobenzene results 97
4.7 Best practice for acquiring SHARPER spectra. 100
4.8 Removal of the imaginary component of FIDs 103
4.9 Experimental details 105

5 SHARPER collapse 109
5.1 Declaration 109
5.2 CPMG SHARPER 109
5.2.1 SHARPER acquisition efficiency 110
5.2.2 Collapsing of 1-phenylethanol 112
5.2.3 Additional power deposition considerations 114
5.2.4 Selecting signals to be collapsed 116
5.2.5 BSPE-SHARPER 122
5.3 SHARPER-DOSY 124
5.3.1 SHARPER-DOSY using μg quantities of sample. 126
5.3.2 Analysis of diffusion coefficients 131
5.4 Experimental 134

6 CSSF-SHARPER 137
6.1 Declaration 137
6.2 Chemical Shift Selective Filter 137
6.3 CSSF-SHARPER 139
6.3.1 CSSF baseline elevation 143
6.4 DOSY-CSSF-SHARPER 145
6.4.1 Preparation of a model mixture 146
6.4.2 DOSY-CSSF-SHARPER results 153
6.5 Experimental 156

7 Conclusions 158

8 References 160

A Appendix 166
A.1 DISPEL 166
A.1.1 1D interleaved DISPEL sequence. 166
A.1.2 DISPEL-TOCSY sequence. 171
A.1.3 DISPEL-TOCSY interleaved sequence 181
A.1.4 DISPEL-TOCSY interleaved processing AU program 194
A.1.5 *J*-RES-DISPEL sequence 198
A.1.6 *J*-RES-DISPEL interleaved sequence 203
A.2 Benchtop SHARPER 209
A.2.1 Table of nutation curve parameters 209
A.2.2 Python script for zeroing imaginary components of Bruker FIDs 209
A.2.3 AU program for zeroing imaginary components of Bruker FIDs 212

A.3 CPMG-DOSY-SHARPER 215
A.3.1 CPMG-SHARPER sequence with BSPE 215
A.3.2 CPMG- DOSY-SHARPER sequence with BSPE 225
A.3.3 AU program to perform subtraction of reference solvent DOSY spectrum from sample spectrum. 237
A.3.4 Julia script for optimization of the duration of the selective pulse and carrier offset. 239
A.4 CSSF-SHARPER 240
A.4.1 CSSF-SHARPER sequence 240
A.4.2 CSSF-DOSY-SHARPER sequence 248

Acronyms

AQ	Acquisition time
BIRD	BIlinear Rotation Decoupling
BSPE	Band selective perfect echo
COSY	Correlation spectroscopy
CPMG	Carr-Purcell-Meiboom-Gill
CSSF	Chemical shift selective filter
CW	Continuous wave
D	Diffusion coefficient
D1	Relaxation time
DIPSI	Decoupling In the Presence of Scalar Interactions
DISPEL	Destruction of Interfering Satellites by Perfect Echo Low-pass filtration
DNI	Distance to Nearest Integer
DOSY	Diffusion ordered spectroscopy
DS	Dummy scans
FID	Free induction decay
FT	Fourier transform
ge	Gradient enhanced
HPLC	High Performance Liquid Chromatography
HSQC	Heteronuclear Single-Quantum Correlation
Hz	Hertz
J-RES	J resolved
NMR	Nuclear magnetic resonance
NS	Number of scans
PFG	Pulsed field gradient
ppm	Parts per million

Presat	Presaturation
RD	Relaxation delay
REBURP	Refocusing Band-selective Uniform-Response Pure-phase
RF	Radiofrequency
SE	Spin echo
sel-	Selective
SHARPER	Sensitive, Homogeneous And Resolved PEaks in Real time
SNR	Signal to noise ratio
SPFGSE	Single pulse field gradient spin echo
SW	Spectral width
T_1	Spin-lattice relaxation
T_2	Spin-spin relaxation
TD	Time domain
TMS	Tetramethylsilane
TOCSY	Total correlation spectroscopy

List of Figures

Figure 1.1: Energy splitting diagram 13

Figure 1.2: Vector model representation of precessional motion 14

Figure 1.3: Vector model representation of a 90° pulse. 16

Figure 1.4: Vector model representation of transverse relaxation 17

Figure 1.5: J-coupling 19

Figure 1.6: Pulse acquire pulse sequence. 21

Figure 1.7: Spin echo pulse sequence 22

Figure 1.8: Vector evolution during a spin echo 23

Figure 1.9: Heteronuclear vs homonuclear vector evolution. 24

Figure 1.10: T_2 measurement pulse sequence. 25

Figure 1.11: Perfect echo pulse sequence. 26

Figure 1.12: The basic scheme of a 2D NMR experiment. 28

Figure 1.13: An example 2D spectrum 29

Figure 1.14: TOCSY pulse sequence 31

Figure 1.15: DOSY pulse sequence. 32

Figure 1.16: *J*-RES pulse sequence 33

Figure 1.17: Theoretical *J*-RES spectrum. 34

Figure 1.18: Decoupling in a pulse acquire experiment. 35

Figure 3.1: ^{13}C satellite example 39

Figure 3.2: X-filter pulse sequence 40

Figure 3.3: Adiabatic X-filter pulse sequence 41

Figure 3.4: DISPEL pulse sequence 42

Figure 3.5: J filter pulse sequence 43

Figure 3.6: Z filter pulse sequence. 44

Figure 3.7: 1D labelled glucose spectra 46

Figure 3.8: DISPEL-TOCSY pulse sequence 47

Figure 3.9: DISPEL-TOCSY pulse sequence with two DISPEL blocks 48

Figure 3.10: DISPEL-TOCSY spectra of ^{13}C labelled glucose 50

Figure 3.11: DISPEL-TOCSY spectra of ^{13}C labelled glucose obtained from addition and subtraction of the spectra shown in figure 3.10 52

Figure 3.12: 800 MHz ^{1}H spectrum of xylose in D_2O 56

Figure 3.13: TOCSY spectrum of xylose 57

Figure 3.14: ^{1}H spectra of xylose samples. 58

Figure 3.15: Labelled TOCSY spectra of xylose identifying cross peaks for enrichment estimates. 60

Figure 3.16: Enrichment comparison for xylose samples. 61

Figure 3.17: ^{13}C---^{13}C TOCSY spectrum of xylose sample 3. 63

Figure 3.18: Conversion of glucose to ethanol in Bakers yeast. 64

Figure 3.19: Formation of malic acid from glycosis of glucose and oxidation of glycerol 64

Figure 3.20: TOCSY spectrum of bakers yeast. 65

Figure 3.21: jresgpprqf pulse sequence. 67

Figure 3.22: J-RES-DISPEL pulse sequence 68

Figure 3.23: J-RES spectra of ^{13}C-1 labelled glucose 69

Figure 4.1: SHARPER pulse sequence 74

Figure 4.2: ^{19}F and SHARPER spectra of fluorobenzene 75

Figure 4.3: sel-SHARPER pulse sequence. 76

Figure 4.4: Selective pulse inversion profiles. 77

Figure 4.5: Improved sel-SHARPER pulse sequence 79

Figure 4.6: SHARPER spectrum comparison on fluorobenzene 80

Figure 4.7: SE sel-SHARPER pulse sequence 82

Figure 4.8: 270° sel-SHARPER pulse sequence 82
Figure 4.9: SHARPER spectrum comparison on pentafluorobenzene 83
Figure 4.10 : Excitation profile of low power 90° rectangular pulse 84
Figure 4.11: Comparison of ^{19}F and rectangular sel-SHARPER spectra 85
Figure 4.12: SPFGSE-sel-SHARPER pulse sequence..... 86
Figure 4.13: Comparison of ^{19}F and SPFGSE-sel-SHARPER spectra..... 87
Figure 4.14: -6.5 dB nutation curve 89
Figure 4.15: 0dB to −18dB nutation curves..... 90
Figure 4.16: Attenuation vs pulse length graph 91
Figure 4.17: Input power vs produced power 92
Figure 4.18: Pulse calibration using SPFGSE sel-SHARPER..... 93
Figure 4.19: 1D gradient echo imaging pulse sequence 95
Figure 4.20: Plot of peak width against proportional shim change 95
Figure 4.21: Comparison of all SHARPER sequences..... 97
Figure 4.22: High and low field ^{19}F spectra of fluorobenzene 98
Figure 4.23: Real component of a sharper FID of fluorbenzene 103
Figure 4.24: Baseline with and without imaginary component. 104
Figure 4.25: SNR values with and without imaginary component of the FID 105
Figure 5.1: Integral intensities vs offset for SHARPER peak 110
Figure 5.2: Signal height vs offset for SHARPER peak..... 111
Figure 5.3: ^{1}H and SHARPER spectra of 1-phenylethanol 113
Figure 5.4: Integral intensities vs offset for SHARPER peak with 90° pulses..... 115
Figure 5.5: Signal height vs offset for SHARPER peak with 90° pulses 116
Figure 5.6: Simulated DNI norm 119
Figure 5.7: Inversion profile 120
Figure 5.8: ^{1}H spectrum of cyclosporine 121

Figure 5.9: non-selective presat SHARPER pulse sequence 121
Figure 5.10: Selective saturation spectra of cyclosporine 122
Figure 5.11: BSPE 1H and BSPE-SHARPER 123
Figure 5.12: BSPE-SHARPER pulse sequence 124
Figure 5.13: SHARPER-DOSY pulse sequence 124
Figure 5.14: DOSY and BSPE-DOSY-SHARPER spectra of cyclosporine. 125
Figure 5.15: Spectra of a 7.7 mM sample of sodium cholate 127
Figure 5.16: BSPE-SHARPER spectra of 5.5μM sodium cholate and D_2O 128
Figure 5.17: DOSY and BSPE-DOSY-SHARPER spectra of 5.5 μM sodium cholate 129
Figure 5.18: SHARPER-DOSY projections showing subtraction 130
Figure 5.19: Subtracted DOSY spectrum 131
Figure 6.1: ge-CSSF pulse sequence. 138
Figure 6.2: ^{1}H and CSSF spectrum of 5.2 kDa dextran 139
Figure 6.3: CSSF-SHARPER pulse sequence 140
Figure 6.4: CSSF-SHARPER peaks of individual dextran signals. 141
Figure 6.5: Simulated CSSF Intensities as a function of frequency 143
Figure 6.6: Simulated CSSF baseline elevation. 145
Figure 6.7: DOSY-CSSF-SHARPER pulse sequence 146
Figure 6.8: Structures of methyl β-d-xylopyranoside, cellobiose and fondaparinux. 147
Figure 6.9: ^{1}H NMR spectrum of the mixed sample. 148
Figure 6.10: CSSF spectra of the mixed sample 149
Figure 6.11: CSSF-SHARPER pulse sequence with additional z-filter 150
Figure 6.12: z-filter vs no z-filter CSSF comparison. 151
Figure 6.13: CSSF-SHARPER spectra of mixed sample 152
Figure 6.14: DOSY spectrum of the mixed sample. 154

Figure 6.15: DOSY vs DOSY-CSSF-SHARPER spectra comparison..... 155

List of Tables

Table 1.1: Spin values 12

Table 3.1: DISPEL-TOCSY combinations 49

Table 3.2: Linear combinations of DISPEL-TOCSY spectra 51

Table 3.3: Additional DISPEL-TOCSY spectra 55

Table 3.4: Xylose samples 58

Table 3.5: Enrichment estimates 61

Table 3.6: Peak assignments for glycerol and L-(-)-malic acid 66

Table 3.7: Estimated ^{13}C enrichment levels glycerol and L-(-)-malic acid 66

Table 4.1: SNR and integral values for the SHARPER spectra 81

Table 4.2: Pulse powers optimised for 180° Gaussian pulses 94

Table 4.3: Maximum gradient strengths produced by shim coils 96

Table 4.4: Single scan vs multiple scan SHARPER experiments 100

Table 4.5: Comparison of SHARPER linewidths 102

Table 4.6: Experimental parameters of SHARPER experiments 106

Table 4.7: Relaxation times of each signal at low field 107

Table 5.1: Diffusion coefficient of sodium cholate 132

Table 5.2: Comparison of determined diffusion coefficients 133

Table 6.1: Integral areas of each peak in 5.2 kDa dextran 142

Table 6.2: Diffusion coefficients calculated from spectra 156

Table A.1: Table of nutation curve parameters 209

1 Introduction

1.1 What is NMR?

Nuclear Magnetic Resonance (NMR) is a physical phenomenon where nuclei placed in a magnetic field produce an electromagnetic signal upon exposure to a weak oscillating magnetic field. The frequency of this electromagnetic signal depends on the magnetic field at the nucleus, so measuring the signal from a nucleus can give information about the electronic structure of the molecule and the presence of functional groups. This technique is called NMR spectroscopy and since its initial development by the independent groups of Bloch at Stanford[3,4] and Purcell at Harvard[5], for which they shared the 1952 Nobel Prize in physics, it has become the go to technique for identifying structures of organic compounds. It is also widely used for structure elucidation of proteins and other biomacromolecules, including polysaccharides, along with many applications in the field of reaction monitoring.

While NMR can be used on solid samples, it is much less common than solution state NMR and for the purpose of this thesis only solution state NMR will be discussed. Unless otherwise stated, the information present in this section is based on the textbook "Understanding NMR spectroscopy" by Dr James Keeler.[6]

1.2 Theory of NMR

NMR arises from an internal property possessed by nuclei called spin, which is defined by the quantum number I, where $I = n/2$ and n is an integer. The spin of a nucleus depends on the number of protons and neutrons present, as shown in Table 1.1.

Table 1.1: Spin values depending on the number of protons and neutrons in the nucleus.

Number of protons	**Number of neutrons**	***I***
even	even	0
odd	odd	Integer (1, 2, 3, …)
even	odd	Half integer (1/2, 3/2, 5/2, …)
odd	even	Half integer (1/2, 3/2, 5/2, …)

Nuclei with a spin value $I \geq ½$ such as ^{1}H ($I = ½$) or ^{14}N ($I = 1$) have a constant magnetic moment which can interact with external magnetic fields and can produce NMR signals. In contrast, nuclei such as ^{12}C and ^{16}O that have spin quantum number $I = 0$ have no magnetic moment and are described as being NMR silent.

Each nucleus that has $I \geq ½$ can occupy $2I + 1$ quantum states ranging from $-I$ to $+I$ that are described by the magnetic quantum number m_I. The energy levels associated with these levels are normally degenerate, however upon exposure to a magnetic field they split as shown in Figure 1.1 for spin ½ nuclei.

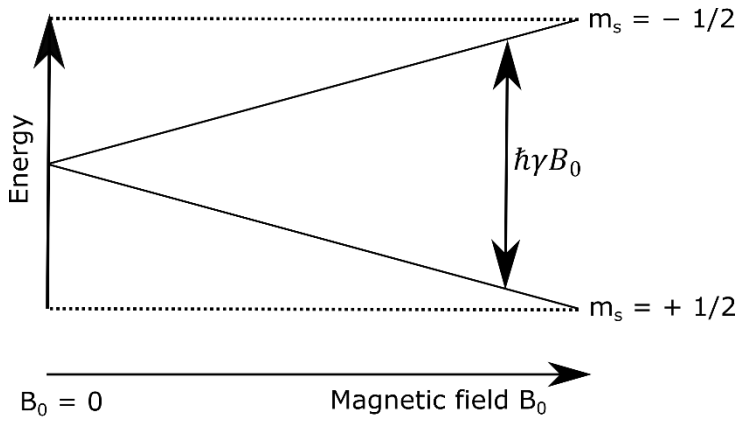

Figure 1.1: Diagram showing the splitting of energy levels in an I = ½ nucleus

The difference between the energy levels depends on the strength of the magnetic field and the gyromagnetic ratio (γ), which is unique to each nucleus. This is shown in Equation 1 where ΔE is the energy difference, $\hbar$ is Planck's constant divided by 2π and B_0 is the magnetic field strength.

$$\Delta E = \hbar \gamma B_0 \qquad (1)$$

For an $I = ½$ nucleus the spin states are labelled as α and β with α representing the $m_s = +½$ spin state which is aligned with the magnetic field and β representing the $m_s = -½$ spin state which is aligned against the magnetic field. Under normal conditions the population of each energy level is related to the Boltzmann distribution as shown in Equation 2, where N_β and N_α are the relative populations of the upper and lower energy spin states, ΔE is the energy difference, k_B is the Boltzmann constant and T is the temperature.

$$\frac{N_\beta}{N_\alpha} = \exp\left(\frac{-\Delta E}{k_B T}\right) \qquad (2)$$

As the α spin state is lower in energy it has a larger population than the β spin state. The size of this population difference is linked to the strength of the magnetic field so in stronger magnetic fields the population of the α spin state is greater. This difference in spin numbers leads to an overall magnetisation of an ensemble of nuclei that matches the direction of the external magnetic field. However, as spins not only possess magnetic moment but also an angular moment, they precess around the B_o axis slightly tilted, as shown in Figure 1.2.

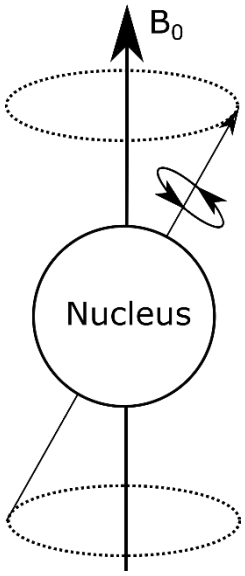

Figure 1.2: Precessional motion of the magnetic moment around the external magnetic field. The solid black arrows represent the external magnetic field and the magnetic moment, and the dotted lines show the precessional orbit.

The frequency of the precessional motion is known as the Larmor frequency (υ_0) and is related to the gyromagnetic ratio and magnetic field strength by Eqn. 3.

$$v_o = \gamma B_0 / 2\pi \qquad (3)$$

This frequency is important, as when a pulse of electromagnetic radiation, called a radiofrequency (RF) pulse, is applied to nuclei at the same frequency as the Larmor frequency the nucleus can absorb energy and be promoted to the β spin state. When this pulse is applied over a short time period, it causes the overall magnetic moment to rotate. After the pulse ends, the magnetic moment starts returning to its position at

thermal equilibrium, aligning with the external magnetic field while precessing around it. The movement of the magnetisation back to thermal equilibrium induces an alternating current in the spectrometer probe coil which is called a free induction decay (FID). This FID is converted into an NMR spectrum by applying Fourier transformation to the raw FID. The process of recording an FID and then producing an NMR spectrum is called Fourier transform (FT) spectroscopy. For the magnetisation to be affected by the pulse of electromagnetic radiation, the frequency of the pulse must match or be close to the Larmor frequency of the nuclei in question. This requirement is known as the resonance condition.

1.3 How a spectrum is obtained

The previous section mentioned that to obtain a spectrum from a sample an external magnetic field, a pulse of electromagnetic radiation and a way to detect an alternating current is required. In a typical NMR spectrometer, a probe holds the sample in the centre of a superconducting magnet that provides a uniform external field on the order of 10 T or more. When a spectrum is taken, a RF pulse is emitted from the probe at an angle of 90˚ to the external field, exciting the sample and changing the position of the magnetisation, generating a transverse component. This magnetisation then decays, producing the FID. The movement of the magnetisation vector and how the current is measured can be visualised with the Bloch sphere method or vector model.

The vector model treats the magnetic moment of the nuclei as a single vector that at equilibrium is aligned along the z-axis, which is the direction of the external field. When an RF pulse that meets the resonance condition is applied along the x direction, it replaces the external magnetic field with the effective magnetic field felt by the nuclei, so the magnetisation vector starts to precess about the effective axis rather than the z-axis. It is the case that for short pulses the applied RF field generates magnetic moment much stronger than the external magnetic field and the effective magnetic moment is fully aligned with the x-axis across a large frequency range. This moves the magnetisation vector to the transverse plane as shown in Figure 1.3.

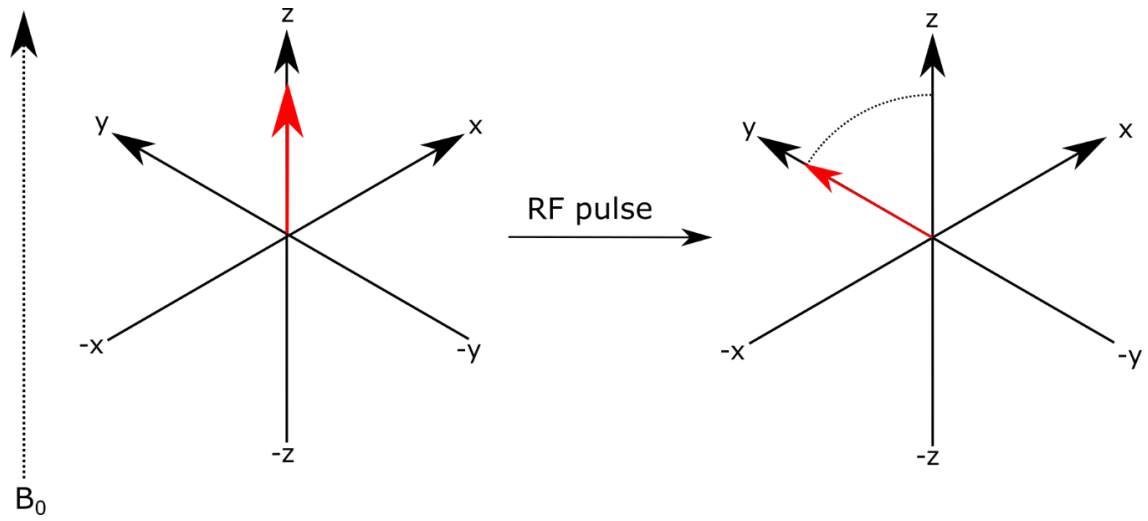

Figure 1.3: Rotation of the magnetic moment of a system from the z-axis to the y-axis upon application of an RF pulse from the x-axis. Throughout this thesis figures use a right-handed axis system.

Once the RF pulse is finished, the external magnetic field becomes the effective magnetic field felt by the nuclei, so the magnetic moment starts precessing around it, and at the same time relaxes back to its equilibrium position. This can be visualised as the magnetisation vector in the transverse plane slowly decreasing to zero while precessing around B_0, and the magnetisation vector in the z-axis increasing back to its equilibrium value. The decreasing vector in the transverse plane induces an oscillating electric current in the receiver coil as a function of signal intensity against time. This is the FID, and after a Fourier transform has been carried out a spectrum of intensity against frequency is produced. Figure 1.4 shows how the decreasing oscillating transverse magnetisation vector produces an FID.

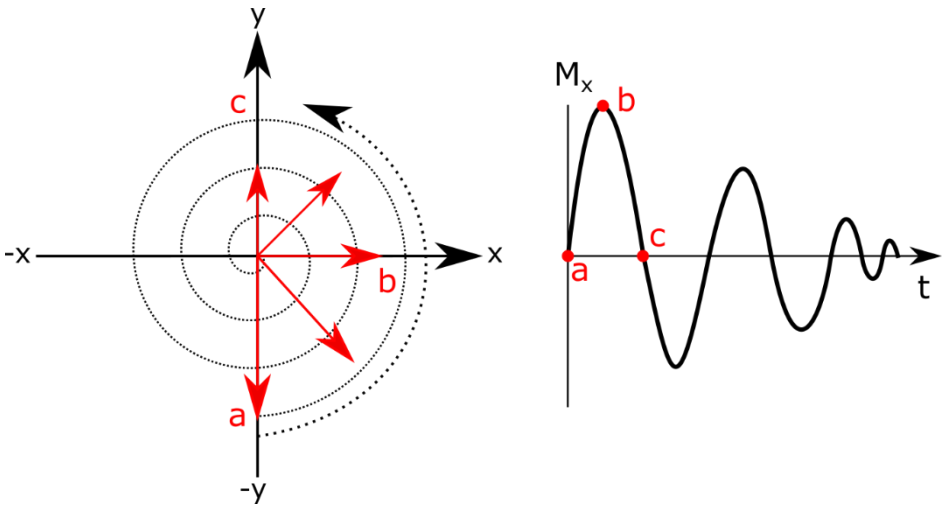

Figure 1.4: Relaxation of the transverse magnetisation from the -y axis following an RF pulse. The x-component (M_x) of the FID produced is shown to the right.

1.4 The NMR spectrum

As mentioned in the previous section, the NMR spectrum is a function of intensity against frequency, with intensity on the y-axis and frequency on the x-axis. The intensity generally correlates to the relative abundance of nuclei. Particularly for ^{1}H and suitable experimental conditions, higher intensities indicate a higher number of protons present in a different environment. In contrast to the simple intensity scale, the scale used on the x-axis is more complicated and is known as the chemical shift. The chemical shift arises due to differences in the local magnetic field experienced by each nucleus and the external magnetic field, which would only be experienced if there were no electrons present. The strength of the local magnetic field is different for different nuclei and chemical environments. This means that each nucleus and chemical environment combination will have a specific resonance frequency and will produce a signal in a certain position on a frequency scale. As the location of different signals is affected by both the strength of the local magnetic field and the frequency of the spectrometer a reference signal is used to remove the dependency of resonances on the spectrometer frequency. This reference signal is for organic solvents tetramethylsilane (TMS) for ^{1}H and ^{13}C spectroscopy due to its very low resonance frequency not interfering with the signals of the compounds. The signals relative to TMS, which are given in Hz, are then divided by the spectrometer frequency to remove the field dependency of the signal distribution and the resulting number is often multiplied by a

million to give a value in units of parts per million (ppm). The conversion to ppm is purely for convenience as most shifts are given on the magnitude of 1×10^{-6} and multiplying by a million converts them to the order of magnitude of 1. Once converted to ppm this value is the chemical shift and can be used to directly compare spectra from spectrometers with different magnetic field strengths and reference frequencies. Equation 4 gives the chemical shift where δ is the chemical shift in parts per million (ppm), υ_0 is the frequency of the signal in Hz, and υ_{TMS} is the frequency of the TMS reference in Hz.

$$\delta = \frac{\upsilon_0 - \upsilon_{TMS}}{\upsilon_{TMS}} \times 10^6 \qquad (4)$$

Since the chemical shift reflects small changes in the electronic environment at a nucleus, it can provide a large amount of information about the structure of a molecule. For example, the presence of an electron withdrawing group such as a carbonyl group removes local electron density from a nucleus 'de-shielding' it and increasing the resonance frequency of the nucleus. An electron donating group has the opposite effect increasing the electron density at the nucleus making it more shielded and lowering the frequency required to excite the nucleus. The dependence of the signal location on the local environment of the nuclei allows information about the immediate neighbours of different nuclei to be determined by comparing the chemical shift of a signal with the known chemical shift ranges of different functional groups. This can be used from gathering information about the presence of functional groups, to the determination of the entire chemical structure of a simple molecule.

After chemical shift, the second main method extracting information from an NMR spectrum is provided by the *J*-couplings. *J*-couplings, which are also known as spin-spin couplings, or scaler couplings, are interactions between spin active nuclei mediated by valence electrons that cause NMR signals to split into multiple peaks that maintain the overall area of the original peak but have distinct spacings and relative intensities. These interactions also occur between the spins of the different nuclei. Whether the interaction raises or lowers the energy of the original spin depends on the signs of both spins. For example, if an interaction between two spins of the same sign raises the energy, an interaction between two opposing spins will lower the energy and vice versa. This is shown in Figure 1.5.

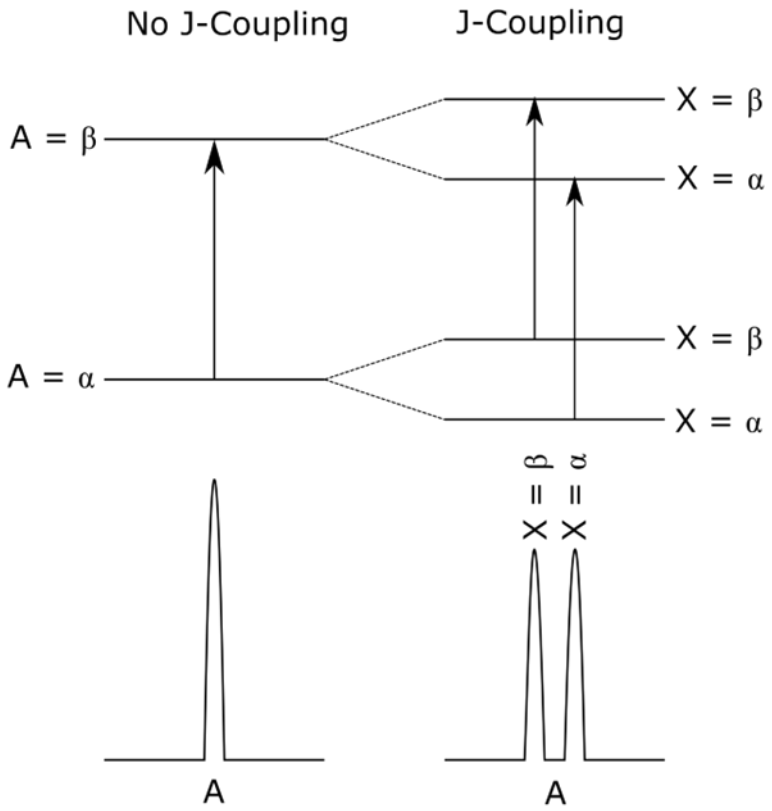

Figure 1.5: The effect of J-coupling on the signal for spin ½ nucleus A in the presence of a second heteronuclear spin ½ nucleus X. The transition of spin states for the X nucleus is not considered as only nuclei A is affected by the RF pulse.

As shown in Figure 1.5, the presence of a second spin active nuclei results in the splitting of the NMR signal into two peaks called a doublet. For spins with $I = ½$, the multiplicity is one more than the number of coupled nucleus; this is known as the n + 1 rule. For a general case of a nucleus coupled to n equivalent nuclei with spin I, the multiplicity is equal to $2nI + 1$. Other than the multiplicity, the magnitude of the coupling can also be used to obtain information about the system. A general expression for the energy of two interacting nuclei is shown in Equation 5 where E is the energy, h is Planck's constant, J_{AX} is the coupling constant and m_A and m_X are the spin quantum numbers of each nucleus.

$$E = h J_{AX} m_A m_X \qquad (5)$$

The magnitude of the coupling, and thus the energy of the interaction between the two nuclei is affected by the distance between the spin of active nuclei with couplings generally decreasing with increasing distance between two nuclei. In aliphatic systems,

the coupling through four bonds or more is normally too weak to be shown in the spectrum. To determine the values of J_{AX} the distance between peaks in the multiplet needs to be measured. The distance between the first and second lines in a multiplet is always a coupling constant and the distance between the first and last line is always the sum of all the coupling constants. While this information is useful for structure determination, *J*-coupling can be an undesirable effect to see within a spectrum as it can lead to considerable peak overlap, and it greatly reduces the signal to noise ratio (SNR). This results in more complicated spectra and makes it more difficult to interpret low intensity signals, therefore decoupling methods are often used. Section 1.8 describes the decoupling process in more detail.

1.5 Benchtop spectroscopy

Traditionally, NMR spectrometers have been developed with stronger magnetic fields to reach higher frequencies and improve resolution and sensitivity. As mentioned in section 1.2, the population difference of the different spin states is affected by the strength of the magnetic field with a greater difference occurring at higher magnetic field strengths. A greater difference in spin state populations increases the strength of the signal produced so higher magnetic fields provide spectra with greater sensitivity. In addition to the increased sensitivity the difference between the Larmor frequency of nuclei of the same kind will also increase, reducing signal overlap and improving the resolution of the spectrum. As a result, most spectrometers used in chemistry research have a ^{1}H frequency between 300 and 800 MHz, although there are spectrometers with frequencies up to 1.2 GHz. While these high-field instruments can provide high quality information, they are expensive, require lots of space and are very high maintenance in terms of requiring liquid nitrogen and helium fills to maintain the superconducting magnets. Consequently, one branch of recent NMR developments has been focused on producing low field benchtop spectrometers. These spectrometers operate at frequencies between 40-100 MHz and are small enough to fit on a lab bench or in a fume cupboard. This small size is possible due to the use of permanent cryogen free magnets and has the added benefit of lowering both the initial cost and the ongoing costs required to run the spectrometer. As a result, these benchtop spectrometers are gaining increasing popularity in the fields of both chemical and biochemical analysis[7], academic teaching[8] and reaction monitoring[9]. The development of these spectrometers

is particularly useful for the field of reaction monitoring as the ability to place the spectrometer in a fume cupboard or even include the spectrometer in a flow system greatly increases the potential to monitor fast or dangerous reactions without the inconveniences of using a high-field facility.

1.6 Building blocks of NMR experiments

1.6.1 Pulse and acquire experiment.

The simplest possible NMR experiment is the pulse and acquire experiment. This is used to record 1D spectra and consists of three separate stages shown in Figure 1.6.

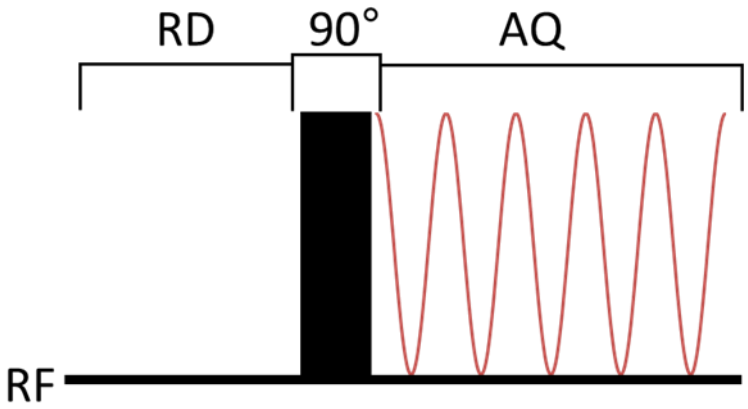

Figure 1.6: A timing diagram of the pulse and acquire experiment where RD is the relaxation delay time, filled rectangle is a RF pulse, in this case with a 90° flip angle and AQ is the acquisition time of the FID. The horizontal axis is a time scale increasing from left to right.

During the relaxation delay the sample reaches equilibrium (or a steady state) in the external magnetic field of the spectrometer which causes a magnetic moment to build up along the z-axis. After the delay, a radiofrequency pulse is applied to the sample causing the overall magnetisation to rotate 90° into the transverse plane and the FID is immediately recorded while the magnetisation is precessing in the transverse plane for time AQ. For a single signal, Fourier transform of the FID will produce a spectrum with a single peak at frequency Ω, where Ω is called the offset, and is the frequency at which the magnetisation vector precesses in the transverse plane relative to the carrier frequency. If there are multiple signals, each will have its own offset value and will precess at a different rate and a Fourier transform will produce a peak for each signal

present in the sample. These offset values can be affected by couplings between spins and by inhomogeneous effects such as the presence of a magnetic field gradient in the external magnetic field. These additional modulations can result in signal overlap and loss of resolution in spectra, which is highly undesirable and limits the usefulness of the simple pulse and acquire sequence.

1.6.2 Spin echo

The spin echo is a simple, yet effective method of countering the negative impact of inhomogeneous magnetic field on spectra and as such is widely used as a building block of many complex experiments in modern NMR. This effect was first observed by Erwin Hahn in 1950[10] and was refined by Purcell and Carr in 1954[11]. The principle of the method is to use a second pulse after the initial 90° pulse in order to refocus the transverse magnetisation so that after a delay, τ, an 'echo' is seen that mimics the initial magnetisation vector present immediately after the first pulse.

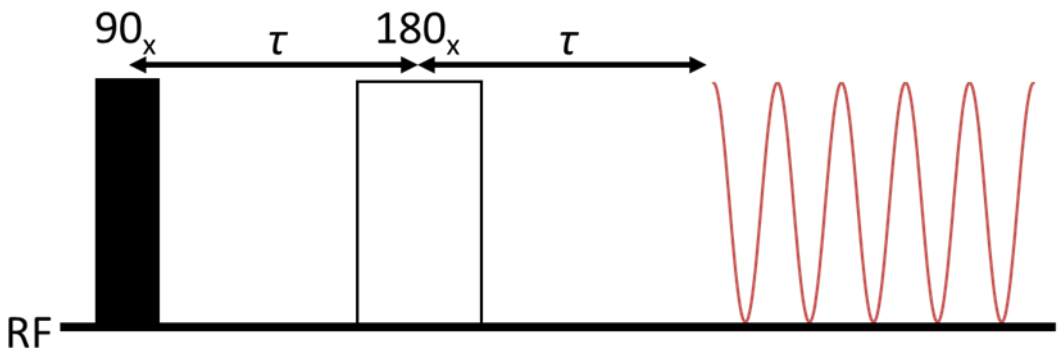

Figure 1.7: Timing diagram, also known as a pulse sequence, for the spin echo experiment. Throughout this report a filled black rectangle represents a 90° hard pulse, and an empty rectangle represents a 180° hard pulse, unless otherwise indicated.

After the initial 90° pulse, during a delay τ, the magnetisation vectors precess in the transverse plane at different rates due to different offsets and inhomogeneous effects. A 180° pulse in the x-axis is then used to flip the magnetisation around the vertical plane perpendicular to the original magnetisation vector as shown in Figure 1.8.

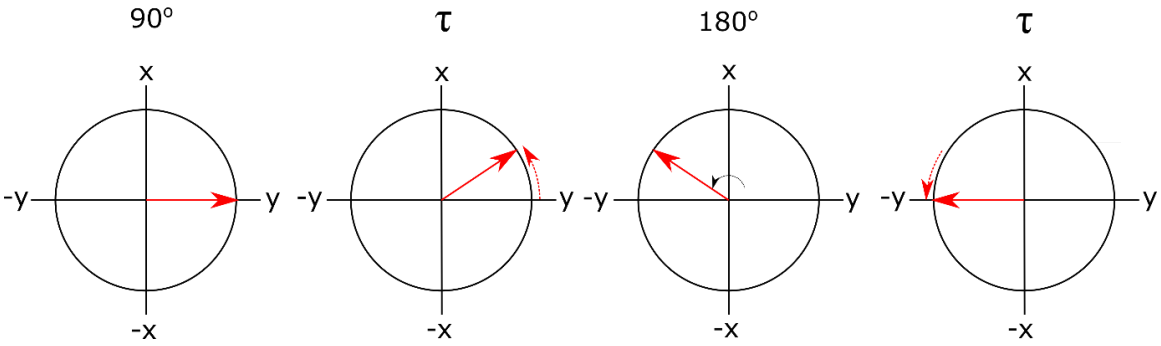

Figure 1.8: The evolution of magnetisation vector during the spin echo sequence. The red dotted arrows represent movement in the xy plane, and the black dotted arrow represents the flipping of the magnetisation through the xz plane.

If the delay after the 180° pulse is the same as the delay between the two pulses, the magnetisation will precess through the same angle and will always refocus for any value of the offset and for this reason the 180° pulse is known as the refocusing pulse. The impact of this on the resulting spectrum is that the effects arising from chemical shift, heteronuclear couplings and magnetic field inhomogeneity are removed and the spin system is returned to its original state, bar the partial relaxation.

1.6.3 Spin echo and coupled systems.

The refocusing of heteronuclear *J*-couplings but not homonuclear *J*-couplings occurs because the 180° pulse is only applied at the frequency of a single type of nuclei, e.g ^{1}H. This means that in a heteronuclear system only one spin experiences the 180° pulse, so the direction of the precession is reversed. In the case of a homonuclear system both spins experience the pulse and direction of the spin precession remains unchanged. These effects are shown in Figure 1.9.

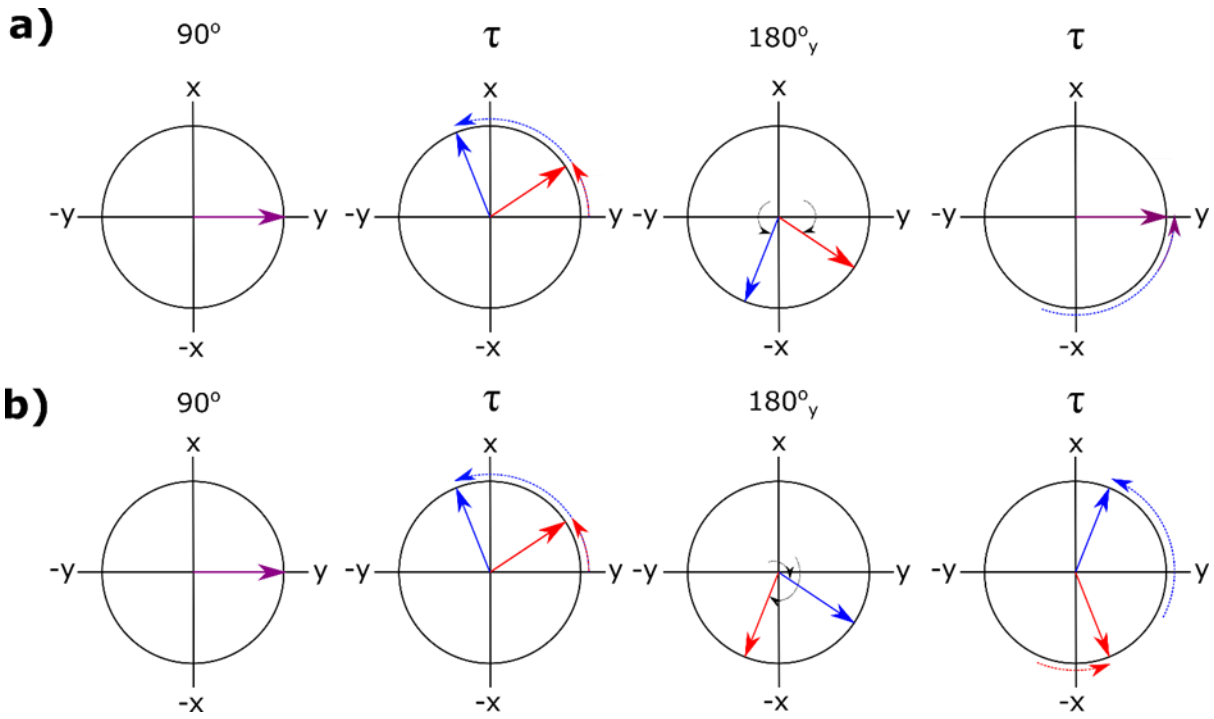

Figure 1.9: The evolution of magnetisation vectors for an a) heteronuclear system and b) homonuclear system. The blue arrows represent the α spin vector, the red arrows represent the β spin vector and the purple arrow indicates when both the α and β spin vectors have the same position.

In some cases, it is desirable to observe the effects of heteronuclear *J*-coupling in order to gain more information about a chemical's structure or to detect labelled metabolites[12]. In these cases, a 180° pulse is also applied to the second nuclei, commonly ^{15}N or ^{13}C, at the same time as the ^{1}H 180° pulse to ensure both spins are flipped, and the couplings are not refocused. One large downside of the spin echo experiment in its basic form is the impact of homonuclear *J*-couplings, otherwise known as *J*-modulation. Since this is unaffected by a nonselective 180° pulse, there is still distortion of the spectrum present. This can be countered for a particular spin if the non-selective pulse is replaced by a frequency selective or soft pulse. The spin system then behaves like the heteronuclear case, where only one of the coupled spin pair was inverted. This of course is not a general solution. To counter this problem a refined version of the spin echo experiment was introduced called the perfect echo[13]. The perfect echo, its scope and limitations are introduced in section 1.6.5.

1.6.4 Spin echo for T_2 measurements

After the initial development of the spin echo sequence by Carr and Purcell in 1954, it found wide use in the measurement of T_2 relaxation times. This was achieved by repeating the 180° pulse at set intervals and recording the echoes that appeared after each 180°. The sequence is shown in Figure 1.10.

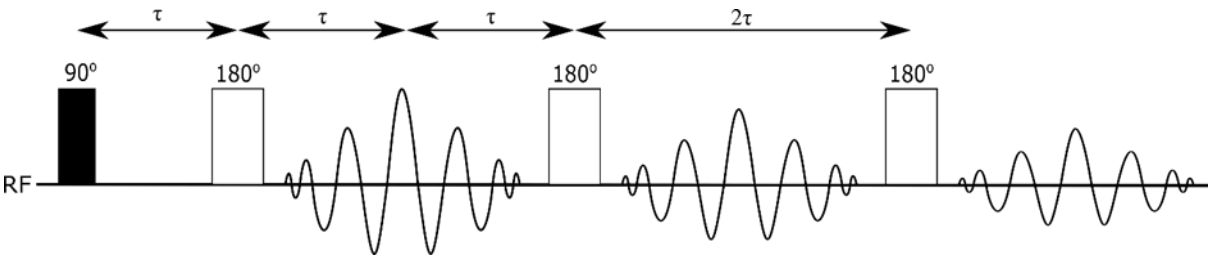

Figure 1.10: Pulse sequence for the measurement of T_2 relaxation times using the spin echo. An echo is present at time τ after each 180° with the amplitude decreasing with successive pulses.

The amplitude of each echo is recorded and the decay in amplitude is exponential with a time constant equal to the T_2 of the signal being measured. While this allowed the measurement of T_2 times, the original method of both the 90° and following 180° pulses being along x resulted in small imperfections in the 180° pulses having a cumulative effect on the echo amplitudes. Each time a pulse is introduced that is not exactly 180° some of the magnetisation is rotated out of the xy plane and successive pulses continue to rotate the magnetisation further out of the xy plane. Over time, the loss of this magnetisation adds up and causes the amplitude of each echo to decay by a larger amount than if only T_2 relaxation was present. These imperfections could be circumvented with a very accurate adjustment of the 180° pulses. However, this was a difficult process and measurements had a very low reproducibility. In 1958 Meiboom and Gill[13] introduced a simple solution to the problem of cumulative imperfection effects which was to give the 180° pulses a phase 90° different to the phase of the original 90° pulse. In practice the 90° pulse is in x and the 180° pulse is in y. It was shown that if a minimum of two 180° pulses are used there is no need to account for pulse imperfections and the reproducibility of T_2 measurements was greatly increased. The reason for this difference is that instead of rotating out of plane magnetisation that results from an imperfect 180° pulse further out of plane a pulse from y returns the

polarisation to the xy plane. This means that any small effect from an imperfect pulse is immediately resolved by the following pulse and has no lasting effect on the measurements. This discovery was also applied to the standard spin echo sequence, resulting in the established phases of x for the 90° excitation pulse and y for all following 180° refocusing pulses. This updated CPMG spin echo sequence also compensates for magnetic field homogeneity, unlike its predecessor.

1.6.5 Perfect echo

Perfect echo is a variation of the spin echo experiment designed to remove the effect of *J* modulation in weakly coupled two spin systems. The technique was first developed in 1988[14] but went widely unused until its rediscovery in 2009[15] and is now increasing in popularity, especially in ^{1}H NMR spectroscopy of small molecules.

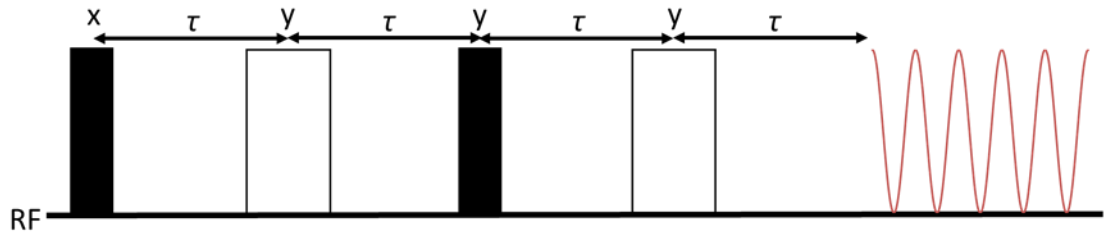

Figure 1.11: Pulse sequence of the perfect echo experiment, the initial 90° pulse is along the x-axis while the remaining three pulses are along the y-axis. The black rectangles represent 90° pulses while the white rectangles represent 180° pulses.

The basis version of the perfect echo sequence is shown in Figure 1.11 and consists of two 180° spin echo pulses with an orthogonal 90° pulse in the middle. The additional 90^{o} pulse together with the second spin echo has the effect of refocusing both the homonuclear and heteronuclear *J*-couplings resulting in a final spectrum that is free from *J* modulation. The key to removing the homonuclear *J*-couplings is the second 90° pulse which inverts the out of phase magnetisation produced by homonuclear *J*-coupling, without affecting the in-phase magnetisation components. Following this, the second spin echo pulse refocuses all the magnetisation components to pure in-phase magnetisation which produces a spectrum free from both homonuclear and heteronuclear *J*-coupling modulation.[15] The perfect echo is perfect for a two-spin system for which it works for any length of the τ delay. In case of multi spin system, evolution of multiple couplings generates out of phase components that are not removed

for arbitrary lengths of the spin-echo interval τ but are minimal for durations less than τ = 5 ms. As the time of the delay increases the intensity distortion increases until it reaches a maximum at the time given in Equation 6 where n is the number of spins and ΔΩ is given by Equation 7.

$$\tau = \frac{(n+1)\pi}{\Delta\Omega} \qquad (6)$$

In Equation 7, Ω_1 and Ω_2 are the chemical shifts of each spin and *J* is the magnitude of the *J*-coupling.

$$\Delta\Omega = \sqrt{(\Omega_1 - \Omega_2)^2 + (2\pi J)^2} \qquad (7)$$

This distortion limits the range of τ values to short values close to 0 when large *J*-couplings are present, as an increase in the value of *J* shortens the value of τ at which the distortion reaches its maximum value.[16]

While this technique is very effective for two spin systems with weak coupling effects, the large distortions arising from strong coupling effects and the modulation reduction is present in more complex systems limits the use of the technique. This was identified as an issue in the 2009 paper. However, it was not addressed at the time. Two later papers by Peter Howe re-examined the experiment and determined that the impact of the strong coupling manifested as an oscillation of multiplet intensities as a function of the chemical shift difference between spins, the echo delay, τ and the *J*-coupling.[16,17] These papers also suggested that the inclusion of a final orthogonal 90° pulse immediately before the acquisition can greatly reduce the impact of strong coupling effects by filtering out any remaining out of phase and anti-phase magnetisation components. This solution is not presented as a universal solution however and it is recommended that upon the addition of the perfect echo sequence to more complicated pulse sequences, a case-by-case analysis should be performed to determine how beneficial a final 90° pulse would be. As a widely used alternative, a z-filter originally developed by Thrippleton and Keeler for removal of zero-quantum artefacts[18], can be appended at the end of the perfect echo. This element also removes the out of phase signals arising in multi spin systems.

1.7 2D NMR

While 1D NMR is very useful for obtaining information about small molecules, it can fall short when looking at more complicated molecules chiefly due to signal overlap. For this reason, two-dimensional NMR is often used as it greatly simplifies the process of structure elucidation by removing or reducing the overlap, but also importantly by providing additional information not present in 1D spectra. The potential of 2D NMR spectroscopy was first realised in 1975 when the first 2D experiment was successfully performed,[19] and since then the field has grown with many 2D experiments now being available for a multitude of different applications.

In contrast to 1D experiments, where there is a single detection period during which the FID signal is obtained, a 2D experiment has two detection periods known as the indirectly detected and directly detected periods. These periods form parts of a general four stage scheme which is common to all 2D experiments; these are preparation, evolution, mixing and detection.

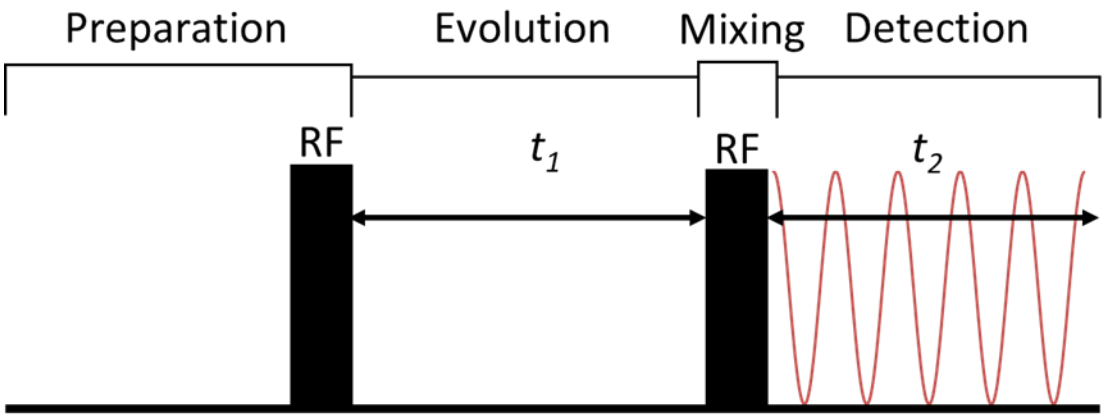

Figure 1.12: The basic scheme of a 2D NMR experiment.

The preparation phase is the same as the equilibrium stage of a 1D experiment where the magnetisation of the spins aligns with the external field and ends with the initial RF pulse exciting the sample. The evolution phase consists of a time delay, t_1, during which the magnetisation is left to evolve. Next, the mixing phase takes place, which consists of further pulses during which the magnetisation is transferred among the coupled spins. Finally, during the detection phase the signal is detected for time t_2 in the directly detected dimension in the same way as for a 1D spectrum. Rather than sampling directly

as for t_2, the t_1 sampling is achieved by varying the duration of t_1 over multiple repeats of the experiment. Recording multiple FIDs provides an indirect way of recording the evolution (chemical shifts or coupling) of the spin system until sufficient resolution is achieved. Once enough FIDs have been collected, typically 50 to 500, two Fourier transforms are performed, one along t_1 and the other along t_2 which gives two frequency scales, F_1 and F_2.

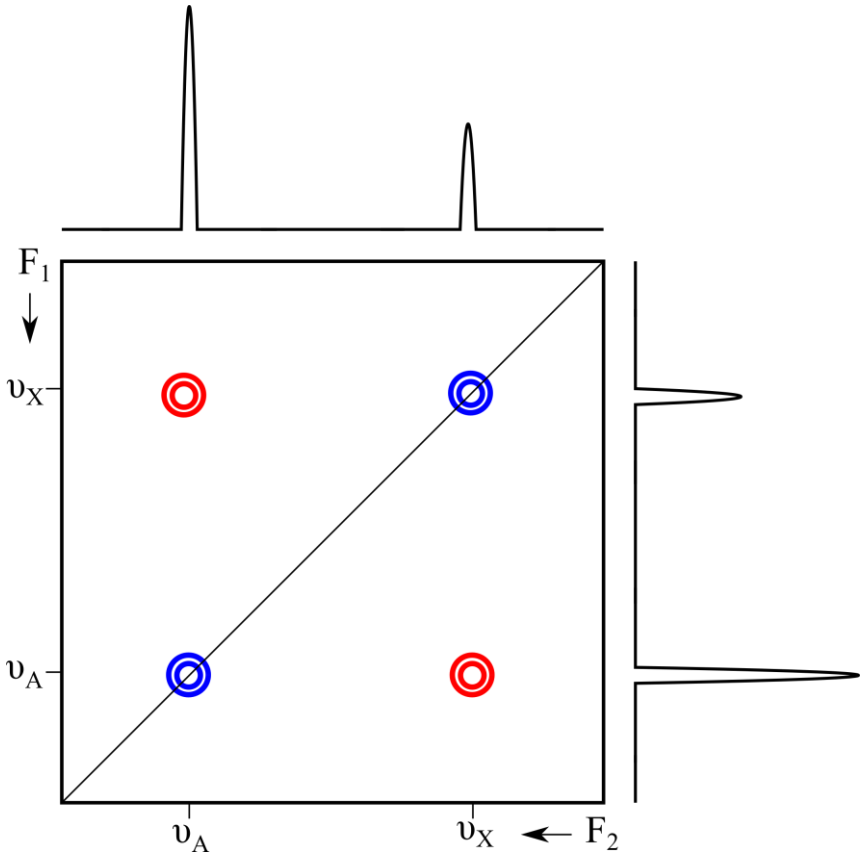

Figure 1.13: An example 2D spectrum for the two-spin system AX. Cross peaks are shown in red and auto correlation peaks are shown in blue.

The spectrum produced is a plot where intensity is shown as a function of two frequencies, rather than simply being plotted against one frequency as is the case in 1D NMR. The frequency axes of the spectra depend on whether the spin system AX was homonuclear or heteronuclear. If the system is homonuclear then the spectrum is symmetrical around the diagonal with auto correlation peaks present at [υ_A, υ_A] and [υ_X, υ_X] and cross peaks present at [υ_A, υ_X] and [υ_X, υ_A]. The cross-correlation peaks indicate transfer of magnetisation between the two spins, whereas the auto correlation peaks are present where magnetisation was not transferred. The spectrum is symmetrical along

the diagonal. In a heteronuclear experiment there are no auto correlation peaks and the spectrum is not symmetrical around the diagonal, as each axis shows the spectrum of a different nucleus, e.g., ^{13}C on the F_1 axis and ^{1}H on the F_2 axis in an HSQC experiment.

1.7.1 COSY

COrrelated SpectroscopY (COSY), the sequence for which is shown in Figure 1.12, is the simplest 2D NMR experiment and was also the first successful 2D experiment.[19] COSY is a homonuclear experiment where a single 90° pulse is used during the mixing period in order to transfer magnetisation between neighbouring *J*-coupled spins. This produces a spectrum with cross peaks appearing where there is direct *J*-coupling, typically between spins separated up to four bonds. In contrast to the in phase diagonal peaks the cross peaks have antiphase character with respect to the active *J*-coupling between the two spins. Passive coupling is also shown by the cross peaks in the form of phase splitting. While this information is very useful for the *J* connectivity of simple molecules, in the cases of larger molecules such as sugars, peptides or proteins, COSY spectra are often overcrowded. In such instances it is desirable to focus on relatively isolated signals and to use them to map the entire spin systems.

1.7.2 TOCSY

TOtal Correlation SpectroscopY (TOCSY) is another simple homonuclear 2D experiment, proposed by Jean Jeneer at the Ampere summer school in 1971 before being experimentally carried out by Ernst in 1983.[20] It is used to correlate all *J*-coupled spins in a spin system regardless of the number of bonds between the two spins. Another difference from COSY is that the cross peaks are in phase which prevents them from disappearing when high mass molecules with large linewidths are studied. This makes TOCSY particularly useful in protein NMR as the correlation of entire spin systems enables the collection of full sub spectra for each individual amino acid present in the protein.[21] The correlation of all coupled spins is achieved by replacing the 90° transfer pulse in the COSY sequence with a spin lock mixing sequence.

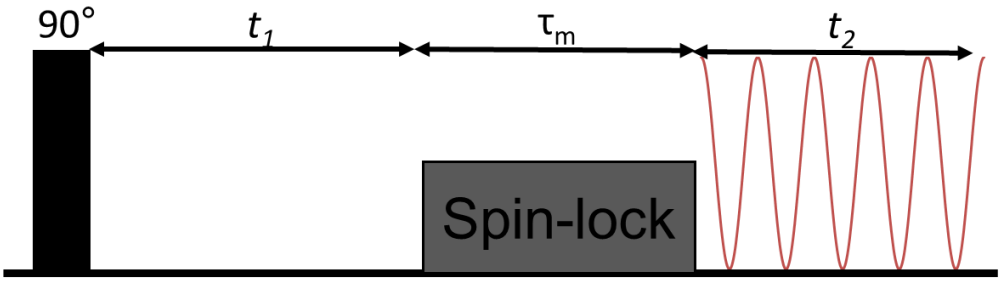

Figure 1.14: Pulse sequence of a basic 2D TOCSY experiment

This mixing sequence lasts for time τ_m and the most basic approach consists of a continuous low power pulse that holds the magnetisation vector in the xy plane, allowing full transfer of magnetisation through *J*-couplings. If τ_m is too short the magnetisation will not have time to fully transfer, and the resulting spectrum will resemble a COSY spectrum with more intense peaks corresponding to shorter range correlations. For this reason, τ_m needs to be sufficiently long so that the magnetisation can fully transfer amongst the spins of individual spin systems. Another more complex spin locking method that is commonly used is called DIPSI-2[22] that enables the spin-locking along any-axis and only produces zero-quantum operators rather a mixture of zero, single and double quantum operators. These zero-quantum operators can then be removed by a z-filter[18] which is discussed in greater detail in section 3.1.

1.7.3 DOSY

Diffusion Ordered SpectroscopY (DOSY) is a 2D NMR technique that separates signals according to the diffusion coefficients of the species they originate from.[23,24] It is comparable to using a combination of HPLC and NMR, where HPLC is used to separate compounds on a physical level which then have 1D NMR spectra recorded, whereas DOSY provides the same information in less detail but much faster and more affordably. The technique involves the recording of a series of spectra with incrementally increasing pulsed field gradient (PFG) strengths. Diffusion of the molecules causes the signals to attenuate, and the rate of decay is linked to the signal intensity by equation 8.

$$I = I_0 e^{-D\gamma^2 g^2 \delta^2 (\Delta - \frac{\delta}{3})} \qquad (8)$$

I is the measured intensity, I_0 is the initial intensity, D is the diffusion coefficient which is affected by the size and shape of the molecule, γ is the gyromagnetic ratio of the nucleus, δ is the duration of the PFG, g is the PFG strength, and Δ the duration of the diffusion. An exponential function is fitted over the range of 1D spectra giving a value of D for each signal. This results in a 2D spectrum with a 1D spectrum present along the F_2 axis while the F_1 axis shows the diffusion coefficient of each signal. This allows identification of signals from the same molecules as the peaks in the 2D spectrum will have the same F_1 value as well as enabling the diffusion coefficient and molecular weight to be calculated. While different versions of the DOSY experiment exist, the one used in this project was based on a stimulated spin echo sequence in its basic form, which is shown in Figure 1.15.

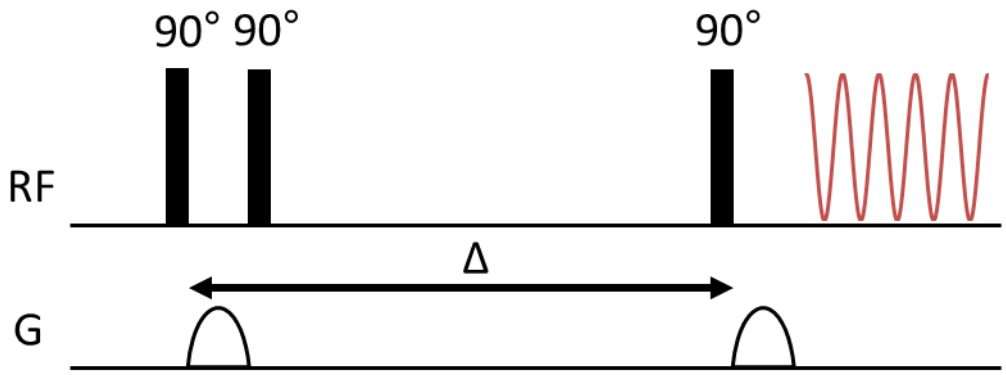

Figure 1.15: Pulse sequence of a simple stimulated echo DOSY experiment. The rounded shapes represent PFG pulses that are incremented in strength for each 1D spectrum.

In this experiment the initial pulse places the spins into the xy plane, and the following gradient encodes them with phase changes that are determined by the position of the molecule. The second 90° pulse moves the spatially diffused spins into the z plane where they diffuse over a set delay Δ. After the delay the third 90° pulse completes the echo and returns the spins to the xy plane where the second gradient cancels the phase changes introduced by the first gradient. This leaves the original signal minus the amplitude loss due to diffusion. The stimulated echo is favoured as the storing of magnetization in z results in a low loss of intensity when studying macromolecules that require a long delay. However, most commonly used sequences feature additional 180°

pulses with PFGs of opposite polarity to remove artifacts and counter effects such as fluid convection.[25]

1.7.4 *J*-RES

J-RESolved Spectroscopy (*J*-RES) is another example of a 2D experiment that can be used to obtain information about the *J*-couplings of a sample. This experiment is another technique developed by Ernst in 1976[26] and was the basis for developing the initial concept of 2D NMR spectroscopy. It has never reached the popularity of experiments such as COSY, due to its more limited range of applications. Where *J*-RES spectroscopy does prove to be useful is in the fields of metabolomics[27] and analysing biological samples[28]. *J*-RES spectra differ from the previously mentioned 2D spectra in that they show a plot of chemical shift along the F_2 axis and *J* multiplets along F_1. This allows easy determination of the multiplicity of different signals that may otherwise be heavily overlapping and difficult to separate, a common issue encountered in benchtop spectroscopy, due to the weaker magnetic field used in these instruments. This is achieved by placing a 180° pulse in the centre of the evolution period that refocuses chemical shift evolution, while leaving *J*-coupling unaffected.

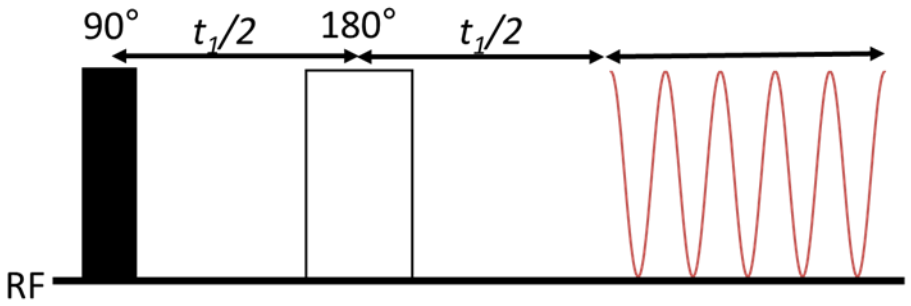

Figure 1.16: Pulse sequence of a basic J-RES experiment

An additional complication that arises for *J*-RES spectra is the evolution of both chemical shift and *J*-coupling during the detection period. This means that after the 2D Fourier transformation the multiplets in the F_1 axis are rotated by 45°. To correct this, the 2D spectrum is tilted by 45° which also has the effect of removing the *J* splitting in the 1D projection of axis F_2. The effect of this tilt on the 2D spectrum is shown in Figure 1.17 along with the effect of removing multiplets from the 1D projection of the F_2 axis.

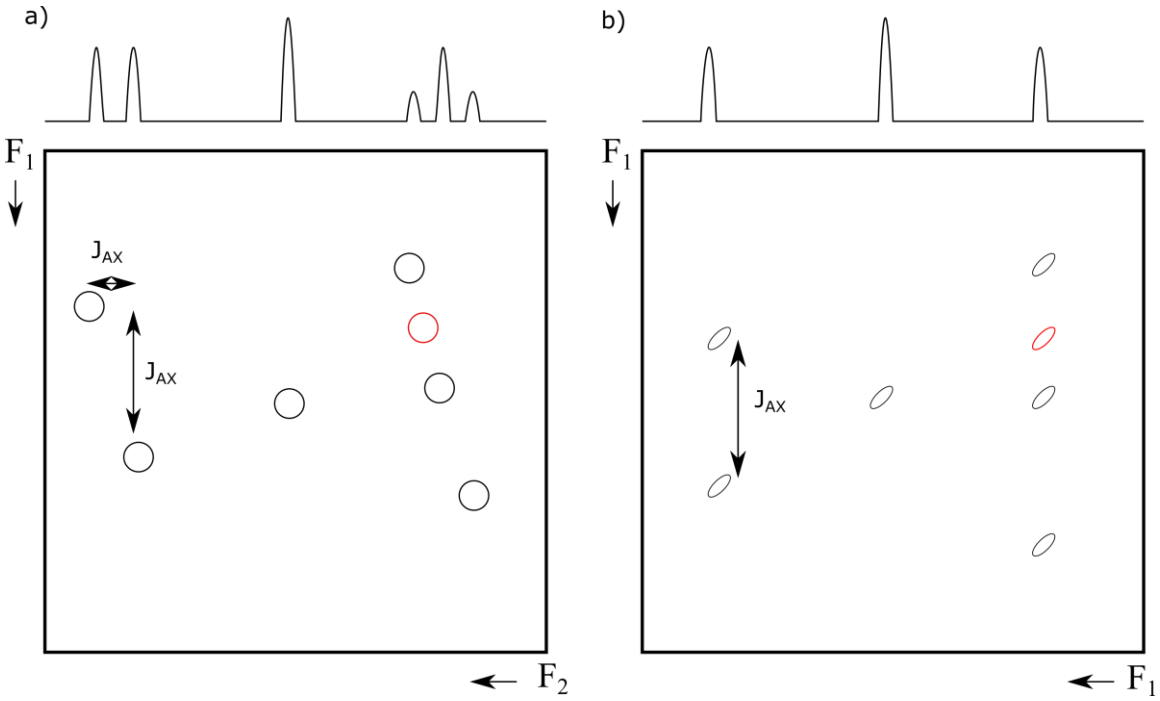

Figure 1.17: A representation of a theoretical *J*-RES spectrum a) after the initial Fourier transform and b) after the tilt has been applied. The red signal is an example of an artefact that would be removed by symmetrisation. Adapted from a Figure by Ludwig and Viant[27].

Another step that can be taken during processing of a *J*-RES spectrum is symmetrisation along the F_1 axis. Since the multiplets should be symmetrical around the centre of the F_1 axis, any artefacts present in the spectra can be removed by comparing the spectrum in each half of the F_1 axis and replacing a higher intensity signal at symmetry related positions by its lower intensity counterpart. These basic *J*-resolved spectra are presented in magnitude mode. More recently, phase sensitive alternatives were developed that deal with J-modulation differently such as the *J*-scaled BIRD-HSQC (BIlinear Rotation Decoupling Heteronuclear Single-Quantum Correlation) experiment[29] and a pure shift modified PSYCHE (Pure Shift Yielded by Chirp Excitation) experiment[30].

1.8 Decoupling

Decoupling is a very useful technique for removing the effect of *J*-couplings on NMR spectra, in this case by completely removing all *J*-coupling arising from a certain nucleus. This is achieved by using a second channel in the spectrometer to irradiate a

nucleus with a stream of broad bandwidth pulses at the Larmor frequency of the targeted nuclei. This is shown in Figure 1.18 with a decoupled example of the pulse acquire experiment.

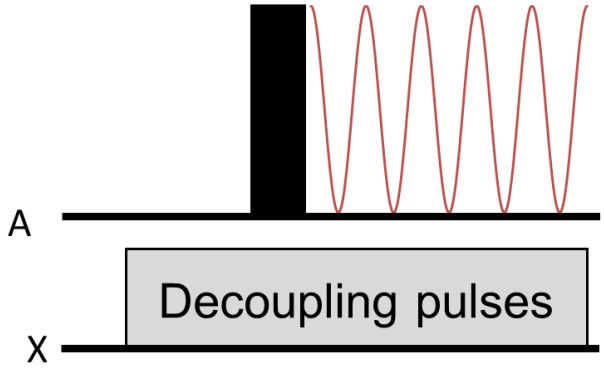

Figure 1.18: Decoupling of X in a pulse acquire experiment on an AX spin system.

The coupling effects of the irradiated nuclei are removed from the spectra and no magnetisation transfer can occur between the irradiated nuclei and the nuclei being observed. Decoupling can be homonuclear or heteronuclear and is most commonly used to remove the effects of proton-carbon couplings in 1D ^{13}C spectra or 2D ^{1}H, ^{13}C hetero-correlated experiments. Many schemes have been developed to achieve a low power broadband decoupling of X nuclei such as WALTZ (Wideband Alternating-phase Low-power Technique for residual splitting)[31], GARP (Globally-optimised Alternating-phase Rectangular Pulses)[32] and MLEV[33]. However, these are limited in the range of frequencies they can cover as well as the power deposition required. To counter this issue adiabatic decoupling has also been developed which uses shaped adiabatic pulses rather than hard rectangular pulses and is growing more common due to the increased abilities of modern spectrometers to produce shaped pulses. The most notable of these is the WURST (Wideband, Uniform Rate, Smooth Truncation) scheme[34,35] and they are popular as the power deposition is much lower than for rectangular pulses which greatly reduces the risk of sample heating. Added to this the shaped pulses can affect a much larger range of frequencies which is suitable for higher field spectrometers, so they are excellent for broadband X nucleus decoupling on high field instruments.

2 Aims and objectives

NMR is a highly versatile analytical technique with a large catalogue of experiments that are composed from smaller building blocks. These experiments provide lot of information and address issues such, limited sensitivity of certain nuclei or spectral overlap. While the building blocks are often useful as standalone experiments, their true potential is realised when they are combined to produce more complex experiments. Once combined, their application scope broadens, and subsequently some become widely used in academia and industry.

The past decades have seen significant progress in widening of the repertoire of NMR experiments, mostly developed at >300 MHz NMR spectrometers. Recent introduction of benchtop NMR instruments operating at 45-100 MHz is helping to widen the use of NMR in non-traditional environment, but calls for development of experiments that can increase the sensitivity of these low field instruments. This helps to break down the financial and logistical barriers and to bring NMR closer to the chemistry fume hoods e.g as a convenient portable reaction monitoring tools.

Two experiments in particular will be the focus of this project. First is the DISPEL (Destruction of Interfering Satellites by Perfect Echo Low-pass filtration) experiment that supresses one bond ^{13}C-^{1}H satellites while leaving the rest of the spectra intact. The second is SHARPER (Sensitive, Homogeneous, And Resolved PEaks in Real time), a pure shift method that removes all heteronuclear and homonuclear couplings from a particular nucleus collapsing the signal into a single sharp peak. Both of these experiments have great scope for further development and applications to different areas of research.

The aims of this project thus are as follows:

- Develop further the DISPEL pulse sequence and combine it with the well-known TOCSY technique.
- Use the new DISPEL-TOCSY experiment to in determining of the site-specific ^{13}C enrichment by NMR.
- Adapt the SHARPER acquisition method for use on low field benchtop NMR spectrometers.

- Combine the SHARPER sequence with other building blocks such as DOSY and CSSF to achieve determination of diffusion coefficients of molecules in mixtures.
- Investigate the potential for using SHARPER to collapse entire spectra, to enable the study of low concentration samples that otherwise cannot not be characterised.

3 DISPEL

3.1 Declaration

The work described in 3.4.2 was in part carried out by Dr Will Kew of the Pacific Northwest national laboratory and final year undergraduate student George Padfield. Will produced the *Saccharomyces cerevisiae* sample and recorded the spectra while George assigned the peaks and identified the present compounds. I carried out the enrichment calculations.

3.2 Introduction to DISPEL

This chapter describes adaptations of a DISPEL (Destruction of Interfering Satellites by Perfect Echo Low-pass filtration) building block, first developed in 2017 by the NMR methodology group at the University of Manchester[36]. These adaptations are intended to improve the practical uses of the DISPEL experiment by both altering the basic experiment and including it in other well-known NMR experiments.

DISPEL aims to suppress the one-bond ^{13}C satellites in ^{1}H NMR spectra without the use of broadband ^{13}C decoupling or sacrificing the signal to noise ratio of the spectrum. These satellites arise due to couplings between ^{1}H nuclei and spin active ^{13}C nuclei and appear either side of the parent peaks at $0.5*J_{CH}$ offset from the parent signal (neglecting the isotope shift) at roughly 0.55% of the parent peak intensity. Providing the ^{1}H spectra show sufficient SNR, one-bond satellites are visible, and these are the target of the DISPEL experiment as illustrated in Figure 3.1. Long-range ^{13}C satellites are hidden beneath the main ^{1}H-^{13}C signals.

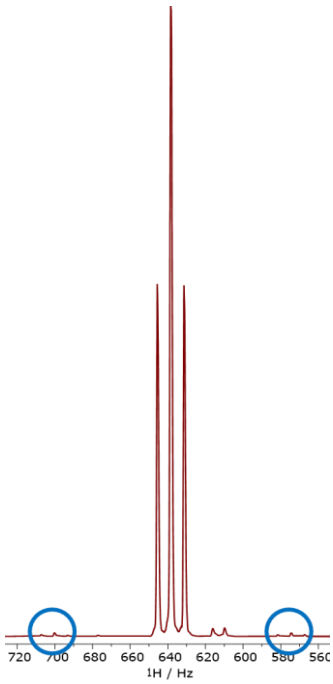

Figure 3.1: An example of a CH_2 ethanol triplet with one bond ^{13}C satellites indicated by the blue circles.

This small intensity is due to the natural abundance of ^{13}C of 1.11%, however, this can still pose major problems when assessing the purity of compounds as these small peaks can mask the signals of impurities or could be mistaken for such. These problems have been addressed in the past using techniques such as changing the solvent or pH of the sample to move the relative positions of the signals[37] but these techniques are time consuming and are sometimes not possible when dealing with sensitive samples. A more suitable approach is the use of X-filters.[37] In the most basic form this involves adding a spin echo with every other scan containing an additional 180° pulse in the X channel at the same time as the 180° pulse in the proton channel as shown in Figure 3.2.

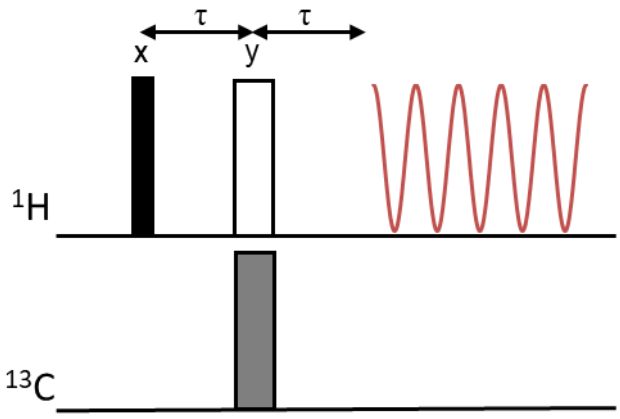

Figure 3.2: Pulse sequence of the basic X filter. The black rectangle represents a 90° hard pulse, white rectangle is a 180° hard pulse, and the grey rectangle is a 180° X channel pulse which is only activated during odd-numbered scans. $\tau = 1/2^{1}J_{CH}$

Following the period of $\tau = 1/2^{1}J_{CH}$, antiphase proton magnetisation changes sign when the 180° X pulse is applied. When this spectrum is added to the spectrum produced in the scan without the X channel pulse, the difference spectrum is free from ^{13}C satellites. The main issue with this technique is that there often is a range of $^{1}J_{CH}$ values in molecules, which means that no single value of τ will result in all proton magnetisation converting fully into antiphase magnetisation. This means that the ^{13}C satellites will not be perfectly cancelled, more so with the increasing difference in $^{1}J_{CH}$ values from the value of $^{1}J_{CH}$ that the τ delay was tuned to. A solution to this problem was proposed by Kupce and Freeman[38] which involves the use of a pair of opposing adiabatic pulses instead of a hard 180° pulse. When long (1-2 ms) adiabatic pulses sweep through the chemical shift range, they invert X-spins at different times. As there is roughly a linear relationship between $^{1}J_{CH}$ magnitude and ^{13}C chemical shifts, it is possible to arrange that aromatic CHs (which have the largest $^{1}J_{CH}$ couplings) are inverted last, i.e., their inversion point is most off-centre with regard to the central ^{1}H 180° pulse, while the methyls (with the smallest $^{1}J_{CH}$) are inverted first. The amount of off centeredness decreases the effective *J* evolution, meaning that optimum *J* evolution time can be achieved for most of the CH_x sites. The use of adiabatic pulses is beneficial, as they greatly increase the effective bandwidth and uniformity of the X nuclei inversion. The initial adiabatic inversion X pulse restores the spin-echo condition on the ^{1}H channel. The resulting pulse sequence is shown in Figure 3.3.

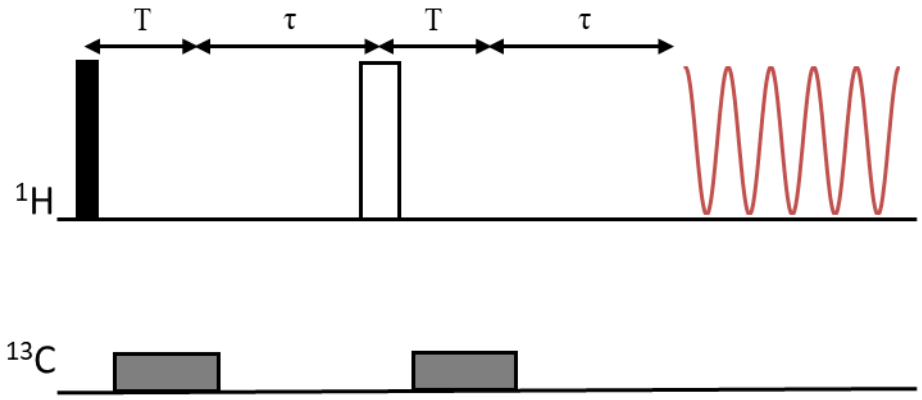

Figure 3.3: Pulse sequence of the adiabatic X-filter. The black, white, and grey rectangles are 90°, 180° and adiabatic pulses respectively. The adiabatic pulses have duration T which is chosen such that $\tau + T = c/J_{min}$ and $\tau - T = c/J_{max}$; c is a constant where c = 0.2 for HSQC experiments and c = 0.5 for isotope filter experiments.

As long as the time T and the parameters of the sweep are appropriately calibrated to the range of $^1J_{CH}$ values present in the sample, this sequence mostly compensates for the difference in $^1J_{CH}$ values. However, the relationship between coupling strength and chemical shift is only approximate so this is not a perfect solution. An example are the anomeric carbons of carbohydrates, which have large $^1J_{CH}$ coupling constants (~170 Hz and ~ 160 Hz for the α and β form, respectively), yet resonate in the 90-105 ppm range, well below the aromatic carbons which have comparable coupling constants.

Another method widely used is broadband decoupling that removes all heteronuclear couplings between protons and ^{13}C. However, this has the major downsides of introducing decoupling sidebands (for enriched ^{13}C compounds in particular) to the spectrum and can lead to sample heating. A major practical limitation is the restricted decoupling time on cryoprobes to 150-200 ms which severely compromises the resulting resolution. In contrast to these techniques DISPEL removes ^{13}C satellites without introducing sidebands, does not require any special sample preparation and has no restrictions on the acquisition time. The pulse sequence of the original DISPEL experiment is shown below in Figure 3.4.

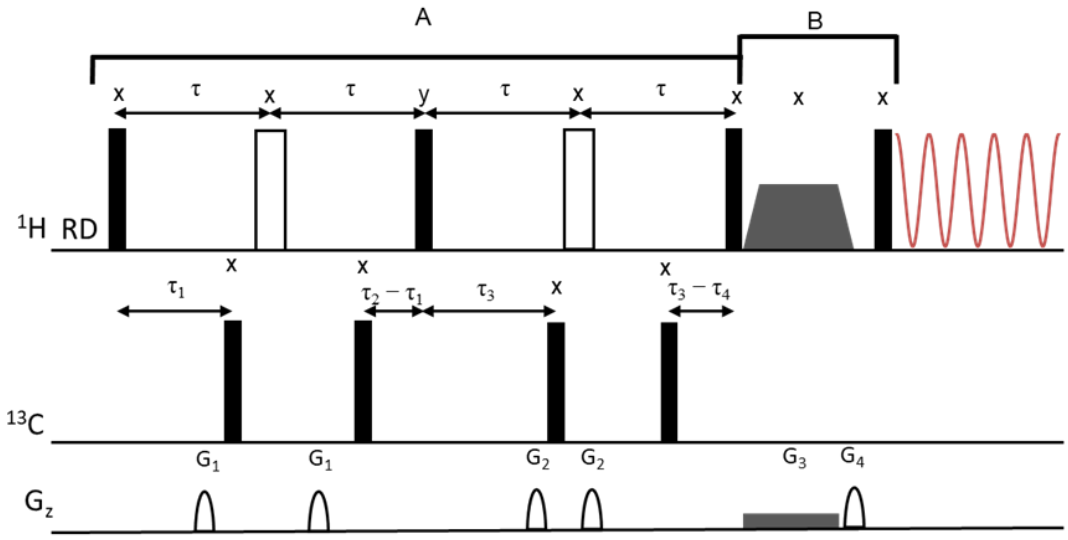

Figure 3.4: Pulse sequence of the original 4-stage DISPEL experiment. The black and white rectangles represent 90° and 180° pulses, respectively, while the white shapes are field gradient pulses. The trapezoid is a 180° smoothed chirp pulse that is applied concurrently with G_3 which is a matched field low power gradient pulse. The phase of each pulse during the first scan is shown above the pulse. Section A is a low pass J filter[39] and section B is a z filter.[40] τ is a set delay chosen to accommodate delays $\tau_{1\text{-}4}$ which are numerically optimized to supress signals of protons with a range of $^1J_{CH}$ coupling constants.

The key outcome of this sequence is that it enables removal of one-bond ^{13}C satellites. This occurs during section A of Figure 3.4 that acts as a low pass *J* filter[39]. Low pass *J* filtering is a technique developed in the 80's that in an ideal case selectively removes signals exhibiting *J*-coupling larger than a lower limit, known as J_{min}. In the case of DISPEL this is achieved by using a series of 90° ^{13}C pulses at different time points that follow the initial 90° excitation pulse in the ^{1}H channel.

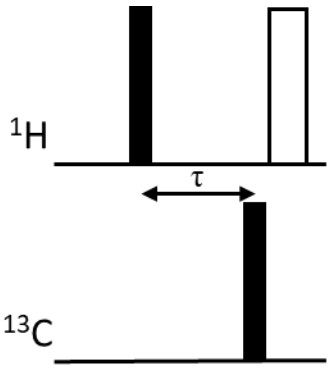

Figure 3.5: Base component of a low pass J filter. The black and white rectangles represent 90° and 180° pulses respectively. The 180° pulse is only required for phase sensitive spectra.

Each 90° ^{13}C pulse takes ^{1}H coherences that are antiphase with respect to ^{13}C and convert them into multiple-quantum coherences that are unobservable and are therefore not present in the final spectra. The reason why multiple repeats of the *J* filter are required is a leakage of magnetisation in case of the mismatch between the actual $^{1}J_{CH}$ coupling constant and the one used to set an evolution delay ($\tau = 0.5/^{1}J_{CH}$). For a single low pass *J*-filter this leakage is inevitable in real samples that exhibit a range of $^{1}J_{CH}$ coupling constants (120 to 250 Hz). Unfortunately, this requires time (2-4 ms[39]) which causes the phases of individual lines of ^{1}H multiplets created by the homonuclear *J*-couplings to diverge. A solution proposed to this problem is the use of a perfect echo to effectively refocus all homonuclear couplings. The range of $^{1}J_{CH}$ couplings affected by each ^{13}C pulse depends on the delay τ between the proton pulse and the ^{13}C pulse. DISPEL was designed with delays τ_1, τ_2, τ_3 and τ_4 set to 3.2, 1.1, 3.95 and 1.56 ms to cover J_{CH} couplings between the range of 120 to 360 Hz. This range thus covers all the one-bond couplings that are encountered in practice and the DISPEL experiment can be used to suppress all one-bond satellites. This suppression is aided by the gradient pulses G_1 and G_2 that are used to select the pathways through which the coherence is transferred.

The second important aspect of this experiment is depicted in Figure 3.6 and is called a z-filter[40].

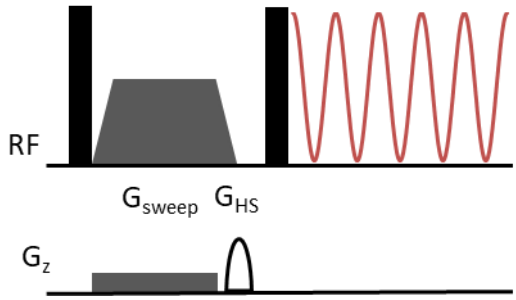

Figure 3.6: Pulse sequence of a z filter, the black rectangles are 90° pulses, the trapezoid is a 180° smoothed swept frequency pulse, G_{sweep} is the gradient pulse for the swept frequency pulse and G_{HS} is a homospoil gradient pulse.

The purpose of the z-filter is to remove out of phase coherences such as homonuclear zero and double quantum terms. These terms result in the appearance of mixed phase multiplets in the spectra by introducing anti-phase dispersive components. Secondary benefits specific to the DISPEL experiment are the elimination of homonuclear J_{HH} modulation that was not completely refocused by the perfect echo and dephasing of any remaining antiphase heteronuclear terms. This is achieved by a PFG, which is applied along the z-axis, changing the Larmor frequency to be a function of the spin's position within the NMR tube. This means that the swept frequency pulse flips the spins in the tube at different times. For example, a spin at the top of the tube may experience the 180° pulse right at the beginning of the sweep time whereas a sample at the bottom of the tube will experience the 180° pulse at the end of the sweep. The length of the spin-echo that refocuses the chemical shift of zero-quantum coherences therefore differs causing the multiple-quantum coherences to acquire different phases. After conversion of these coherences into observable magnetisation this phase is preserved, thus cancelling each other out and removing the zero-quantum artefacts in the final spectrum. The double-quantum coherences can also be removed by phase cycling while the in phase magnetisation, stored along the z-axis, is not affected by the PFGs.

One final important feature of this experiment that was not discussed in the original paper but is used in this project is the addition of a presaturation pulse[41] at the beginning of the sequence in order to suppress any solvent peaks. As many of the samples used during this project are aqueous an efficient solvent suppression mechanism was required. It has previously been shown that presaturation is compatible with the

DISPEL experiment[36]. Presaturation is a solvent suppression technique that consists of saturating a specific frequency, often water, with a long, low power RF pulse to remove the presence of a solvent peak from a spectrum. This can greatly improve the signal to noise ratio of the rest of the spectrum and reveal peaks that may be present at a frequency close to that of the solvent.

The combination of a low-pass *J* filter and z-filter enables DISPEL to effectively remove one-bond ^{13}C satellites from the spectra with negligible sample heating and no impact on the final spectral resolution. While this is very useful by itself, the DISPEL element can also be incorporated into other experiments. This has already been demonstrated by the inclusion of the sequence in the DOSY (Diffusion Ordered SpectroscopY) experiment[42] so this project has focused on adapting the original sequence and adding it to two other experiments.

3.3 1D interleaving.

The first task of this project was to improve upon the basic 1D DISPEL experiment by producing an interleaved version where a single experiment would yield two spectra, one with suppression of ^{13}C satellites and the other with the ^{13}C satellites still present. The spectra without the satellites are obtained by a standard DISPEL setting, while the spectra with satellites are obtained using the identical pulse sequence, but setting the power of the ^{13}C channel to 0 W. This arrangement ensures that these spectra are otherwise identical, including any minor distortions to proton multiplets and signal attenuation caused by relaxation. The spectra without ^{13}C satellites can then be subtracted from the spectra containing ^{13}C satellites to give a third spectrum that only contains ^{13}C satellites. This third spectrum is particularly useful for quantification of ^{13}C enrichment e.g., in biological studies without interference from intense signals of ^{12}C attached protons.

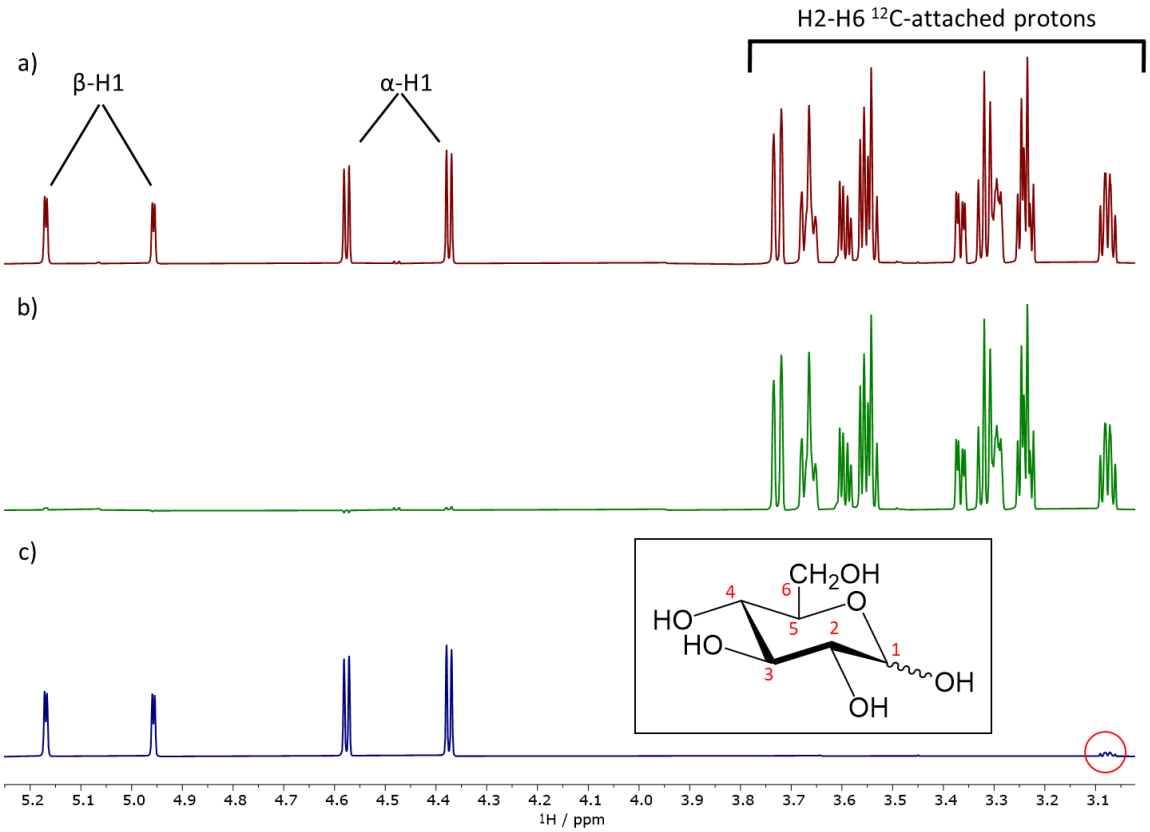

Figure 3.7: Spectra of labelled glucose with ^{13}C placed at position 1 obtained using an interleaved DISPEL sequence. a) shows the spectrum with ^{13}C satellites present (no power in ^{13}C channel), b) is the spectrum without ^{13}C signals (full power in ^{13}C channel) and c) is the spectrum only containing ^{13}C satellites obtained by subtracting b from a. The red circle indicates a residual signal of H2β. The inset shows the structure of glucose and the assignments of the protons.

The reasons that this procedure requires to acquire spectra in an interleaved manner rather than running the two experiments sequentially one after the other are the spectrometer instabilities, including lock instabilities. These instabilities cause the exact frequencies of peaks in a spectrum to shift slightly so two spectra, even if they are obtained in quick succession, will not perfectly overlap resulting in large cancellation artefacts. In contrast to running two separate experiments where the lock is set up twice, an interleaved experiment only has one lock point. This minimises the impact of lock instabilities on the obtained spectra. To interleave these two experiments a new pseudo 2D pulse program was written that records data into two separate files, one that contains an FID from scans with power in the carbon channel and the other

containing a FID from scans with no power in the carbon channel. These scans are interleaved so only every other scan has DISPEL 'switched on' and the final spectra are much less impacted by spectrometer instabilities resulting in artefacts with greatly reduced intensities. Two examples of spectra obtained using this interleaved experiment are shown in Figure 3.7. In this spectrum, in addition to $^{1}J_{CH}$ satellites, also a residual signal of H2β is visible. This is due to a large $^{2}J_{C1H2}$ coupling constant (5.5 Hz)[43] that also evolved during the DISPEL pulse sequence, causing H2β to be marginally attenuated in the spectrum with full power ^{13}C pulse.

3.4 2D ^{1}H-^{1}H TOCSY

After the 1D interleaved DISPEL experiment was developed, the sequence was added to a 2D TOCSY program from the Bruker list of standard experiments that uses the DIPSI2 (Decoupling In the Presence of Scalar Interactions) mixing sequence[44].

Figure 3.8: Pulse sequence of a 2D TOCSY experiment that DISPEL was added to. The black rectangles are 90° pulses, the trapeziums are adiabatic shaped pulses, the grey rectangles are gradient pulses, and the white rectangle is the DIPSI2 mixing time.

Since the TOCSY experiment shows correlations between the donor and acceptor spins there are two ways in which the DISPEL sequence can be utilised in this experiment. These both involve replacing a 90° pulse with the DISPEL sequence and are marked as A and B in Figure 3.8. As A is before the mixing time, if it is replaced, the DISPEL transfer will only occur from protons that are attached to ^{12}C nuclei so in the final spectrum ^{13}C peaks will only appear along the F_2 axis. In contrast, since B is after the mixing time, transfer will only occur to ^{12}C nuclei and ^{13}C peaks will only occur along

the F_1 axis. Finally, if both A and B are replaced with DISPEL, then magnetisation will only transfer through *J*-couplings between protons that are attached to ^{12}C nuclei.

Initially, separate pulse programs were created for DISPEL in each position to confirm that the experiment worked and then a master experiment was produced that uses definitions defined by the user when setting up the experiment to determine which DISPEL sequences are active.

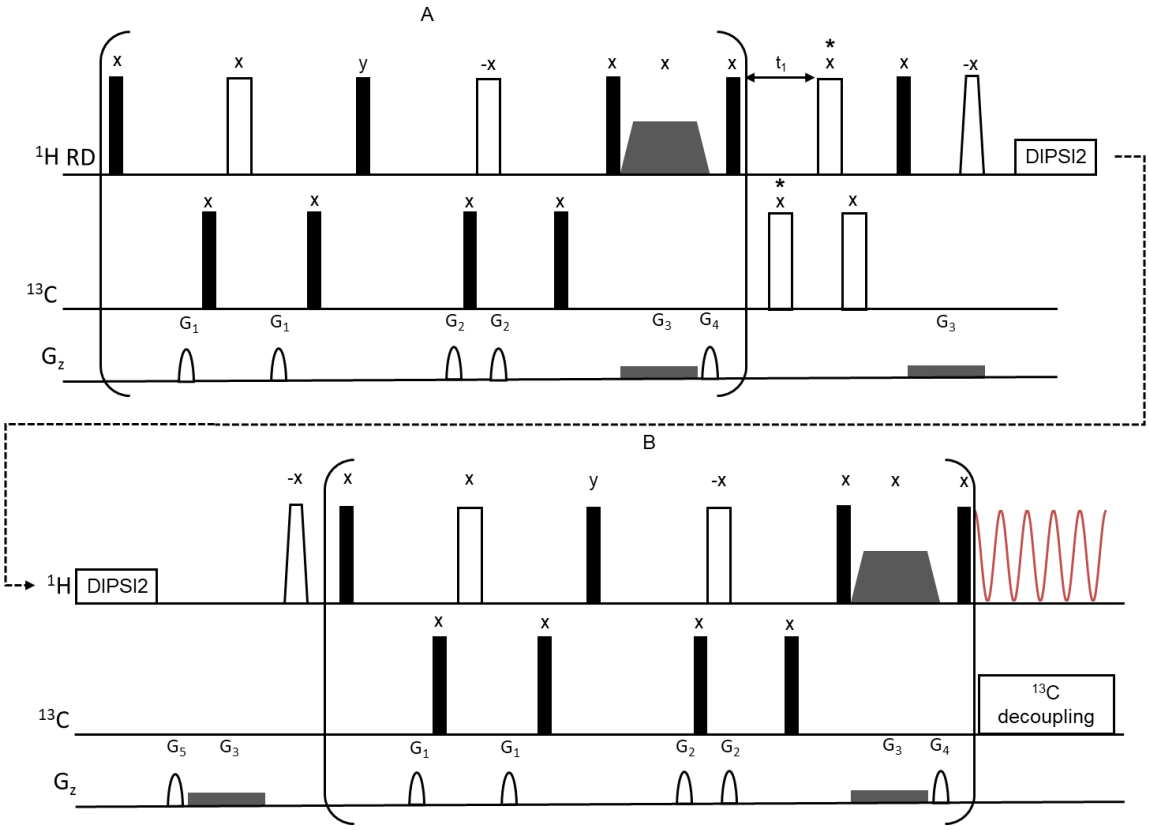

Figure 3.9: Pulse sequence of the 2D DISPEL-TOCSY experiment split over two lines with the DIPSI2 mixing time at the separation point. A and B correspond to A and B in Figure 3.8 and show where the DISPEL sequence has been substituted in. The black rectangles are 90° pulses, the white rectangles are 180° pulses, the white trapeziums are adiabatic shaped pulses, the grey trapeziums are 180° smoothed chirp pulses, the white shapes are gradient pulses, and the white rectangle is the DIPSI2 mixing time.

Three additional 180° pulses are shown in Figure 3.9 which are marked by asterisks. The first ^{13}C channel pulse occurs in the middle of the t_1 period and refocuses the C-H couplings preventing them from evolving and thus acting as carbon decoupling in F_1. It is repeated before the 90° ^{1}H pulse. Typically, this arrangement is used to eliminate

phase distortions caused by inversion rather than refocusing ^{13}C pulses. The pulse in the ^{1}H channel is an additional 180° pulse which is required to remove the ^{1}H chemical shift evolution during the central ^{13}C inversion pulse. This accounts for the sampling delay at the beginning of the t_1 period, potentially setting it to 0. Alternatively, the first sampling point is set to half the t_1 dwell time and a 90, -180° zero and the first order phase corrections are used to avoid baseline distortion as described by Bax et al.[45]

In order to deactivate the DISPEL sequence either before or after the mixing time, the power of the ^{13}C channel is changed to zero for the duration of the DISPEL section of the experiment. This maintains the time delays for the proton channel but prevents the suppression of ^{13}C satellites giving identical ^{12}C peaks to when the sequence is activated. As the sequence is placed both before and after the mixing time there are 4 possible combinations which will result in spectra showing different peaks. The different combinations and the magnetisation transfer present in the final spectra are shown below in Table 3.1.

Table 3.1: DISPEL-TOCSY combinations and the peaks that will be observed in the resulting spectra.

Experiment number	DISPEL before?	DISPEL after?	Transfer observed?			
			^{12}C--^{12}C	^{12}C--^{13}C	^{13}C--^{12}C	^{13}C--^{13}C
1	No	No	Yes	Yes	Yes	Yes
2	No	Yes	Yes	No	Yes	No
3	Yes	No	Yes	Yes	No	No
4	Yes	Yes	Yes	No	No	No

An interleaved version of this experiment was written that obtains all four combinations of DISPEL before and after in a single run and enables easy comparison of the different spectra. The results from this experiment on a C_1 ^{13}C-labelled sample of glucose are shown in Figure 3.10. The two satellites are clearly visible in the F_2 dimension. However, there is only a single peak for each ^{13}C attached proton in the F_1 dimension due to carbon-13 decoupling in F_1. This demonstrates the effective removal of the ^{13}C attached signal both when it is present as satellites with no decoupling and when decoupling has collapsed the satellites into the central frequency.

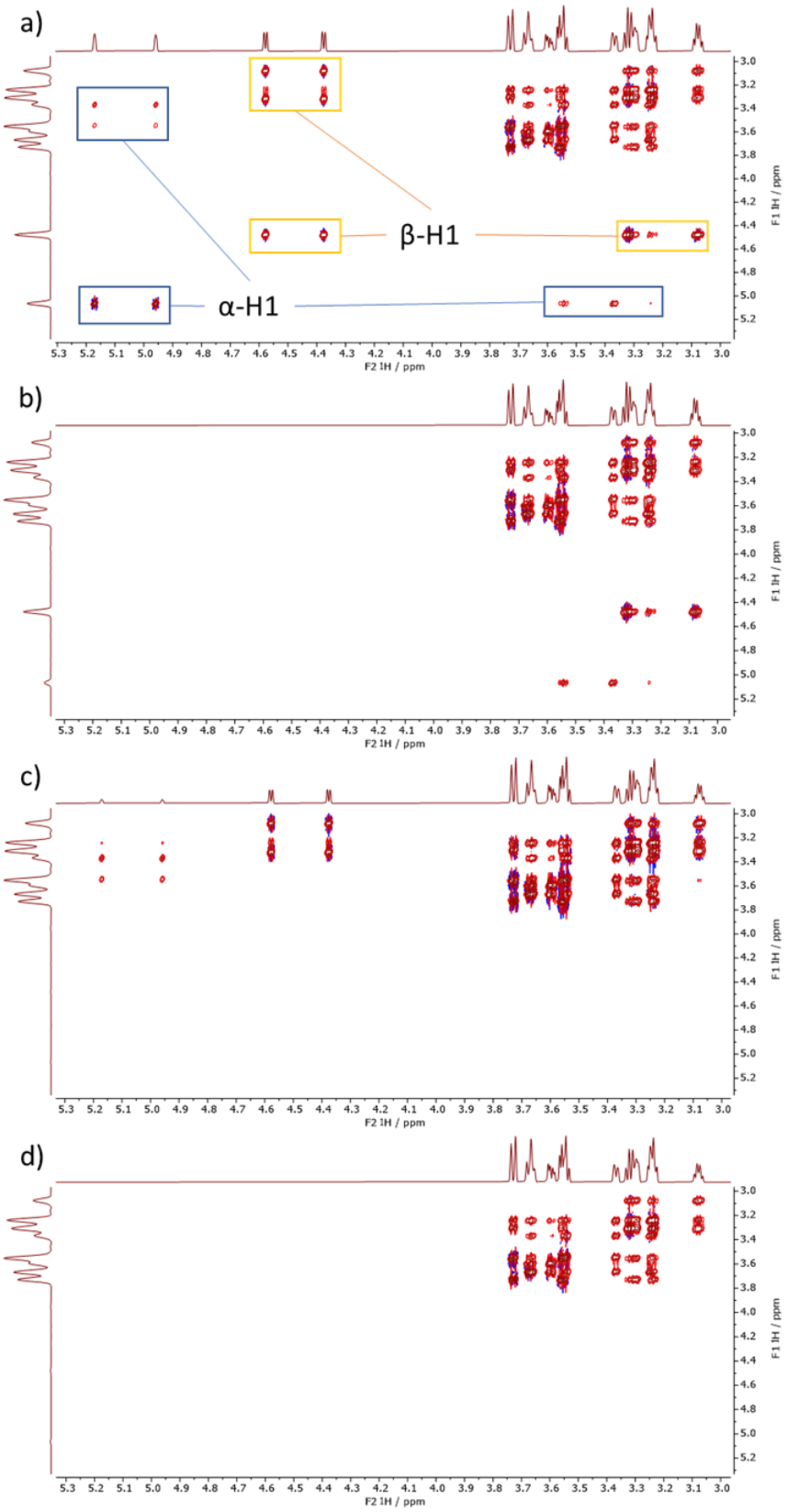

Figure 3.10: 2D DISPEL-TOCSY spectra of ^{13}C labelled glucose obtained from a single experiment with a 60 ms mixing time. a) no DISPEL sequences active, b) DISPEL

active after the mixing time, c) DISPEL active before the mixing time and d) DISPEL active both before and after mixing. ^{13}C decoupling was utilised in the F_1 dimension but not F_2.

While the combinations introduced in Table 3.1 and shown in Figure 3.10 are all the options possible to directly record, addition and subtraction of spectra can be used to produce spectra consisting of different transfer pathways and indeed isolate each individual transfer. Table 3.2 is an extension of Table 3.1 and shows the possible combinations that can be obtained by a linear combination of the spectra recorded using the interleaved DISPEL-TOCSY sequence.

Table 3.2: Linear combinations of DISPEL-TOCSY spectra along with the original spectra. The type of polarisation transfer present in the final spectra is highlighted.

Experiment combination	Addition/subtraction	Transfer observed?			
		^{12}C--^{12}C	^{12}C--^{13}C	^{13}C--^{12}C	^{13}C--^{13}C
1	-	**Yes**	**Yes**	**Yes**	**Yes**
2	-	**Yes**	No	**Yes**	No
3	-	**Yes**	**Yes**	No	No
4	-	**Yes**	No	No	No
5	3−4	No	**Yes**	No	No
6	2−4	No	No	**Yes**	No
7	1−4	No	**Yes**	**Yes**	**Yes**
8	1−2−3+4	No	No	No	**Yes**

In order to aid this processing, an AU program has been written that takes the original interleaved TOCSY file, splits it into the four separate recorded spectra and then performs all the necessary additions and subtractions producing the eight spectra that are mentioned in Table 3.2. The interleaved nature of the acquisition means that despite the long times taken to record the TOCSY spectra, factors such as temperature, lock or

electronic instabilities will not have an impact on the final spectra. This means the addition and subtraction can be carried out automatically without having to first align the spectra using a reference such as TMS. The results of this addition and subtraction are shown below on the same sample of labelled glucose as used for Figure 3.10.

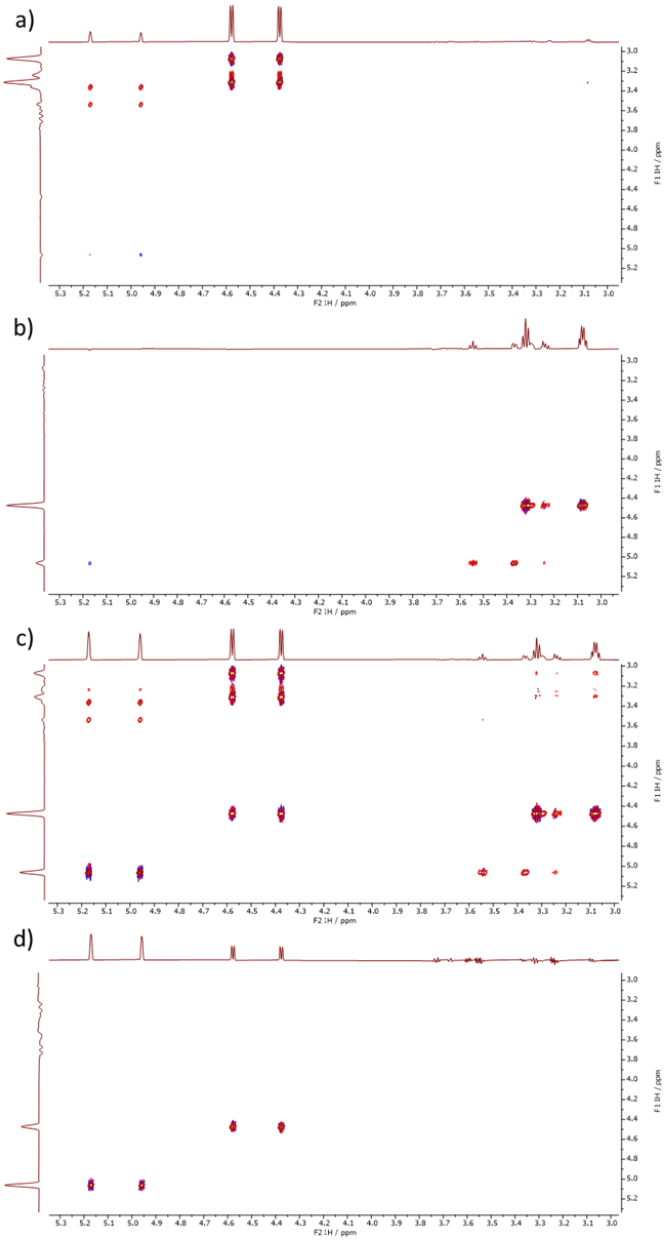

Figure 3.11: 2D DISPEL-TOCSY spectra of ^{13}C labelled glucose obtained from addition and subtraction of the spectra shown in Figure 3.10. a) 3−4 only showing cross peaks resulting from transfer from a ^{12}C attached proton to a ^{13}C attached proton, b) 2−4 only showing cross peaks resulting from transfer from a ^{13}C attached proton to a ^{12}C attached proton, c) 1−4 showing cross peaks resulting from any transfer involving

a ^{13}C attached proton and d) 1−2−3+4 showing exclusively transfer from ^{13}C attached protons to a second ^{13}C attached proton.

The spectra in Figure 3.11 show how the individual transfer pathways present in the TOCSY spectra manifest in the form of peaks. Spectra in Fig11a and b only contain cross peaks as the transfer is between protons attached to different isotopes of carbon. Therefore, diagonal peaks are not present as it would mean that a proton is bonded to both a ^{12}C and ^{13}C atom at the same time. It is also possible to determine which proton is attached to the ^{12}C and which to the ^{13}C as the magnetisation starts on the diagonal then transfers horizontally to a cross peak then vertically down back to the diagonal. Similarly, if transfer shown is ^{12}C to ^{13}C the peaks present will have the same F_1 ppm as the ^{12}C proton. In contrast the spectrum in Fig 11d only contains diagonal peaks as with the high enrichment of the position 1 carbon and the natural abundance ^{13}C on other peaks the only significant transfer from ^{13}C to ^{13}C attached protons occurs when the magnetisation starts and finishes on the same proton. In a case where the abundances were more mixed the cross peaks would indicate that both the start and end proton are bonded to ^{13}C and by choosing the right cross peaks it would enable identification of ^{13}C–^{13}C pairs in the backbone of a molecule. Finally, the spectrum in Fig 11c shows both diagonal peaks and cross peaks as it only eliminates signals arising from ^{12}C–^{12}C pairs so will show any transfer that involves a ^{13}C attached proton.

3.4.1 ^{13}C enrichment estimation

While the original intention of the DISPEL sequence was to remove natural abundance satellites from spectra in order to identify low intensity peaks[36], the isolation of specific transfer pathways demonstrated in section 3.3.1 opens up the potential for the technique to be used in determining levels of isotopic enrichment in non-natural ^{13}C abundance samples. A key research application where isotopically enriched samples are encountered is in the field of metabolite studies.[46–49] In order to understand the formation of metabolites within bacteria and other microorganisms, partially labelled ^{13}C sources such as a mixture of ^{12}C and ^{13}C glucose are fed to the organism and the resulting metabolites are studied. The enrichment of the metabolite allows the pathway by which it was formed to be determined as the pathways that utilised this source will show higher levels of incorporation.

Traditionally, NMR has not been particularly useful in this field, requiring isolated signals where the area of the satellite peaks and central peak can be fully integrated whereas the spectra are often very complex with many overlapping peaks. This difficulty is eased by the use of 2D techniques such as COSY and TOCSY which will help to isolate overlapping signals. In their basic forms, these experiments will still produce a large number of cross peaks due to $^{1}J_{CH}$ splittings in both dimensions. By using a combination of DISPEL-TOCSY and ^{13}C decoupling in F_1 and F_2 to collapse the satellites into the central peak it is possible to estimate the ratio of ^{12}C to ^{13}C in a particular position by integrating specific cross peaks in the spectrum. This works by comparing the area of peaks in spectra isolating specific transfer pathways to the area of the same peak in a 2D DISPEL-TOCSY spectrum where the DISPEL was not activated at all (Spectrum 1) as shown in Table 3.3.

Table 3.3: Each additional DISPEL-TOCSY spectra and basic TOCSY peak comparison and the resulting information that can be obtained. Receiving proton refers to the proton that the magnetisation is transferred to during the mixing time and the starting proton is the source of the initial magnetisation.

Experiment division	Transfer(s) measured	Estimate obtained
2/1	$^{12}C/^{13}C$--^{12}C	Cross peaks provide ^{12}CH % of receiving protons
3/1	^{12}C--$^{12}C/^{13}C$	Cross peaks provide ^{12}CH % of starting protons
4/1	^{12}C--^{12}C	Cross peaks provide % of pairs where both starting and receiving protons are ^{12}CH. Diagonal peaks provide ^{12}CH %
5/1	^{12}C--^{13}C	Cross peaks provide % of pairs where starting proton is ^{12}CH and receiving protons is ^{13}CH.
6/1	^{13}C--^{12}C	Cross peaks provide % of pairs where starting proton is ^{13}CH and receiving protons is ^{12}CH.
7/1	^{12}C--^{13}C, ^{13}C--$^{12}C/^{13}C$	Cross peaks provide % of pairs where starting or receiving protons aren't both ^{12}CH. Diagonal peaks provide ^{13}CH %
8/1	^{13}C--^{13}C	Cross peaks provide % of pairs where both starting and receiving protons are ^{13}CH. Diagonal peaks provide ^{13}CH %

In order to test this technique a model compound was required that would have isolated peaks in a 2D spectrum but would also allow estimates of enrichment from 1D spectra. Xylose was chosen due to its simple ring structure enabling full magnetisation transfer between protons, generating a large number of TOCSY cross peaks and the availability of different labelled samples.

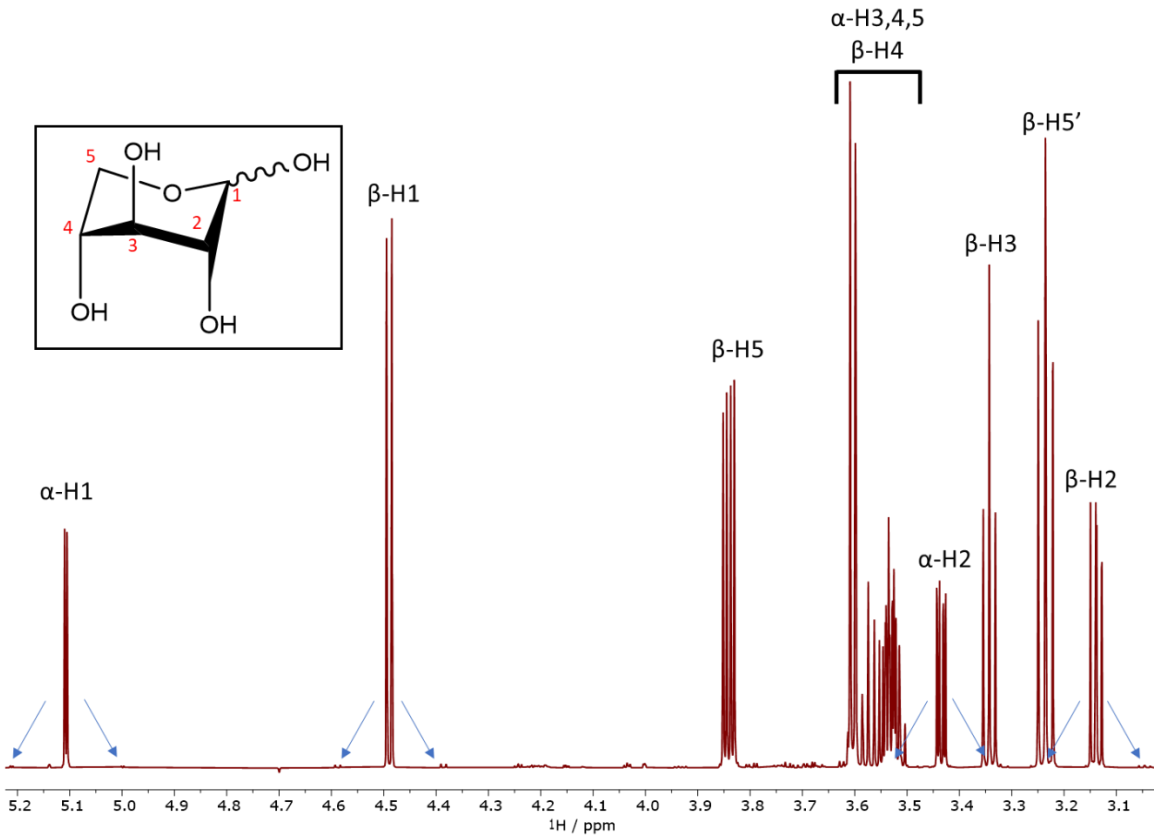

Figure 3.12: 800 MHz ^{1}H spectrum of xylose in D_2O recorded with water suppression. The inset shows the structure, and the separated peaks are labelled with blue arrows indicating the positions of the ^{13}C satellites relative to the signals from protons 1 and 2 in both the alpha and beta forms.

As Figure 3.12 shows, the spectrum of xylose has highly separated H1 signals for both anomeric forms and ^{12}C and ^{13}C isotopomers, but H2 signals are only separated for the ^{12}C isotopomer, while the ^{13}C isotopomer, these fall under other larger signals (with the exception of one of the H2β satellites). This enables the DISPEL-TOCSY method to be tested on both isolated signals, where normal 1D integration would suffice, but also

on overlapped signals where 1D integration would be ineffective. Another benefit which is demonstrated by the TOCSY spectrum below is that for the β-form all the peaks barring those involving transfer to H4 are distinct and free from overlap. This means that the ^{13}C decoupled peaks can be cleanly integrated for the enriched samples and multiple integrals compared to determine the accuracy of the enrichment estimate and if the distance the magnetisation travels impacts the final calculated value.

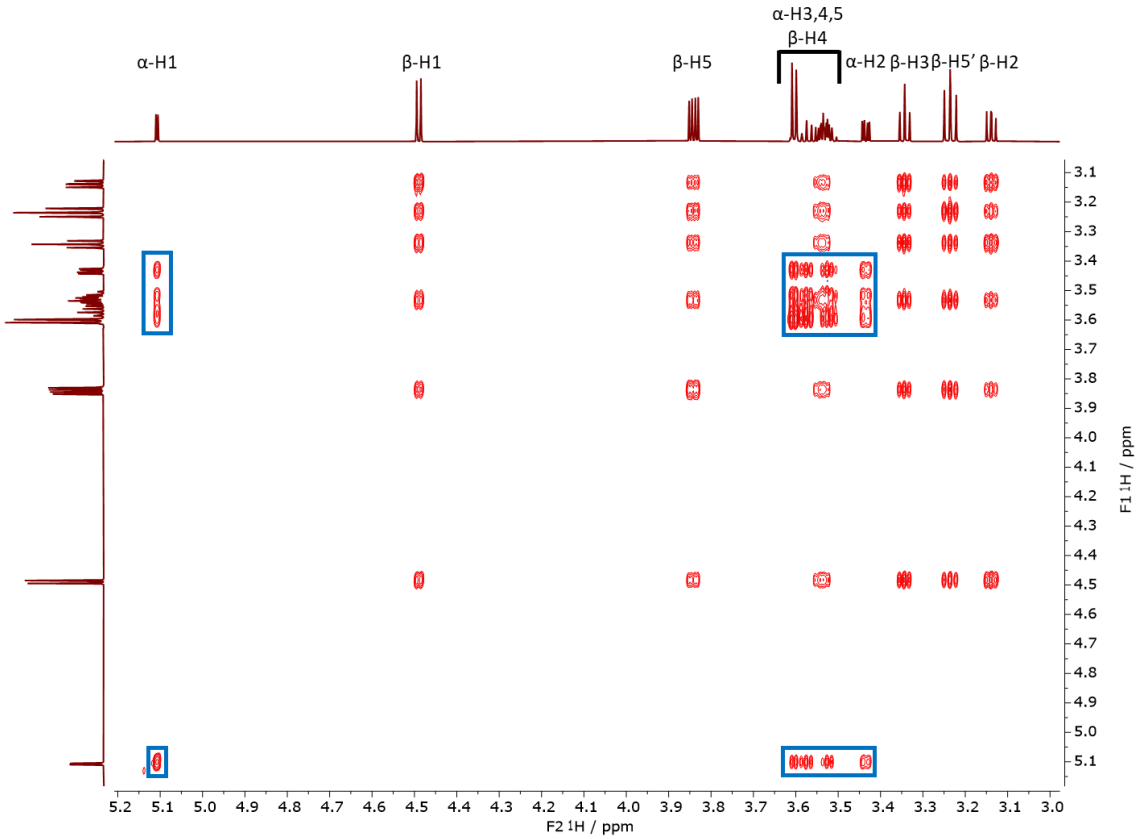

Figure 3.13: DISPEL-TOCSY spectrum of xylose acquired with both DISPEL blocks inactive and ^{13}C decoupling in F_1 and F_2. The mixing time was 120ms. The blue boxes indicate the peaks arising from the α-form which are heavily overlapped while the remaining peaks are from the β-form.

Four samples were prepared containing a mixture of unlabeled, 1-^{13}C, 99% and 1,2-^{13}C, 99% D-xylose in the relative proportions shown in Table 3.4. The full details of the sample preparation are given in the experimental section of this chapter.

Table 3.4: Xylose samples with levels of enrichment of each carbon atom and the total enrichment of the mixture adjusted to reflect the 1.1% natural abundance of ^{13}C.

Sample number	% unlabelled xylose	% 1-^{13}C xylose	%1,2-^{13}C xylose	1-^{13}C % enrichment	2-^{13}C % enrichment
1	65.5	34.5	0	35.2	1.1
2	51.6	0	48.4	48.9	48.9
3	51.1	33.0	15.9	49.5	16.8
4	33.8	33.8	32.4	66.6	33.1

The ^{1}H spectra of each sample are shown in Figure 3.14, showing the increase in size of the ^{13}C satellites due to the varying levels of enrichment.

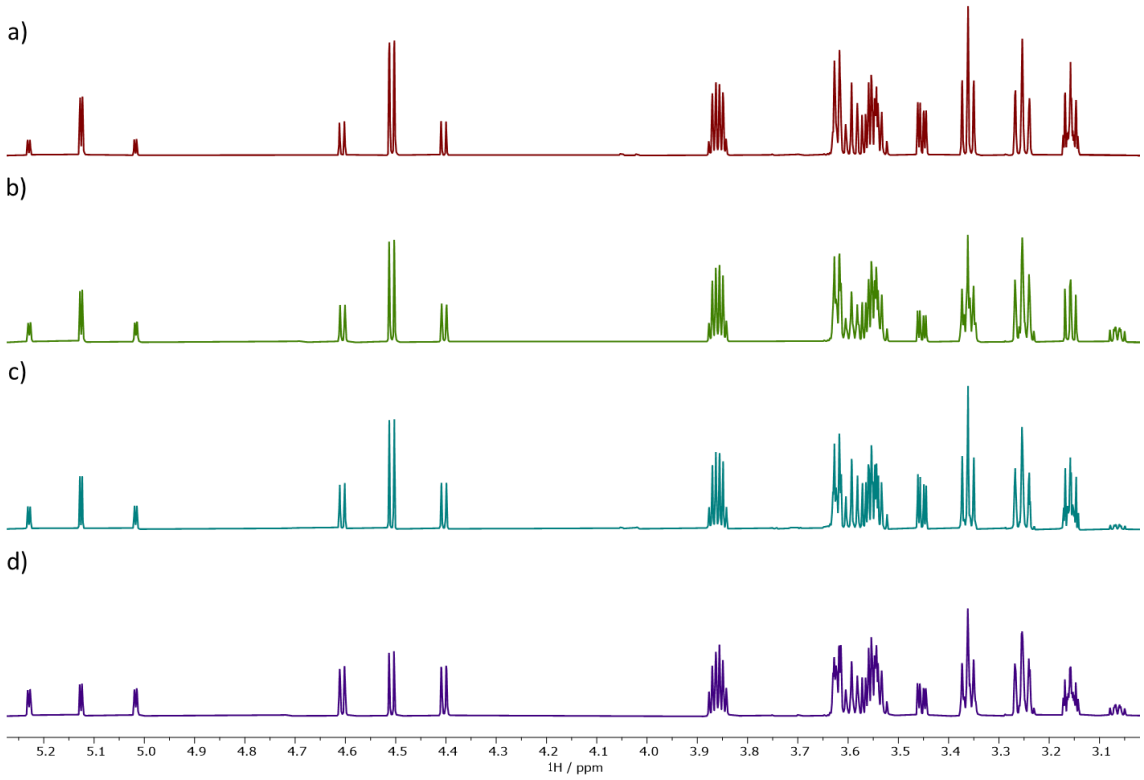

Figure 3.14 ^{1}H spectra of samples 1-4 acquired with water suppression. a) sample 1 with 34.5% 1-^{13}C enrichment, b) sample 2 with 48.4% 1,2-^{13}C enrichment, c) sample 3 with 48.9% 1-^{13}C enrichment and 15.9% 2-^{13}C enrichment and d) sample 4 with 66.2% 1-^{13}C enrichment and 32.4% 2-^{13}C enrichment. The intensities have been normalised relative to the β-H5 peak at 3.87 ppm.

In order to confirm the compositions of the samples, the 1D interleaved DISPEL spectra were collected for each sample and edited spectra obtained. This isolated the ^{13}C satellite peaks and enabled standard 1D integration to be used. The absolute integrals of both satellites for each signal of the protons 1-^{13}C and 2-^{13}C across both forms were compared to give an estimate of the amount of ^{13}C present at each position. Interleaved DISPEL-TOCSY spectra were than acquired for these samples and only the beta form was analysed due to the lack of peak overlap. Integral areas were defined encompassing individual peaks seen in Figure 3.13. The absolute integrals were then extracted and compared for 8 combination spectra as defined in Table 3.3. This produced a separate estimate for the ^{13}C enrichment of each carbon site for every cross peak in the spectrum. As every isolated cross peak can be used a longer mixing time is recommended to allow full transfer of magnetisation to distant peaks. For estimation of the enrichment of the nuclei in positions 1 and 2, ten values were averaged, five cross peaks from the F_1 dimension and five from the F_2 dimension. The integrals were obtained from the F_1 cross peaks in the 2/1 calculation and each F_2 cross peak in the 3/1 calculation. These represented the magnetisation being transferred to and from ^{12}C attached protons respectively. Figure 3.15 shows the chosen peaks for estimating position 1.

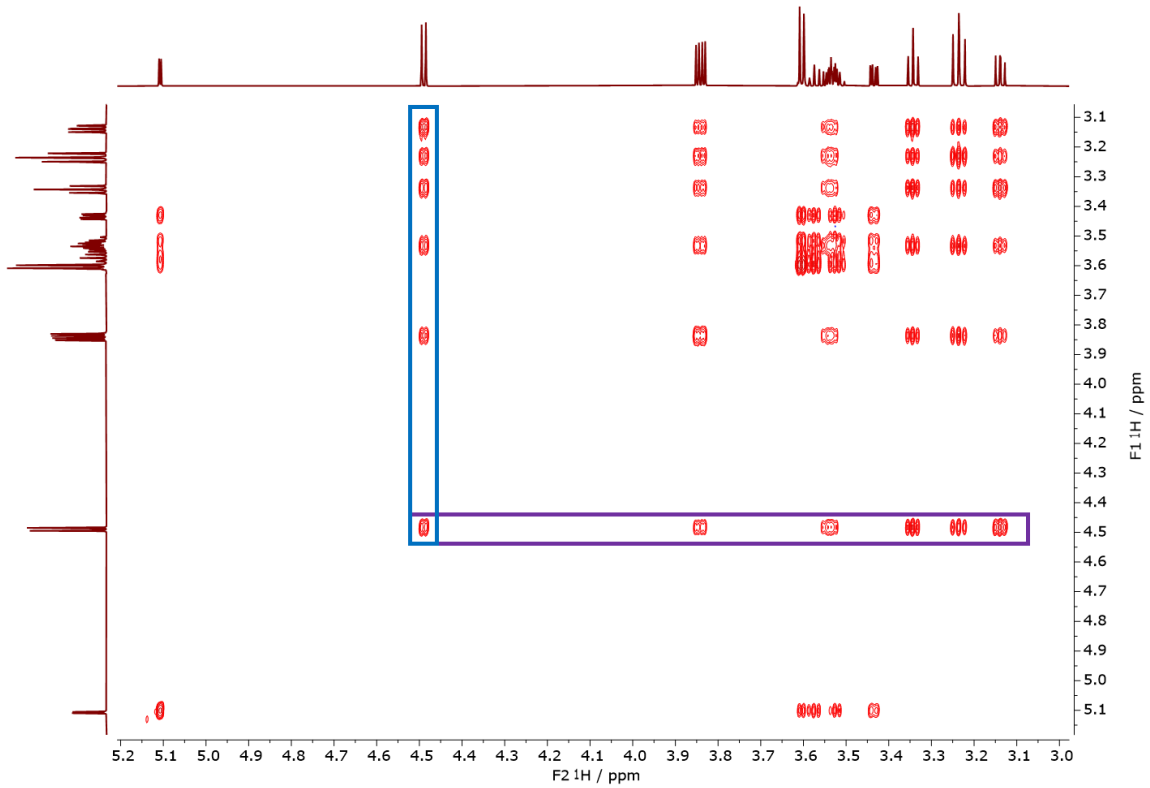

Figure 3.15: The cross peaks used to estimate the ^{13}C enrichment of carbon 1 in the beta form of xylose. The blue box indicates the areas measured for the combination of 2/1 and the purple box indicates the peaks used for 3/1.

Once the estimate from each individual cross peak was calculated the ten values were all averaged to give a single estimate from the overall DISPEL-TOCSY experiment for each site. These values are presented in Figure 3.16 with the numerical results presented in Table 3.5.

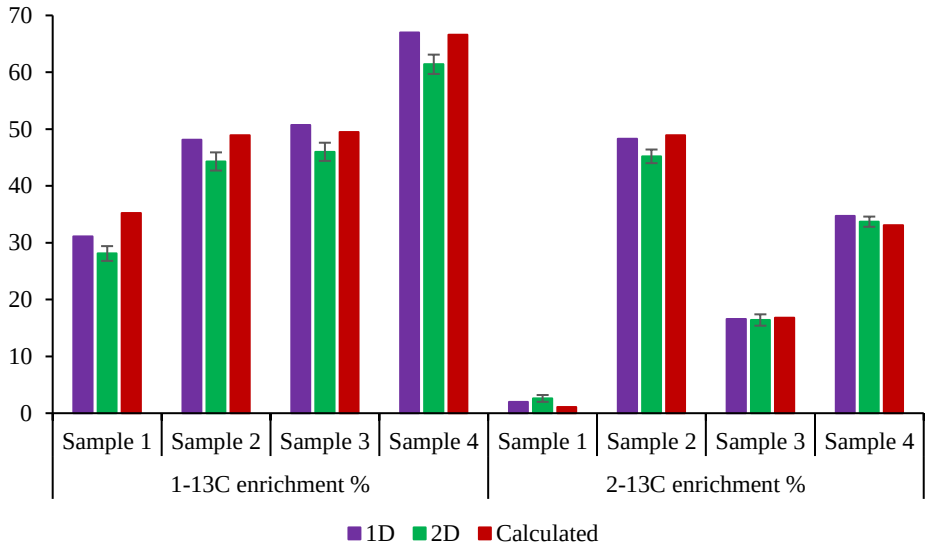

Figure 3.16: A comparison of the experimentally determined enrichment levels of 1-^{13}C and 2-^{13}C in samples 1-4, and the calculated enrichment determined from the concentration of the sample. All TOCSY spectra were acquired with a DIPSI2 mixing time of 100 ms and 4 scans while the 1D spectra used 16 scans. The error bars indicate the standard deviation calculated from the averaging of the 10 cross peak integral areas.

Table 3.5: Tabulated data used to produce Figure 3.15 along with standard deviation for each averaged DISPEL-TOCSY value.

Sample	1-^{13}C enrichment %			2-^{13}C enrichment %		
	1D	2D	Sample prepared	1D	2D	Sample prepared
1	31.1	28.4 ± 0.9	35.2	2.0	2.6 ± 0.5	1.1
2	48.1	44.7 ± 0.8	48.9	48.3	45.2 ± 1.1	48.9
3	50.7	46.6 ± 0.6	49.5	16.6	16.6 ± 1.2	16.8
4	67.0	62.0 ± 0.6	66.6	34.7	34.1 ± 0.8	33.1

It can be seen that the estimates obtained from the 2D spectrum are consistently lower than the true values and the 1D estimates while the standard deviations are smaller than the difference. This shows that the method is precise and has low variation, however there is a systematic error that prevents it from being truly accurate. Repeated tests with different mixing times and relaxation delays did not remove this discrepancy and

therefore incomplete magnetisation transfer and effects arising from different relaxation times of ^{12}C and ^{13}C attached protons can be disregarded as the cause. This is an area for future work in order to determine why the magnetisation arising from ^{12}C attached protons appears more prominently than that of ^{13}C attached protons and to see if the loss can be countered or a correction introduced.

Nevertheless, average % enrichment estimate obtained by integrating cross peaks in a 2D DISPEL-TOCSY spectra are close to the true enrichment values of the samples. This is a significant achievement that increases the potential of NMR to be used as a non-destructive way of estimating ^{13}C enrichment in samples.

An additional piece of information that can be obtained from the series of spectra produced by the DISPEL-TOCSY sequence is the ability to determine the concentration of directly bonded ^{13}C-^{13}C pairs within the backbone of a molecule. This is particularly significant for experiments such as INADEQUATE[21,33] that rely on ^{13}C-^{13}C pairs in a carbon backbone to trace out the structure of the full molecule. DISPEL-TOCSY can help determine the concentration of these pairs by using the same method as for single site enrichment but only examining cross peaks. Since spectrum 8 only contains cross peaks arising from transfer between ^{13}C attached protons the cross peak of two neighbouring protons will only contain signal from molecules that contain two neighbouring ^{13}C nuclei. This is demonstrated by looking at sample 3 which contains both 1-^{13}C and 1,2-^{13}C labelled xylose as well as unlabeled. The ^{13}C-^{13}C transfer spectrum of sample 3 is presented in Figure 3.17.

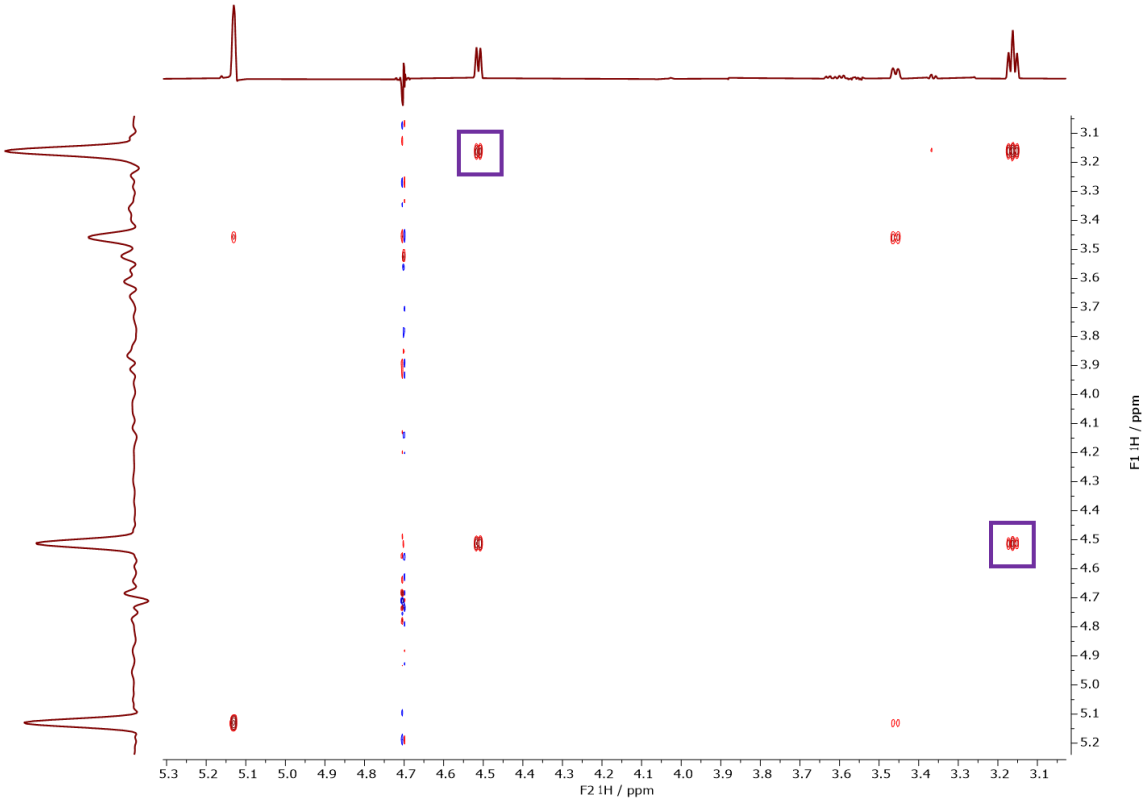

Figure 3.17: Spectrum 8 of sample 3 showing only peaks that arise from transfer between two ^{13}C bonded protons. The purple boxes indicate the 1-2 cross peaks for the β-D-xylose.

When the two boxed peaks were integrated and compared to the standard TOCSY spectrum they returned values of 16.3 % and 14.7 % for transfer from 2-1 and 1-2 respectively. These are very close to the true value of 15.9 % which is based on the % of the sample which is 1,2-^{13}C xylose. This shows that the cross peaks can be used to accurately determine the % of ^{13}C-^{13}C pairs in a site-specific manner. Using the same logic, but different spectra, it would be possible to calculate the % of ^{12}C-^{13}C (spectrum 5), ^{13}C-^{12}C (spectrum 6) or ^{12}C-^{12}C pairs (spectrum 4). Unfortunately, this technique can only be applied to identify directly bonded pairs. As the magnetisation transfer pathway is unaffected by DISPEL with only the final signals being removed, it is impossible to gather information about the intermediary carbon atoms between the two CH groups that contribute to a cross peak.

3.4.2 Application to metabolite samples

Having demonstrated the efficacy of the DISPEL-TOCSY sequence at analysing the ^{13}C enrichment, the next step was to apply the sequence to a real system. The system studied is the fermentation of Glucose by *Saccharomyces cerevisiae*[50], commonly referred to as Baker's yeast. This process consumes glucose and produces ethanol and carbon dioxide, although other metabolites can also be formed, particularly glycerol.[51]

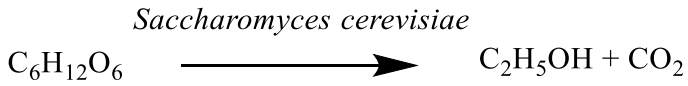

Figure 3.18: Conversion of glucose to ethanol in Bakers yeast.

A sample of Bakers yeast was produced by Dr Will Kew at the Pacific Northwest National Laboratory and the DISPEL-TOCSY spectra were run by him. Experimental details are given in the Experimental section of this chapter. The spectrum of the sample is shown below and clearly contains a large amount of glycerol. This is likely due to the yeast cells accumulating glycerol in response to osmotic pressure.[51] Another compound which was identified is L-(-)-malic acid that is present in much lower concentrations which is to be expected. This is due to L-(-)-malic acid being produced from both glucose and glycerol as shown in Figure 3.19.[52–54]

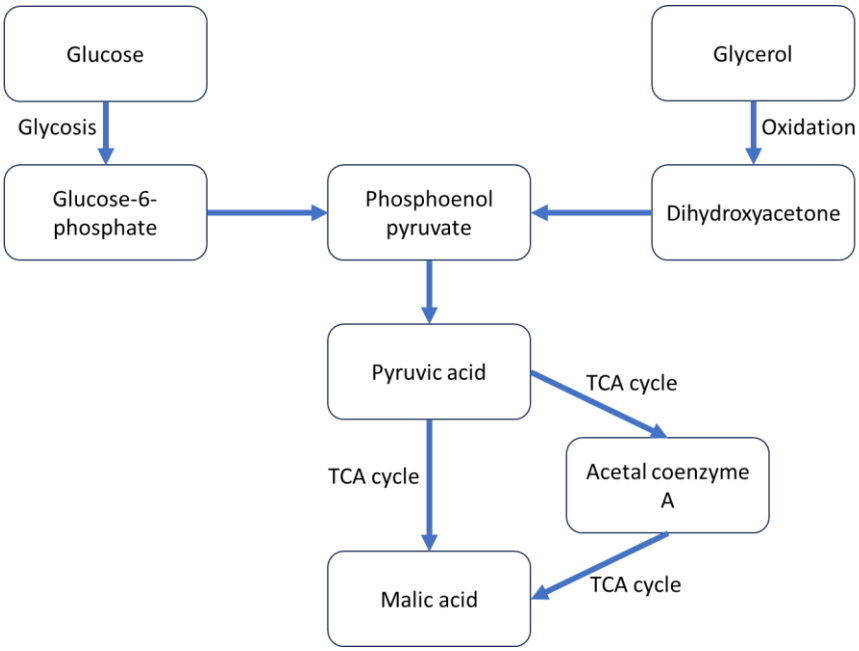

Figure 3.19: Formation of malic acid from glycosis of glucose and oxidation of glycerol via phosphoenol pyruvate.[53,54]

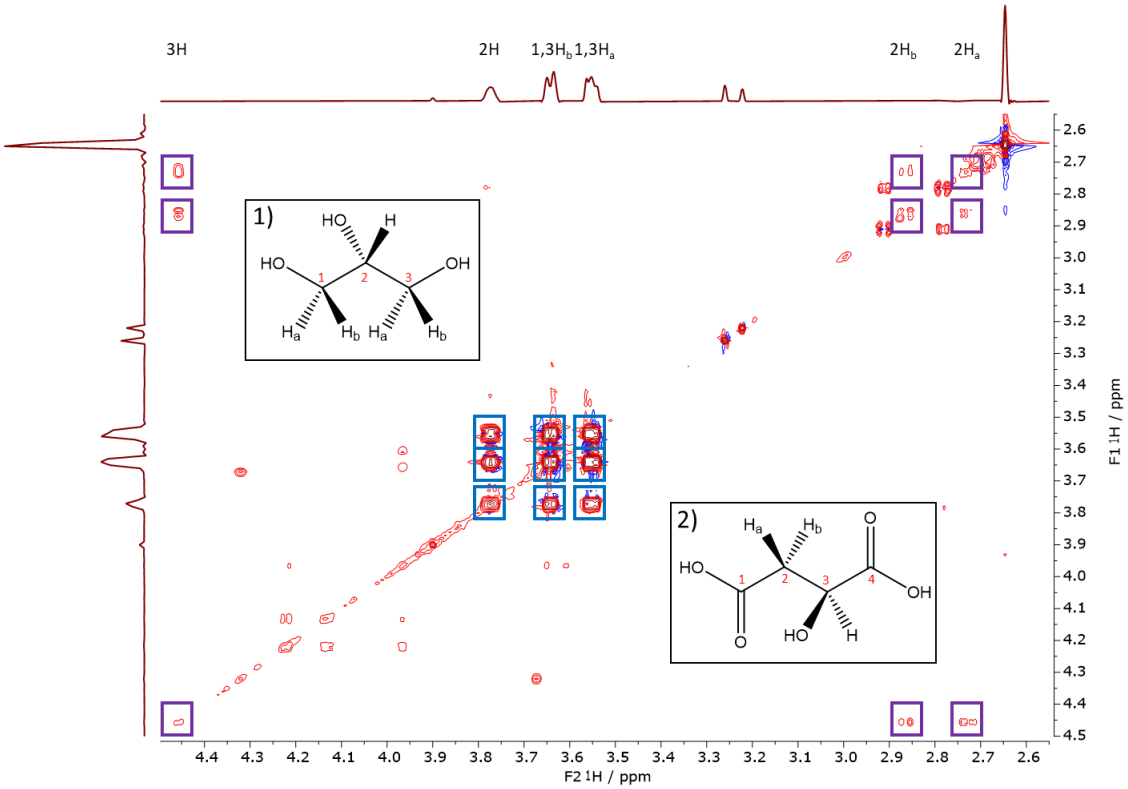

Figure 3.20: TOCSY spectrum of the bakers yeast sample recorded with a 60 ms mixing time. 1) shows the structure of glycerol, the peaks of which are marked by blue boxes and 2) is the structure of L-(-)-malic acid, the peaks of which are marked by purple boxes

The peaks of glycerol and malic acid were assigned by project student George Padfield using literature values which are tabulated below. The small discrepancy between the literature values and observed values is attributed to the different pH of the sample affecting the equilibrium of the protonated and unprotonated species, which moves the ^{1}H chemical shift. A lower pH will move the equilibrium closer to the protonated state, and the lack of a charge will result in a smaller difference between the chemical shifts of the two H2 signals. This is due to the shielding effect of the negative charge of the carboxylate groups. At a pH of 2.65 most malic acid molecules are neutral so the shielding difference between $H2_a$ and $H2_b$ is smaller. This will shift the $H2_a$ signal downfield towards $H2_b$ but to a smaller extent than reported in the literature.[55]

Table 3.6: Peak assignments for glycerol and L-(-)-malic acid in the bakers yeast sample. The literature value for malic acid was obtained at a pH of 6.5 whereas the sample pH was measured to be 3.7.

Compound	Glycerol			L-(-)-malic acid		
Signal	2H	$1H_b$, $3H_b$	$1H_a$, $3H_a$	$2H_a$	$2H_b$	3H
δ ^{1}H/ppm Exp.	3.77	3.64	3.55	2.72	2.86	4.45
δ ^{1}H/ppm, Lit.[55,56]	3.77	3.59	3.59	2.4	2.7	4.3

The same analysis as for the labelled xylose sample was carried out on these two compounds and the results are presented below. For glycerol the symmetry of the molecule ensures that protons a and b on carbon atoms 1 and 3 are chemically equivalent so instead of producing an estimate for the enrichment of carbon 1 and 3 separately two average enrichments are obtained. This is a limitation of the technique. However, it is rare that symmetrical molecules of this nature are encountered so it will not hinder application of this technique to wider research.

Table 3.7: Estimated ^{13}C enrichment levels with standard deviation, of carbon atoms in glycerol and malic acid from the bakers yeast sample. The mixing time for the DISPEL-TOCSY experiment was 60 ms.

Compound	Peak	^{13}C % enrichment
Glycerol	2H	14.7 ± 2.9
	$1H_b$, $3H_b$	30.1 ± 2.3
	$1H_a$, $3H_a$	31.8 ± 3.3
L-(-)-malic acid[57]	$2H_a$	29.6 ± 5.7
	$2H_b$	31.2 ± 4.4
	3H	35.0 ± 3.2

The results in Table 3.7 show that both compounds have raised levels of ^{13}C enrichment compared to natural abundance, which correlates with the microorganisms being fed labelled glucose and both compounds being present in the metabolic pathway of glucose. This however doesn't explain the difference in enrichment between C2 and

C1, C3. Following the metabolic pathway all the carbon atoms come from the starting glucose sample so if the initial glucose is uniformly enriched uniform enrichment of the glycerol would be expected. It is also interesting that the values for malic acid are close to those for C1, C3 of the glycerol molecule. This would make sense with the pathway as malic acid appears further down the pathway and is a possible product if glycerol is not formed.[58] The discussion of how these enrichment values occur is beyond the scope of this thesis, but these results show that DISPEL-TOCSY can also be applied to real samples to determine enrichment levels in a site-specific non-destructive manner.

3.5 *J*-RES-DISPEL

The second 2D experiment that DISPEL was incorporated into was a *J*-RES[26] experiment which is used to determine the scalar coupling of multiplets. The initial sequence (Figure 3.21) was a homonuclear 2D *J*-resolved experiment with pre-saturation during relaxation delay using PFGs that is included in the standard Bruker library under the name of jresgpprqf.

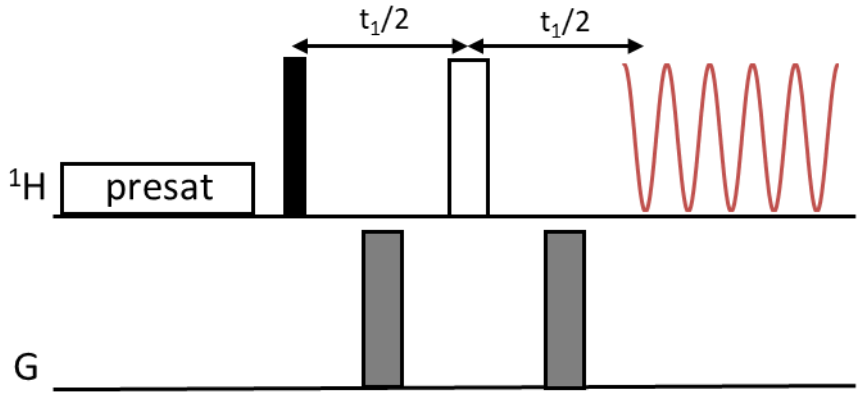

Figure 3.21: Pulse sequence of the jresgpprqf experiment used as a basis for the J-RES-DISPEL sequence. The black and white rectangles are 90° and 180° pulses respectively while the grey rectangles are gradient pulses.

As when DISPEL was added to the TOCSY sequence, the whole original DISPEL sequence replaces the initial 90° pulse leaving the rest of the sequence unaffected. The resulting sequence is shown below in Figure 3.22.

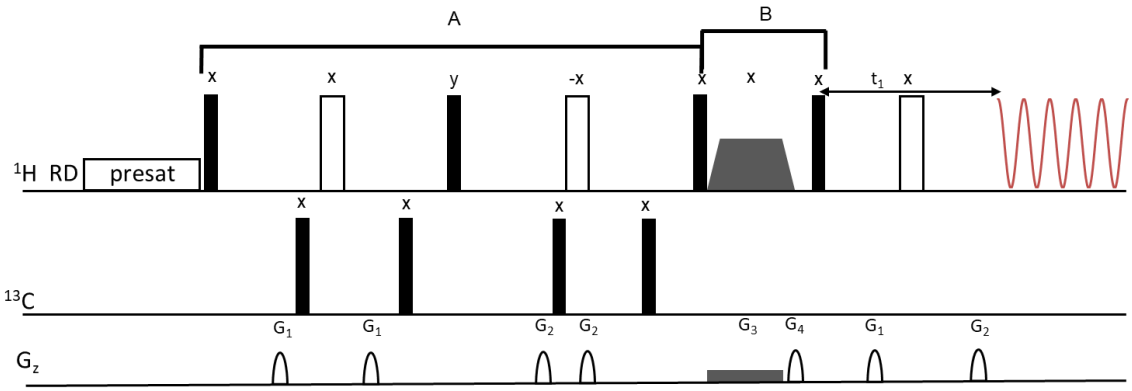

Figure 3.22: Pulse sequence of the J-RES DISPEL experiment showing the presence of DISPEL instead of the 90° pulse present in the original J-RES experiment. The black rectangles are 90° pulses, the white rectangles are 180° pulses, the grey trapezium is a 180° smoothed chirp pulses, the white shapes are gradient pulses, and the white rectangle is the presat mixing time. Section A is the DISPEL building block and B is the z-filter.

As with the TOCSY-DISPEL experiment, the *J*-RES-DISPEL experiment was interleaved although there are only two spectra produced as DISPEL is either activated or not before the t_1 period. This sequence was also tested on a ^{13}C labelled glucose sample, and the resulting spectra are shown in Figure 3.23.

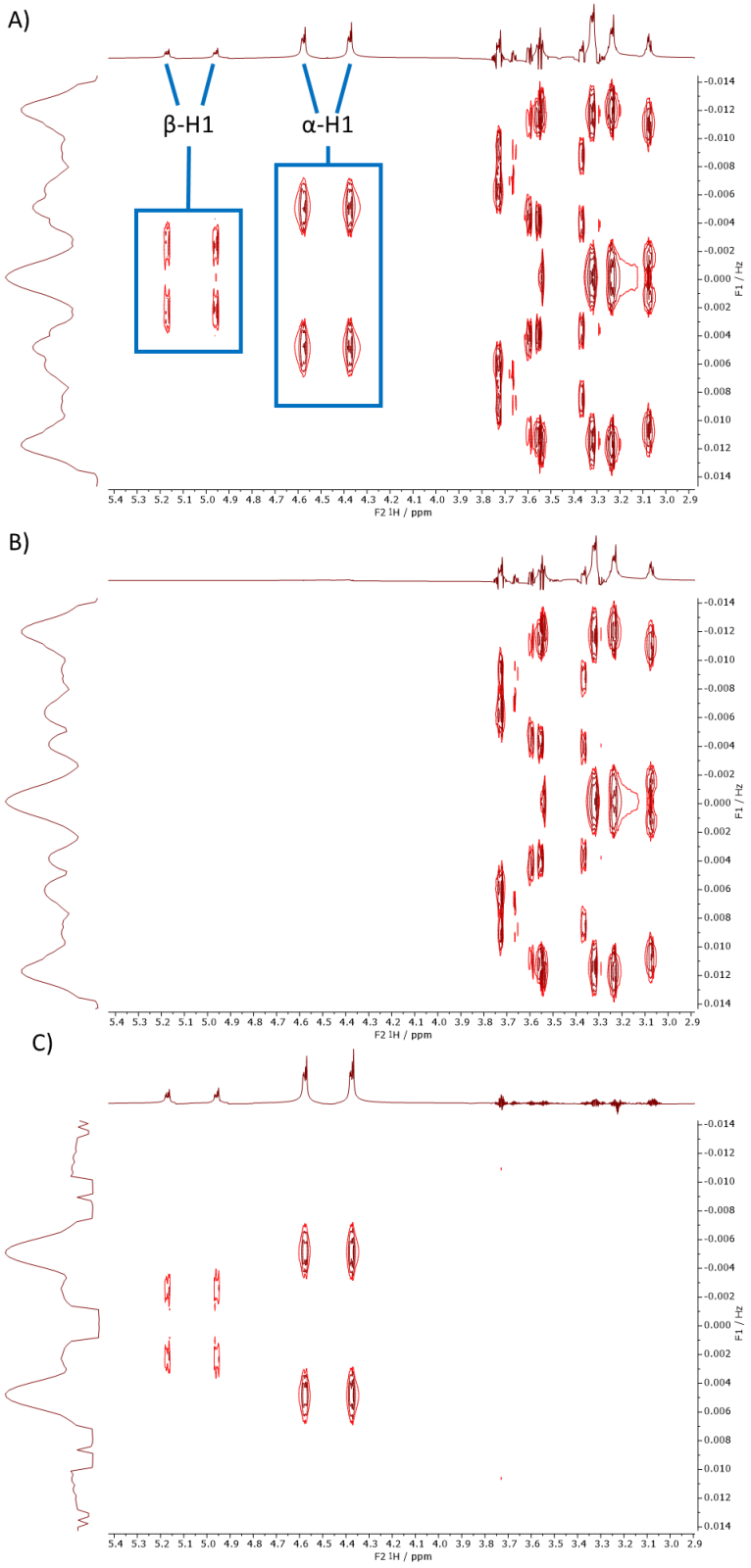

Figure 3.23: J-RES spectra of a ^{13}C-1 labelled glucose. a) without DISPEL, b) with DISPEL active and c) With only the ^{13}C peaks present which is obtained by subtracting spectrum b from spectrum a.

In this sample the labelled sites carry protons that resonate outside of the area of ^{12}C-bonded protons, hence information content of regular *J*-resolved spectra is not enhanced by DISPEL editing. Nevertheless, this is not the case generally and JRES-DISPEL spectra of labelled samples and overlapping ^{1}H resonances will benefit from this approach. It should be mentioned that separation of cross peaks of protons directly attached to ^{13}C atoms can be achieved by applying a 180° ^{13}C pulse simultaneously with the ^{1}H 180° pulse in the middle of the t_1 period, provided that the spectral width is increased[59]. This will however complicate structures of cross peaks of protons long-range coupled protons on ^{12}C.

3.6 Experimental details

The 1-^{13}C glucose sample (20 mg in 600 µl of D_2O) spectra were all acquired on a Bruker 600 AVANCE III MHz spectrometer equipped with a TCI cryoprobe. The interleaved DISPEL, DISPEL-TOCSY and J-RES DISPEL spectra were acquired with the following common parameters: 1 s relaxation time (D1), 4 dummy scans and 16 real scans. The 1D interleaved DISPEL sequence was acquired with 6009.6 Hz spectral width (SW), 2.56 s acquisition time (AQ) and 30720 time domain points (TD). All DISPEL specific parameters were used as in the original paper[1]. For the DISPEL-TOCSY experiment the parameters were SW = 2102 Hz in F_1 and 3004 Hz in F_2, AQ = 0.170 s and TD = 128 in F_1 and 2048 in F_2. For the *J*-RES -DISPEL spectrum SW = 30 Hz in F_1, 3000 Hz in F_2, AQ = 0.5 s and TD = 90 in F_1 and 2998 in F_2.

The xylose samples were prepared from solutions of two unlabeled xylose a) (M_w = 150.13 g mol^{-1}, 9.8 mg in 600 µl of D_2O) and b) (M_w = 150.13 g mol^{-1}, 10.4 mg in 600 µl of D_2O), 1-^{13}C xylose (M_w = 151.12 g mol^{-1}, 10.4 mg in 600 µl of D_2O) and 1,2-^{13}C xylose (M_w = 152.12 g mol^{-1}, 9.9 mg in 600 µl of D_2O). These were then mixed in the ratios 400 µl of unlabelled solution a and 200 µl of the 1-^{13}C xylose to produce sample 1, 300 µl of unlabelled solution b and 300 µl of 1,2-^{13}C xylose to produce sample 2, 300 µl of unlabelled solution b, 200 µl of 1-^{13}C xylose and 100 µl of 1,2-^{13}C xylose to produce sample 3 and 200 µl of unlabelled solution a, 200 µl of 1-^{13}C xylose and 200 µl of 1,2-^{13}C xylose to produce sample 4. This produced 4 samples with the relative concentrations shown in Table 2.4.

The spectra were acquired in TopSpin 4.1 on an 800 MHz BRUKER NEO NMR spectrometer equipped with a TCl cryoprobe. The common parameters were DS = 4 scans, NS = 16 scans and D1 = 20 s. The interleaved DISPEL spectra were acquired with AQ = 1.97 s, SW = 16667 Hz (20.848 ppm) and TD = 65536. For the DISPEL-TOCSY experiments AQ = 0.250 s, SW = 8196 Hz (10.25 ppm) in F_2 and 1860 Hz (2.3266 ppm) in F_1 and TD = 4096 in F_2 and 76 in F_1 and the mixing time was 100 ms.

The NMR spectra of the yeast was acquired at the Pacific North-West Laboratory by Dr Will Kew on a Bruker NEO spectrometer equipped with a TCI Cryogenically cooled probe and 800 MHz shielded magnet. A yeast solution/ suspension was made by mixing around 1 gram of dried instant yeast (bakers yeast from a local grocery store) with 10 mL of miliQ (18MOhm) H_2O with vortex mixing. The mix was left for 5 minutes. 200 µL of the solution was mixed with C1 labelled glucose (100 mg) and 10 mL of miliQ water. This was vortex mixed for 20 seconds and then left to rest at room temperature for 4 days in the dark. The samples were centrifuged at 4°C, 4000 RPM for 10 minutes. An aliquot of the supernatant was removed for NMR analysis. The remaining supernatant was dried using a rotary evaporator. The dried sample was re-suspended in 180 µL of D_2O and a further 20 µL of D_2O containing 0.01% NaN_3 and 4.48 mM DSS-d_6 was added. The DISPEL-TOCSY sequence was run with D1 = 1.5 s, DS = 128, NS = 8, AQ = 0.187 s, SW = 8196 Hz (10.242 ppm) in both F_1 and F_2, TD = 3072 in F_2 and 1024 in F_1 and a 60 ms mixing time.

4 Benchtop SHARPER

4.1 Declaration

This chapter contains work published in the following paper:

Dickson, Claire L., Peat George, Rossetto Matheus, Halse Meghan E. and Uhrín Dušan. SHARPER-enhanced benchtop NMR: improving SNR by removing couplings and approaching natural linewidths. *Chemical Communications*, 2022, **36**, 5534.

https://doi.org/10.1039/D2CC01325H

Claire performed the majority of the data analysis and experiment design while I contributed to experiment design, prepared the samples, implemented the new sequences on the spectrometer and performed all data acquisition. Matheus contributed the code to produce a shaped gaussian pulse.

4.2 Introduction to SHARPER

The second project to be covered in this thesis involves further development of a pure shift experiment called SHARPER (Sensitive, Homogeneous, And Resolved PEaks in Real time), first developed in 2017 by researchers at the University of Edinburgh[2].

In contrast to DISPEL and most conventional NMR experiments that provide a spectrum of a sample in order to determine a molecular structure or a composition of a mixture, SHARPER is a pure shift technique that produces an extremely narrow singlet of a selected resonance. It does this by selecting a single signal that is present in a spectrum and collapsing it from a low intensity multiplet to a high intensity sharp peak. This singlet can be used to measure molecular parameters such as scalar or dipolar couplings, diffusion coefficient or to track the progress of a reaction and study reaction kinetics.

4.2.1 Pure shift reaction monitoring

Pure shift NMR, also known as broadband homonuclear decoupling, is a widely used 1D or 2D NMR technique that has been developed in order to simplify spectra by collapsing overlapping multiplets into more intense singlets.[60] This is useful for spectra that contain many overlapping proton spectra such as natural products. To the contrary, SHARPER is a 1D NMR method that focuses on one signal. It is a real-time pure shift

method[61] that can acquire signal in one scan. Signal acquisition in real-time pure shifts methods consists of a series of FID data chunks, that are put together by the software and generally do not require additional advanced data processing. Data chunks are periodically interrupted by radio frequency pulses that refocus the evolution of scalar couplings. The acquisition is halted during these interruptions and resumes after the evolution of the signal due to couplings has been reversed. In standard real-time pure-shift methods such as HOBS (HOmodecoupled Band-Selective)[62] this refocusing takes the form of two 180° inversion pulses, where both inversions are felt by the active, detected nuclei, while the passive coupled spins only feel one inversion. As a result, chemical shift is left to evolve as normal, but intergroup couplings are removed. Although this approach removes the splitting and enhances the signal, it does not compensate for the magnetic field inhomogeneity. More complex pure shift methodologies have been introduced that do not require signal separation such as the Zangger-Stark based method introduced by Aguilar et al which utilises PFGs during selective pulses to remove couplings[63]. The advantage of Zangger –Stark method is that that it produces complete spectra with no multiplet structures at the cost of reduced sensitivity compared to a reference spectrum. Another method that provides a complete spectrum but degrades sensitivity even further is based on the detection of ^{13}C-attached protons. It uses BIRD[64] pulses to selectively invert these protons. In contrast SHARPER only focuses on a single signal in a spectrum and provides a sharp peak with a much greater SNR than would be expected from the removal of the *J* splittings. It achieves this by a selective inversion of the active spin, while not inverting the passive spins.

4.2.2 Non-selective or 'hard' SHARPER

While this focus on a single signal may at first seem to be a disadvantage when other pure-shift methods exist that remove the coupling from all signals[2], inversion of the active spin avoids the need to pulse on X-channels, e.g., in case of ^{1}H-^{19}F coupling constants. This circumvents a hardware limitation present in many conventional spectrometers that prevents the use of broadband decoupling which is a common issue when studying fluorinated compounds. As most spectrometers are incapable of pulsing on both ^{19}F and ^{1}H during the same experiment, recording of ^{1}H decoupled ^{19}F spectra is very rare.

To select the signal of interest, the RF carrier is matched to the chemical shift of the monitored nucleus. This removes any chemical shift modulation and allows the acquisition of signal within continuous spin-echoes, eliminating line broadening due to magnetic field inhomogeneity producing a sharper, more intense peak. The combination of heteronuclear decoupling without X-channel pulses and removal of chemical shift modulation results in the ability of the original SHARPER sequences to produce a sharp peak, free of heteronuclear couplings. The pulse sequence for this experiment is shown in Figure 4.1.

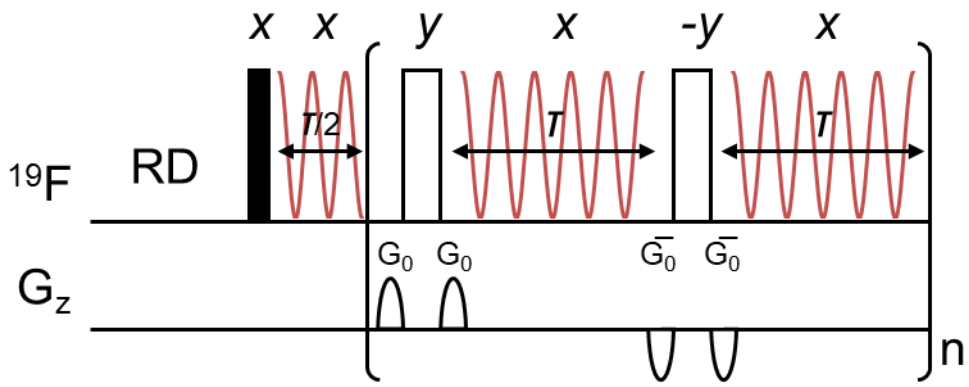

Figure 4.1: Pulse sequence of the original SHARPER experiment[2]. The narrow and wide black rectangles are 90° and 180° pulses, respectively and the rounded blocks are sine-shaped pulsed field gradients. RD stands for relaxation delay and $\tau = AQ/(2n)$, where AQ is the total acquisition time and n is the total number of loops.

In Figure 4.1 it can be seen that refocusing is achieved by the periodic application of non-selective 180° pulses flanked by pulsed field gradients with the time of each acquisition chunk depending on the number of repeats, n, of the two-chunk block. The pulsed field gradients have different polarities to minimise the impact on the static magnetic field and protect the lock circuitry. The phase sequence of x y -y was chosen to maintain a 90° difference between the initial 90° pulse and the repeating 180° pulses. This means that the sequence has the same form as the widely used CPMG (Carr-Purcell-Meiboom-Gill) experiment[7] which minimises the impact of pulse imperfections and magnetic field inhomogeneity on the spectrum. This basic SHARPER pulse sequence is designed for singly fluorinated compounds that do not exhibit fluorine-fluorine couplings, e.g.fluorobenzene.

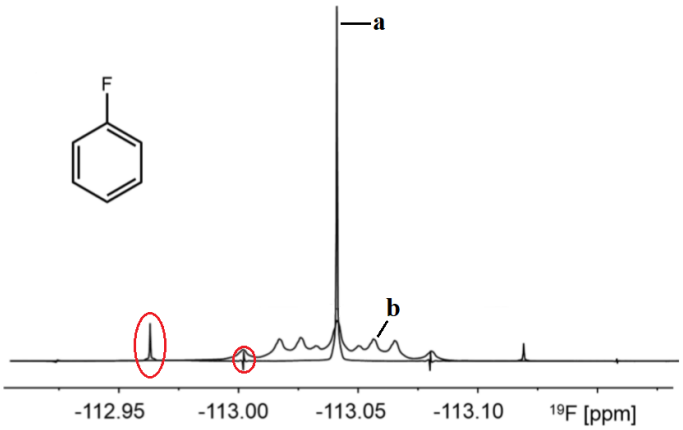

Figure 4.2: Overlaid spectra of fluorobenzene. a) is a ^{19}F SHARPER spectrum which has a $\Delta_{1/2}$ value of 0.14 Hz and b) is the ^{1}H-coupled ^{19}F spectrum. The red circles indicate chunking artefacts present in the SHARPER spectrum with the larger circle showing the first sideband which is present at 1000/34 = 29.41 Hz. Adapted from reference 2.

As shown in Figure 4.2 the original ^{19}F spectra of fluorobenzene contains a triplet of triplets which arises from coupling between the fluorine nucleus and the chemically equivalent pairs of ortho and meta protons. The coupling constant with the para proton is close to zero. The SHARPER spectrum contains a single narrow and sharp peak at the frequency of the ^{19}F resonance along with small chunking artefacts that appear as sidebands that decay further away from the main peak. These artefacts are caused by discontinuities between acquisition chunks and can be reduced in size by including an initial half chunk at the start of the sequence[2]. As their distance from the main peak is inversely proportioned to the length of the chunks, they can be moved away by employing short chunk times. Generally, their length should be $\leq 0.25/J$ and shorter chunk times need to be used for large coupling constants. This, however, leads to more frequent application of the refocusing pulses, which shortens the effective relaxation time of the nucleus and broadens signals. When the sideband intensity is high, these should be considered in quantitative analysis and their integral intensities should be included in the overall integrals.

^{19}F SHARPER spectra have flat baselines and do not contain signals that arise from fluorinated material present in NMR probes. This greatly increases the applicability of

this technique to the study of reaction kinetics as reliable signal integration can be carried out without accounting for background artefacts.

4.2.3 *Sel*-SHARPER

A second more robust version of SHARPER exists called selective (*sel*-) SHARPER. This is very similar to the original SHARPER sequence but has the key distinction of performing homonuclear as well as heteronuclear decoupling. This is achieved by the replacement of the initial 90° excitation pulse with a single pulsed-field gradient spin echo[65] and the replacement of the nonselective 180° inversion pulses with selective inversion pulses.

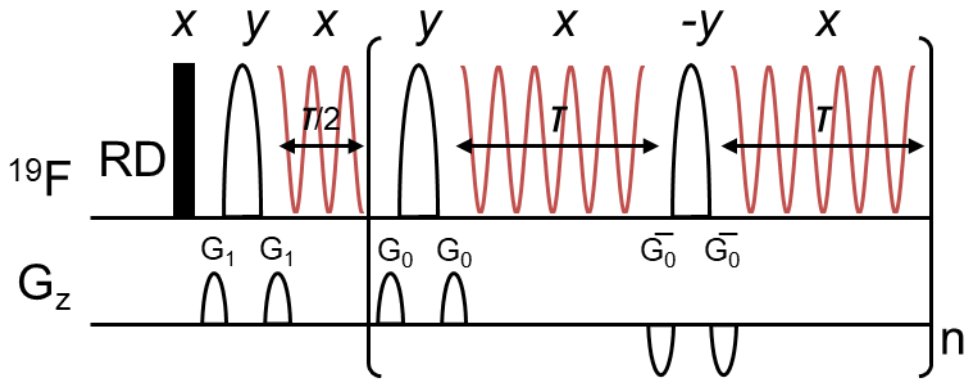

Figure 4.3: Pulse sequence of the sel-SHARPER experiment. The black rectangle is a non-selective 90° pulse, the large rounded white blocks are selective 180° pulses and the rounded white blocks are sine-shaped pulsed field gradients. $\tau = AQ/(2n)$, where AQ is the total acquisition time and n is the total number of loops.

The addition of the spin echo before the chunk acts to select the signal of interest and the selective 180° pulses ensure that no homonuclear coupling effects are present in the final spectrum. The 180° pulses can take the form of an adjusted rectangular 180° pulse that needs to be calibrated for each sample and is applicable for samples with limited number of resonances with sufficient chemical shift separation (situation frequently encountered for compounds with multiple ^{19}F atoms). More generally shaped selective refocusing pulses are needed. The purpose of shaped pulses is to provide a frequency domain excitation profile as close to an ideal "top hat" profile as possible[66]. This top hat profile is desirable as it uniformly excites signals within a set frequency range and has no impact on signals outside of this range. Nevertheless, in most cases the shaped

pulse used is a Gaussian pulse as it provides a better inversion profile than a simple rectangular pulse without increasing the pulse time by a large margin. For demanding cases where an inversion profile close to the ideal 'top-hat' profile is required, such as slice selection, neither rectangular or gaussian pulses are suitable so the more complex π refocusing, or REBURP (REfocusing Band-selective Uniform-Response Pure-phase) pulse designed by Geen and Freeman[67] is used. While this pulse has the most complex radiofrequency pulse shape and takes the longest amount of time to produce, it also has an excitation profile that is very close to the ideal top hat shape as shown in Figure 4.4.

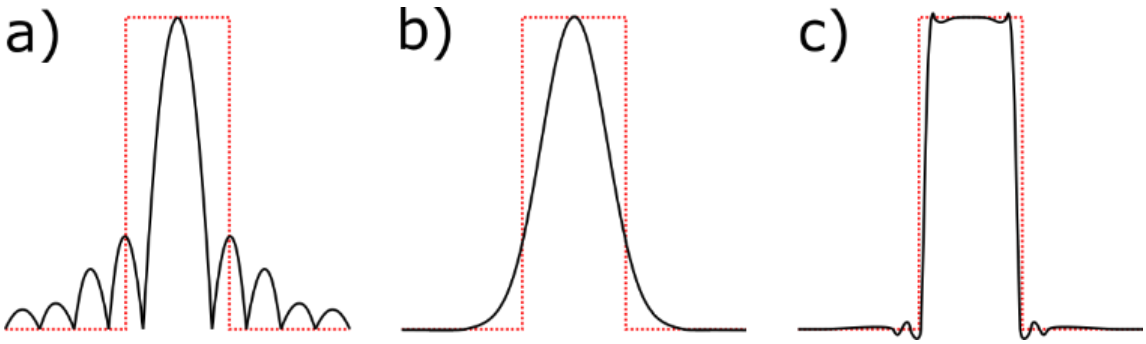

Figure 4.4: Inversion profiles of a) a rectangular pulse, b) a Gaussian pulse and c) a REBURP inversion pulse. The red dotted profile represents the 'perfect' top hat profile.

The calibration process of rectangular pulses involves positioning the signals of any coupled spins in the spectra between the lobes of the rectangular pulses sinc excitation profile, minimising the length of the pulse needed. A short pulse is desirable as minimal spin relaxation can occur during the pulse time which results in a narrower lineshape. Since shaped pulses take more time to invert the spins, it gives the spins time to relax which broadens the final signal. This counters the line narrowing properties of SHARPER so the benefits of avoiding calibration must be weighed against the reduced line narrowing potential when deciding which pulse to use. The main advantage of the *sel*-SHARPER method over the original sequence is the increased versatility regarding which molecules it can be applied to. While the basic SHARPER sequence only removes heteronuclear coupling while leaving homonuclear couplings intact, *sel*-SHARPER can successfully account for homonuclear couplings.

The original paper also studied the effect of static and dynamic magnetic field inhomogeneity on SHARPER and *sel*-SHARPER spectra and found that in both cases the impact on their performance was minimal. This further supported the possible

application of the technique in reaction monitoring where dynamically inhomogeneous samples may be encountered, but also indicated that it would be of great use in the field of benchtop spectroscopy, where generally the magnetic field homogeneity is poorer.

4.3 Why take SHARPER to benchtop?

The potential for SHARPER as a tool in benchtop spectroscopy was originally identified in the 2017 paper[2] which first introduced the technique where it was suggested that its tolerance of poor magnetic field homogeneity would greatly increase the sensitivity of benchtop spectrometers. As previously mentioned, benchtop spectrometers have much weaker and more inhomogeneous magnetic fields than their high field counterparts, so sensitivity is often a significant issue. Added to this, in some instances, reaction monitoring is particularly difficult due to the dynamic inhomogeneity caused by factors such as gas bubbles. Despite these downsides, benchtop spectrometers are gaining popularity in reaction monitoring due to the low cost, low maintenance, simplicity, and flexibility when compared to high field NMR[9]. Rather than having to maintain an expensive high field NMR spectrometer that may be on the other side of a building to where the reaction is taking place a benchtop spectrometer can be placed close to the reaction or even as part of a flow system[68]. This makes monitoring of fast reactions and the study of reaction dynamics by NMR much more achievable. Once implemented on benchtop spectrometers SHARPER would enable real time monitoring of reaction mixtures with no homo- or heteronuclear couplings present and a much higher signal to noise ratio than would normally be possible.

While these benefits will be considerable for studying ^{1}H nuclei the SHARPER sequence shows even more potential when considering ^{19}F nuclei. As fluorinated organic molecules account for up to 60% of agrochemicals[69] and a growing proportion of pharmaceuticals[70] the field of fluorine chemistry is large and has a great impact on reaction monitoring[71]. Added to this, fluorine is also a suitable nucleus for study by SHARPER at low fields as its large chemical shift dispersion means that signals are often isolated, even at low fields, allowing them to be individually enhanced by *sel*-SHARPER. Another reason why ^{19}F nuclei are a promising target at low fields is the method in which most benchtop spectrometers are designed. Since ^{1}H and ^{19}F have similar Larmor frequencies at 1-2 T, most systems use a single coil that can be tuned to

detect either nucleus. This allows most spectrometers to detect ^{19}F but since the coils are optimised for ^{1}H the spectra for ^{19}F suffer from reduced sensitivity, lowering the SNR. The SNR is further lowered by lower field homogeneity compared to high field magnets and the complex peak shapes that show contributions from numerous J_{FF} and J_{HF} couplings and higher order effects between coupled ^{1}H nuclei. As low field spectrometers often lack a separate coil that could be used for ^{1}H decoupling this greatly impacts the resulting spectra. SHARPER provides a solution to all these issues so ^{19}F nuclei at low field show a great deal of potential for the SHARPER sequence.

There is however one major obstacle standing in the way of using the published SHARPER pulse sequences on benchtop spectrometers, which is the lack of gradient coils so inability to produce PFGs present in many of the currently available models.[72] To counter this an adaptation to the SHARPER sequence has been developed that does not require PFGs.

4.4 SHARPER without PFGs

This new development focused on improving the SHARPER sequence involves changing the phasing of the ^{19}F pulses from y, −y, y to x, y, y for the first scan. This change, which is shown in Figure 4.5, removes the need for gradient pulses while still providing the same results as the *sel*-SHARPER experiment.

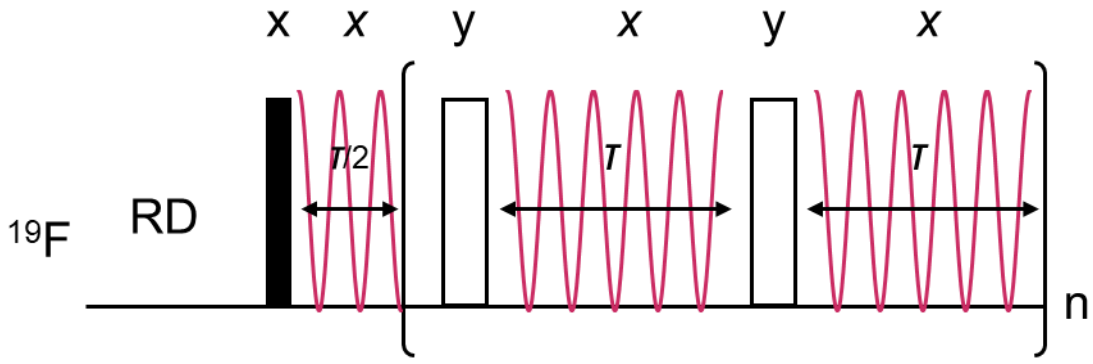

Figure 4.5: Pulse sequence of the improved sel-SHARPER experiment. The black rectangle represents a 90° hard pulse, and the white rectangles represent hard 180° pulses. and τ = AQ/(2n), where AQ is the total acquisition time and n is the total number of loops.

The new phase cycling is the same as that used for CMPG experiments[11,13] and leads to greater sensitivity of SHARPER experiments. This sensitivity increase is due to multiple factors including a reduction in relaxation and diffusion effects as a result of the shorter experiment, fewer eddy current effects and fact that PFGs eliminate magnetisation that has not received perfect inversion, e.g., due to B_1 inhomogeneity of pulses, while the CPMG phase cycling without PFG preserves it. Figure 4.6 demonstrates the increase in signal to noise obtained when the PFG free sequence is used in comparison to the original SHARPER sequence in both homogenous and inhomogeneous magnetic fields.

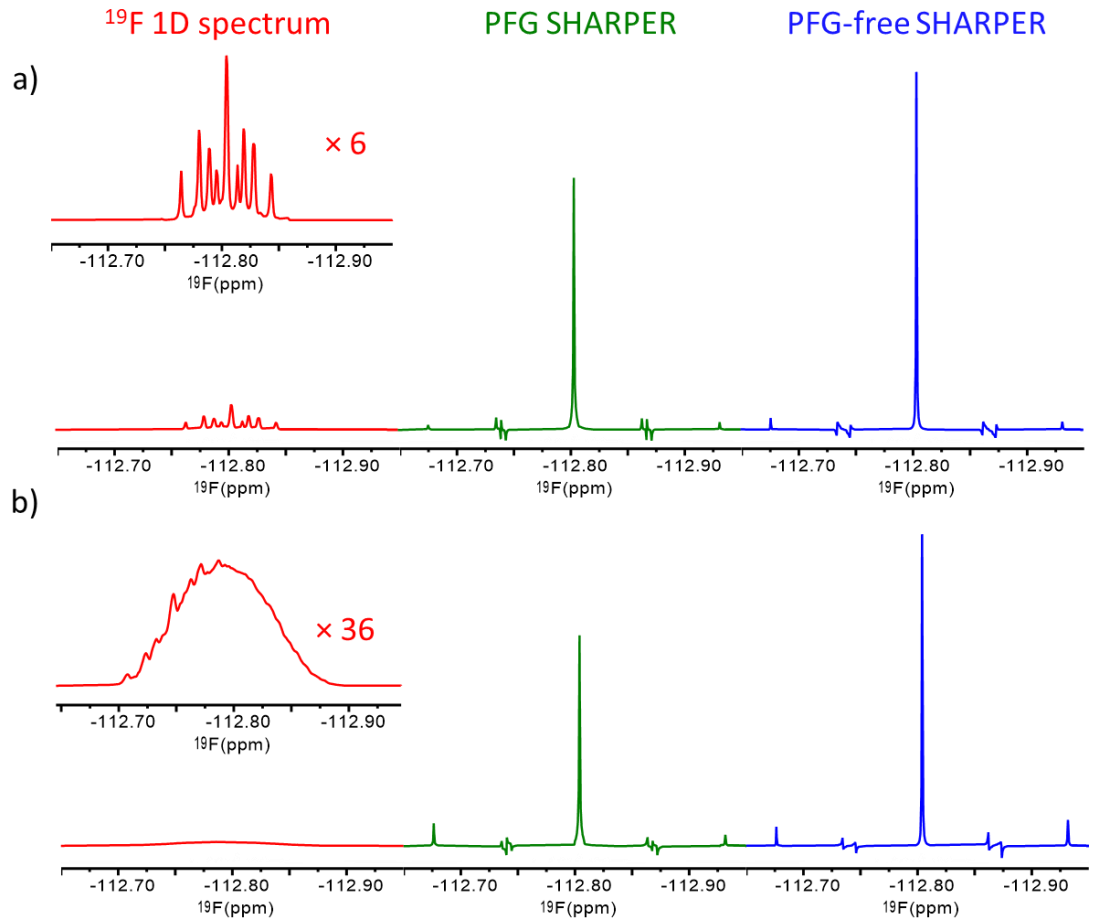

Figure 4.6: 376.5 MHz spectra of fluorobenzene in toluene-d_8 comparing the relative intensities of the original SHARPER pulse sequence containing PFGs (green) and the optimised sequence with the CPMG phase cycling (blue). The red spectra are 1D ^{19}F to demonstrate the signal amplification of the sharper sequence and the insets are expanded by the scaling shown to highlight the increase in SNR. The exact values are

shown in Table 4.1. a) shows spectra recorded in a homogenous magnetic field and b) shows spectra recorded in an inhomogeneous magnetic field where a value of +400 had been added to the z shim.

Table 4.1: SNR and integral values for the spectra shown in Figure 4.6

Magnetic field	Homogenous			Inhomogeneous		
Sequence	1D ^{19}F	PFG SHARPER	PFG-free SHARPER	1D ^{19}F	PFG SHARPER	PFG-free SHARPER
Relative SNR	1	10.1	17.6	1	46.1	79.4
Relative Integral	100%	93.5%	92.5%	100%	80.2%	80.7%

The integral values in Table 4.1 demonstrate that in this instance, despite the increase in SNR, the integral values of the peak remain the same as for the original sequence showing that the signal loss is due to the interrupted acquisition process itself rather than the presence of PFGs.

In addition to this basic gradient free SHARPER sequence shown in Figure 4.6, three other pulse sequences not utilising gradients were developed for use at low fields. This is due to the loss of selectivity resulting from the removal of the gradient pulses requiring alternate selection methods to be utilised. The first of these, which is shown in Figure 4.7, utilises a spin-echo prior to the SHARPER loop along with a two-scan phase cycle to efficiently remove the off-resonance signals.

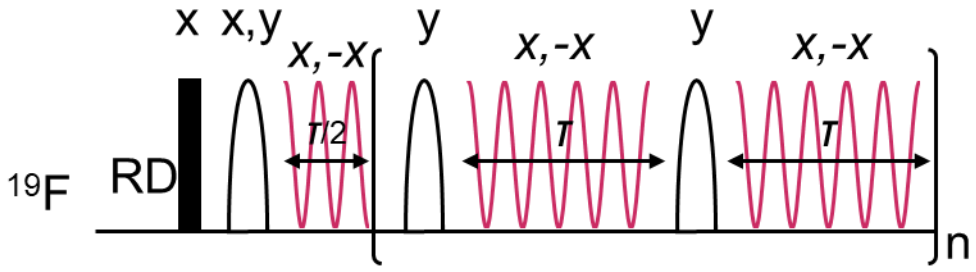

Figure 4.7: Pulse sequence of the SE sel-SHARPER experiment showing the two-step phase cycle. The black rectangle represents a 90° hard pulse, and the white rounded blocks represent shaped gaussian 180° pulses. τ = AQ/(2n), where AQ is the total acquisition time and n is the total number of loops.

Without the two-step phase cycle spectra contain considerable artefacts, therefore two scans are required to enable off-resonance peak cancellation. This reduces the applicability of the pulse sequence to reaction monitoring of fast reactions. To counter this effect, a third gradient free sequence was developed, which replaces the spin echo with a single 270° Gaussian pulse,[73] and has the benefits of selecting a specific signal in a single scan. This means it is suitable for monitoring fast reactions where a single scan per time point is necessary.

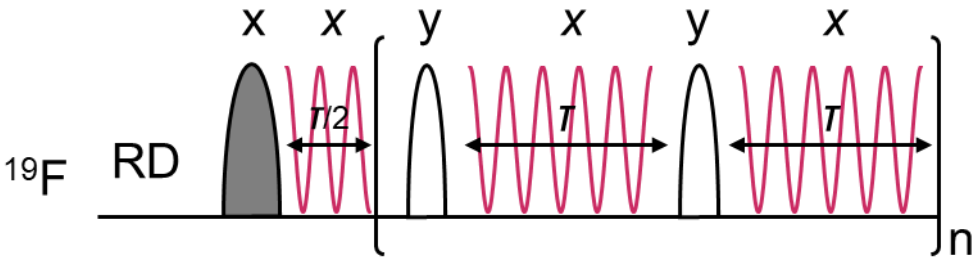

Figure 4.8: Pulse sequence of the 270° sel-SHARPER experiment. The grey rounded block represents a shaped gaussian 270° pulse, and the white rounded blocks represent shaped gaussian 180° pulse. τ = AQ/(2n), where AQ is the total acquisition time and n is the total number of loops.

Spectra from both a two scan SE-*sel*-SHARPER and one scan 270°-*sel*-SHARPER experiment on the central F3 ^{19}F signal in a sample of fluorobenzene are shown below to demonstrate the effectiveness of the selective pulses.

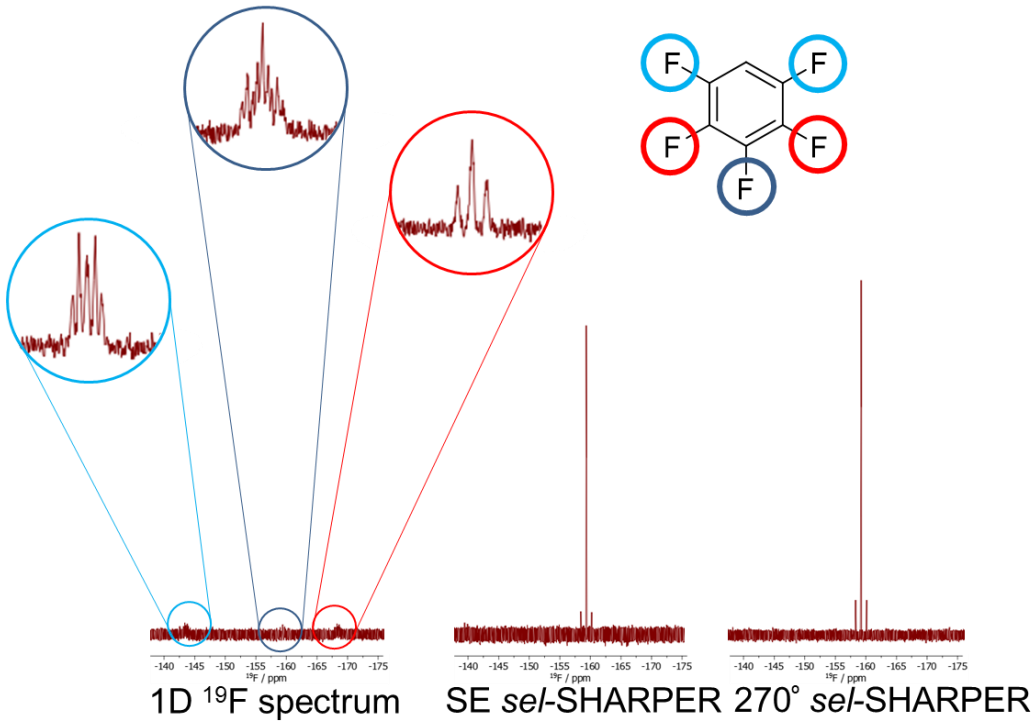

Figure 4.9: A 1D ^{19}F spectrum of pentafluorobenzene in $CDCl_3$, two scan SE-*sel*-SHARPER spectra using a 5 ms 180° Gaussian pulse and one scan 270° *sel*-SHARPER spectra using a 7.7 ms 270° Gaussian pulse. Selective pulses were applied to F3 of pentafluorobenzene which is indicated by the dark blue circle.

The final sequence implemented that doesn't involve gradients, which is termed rectangular *sel*-SHARPER, is a modification of the sequence shown in Figure 4.5 where the hard pulses are replaced with lower power rectangular pulses. As shown in Figure 4.10 this variation achieves signal selection in systems with two resonances in the spectrum by adjusting the pulse length to place the first zero point of the excitation profile at the same frequency as the off-resonance signal. This ensures that no excitation occurs for the off-resonance peak, effectively selecting the on-resonance signal.

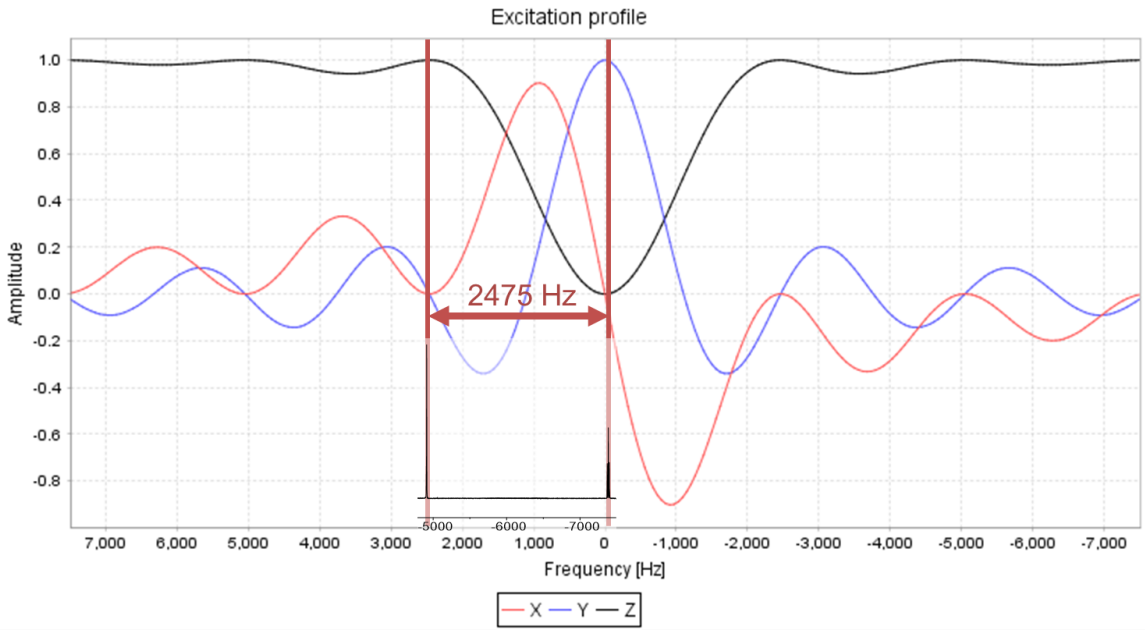

Figure 4.10 : Excitation profile of a 393 µs low power 90° rectangular pulse which was used to selectively remove the CF_3 signal from a pentafluoropropanol sample. The spectrum is overlaid to demonstrate the distance between the two peaks matching the position of the first zero point in the excitation profile.

To calculate the length of the rectangular pulses, Equations 9 and 10 are used where Δ is the frequency difference between the two signals. This sequence would be most appropriate when studying a reaction utilising a monofluorinated reactant and product where only two ^{19}F signals would be present in the spectrum. This sequence also has the benefit of being suitable for use of benchtop instruments where it is not possible to produce shaped pulses allowing a degree of selectivity to be obtained by just varying the power level of pulses.[74] The 180° pulses used during the spin echo were also adjusted to match the rectangular 90° pulses by increasing their duration to be double that of the 90° pulse.

$$pw_{90} = \frac{\sqrt{15}}{4\Delta} \qquad (9)$$

$$pw_{180} = \frac{\sqrt{3}}{2\Delta} \qquad (10)$$

The results from this sequence are shown in Figure 4.11 on a sample of 2,2,3,3,3,-pentafluoropropanol in D_2O with one scan.

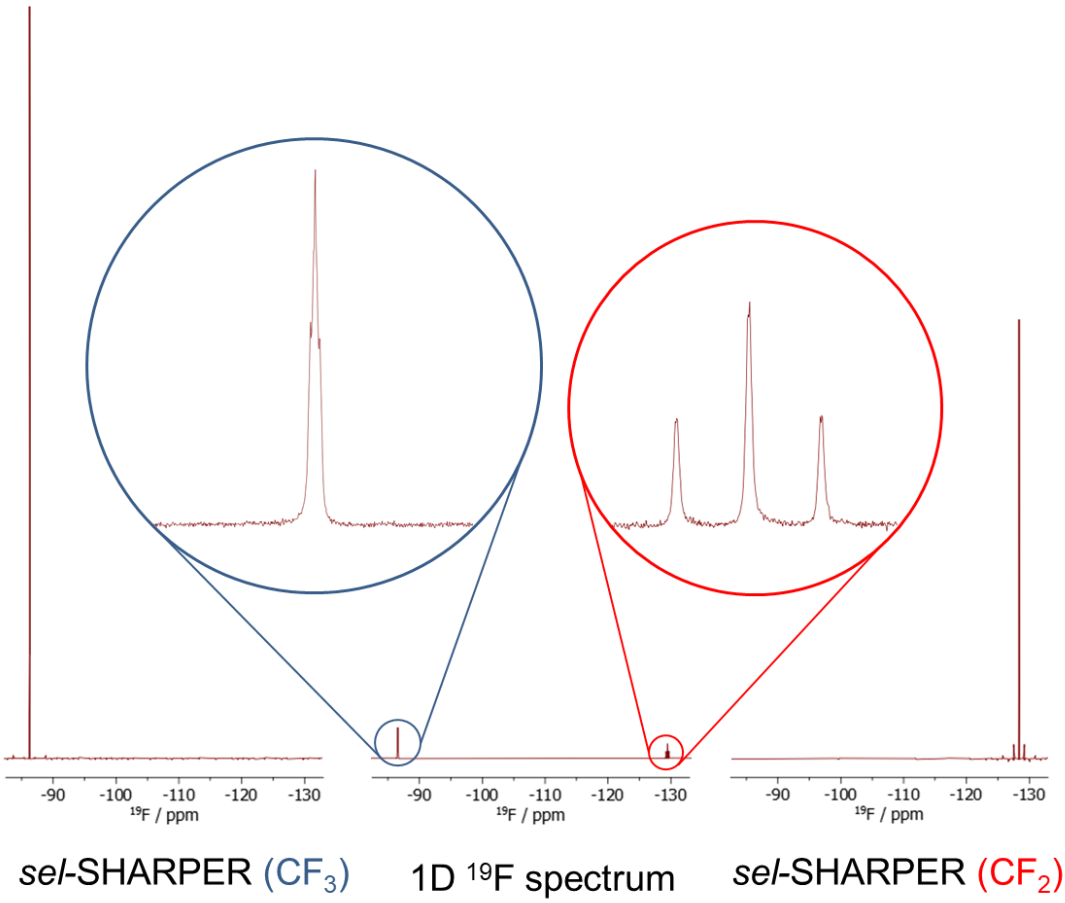

Figure 4.11: Spectra comparing a 1D ^{19}F spectrum of 2,2,3,3,3,-pentafluoropropanol to 1 scan rectangular *sel*-SHARPER spectra acquired to select each peak.

Together these sequences can be used for a range of different reaction monitoring purposes on instruments that do not have the capacity to produce PFGs. However, some instruments do have this capacity so an updated *sel*-SHARPER sequence using single pulsed field gradient spin echo for the selection was implemented. The pulse sequence is shown in Figure 4.12 and has a distinct advantage over the gradient free SE-*sel*-SHARPER in that it can be run with a single scan due to the PFGs removing signals outside of the inversion window of the selective pulse.

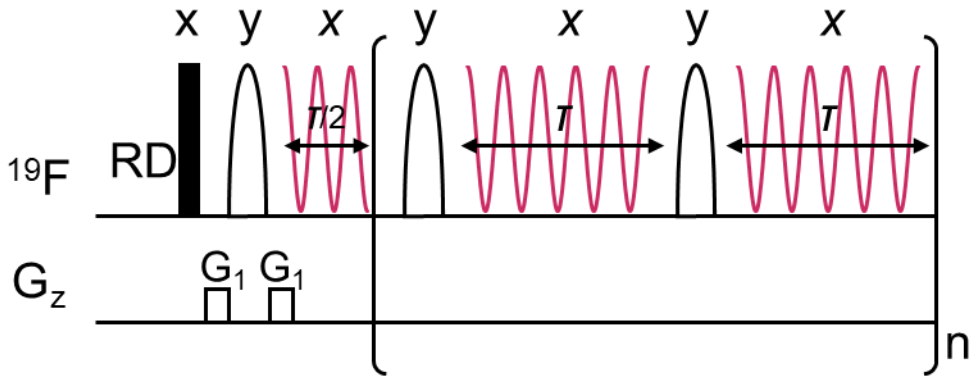

Figure 4.12: Pulse sequence of the SPFGSE-*sel*-SHARPER experiment. The black rectangle is a non-selective 90° pulse, the large rounded white blocks are selective 180° pulses and the white rectangles are PFGs. $\tau = AQ/(2n)$, where AQ is the total acquisition time and n is the total number of loops.

This sequence was implemented on pentafluorobenzene in D_2O. Figure 4.13 shows the three spectra acquired with the one-scan SPFGSE-*sel*-SHARPER and demonstrates the significant enhancement of individual ^{19}F signals.

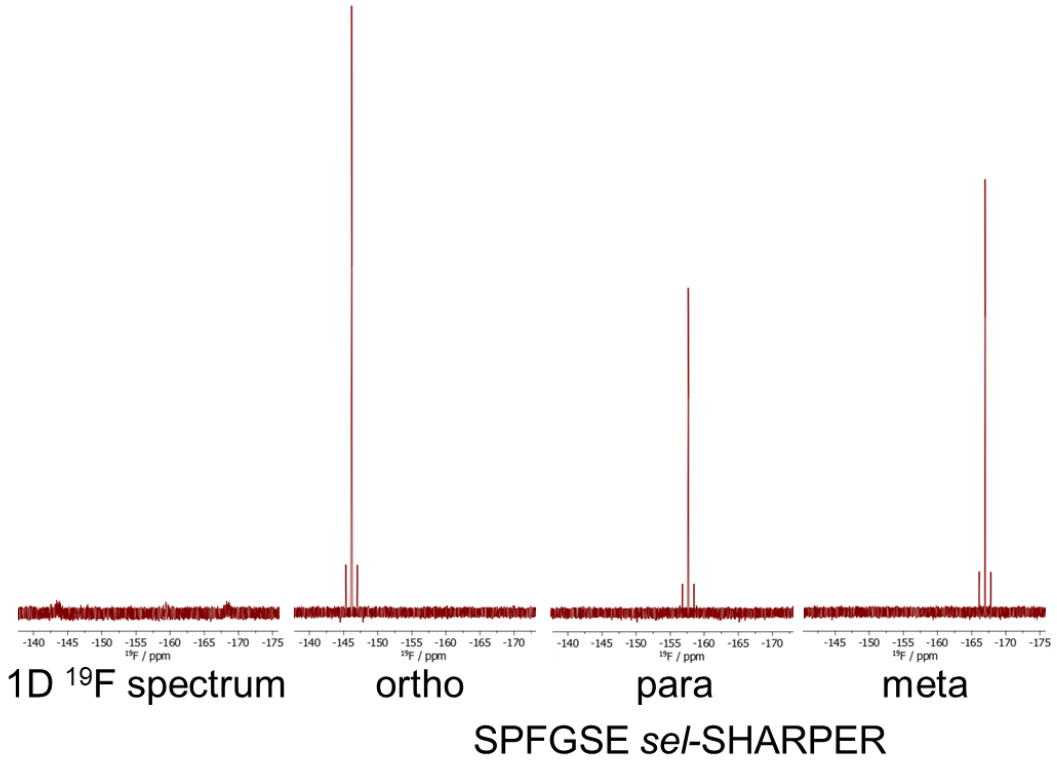

Figure 4.13: A one scan 1D ^{19}F spectrum of pentafluorobenzene compared to the one scan SPFGSE-*sel*-SHARPER used to select each of the ^{19}F signals.

4.5 Practicalities of SHARPER on benchtop NMR spectrometers

This section will address technical issues encountered during implementation of SHARPER pulse sequences on low field instruments. As these are to some extent unique to each system, this discussion is particularly relevant to the Magritek Spinsolve 60 MHz spectrometer using the SpinsolveExpert software.

4.5.1 Shaped pulses

Unlike Bruker TopSpin software, SpinSolve expert does not have pre-saved files for shaped pulses; instead, users are required to generate them. This is mainly caused by the non-linearity of amplifiers, particularly encountered on older instruments. To counter these effects Mattheus Rossetto, a member of the Halse Group at the University of York, wrote a section of code that generates a table of amplitudes with n steps which correspond to the power required for a Gaussian pulse. A Gaussian pulse was chosen due to the simple implementation as well as the large gaps between fluorine signals not requiring a greater level of selectivity which would be provided by more complex

shapes. This table has a wide range of power values and requires careful control of the RF amplitudes. Calibration step is required to ensure that the powers are at correct values, successfully producing a Gaussian pulse.

4.5.2 Power calibration

As discussed in the previous section the production of shaped pulses requires precise power variation at levels far lower than the maximum power. On Magritek instruments the convention is that the power scale is logarithmic and measured in decibels with 0dB being maximum power and a change of -6dB quartering the power level and doubling the pulse length. This means that a pulse produced with power of -18dB should be at 1/64 of the maximum power. While a new instrument should have a linear power scaling it was observed by our colleagues in York that their older instrument suffered greatly from power drift, so the reported power level was often quite far from the actual, necessitating a calibration process.

The theoretical dependency of the pulse length on the dB value is shown below for 180° pulses, as these are more commonly used by the SHARPER sequences.

$$pw_{180} = pw_{180}^{0dB} 10^{\frac{-dB}{20}} \qquad (11)$$

The calibration process consisted of recording a series of nutation curves at sequentially lower powers to determine the 90° pulse duration at each power to confirm if the amplifiers were linear or not. If linear, a drop in power of −6dB would result in the pulse length doubling. The nutation curves were recorded using a standard ProtonDurationSweep experiment modified for ^{19}F. This experiment recorded a series of pulse acquire 1D spectra with incremented pulse duration, 1 scan and 10s relaxation time but fixed power level. Magnitude mode spectra of the singlet peak from a neat sample of 2,2,3,3,3-pentafluoropropanol were integrated. High concentration allowed clear definition of the peak and the results were plotted on a graph of integral value *vs* pulse time as shown in Figure 4.14.

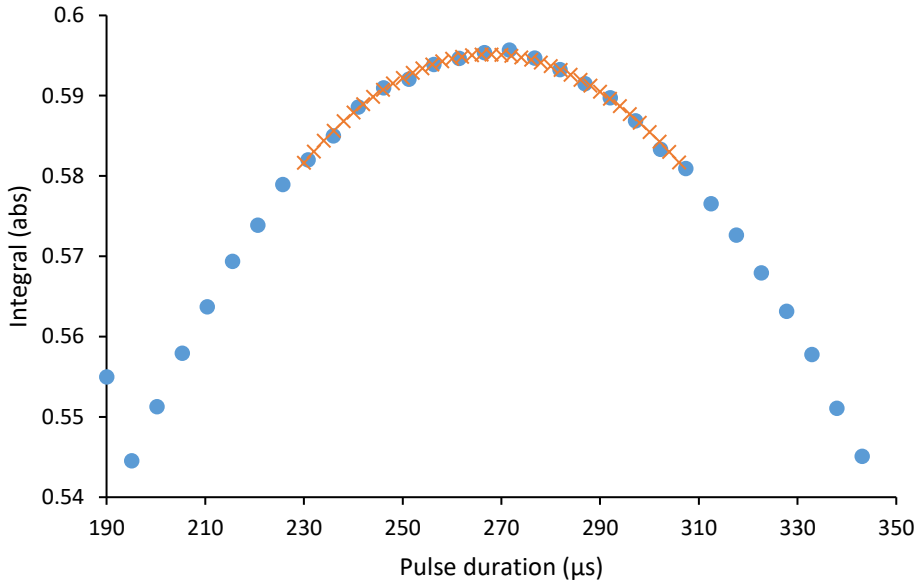

Figure 4.14: Integral area vs pulse time at −6.5dB. The blue dots represent experimentally determined values and the crosses show the predicted points produced by fitting a 4th order polynomial to the curve to find the precise 90° pulse duration.

The crosses shown in Figure 4.14 represent points calculated by fitting the raw data to a 4th order polynomial and then finding the curve maximum to give a precise value for the 90° pulse duration. As can also be observed the first scan of the sequence often had a larger integral than was expected so it was omitted from the fitting procedure.

Calibration curves were recorded for powers down to −18dB as this is when the rectangular pulse length reached 1 ms which is the maximum pulse duration possible on a Magritek spectrometer due to manufacturers specifications. Longer pulses are possible but require different coding with the transmitter to be switched on for a certain time corresponding to the desired pulse length and then switched off. This was not compatible with the sweep experiment. For each power level 40 steps were used with the minimum pulse being chosen in order to centre the maximum in the middle of the recorded times. The pulse step size (µs) was also varied as at lower power levels the smaller integral values of the peak required greater time variations to be able to produce a full nutation curve. Table A1 in the appendix shows the range of powers, pulse lengths and step sizes used to obtain the nutation curves.

The full range of nutation curves are shown below in Figure 4.15 to demonstrate the widening of the curve. The integral values have been normalised to present the data more clearly.

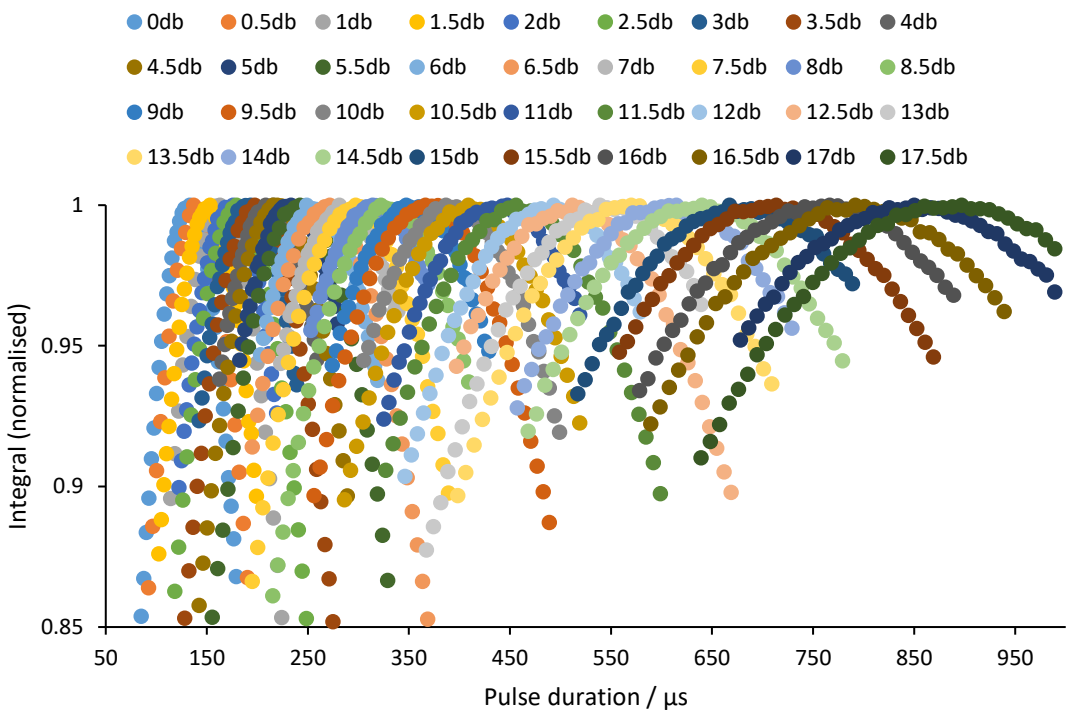

Figure 4.15: Normalised nutation curves from 0dB to −18dB at 0.5dB increments.

Once the 90° pulse time had been obtained for each power from 0 to -17.5dB these values were doubled to obtain the 180° pulse time. These pw_{180} values were then plotted against the power level (dB scale) and extrapolated beyond the 2 ms value using a 5th order polynomial function. The theoretical dependency was also calculated using the calibrated 0 dB pulse length as the initial value.

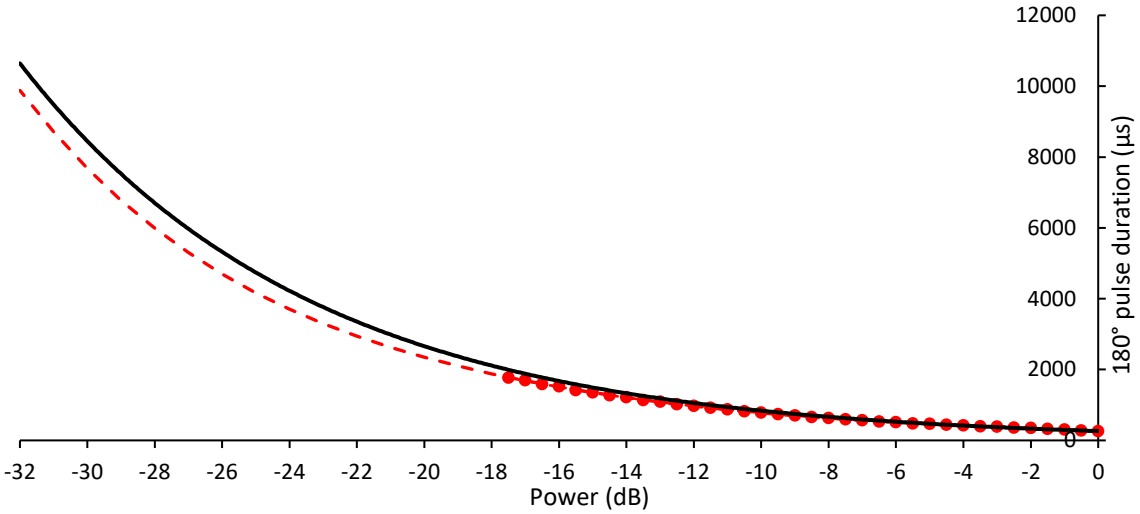

Figure 4.16: Relationship between the attenuation and the pulse length. Experimental values are given between 0 and −17.5 dB and are represented by red circles. The dashed line represents extrapolation of the experimental values to −32 dB and the black line is the theoretical dependency, where $pw_{180}^{0dB} = 264\mu s$.

The predicted pulse lengths were then converted to decibels using Equation 12.

$$dB(i) = \log_{\frac{t(e)}{t(i)}} 0.890898718 \qquad (12)$$

dB(i) is the ideal power in decibels, t(e) is the pulse time from the experimental prediction and t(i) is the pulse time from the perfect power scaling. 0.890898718 is a constant obtained from solving Equation 13 where the power (dB) was -6 and t (pulse time) was equal to 2*t_0 which is pulse time at 0dB for c. C is 0.890898718

$$t = t_0 c^{dB} \qquad (13)$$

This enabled the plotting of input power *vs* actual power as shown in Figure 4.17.

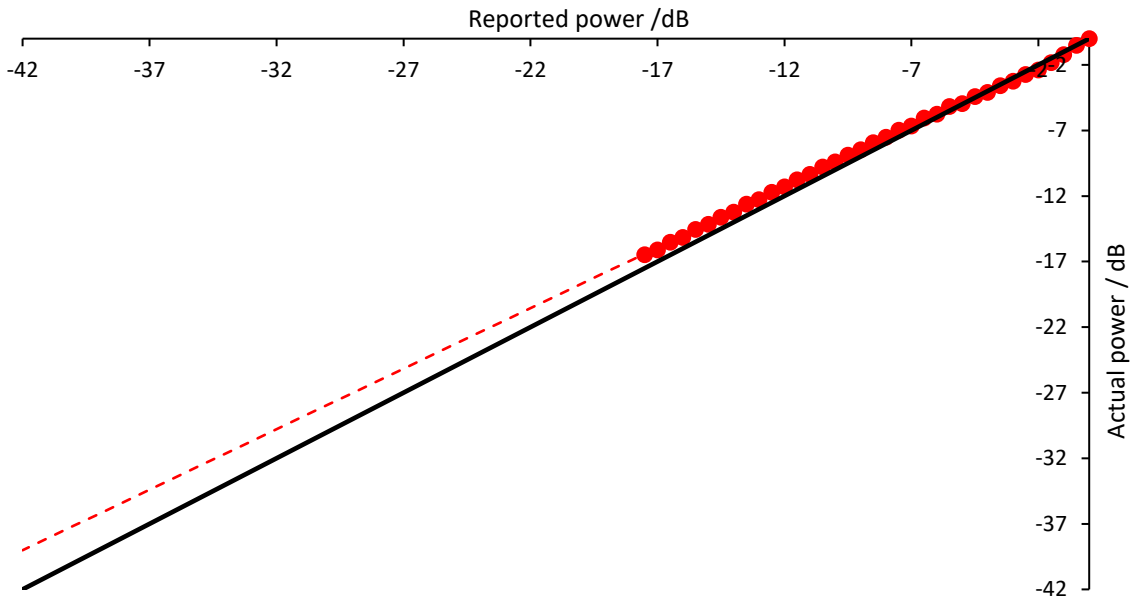

Figure 4.17: The relationship between input power and produced power in dB. The black line is the ideal power based on linear scaling and the pulse length at 0 dB, the red dots are the observed power values, and the dashed line represents the predicted power levels.

Figure 4.17 shows that at lower powers the spectrometer produced pulses at a slightly higher power than that input, however the overall relationship retains its linearity. A correction was included in the pulse sequences to account for this and is applied after attenuation has been converted to a linear scale for application of the Gaussian pulse and simply multiplies the amplitude by a factor of 0.923. After this it was converted back into a 14bit number for use by the spectrometer. The predictions used to obtain pulse length values at very low powers have been shown to be accurate as selective shaped and rectangular pulses based on the prediction accurately select the correct peak at powers as low as -26.52 dB.

It is also possible to use the SHARPER experiment itself to double check the accuracy of the calibration or to calibrate on individual samples. The SHARPER peak is sensitive to pulse power and duration of the spin-echo pulses: if the 180° pulses are miss-set there will be a decrease in the intensity of the main signal and the lineshape will deteriorate significantly. An added bonus is that the increased sensitivity of the SHARPER singlet allows the use of real samples to fine tune the calibration rather than requiring standard

samples. Samples of fluorobenzene, pentafluorobenzene and both neat and diluted in D_2O 2,2,3,3,3-pentafluoropropanol were used for this purpose. The results for fluorobenzene are shown in Figure 4.18 and the rest is presented in Table 4.2. In the case of fluorobenzene there is only a small difference of signal intensity between the predicted value and the optimised value showing that the calibration procedure is reliable.

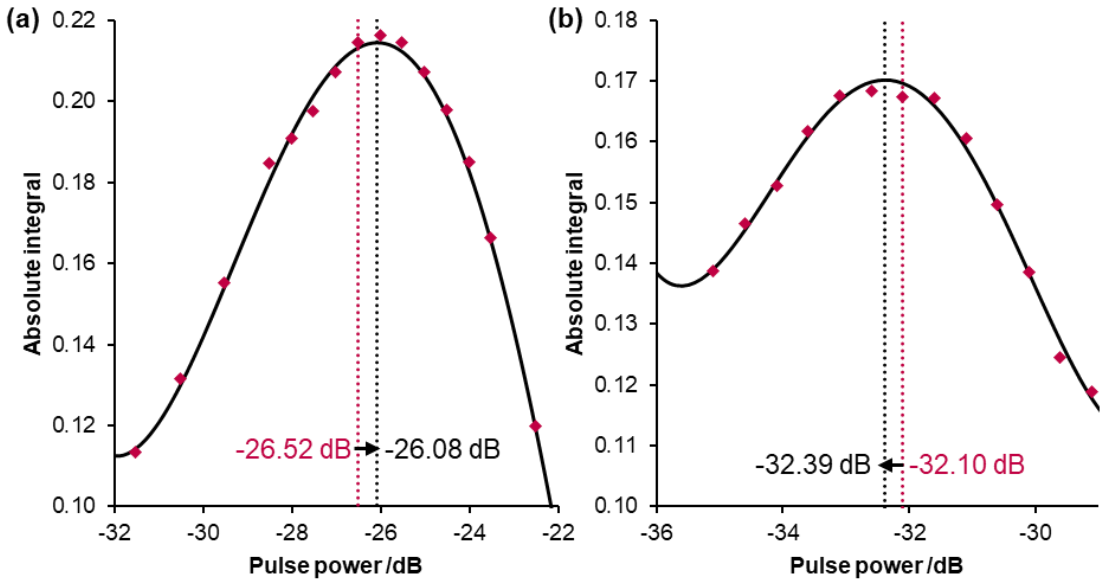

Figure 4.18: Pulse calibration using SPFGSE-*sel*-SHARPER measured for fluorobenzene in toluene-d_8. (a) and (b) show 5 ms and 10 ms 180° Gaussian pulses, respectively. The red and black dotted lines indicate the power levels predicted by nutation experiments and the *sel*-SHARPER calibrated values, respectively.

Table 4.2: Pulse powers optimised for 180° Gaussian pulses using SPFGSE *sel*-SHARPER.

Compound	Solvent	Pulse length /ms	Predicted power (PP) /dB	Optimised power (OP)/dB	PP-OP/dB
Fluorobenzene	Toluene-d_8	5	-26.52	-26.08	-0.44
Fluorobenzene	Toluene-d_8	10	-32.10	-32.39	0.29
Pentafluorobenzene	$CDCl_3$	5	-26.52	-25.81	-0.71
2,2,3,3,3-pentafluoropropanol	Neat	5	-26.52	-25.92	-0.6
2,2,3,3,3-pentafluoropropanol	D_2O	5	-26.52	-26.00	-0.52

4.5.3 Gradient pulses

As previously mentioned, the instrument we were using did not have gradient coils so initially we did not think gradient pulses would be possible. However, upon consulting with the manufacturer we were advised that gradients could be produced by purposely miss-setting the shim coils. This would simulate the use of a simple on/off gradient pulse and while it would lack the capabilities of a shaped or ramped gradient pulse it would still have the desired effect within the pulse sequence and would be suitable to test the capabilities of the SPFGSE-*sel*-SHARPER experiment. To check the linearity of the shim coils and if they are producing suitable field gradients, a 1D gradient echo imaging pulse sequence shown in Figure 4.19 was used.

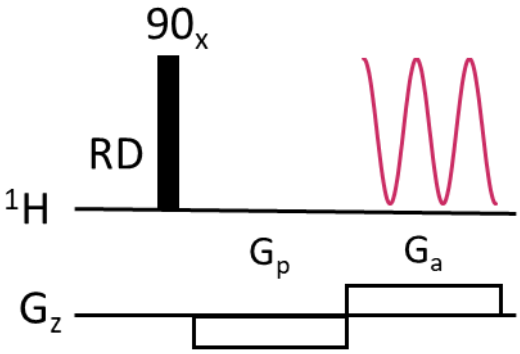

Figure 4.19: 1D gradient echo imaging pulse sequence used to test the shim coil produced gradient strength. The black rectangle is a 90° hard pulse, G_p is the initial gradient pulse which has a duration equal to the acquisition time and G_a is an opposite gradient pulse that runs during the acquisition.

A series of spectra were recorded using the reference water sample provided with the spectrometer for shimming and were then processed in magnitude mode with the base width of the resulting peak measured in Hz. In order to determine the linearity of the coils these spectra were recorded in series with each of the x, y and z coils being used to simulate gradients ranging in power from 100% to -100% of the maximum shim output. The results are shown in Figure 4.20.

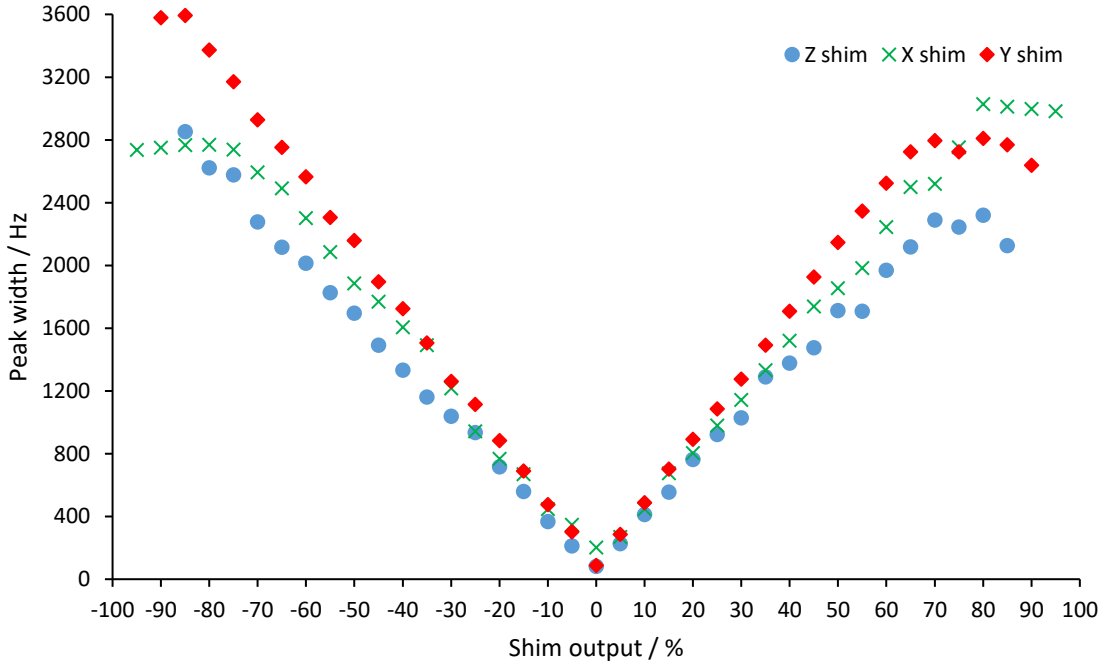

Figure 4.20: Plot of peak width against proportional shim change

As Figure 4.20 shows the gradients were highly linear at low outputs. However, they reached a maximum at roughly ±75% output. Furthermore, the spectra above a certain threshold for each coil (96% for the x coil, 90% for the y and 87% for the z) contained no peaks at all. This is likely due to the shim coils not being intended for use simulating gradients so not working ideally at higher powers. In order to calculate the maximum strength of each gradient Equation 14 was used where G is gradient strength in T m^{-1}, pw is peak width in Hz, FOV is extent of the object in the given direction in m (for x and y this is the width of the NMR tube and for z is the length of the coil) and γ is the gyromagnetic ratio in Hz T^{-1}.

$$G = \frac{pw}{FOV \times \frac{\gamma}{2\pi}} \qquad (14)$$

Taking the maximum values of peak width for each coil the values in Table 4.3 were calculated. Since each gradient pulse needs to be matched by an equal amplitude pulse of opposite magnitude the lower strength value from the positive and negative outputs must be used which led us to settle on using ±70% z coil gradients for the SPFGSE-*sel*-SHARPER sequence. The gradient strength of 1.08 mT m^{-1} for the positive gradient and 1.07 mT m^{-1} for the negative gradient are close enough to match for the purposes of this experiment.

Table 4.3: Maximum gradient strengths produced by shim coils at low field. The variation in maximum power output is due to the lack of peaks in the spectra at different intensities after the peak width plateau observed at roughly 75% output.1.08 +ve 1.07 -ve

Coil	**Power output / %**	**Peak width / Hz**	**Gradient strength / mT m^{-1}**
X	+80	3028	1.65
X	-80	2769	1.51
Y	+80	2809	1.53
Y	-85	3593	1.96
Z	+70	2320	1.09
Z	-85	2852	1.34

4.6 Application to model compounds

The implementation of these sequences and demonstration of their efficacy required the use of a series of model compounds. The compounds chosen were fluorobenzene in toluene-d_8, 2,2,3,3,3-pentaflurorpropanol both in D_2O and neat and pentafluorobenzene in deuterated chloroform. These compounds were chosen due to the suitability of the fluorine signals for demonstrating the capabilities of the different sequences. Fluorobenzene has a single peak so can demonstrate the basic SHARPER sequence, 2,2,3,3,3-pentafluoropropanol has two clearly separated peaks so is suitable for demonstrating the selection capabilities of rectangular *sel*-SHARPER and pentafluorobenzene has three distinct signals so is suitable for demonstrating SE-*sel*-SHARPER, 270° *sel*-SHARPER and SPFGSE-*sel*-SHARPER.

4.6.1 Fluorobenzene results

In order to compare the performance of each sequence they were all initially tested on fluorobenzene using 4 scans with a constant repetition time of five times the T_1 of the ^{19}F nucleus in fluorobenzene. The T_1 was determined experimentally using inversion recovery to be 3.2 seconds. The results are shown in Figure 4.21.

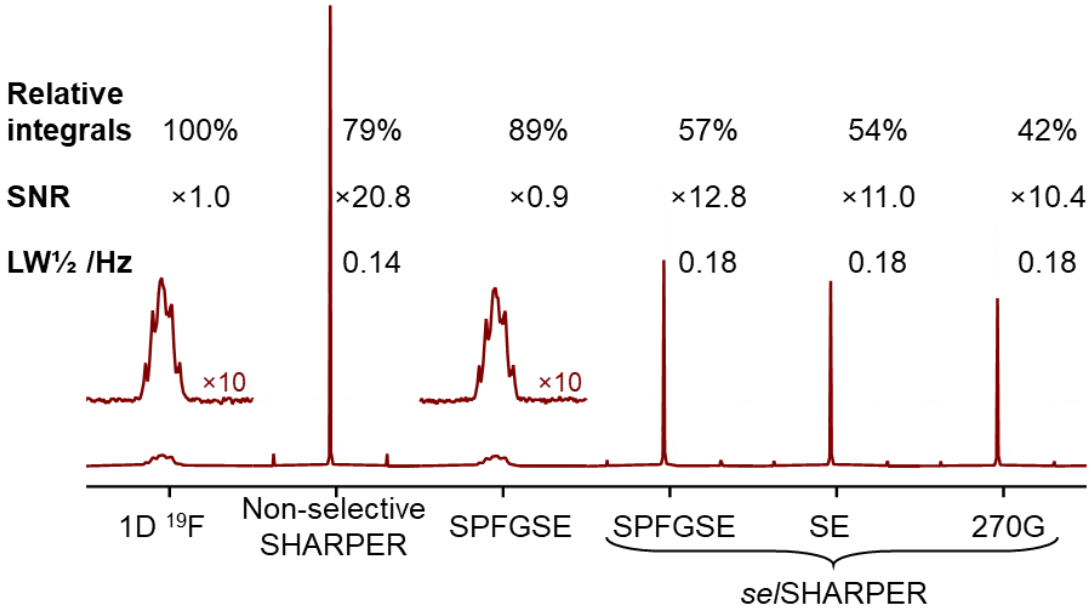

Figure 4.21: 56.46MHz spectra of fluorobenzene in toluene-d_8 showing the SNR improvements and relative integrals of each SHARPER sequence. 4 scans and a repetition time of 5 × T_1 was used for each spectrum. The spectra have been processed

without the imaginary component of the FID which is discussed further in section 4.1.2. Reproduced from reference 72.

As shown in Figure 4.21 there were significant increases in SNR for each SHARPER sequence with the maximum increase of × 20.8 for the non-selective SHARPER sequence. The selective sequences showed a minimum SNR increase of × 10.4 which is greater than the previously reported × 8 gain observed on a 400 MHz instrument.[2] This is a larger gain than would be expected from the removal of PFGs. However, this can be accounted for by the emergence of higher order HH coupling effects at low field that resulted in the appearance of combination lines in the ^{19}F signals, reducing the resolution of the peak. The AA'BB'C ^{1}H spin system of fluorobenzene at 60 MHz is not present at 400 MHz. This is the reason for different appearance of ^{19}F signals at 56.5 and 376.5 MHz (see Figure 4.22).

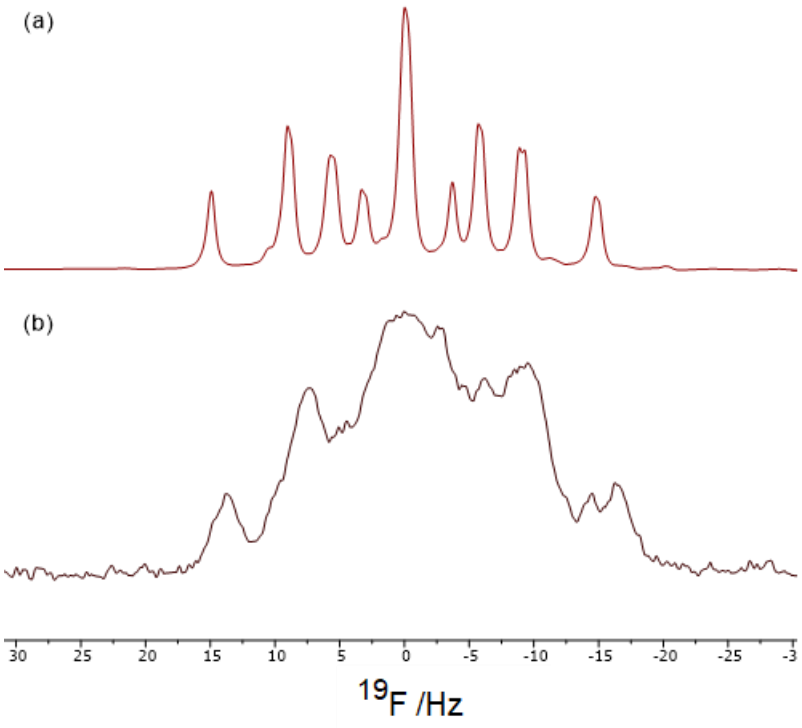

Figure 4.22: ^{19}F spectra of fluorobenzene recorded at a) 376.5 and b) 56.5 MHz demonstrating the impact of the higher order HH couplings on peak shape.

Figure 4.21 also shows that all the SHARPER sequences lose integral intensity with the smallest impact being observed for the non-selective SHARPER sequence and the

largest loss occurring with the 270° SHARPER sequence. This is likely due to imperfections in the selective pulses caused by the inhomogeneity observed in B_1 at a benchtop instrument.

Another key observation is the increase in signal linewidth from 0.14 Hz to 0.18 Hz when selective pulses are used rather than hard pulses in non-selective SHARPER. This is due to the increased time duration of the selective pulses, which are on the order of 5 ms, increasing the relaxation experienced by the nuclei during signal acquisition. The spectra in Figure 4.21 were acquired with 4 scans and a fixed repetition time that was determined based on the T_1 time of the ^{19}F signal in fluorobenzene which is 3.21 s. As the SHARPER experiments used the same repetition time as the 1D spectrum the spins had less time to relax due to the refocusing pulses present in the SHARPER sequence during acquisition. This hinders the SNR increase observed from using SHARPER so a one scan experiment with variable acquisition times was considered. The results from this are shown below in Table 4.4 and show that when considering the enhancement per unit time SHARPER provides even greater SNR enhancements. Table 4.4 shows the results of different experiments using a single scan and variable acquisition times in order to demonstrate the enhancements achieved per unit time from the SHARPER experiments.

Table 4.4: Single scan vs multiple scan SHARPER experiments on fluorobenzene in toluene demonstrating increases in SNR per unit time.

Experiment	Acquisition time	Available relaxation time / s	Multiple scan SNR (relative to 1D ^{19}F)	Single scan SNR (relative to 1D ^{19}F)
1D ^{19}F	10.95	17.0	1.0	1.0
SPFGSE ^{19}F	10.95	17.0	0.9	0.9
SHARPER	11.09	5.9	20.8	24.7
SPFGSE-*sel*-SHARPER	13.68	3.3	12.8	19.9
SE-*sel*-SHARPER	13.68	3.3	11.0	17.1
270°-*sel*-SHARPER	13.68	3.3	10.4	16.1

4.7 Best practice for acquiring SHARPER spectra.

To achieve the increases in SNR demonstrated in the previous sections, specific acquisition and processing parameters need to be used. The acquisition time required to fully digitise the SHARPER signal is often several seconds, or even tens of seconds and the relaxation of spins only happens in the inter-scan relaxation delays, so optimisation is required. This also allows the sequence to be applied to reaction monitoring where sampling points in chemical reactions need to be as close as possible for optimal results. This section will address the optimal solutions to these problems from both acquisition and processing standpoints.

It has been shown that when recording an FID, after $3T^*_2$ seconds the data points consist mostly of noise and the signal has decayed to below 5% of the starting value so further data collection is pointless.[75] As T^*_2 is the effective spin-spin relaxation time which is normally contributed to by magnetic field inhomogeneity, which is removed by

SHARPER, a different value is required for SHARPER acquisition. This is complicated by the additional relaxation contribution that arises from the refocusing pulses in the SHARPER acquisition. To determine a new value for optimal recording time both standard and *sel*- SHARPER spectra were acquired on fluorobenzene, pentafluorobenzene and pentafluoropropanol and the measured linewidths of the Lorentzian SHARPER peaks ($\Delta^S_{1/2}$) were compared to the theoretical linewidths calculated from T_2 times observed in CPMG experiments ($\Delta_{1/2} = 1/\pi T_2$). These results are shown below in Table 6 and demonstrate that while the $\Delta^S_{1/2}$ linewidths are slightly larger than the $\Delta_{1/2}$ derived from T_2 values, they are much smaller than those of normal 1D ^{19}F spectra. This shows that the SHARPER singlets are very close to the natural linewidth of each resonance so are suitably removing the magnetic field inhomogeneity contribution.

Table 4.5: Comparison of theoretical linewidths obtained from CPMG experiments and experimental linewidths obtained from SHARPER experiments with a chunk time of 20 ms.

Sample	Solvent / Atom (s)	180° pulse	Pulse length / μs	T_2 / s	$\Delta_{1/2}$ / Hz	$\Delta^S_{1/2}$ / Hz
Fluorobenzene	F	Hard	264	2.99	0.11	0.14
Pentafluorobenzene	F1,5	Gaussian	5000	3.00	0.11	0.12
	F2,4	Gaussian	5000	2.63	0.12	0.16
	F3	Gaussian	5000	3.44	0.09	0.14
Pentafluoropropanol	Neat CF_2	Rectangular	786	1.31	0.24	0.31
	Neat CF_3	Rectangular	786	1.23	0.26	0.30
	D_2O CF_2	Rectangular	786	5.84	0.05	0.08
	D_2O CF_3	Rectangular	786	4.77	0.07	0.07

From this data it can be concluded that the optimal acquisition time for the SHARPER experiment is $3T^S_2$ where T^S_2 is the effective T_2 relaxation experienced by the resonance during the SHARPER acquisition. For processing, matched filters[76] have been shown to maximise the SNR of an NMR signal when exponential line broadening is utilised with a value determined to match the decaying FID in the form $\exp(-\pi t\Delta_{1/2})$. This line broadening is applied before the Fourier transform and maximises the SNR but doubles the observed linewidth. This means that the optimal line broadening value for processing is LB = $\Delta^S_{1/2}$ Hz. To determine these parameters, a SHARPER spectrum should be acquired with a long acquisition time and from this the relevant parameters of $\Delta^S_{1/2} = 1/\pi T^S_2$ can be calculated and applied for further acquisitions.

4.8 Removal of the imaginary component of FIDs

In addition to the standard processing steps used for NMR spectra such as phasing and line broadening, an additional technique has been developed that significantly increases the SNR ratio of the SHARPER peak while simultaneously reducing the presence of associated artefacts. To explain this technique the appearance of the FID (see Figure 4.23) needs to be discussed first.

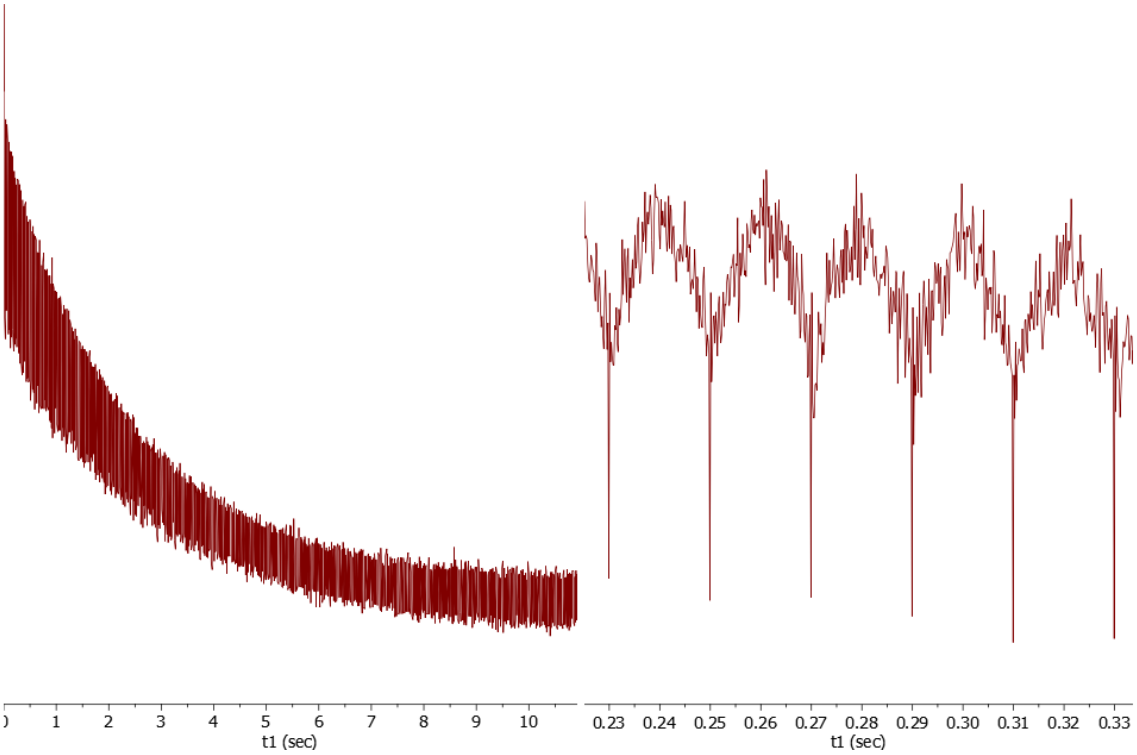

Figure 4.23: The real component of a sharper FID of fluorbenzene in toluene-d_8 at 56.46 MHz with signal directed to the real channel. The expansion shows a 100ms section of the FID (= 5 × τ) showing the evolution and subsequent refocusing of the scalar couplings during each τ period.

Low amplitude modulation of the signal is caused by evolution of scalar couplings during the acquisition chunks and the relaxation during the pulsed interval. These lead to the presence of artefacts and sidebands in the spectra at frequencies of $\pm n/\tau$ where τ is the acquisition chunk duration. As the SHARPER signal is a single exponential it can be directed into a single (real) channel and the signal collected by the imaginary channel can be discarded. This treatment improves the SNR by a factor of √2 and reduces the intensity of artefacts. The symmetrisation of spectra, as a consequence of the removal of the imaginary component, reduces the half chunk artefact in particular (see Figure

4.24). The removal of the imaginary component can be achieved by either using a python script, Bruker AU program after the acquisition or directly by storing only the real data when programmed in Spinsolve.

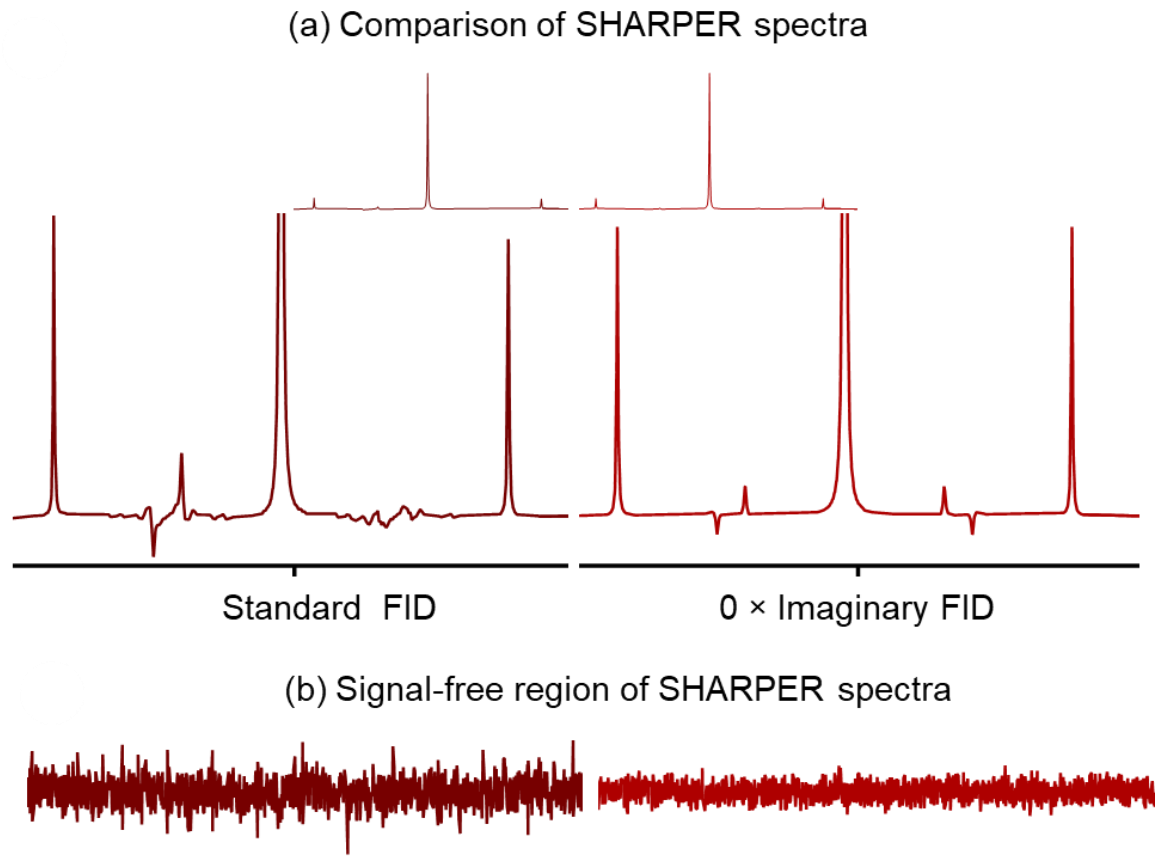

Figure 4.24: a) shows spectra produced by the Fourier transformation of FIDs with and without an imaginary component. b) shows a 1:1 comparison of the noise present in each spectra away from signal containing regions.

The direct SNR increase observed for each sequence is close to an additional 50% as shown below in Figure 4.25 when looking at the fluorobenzene sample. This is slightly greater than the 41% increase suggested by the theoretical factor of $\sqrt{2}$. This discrepancy is quite small however and may be due to small levels of uncertainty in the SNR ratio measurements or could be due to the signal intensity that would be present in the artefacts reappearing in the central peak.

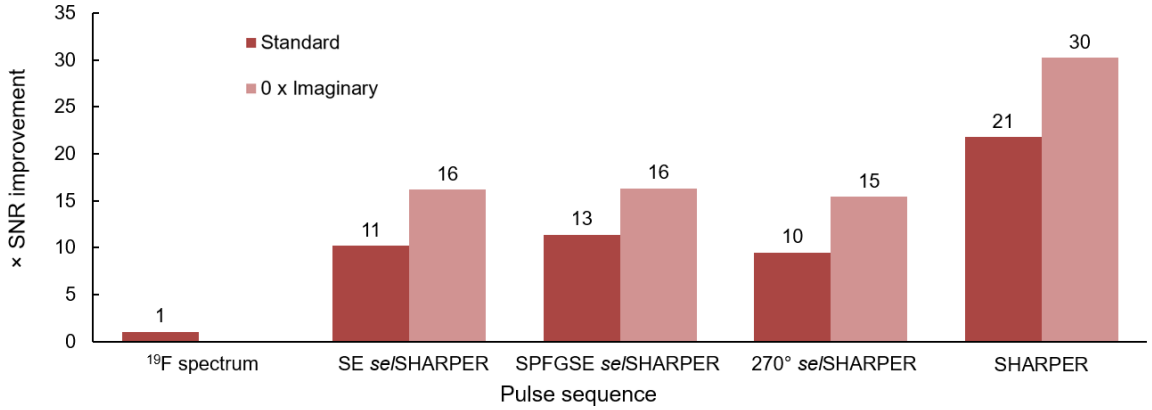

Figure 4.25: Comparison of SNR values of fluorobenzene with and without the removal of the imaginary component of the FID.

4.9 Experimental details

The samples used were fluorobenzene (50µl and 550 µl of toluene-d_8), pentafluorobenzene (30.8 mg in 600 µl of $CDCl_3$), and 2,2,3,3,3,-pentafluoropropanol (neat or 43 µl in 500 µl of D_2O)

All the low field spectra were acquired on a Spinsolve Ultra 60 MHz Carbon benchtop spectrometer with a full power 90° ^{19}F pulse of 132 µs for all samples.

The ^{19}F SPFGSE/SE *sel*-SHARPER experiment used 5 ms 180° Gaussian refocussing pulses; direct excitation in the 270° *sel*-SHARPER was achieved by a 7.5 ms 270° Gaussian pulse. The rectangular *sel*-SHARPER used a 90° pulse of 393 µs which was doubled to obtain a 180° rectangular pulse of 786 µs for both the neat and diluted samples of fluorobenzene. Rectangular PFGs in the SPFGSE-*sel*-SHARPER experiment were applied for 300 µs using a 70% proportional change to the z shim coils. Two dummy scans were used for all experiments with a chunk time of 20 ms for all samples other than fluorobenzene which used a chunk time of 20.04 ms. Parameters which varied for each sample are shown in Table 4.6

Table 4.6: Experimental parameters of SHARPER experiments

Sample	**Scans**	**Repetition time / s**	**Acquisition time / s**	**Dwell time / μs**
Fluorobenzene	1, 2, 4	17	10.9445	167
Pentafluorobenzene	16	23	8.192	125
Neat 2,2,3,3,3, pentafluoropropanol	4	13	6.488	99
D_2O dissolved 2,2,3,3,3, pentafluoropropanol	16	29	19.6608	300

These values were chosen based on the relaxation times of the signals in each sample which were determined by CPMG and inversion recovery methods and are presented in Table 4.7.

Table 4.7: Relaxation times of each signal in the samples used at low field determined from inversion recovery and CPMG methods.

Sample	**Solvent**	**Signal**	**^{19}F δ / ppm**	**T_1 / s**	**T_2 / s**
Fluorobenzene	Toluene-d_8	F	-112.96	3.2	3.0
Pentafluorobenzene	$CDCl_3$	F1,5	-138.62	4.2	3.0
		F3	-153.54	4.3	3.4
		F2,4	-161.98	4.3	2.6
2,2,3,3,3, pentafluoropropanol	Neat	CF_3	-84.199	1.3	1.2
		CF_2	-126.51	1.3	1.3
2,2,3,3,3, pentafluoropropanol	D_2O	CF_3	-81.642	5.1	4.8
		CF_2	-123.75	5.7	5.8

The spectra were processed by zero-filling to 256k points, automatic baseline correction with a 3rd order polynomial and exponential line broadening to π / AQ, where AQ is the acquisition time of the spectra, to measure integrals and linewidth at half height ($\Delta^S_{1/2}$). The applied line broadening was subtracted to produce the reported values.[76] The measurements of SNR were performed on SHARPER spectra using matched filters line-broadening, LB = $\Delta^S_{1/2}$. The measurement of SNR on 1D ^{19}F and SPFGSE spectra for comparison to SHARPER spectra was done using line-broadening (LB = 0.64 Hz). determined to maximise SNR while retaining resolved multiplets and following the decay[77] of the FIDs that was visible up to 0.5 s (hence LB = 1/0.5π = 0.64 Hz). The removal of the data from the imaginary channel of the SHARPER FIDs was performed within the Spinsolve program by zeroing the imaginary channel prior to saving the FID. SNR calculations were performed in Mestrenova 14.2.1.27684 using its in-built manual

SNR function. The tallest peak of the investigated multiplet in 1D spectra was considered. Identical chemical shift window was chosen to evaluate the white noise in the 1D and SHARPER spectra. This window was free from chunking sidebands, impurities or baseline issues.

The 376.5 MHz ^{19}F spectra shown in Figure 4.22 were acquired on a three-channel Bruker Avance III NMR spectrometer equipped with a 5 mm z-gradient BB TBO ^{1}H, ^{19}F probe using one scan, a total acquisition time (AQ) of 10.0 s, dwell time of 66.4 μs and a 90° rectangular pulse of 16.373 μs. The ^{19}F SHARPER loop used chunk lengths (τ) of 20.8 ms. The PFG spectra used, 300 μs sine shaped PFGs set to ±1% of the nominal value followed by a 200 μs gradient recovery delay. The spectra were processed by retaining both real and imaginary data points and zero-filling to 524k points. Exponential line-broadening (1.15 Hz) was used prior to FT for the determination of integral values. The measurement of SNR was performed on spectra without any line-broadening.

5 SHARPER collapse

5.1 Declaration

This chapter contains work published in the following paper:

Peat George, Dickson Claire L., Boaler Patrick J., Lloyd-Jones, Guy C. and Uhrín, Dušan. SHARPER-DOSY: Sensitivity enhanced diffusion-ordered NMR spectroscopy. *Nature Communications*, 2023, **14**, 4410.

https://doi.org/10.1038/s41467-023-40130-2

I contributed to experiment design, data acquisition and analysis, and produced the AU program for the subtraction of 2D DOSY data sets. Claire contributed to experiment design and Patrick contributed to experiment acquisition and analysis and provided the work on optimization of signal suppression and removal of imaginary time data.

5.2 CPMG SHARPER

As discussed in the previous section the SHARPER experiment uses acquisition embedded within a CMPG pulse sequence[11,13] which eliminates effects arising from magnetic field inhomogeneity and thus generates extremely narrow signals with widths close to that of the natural linewidth. The interruption of this acquisition removes all the heteronuclear couplings present in the signal and the use of 180° selective pulses removes the homonuclear couplings as well. In the original SHARPER experiments the chunk times, τ, were chosen to eliminate J evolution so were calculated to be $< 0.25/J$. This means that to remove a coupling of 12.5 Hz a chunk length shorter of roughly 20 ms would be required. It has previously been demonstrated that spin echo intervals of time < 1.0 ms can be combined with non-selective 180° pulses to also remove J evolution[78] and it is this effect that enables the use of CPMG sequences to measure spin-spin relaxation times[13]. This would mean that using much shorter intervals would enable the collapse of signals over a scale of several thousand Hz by removing frequency modulation. This was not yet explored at high fields as the shorter intervals result in the pulses being close enough to mimic CW irradiation and as such risk damage to the electronics of the probes, particularly if a more fragile cryoprobe was used. However, at low field the power limitations are much less stringent, and the instrument can tolerate much higher power CW irradiation. This inspired us to test the collapsing

potential and then reinvestigate the potential for collapsing spectra at high field using 'softer' 180° pulses with a sufficiently long duration and lower power deposition in line with spectrometer specifications. This chapter describes the use of SHARPER to collapse spectra and the further combination with the DOSY experiment allowing diffusion coefficient measurements on samples at micromolar concentrations.

5.2.1 SHARPER acquisition efficiency

The first step taken to assess the collapsing potential of SHARPER was to inspect the efficiency of the acquisition. This was achieved by using a sample of doped D_2O and measuring the integral intensity of the central SHARPER peak as a function of offset from the resonance frequency of the HOD protons. The results are shown in Figure 5.1 and show the change in intensity over a 2400 Hz frequency range with chunk times of 100, 200 and 400 μs.

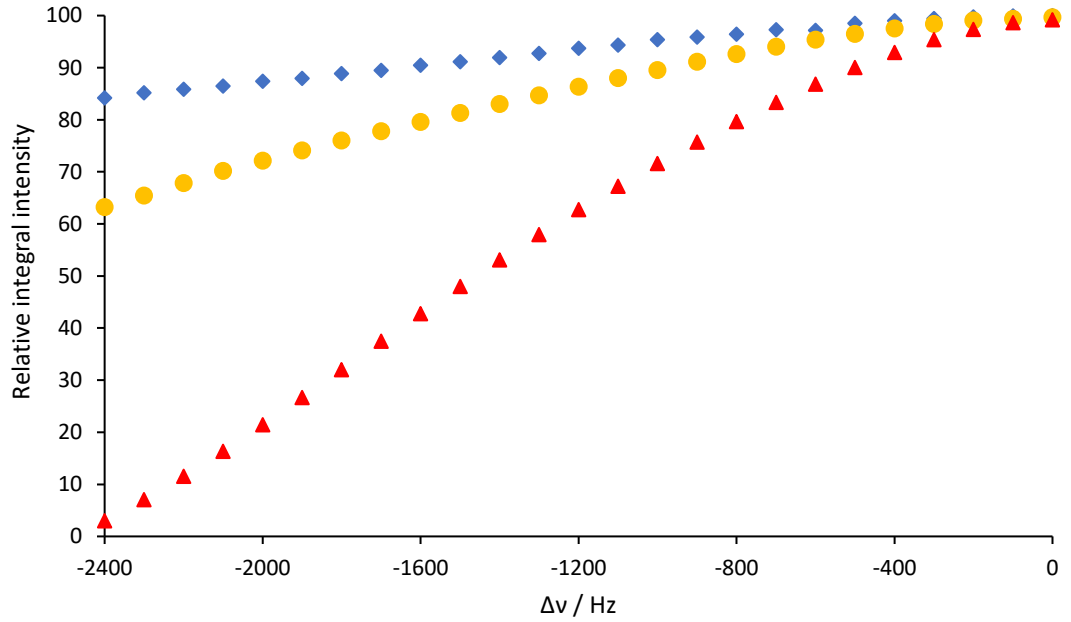

Figure 5.1: Relative integral intensity as a function of offset, Δν, from the HOD signal in doped D_2O recorded at 400 MHz with a 180° pulse length of 60 μs. The red triangles represent chunk time τ = 400 μs, orange circles are τ = 200 μs and blue diamonds are τ = 100 μs. The data has been normalised to the integral intensity of the on-resonance signal of HOD for τ = 100 μs.

As shown in Figure 5.1 the integral intensity shows negligible variation between chunk times when on resonance but as the offset increases the intensity of the NMR signal

associated with the 400 μs chunks drops rapidly when compared to the shorter τ values. There is also an observable drop in intensity for the shorter chunk times. However, this is nowhere near as severe with the intensity at 2400 Hz offset being 84 and 63% respectively for 200 and 100 μs whereas the intensity for 400 μs is at 3%. This shows that when collapsing large areas, it is essential to use short chunk times in order to avoid losing large amounts of signal. Short chunk times aren't always beneficial though as shown by Figure 5.2. In this graph the same spectra were used but the signal height is plotted instead of integral intensity.

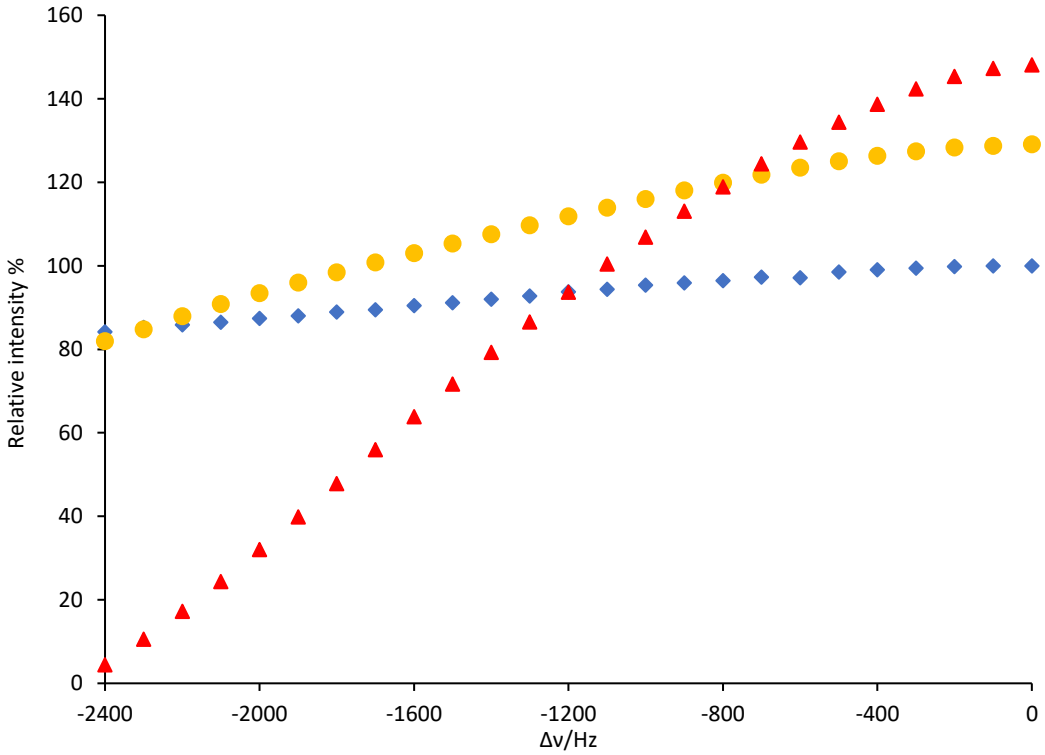

Figure 5.2: Signal height of the SHARPER signal as a function of offset. Signal height is calculated as $H(\Delta\nu) = T_2^S \times I(\Delta\nu)$ where T_2^S is the effective relaxation time of the sample. The red triangles represent chunk time τ = 400 μs, orange circles are τ = 200 μs and blue diamonds are τ = 100 μs. The data has been normalised to the integral intensity of the on-resonance signal of HOD for τ = 100 μs.

The signal height H is calculated from T_2^S which is the effective relaxation time of a nucleus during SHARPER acquistion and characterises the absorption Lorentzian line produced by Fourier transformation of the SHARPER signal of a single nucleus as shown in Equation 15.

$$S(\upsilon) = \frac{1/T_2^S}{(1/T_2^S)^2 + 4\pi^2(\nu - \nu_L)^2} \qquad (15)$$

The maximum intesity at $\nu = \nu_L$ is equal to T_2^S, where ν_L is the Larmor frequency of the SHARPER signal. The peak width at half height, $\Delta_{1/2}^S$, which is a more convenient method of comparing SHARPER peaks acquired under different conditions, is linked to T_2^S by Equation 16.

$$\Delta_{1/2}^S = (1/\pi T_2^S) \qquad (16)$$

This shows that the intensity of the Lorentzian line is therefore proportional to T_2^S and inversely proportional to $\Delta_{1/2}^S$ so, by factoring in T_2^S, the signal height can be quantified while accounting for varying spin-spin relaxation due to differences in the SHARPER experiment conditions.

Looking at Figure 5.2 it is clear that while at large offsets a shorter chunk time is desirable when the offset is small the greatest signal intensity is achieved when using longer chunk times. This is due to to the lower frequency of refocusing pulses slowing down the effective relaxation of the signal which results in taller, narrower signals and larger SNR values. This means that while shorter chunk times are much more favourable for collapsing wide spectral regions, for small regions a longer chunk time will produce optimal results.

5.2.2 Collapsing of 1-phenylethanol

Having shown the efficiency of SHARPER acquisition over a range of offsets the next step was to collapse a real spectrum. The sample chosen is 1-phenylethanol due to containing signals in a range of 6 ppm. Both the 1D ^{1}H and collapsed SHARPER spectra are shown in Figure 5.3. The spectra were both acquired on a 400 MHz spectrometer with identical parameters and the FIDs were Fourier transformed without any apodisation.

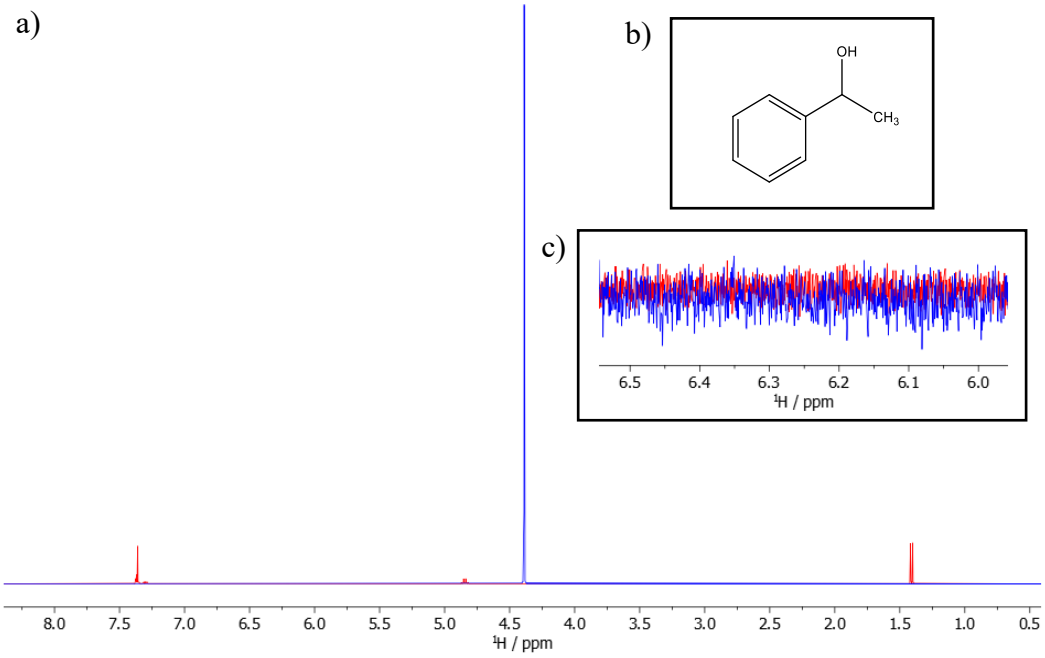

Figure 5.3: (a) 400 MHz ^{1}H (red) and SHARPER (blue) spectra of 1-phenylethanol in D_2O. SHARPER spectrum was acquired using a chunk time of 200 μs and 60 μs 180° refocusing pulses. Both the real and imaginary components of the FID were used and no apodisation was applied to either spectrum. (b) Structure of 1-phenylethanol which has nine non-exchangeable protons. (c) scaled up signal free region of (a) to show that both spectra have identical noise levels. The small amount of noise offset is due to baseline correction applied during the processing of the spectra.

The SHARPER peak in figure 2 has a linewidth of 0.11 Hz which is 5. 4 × narrower than that of the CH_3 doublet at 1.4 ppm that has a linewidth of 0.59 Hz. The SHARPER singlet is also 25 ×taller than the doublet which can be accounted for using Equation 17.

$$Intensity\ ratio = \left(\frac{9 * 2}{3}\right) * \frac{T_2^S}{T_{2eff}^{CH_3}} * collapse\ efficieny = 6 * \frac{1.372}{0.289} * 0.87 = 24.7, \qquad (17)$$

In Equation 17 the initial factor accounts for the differing number of protons in each signal and the fact that we are comparing a singlet and a doublet. The T_2 ratio quantifies the narrowing of the SHARPER acquisition and 0.87 is a factor calculated as a weighted sum of integrals of the signals of individual protons based on the distance from the carrier frequency based on the results in Figure 1. The result of 24.7 is in perfect

agreement with the observed intensity ratio which shows that all peaks have been successfully collapsed. When the SHARPER peak is integrated the result is 87.1% of the total integral of the integral of the entire reference ^{1}H spectrum. This is also in agreement with the weighted value calculated based on the number of protons and position compared to the carrier frequency when compared to the frequency profile present in Figure 1. Together the agreement between intensity ratio and integral region with that predicted using the frequency profiles of Figure 1 demonstrate that the collapsing efficiency of the SHARPER acquisition can be effectively measured and accounted for when collapsing a broad spectral region.

Further improvements to the SNR were achieved using the previously described processing techniques of removing the imaginary component of the FID and utilising a matched filter; the latter favoured noise suppression in the 1D spectrum. The initial gain from removing the imaginary component was a factor of 1.41 and with line broadening of 0.11 Hz to the SHARPER singlet and 0.59 Hz to the ^{1}H spectrum a 11.4 ×higher SNR was achieved. This large improvement is due to the magnetic inhomogeneity of the spectrometer impacting the 1D SNR while the SHARPER singlet is unaffected due to the self-compensating nature of SHARPER acquisition.

5.2.3 Additional power deposition considerations

As previosuly mentioned the use of multiple high power pulses in sequence risks crossing the safe power limits for probes and cryoprobes, however, this can be avoided by using longer but less powerful 180° pulses during the acquisition. An additional method which will be addressed here is to reduce the flip angle, α, of the spin echo pulses. As Figure 5.4 shows this will reduce the signal recovery which scales with $\sin(\alpha/2)$ for a train of spin echoes over a $1/\tau$ Hz frequency range by 29% when comparing $\alpha = 90°$ to $\alpha = 180°$,[79,80] resulting in lower integral intensities for the SHARPER peak.

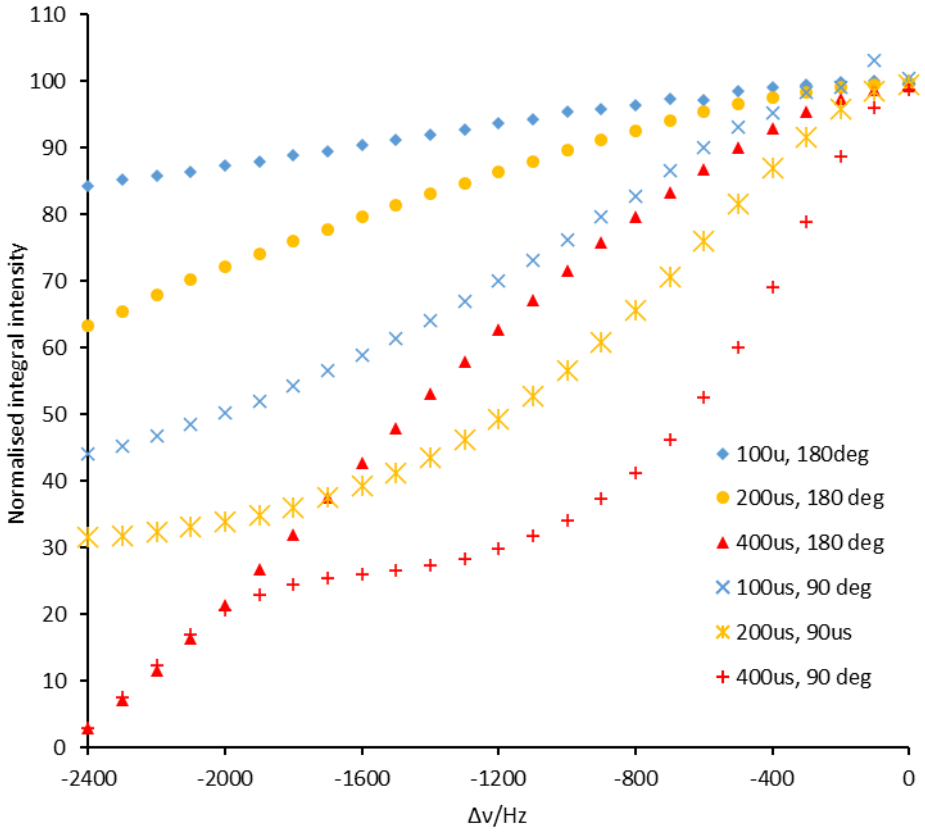

Figure 5.4: Relative integral intensity as a function of offset, Δν, from the HOD signal in doped D_2O recorded at 400 MHz with additional data points from experiments with 90° pulses replacing the 180° spin echo pulses. The data has been normalised to the integral intensity of the on-resonance signal of HOD for the 180° τ = 100 μs dataset.

This loss of integral intensity when using shorter pulses is a drawback but is largely compensated for by the narrowing of the SHARPER singlet. There are two reasons for the narrowing of the peak, and both are related to T_2^S. Firstly, T_2^S is increased by the larger ratio of acquisition chunk time *vs* pulse time, secondly spin lattice relaxation contributes towards T_2^S during 90° pulses which leads to a further increase in T_2^S for molecules that lie outside the extreme narrowing limit ($T_1 > T_2$)[81]. These factors together greatly narrow the peak and mean that 90° pulses actually produce more intense peaks when adjusted for T_2^S as shown in Figure 5.5.

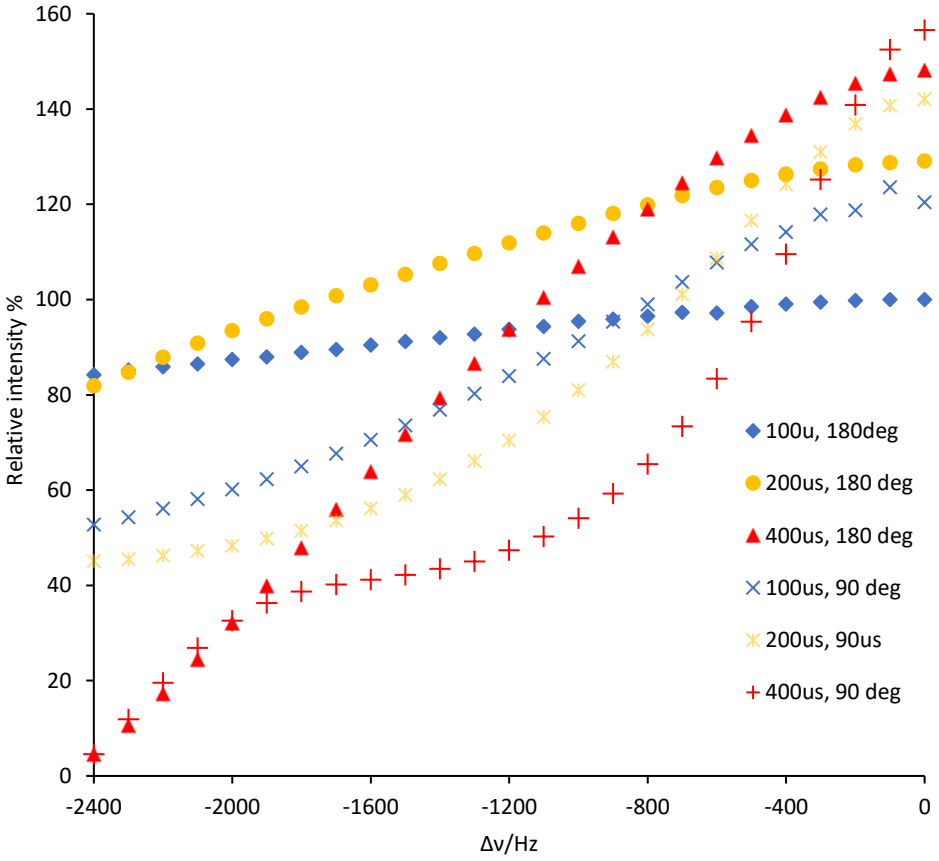

Figure 5.5: Signal height of the SHARPER signal as a function of offset. Signal height is calculated as $H(\Delta\nu) = T_2^S \times I(\Delta\nu)$ where T_2^S is the effective relaxation time of the sample. The data has been normalised to the integral intensity of the on-resonance signal of HOD for the 180° τ = 100 μs dataset.

These graphs show that the power deposition can be halved while maintaining most of the integral intensity and actually increasing signal intensity over small frequency ranges. This means that 90° pulses can be an effective substitute for systems spanning a smaller frequency range if power deposition is a concern. However, for wider ranges 180° pulses are still superior in terms of integral and signal intensity.

5.2.4 Selecting signals to be collapsed

While the previous section has shown that very broad frequency ranges can be selected and collapsed, it may not always be desirable to collapse an entire region as other signals could interfere. In DOSY measurements this would include signals from the solvent or labile protons in the sample that may exchange with the solvent or water.

These signals would contribute to the diffusion coefficient that is measured from a SHARPER peak and give an inaccurate value, so it is important to avoid them.

An example system that has undesirable signals is cyclosporine in benzene-d_6 ($C_{62}H_{111}N_{11}O_1$, M_w = 1,202.61 g mol^{-1}). The signals in question are the weak H_2O/OH signals at 0.55 ppm due to a small amount of H_2O present that is in slow exchange with the OH and four NH protons, and a very intense C_6HD_5 signal at 7.2 ppm. Normally, the carrier frequency would be set to that of the largest signal to be suppressed to achieve its most effective pre-saturation, however this is not possible for SHARPER as the carrier frequency needs to be placed in the centre of the collapsed region, in this case at 3.27 ppm. This doesn't prevent the off resonance C_6HD_5 and OH signals from being suppressed as it is possible to suppress off- resonance signals using low power rectangular pulses[82]. This approach uses ~20-80 ms phase-ramped, low power rectangular pulses applied in a loop with the pulse length adjusted to allow a $2n\pi$ (n is an integer) rotation for the off-resonance signal. Here we have introduced a numerical solution that allows the technique to be applied to multiple signal suppression sites enabling the signals to undergo close to a multiple number of full rotations.

In the rotating frame, off resonance signals precess around a magnetic field according to Equation 18,

$$\Delta\nu = \frac{\gamma \Delta B}{2\pi} \qquad (18)$$

where, ΔB is the residual magnetic field and $\Delta\nu$ is the rotating frame frequency. The angle of precession around the field of an off-resonance signal during a pulse length τ is calculated as

$$\theta = \gamma \Delta B \tau \qquad (19)$$

Hence, the number of rotations (x) of this signal is given as

$$\theta = 2\pi x \qquad (20)$$

Substituting and solving for $\gamma \Delta B$ gives

$$\gamma \Delta B = \frac{2\pi x}{\tau} \qquad (21)$$

Substituting Equation 4 into Equation 7 and taking x as an absolute value gives

$$x = \tau\, \Delta\nu \qquad (22)$$

For a single off-resonance signal, x and τ can be calculated exactly, while for multiple signal suppression, the x and $\Delta\nu$ components of Equation 22 can be generalised as vectors $\mathbf{x}$ and $\boldsymbol{\Delta\nu}$.

$$\mathbf{x} = \tau\, \boldsymbol{\Delta\nu} \quad \text{where} \quad \mathbf{x}, \boldsymbol{\Delta\nu} = \begin{pmatrix} x_1 \\ x_2 \\ \vdots \\ x_n \end{pmatrix}, \begin{pmatrix} \Delta\nu_1 \\ \Delta\nu_2 \\ \vdots \\ \Delta\nu_n \end{pmatrix} \qquad (23)$$

For effective presaturation of multiple signals, an integer number of rotations is required for each component ($x_n \in \mathbb{Z}$). The distance to nearest integer (DNI) function (Equation 24) can be applied to the vector to give the total distance of all components of the vector from an integer as a single value, referred to here as the "DNI norm" $\|\mathbf{x}\|_{DNI}$ (Equation 25). Minimising this norm by varying τ gives an optimised pulse length, which will often be very close to integer rotations in all components.

$$DNI(x) = \min\{|x - m| \mid m \in \mathbb{Z}\} \qquad (24)$$

$$\|\mathbf{x}\|_{DNI} = \sum_i DNI(x_i) \qquad (25)$$

The optimal pulse-length τ_{opt} is then given by Equation 26.

$$\tau_{opt} = \min\|\tau\, \boldsymbol{\Delta\nu}\|_{DNI} \qquad (26)$$

Because the DNI norm surface of $\boldsymbol{\Delta\nu}$ is rough, minimisation using iterative methods leads to many local minima, which often correspond to highly suboptimal presaturation parameters. To combat this a brute-force method was employed to search for minima within a small range of a starting pulse-length (± 20%). Figure 5.6 shows a simulated DNI norm for three offset frequencies $\boldsymbol{\Delta\nu} = (573, -573, -747)^T$ as a function of pulse-length highlighting the difficulty of iterative minimisation. This corresponds to

the resonances of tetrahydrofuran and water in $CDCl_3$ at 600MHz (2256 Hz, 1110 Hz, 936 Hz) when the carrier frequency is set at 1683 Hz, directly between the two tetrahydrofuran resonances.

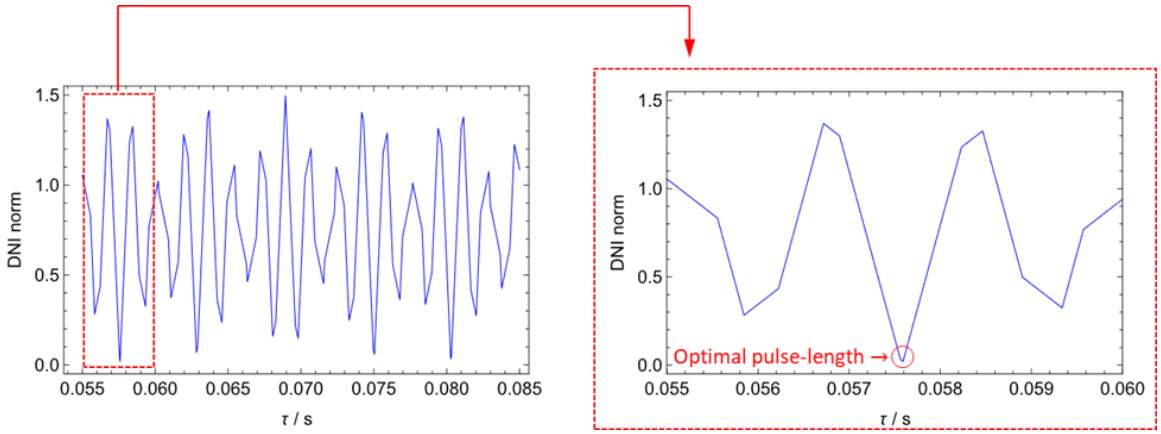

Figure 5.6: Left) simulated DNI norm $\|\mathbf{x}\|_{DNI}$ (where the vector x is equal to $\boldsymbol{\tau}$ **(573,-573,-747)**^{T} **)** as a function of pulse-length $\boldsymbol{\tau}$ between 55 ms and 85 ms. Right) simulated DNI norm for the same vector between 55 ms and 60 ms, highlighting the minimum.

In cases where the carrier frequency is not critical (e.g. collapsing SHARPER spectra), the presaturation can be further optimised by redefining the vector $\boldsymbol{\Delta\nu}$ as the difference between the absolute frequencies $\boldsymbol{\nu}$ and the carrier frequency ν_0. Minimisation of the DNI norm with respect to both τ and ν_0 provides significantly improved presaturation and is suitable for experiments in which the exact value of ν_0 is not critical. In these cases, the optimal parameters are given by Equation 27.

$$\tau_{opt}\,, \nu_{0\,opt} = \min\|\tau\,(\boldsymbol{\nu} - \nu_0)\|_{DNI} \qquad (27)$$

Minimisation only with respect to τ and ν_0 was implemented as a package written in the Julia programming language.

When implementing the calculated parameters into TopSpin, for one off resonance signals the offset can be inputted in the foreground using the spoffs[x] parameter. For multiple suppression sites, a phase ramp is imposed on a rectangular shape of optimal duration, $\boldsymbol{\tau}$, using $\boldsymbol{\Delta\nu}$ frequencies.

When simulated in ShapeTool for pulse length 68936 µs and $\gamma B_1/2\pi$ = 21.76 Hz (= 3*1/4*pw_{90}), the profile shown in Figure 5.7 was obtained for a three-site suppression.

Note that changing the power level of the presaturation pulse has minimal influence on the level of suppression, stronger irradiation affects a wider range of signals.

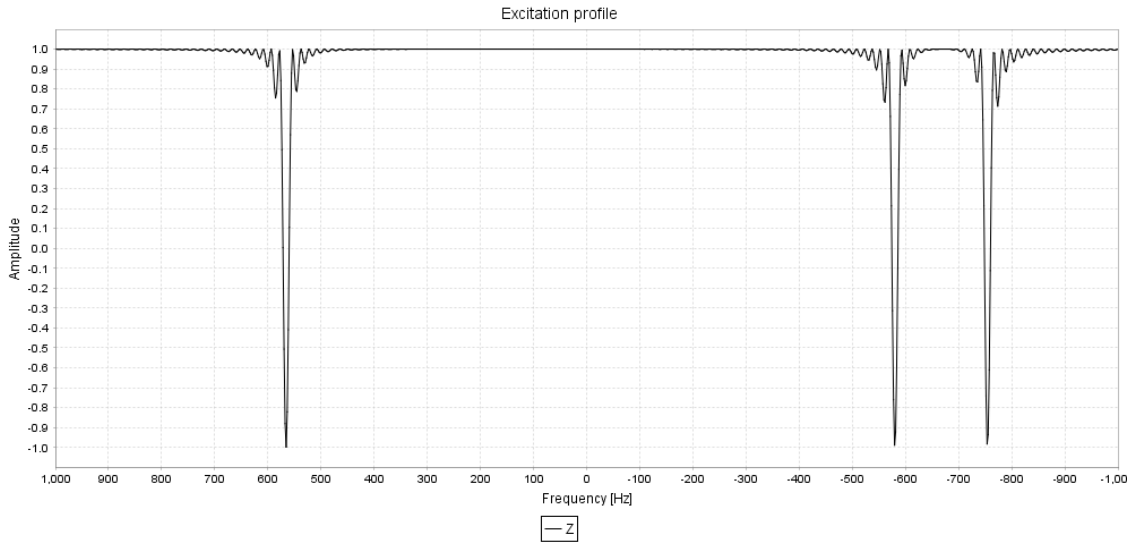

Figure 5.7: Inversion profile using $\gamma B_1/2\pi$ = 21.76 Hz at 565.73 -580.27 -754.27 Hz relative to o1=1690.27 Hz. The half width of individual profiles is ~ 9Hz.

The result of using this method to selectively supress the C_6HD_5 and H_2O/OH peaks is shown below in Figure 5.8. Low power ^{13}C decoupling was also utilised during the pre-saturation period to remove ^{13}C satellites of C_6HD_5 that were also intense due to the large height of the parent signal.

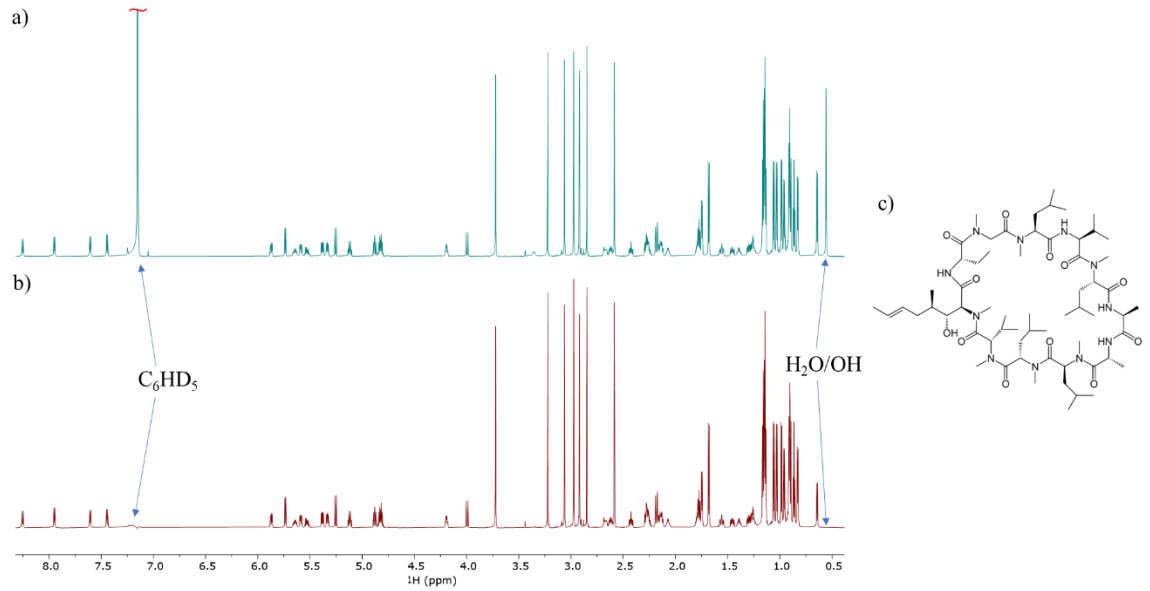

Figure 5.8: a) 1D ^{1}H spectrum of cyclosporine, b) 1D ^{1}H spectrum with selective saturation of the H_2O/OH, C_6HD_5 and C_6HD_5 ^{13}C satellite protons. The parameters for this experiment are given in the experimental c) The structure of cyclosporine.

The pulse sequence used to produce the spectrum in Figure 5.8b is presented in Figure 5.9

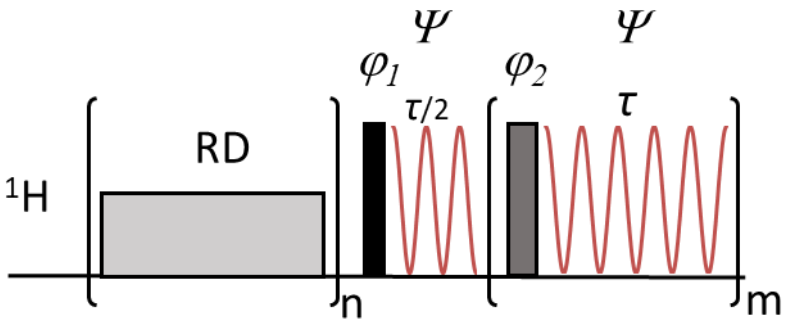

Figure 5.9: Pulse sequence of the non-selective SHARPER experiment with a pre-saturation module used to obtain the spectrum in Figure 5.8b. The black rectangle represents a 90° non-selective pulse, while a reduced power grey pulse of the SHARPER module can have arbitrary flip angle (180° or 90° recommended). τ is the acquisition chunk time. The following phases were used: φ_1=2x, 2(-x); φ_2=y,-y; Ψ = 2x, 2(-x).

5.2.5 BSPE-SHARPER

While the presaturation sequence effectively suppresses several undesirable signals there is still the potential for interference arising from exchange with the NH protons in cyclosporine and water. These are the four signals centred at 8 ppm in Figure 8, which means that the use of a perfect echo containing short 180° ReBurp pulses surrounded by PFGs rather than the non-selective 180° spin echo pulses can be used to efficiently select the remaining 106 protons. This technique is termed Band Selective Perfect Echo (BSPE) and has a signal selection efficiency of 90% as shown in Figure 5.10.

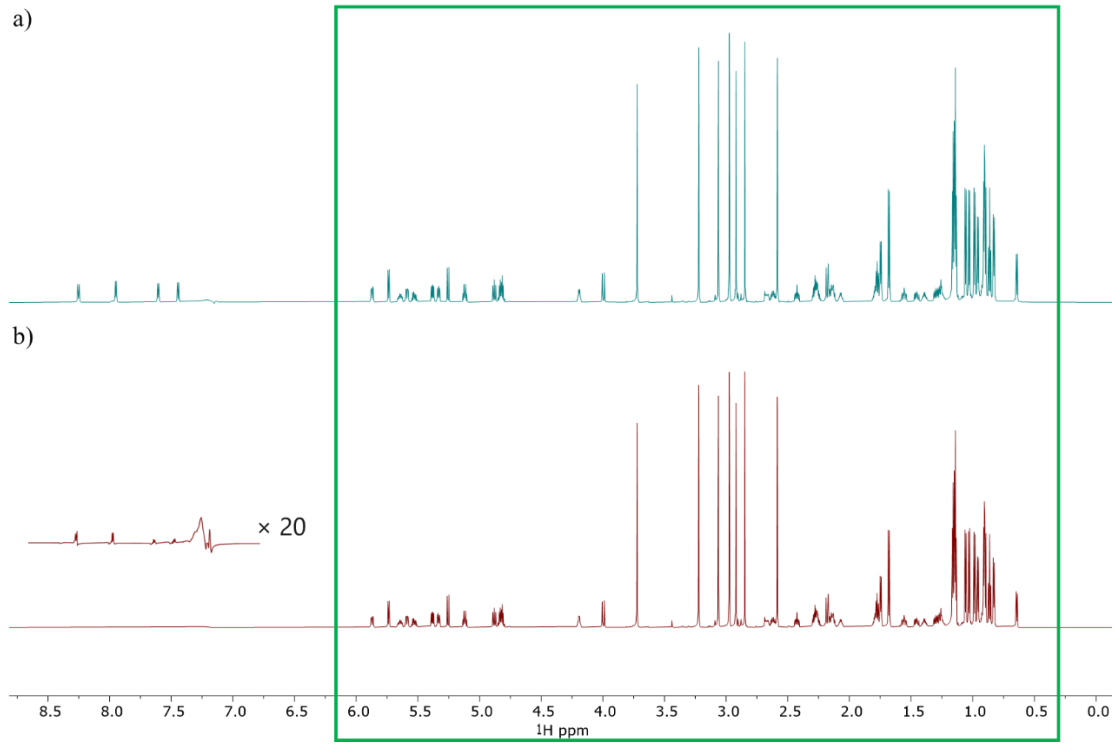

Figure 5.10: a) 1D ^{1}H spectrum with selective saturation of the H_2O/OH, C_6HD_5 and C_6HD_5 ^{13}C satellite protons. b) 1D ^{1}H spectrum with selective saturation of the H_2O/OH, C_6HD_5 and C_6HD_5 ^{13}C satellite protons and additional band selection within the green box. The NH signals have been expanded 20 times to show the selection efficiency. The parameters for this experiment are given in the experimental.

When the SHARPER acquisition block is added to the BSPE experiment the efficiency of signal recovery is 97% for 180° pulses and 75% for 90° pulses relative to the BSPE spectrum shown in Figure 5.10b. To compare these results Figure 5.11 shows an

overlay of the BSPE and both 90° and 180° BSPE-SHARPER spectra processed to remove the imaginary components of the SHARPER FID and matched exponential filters.

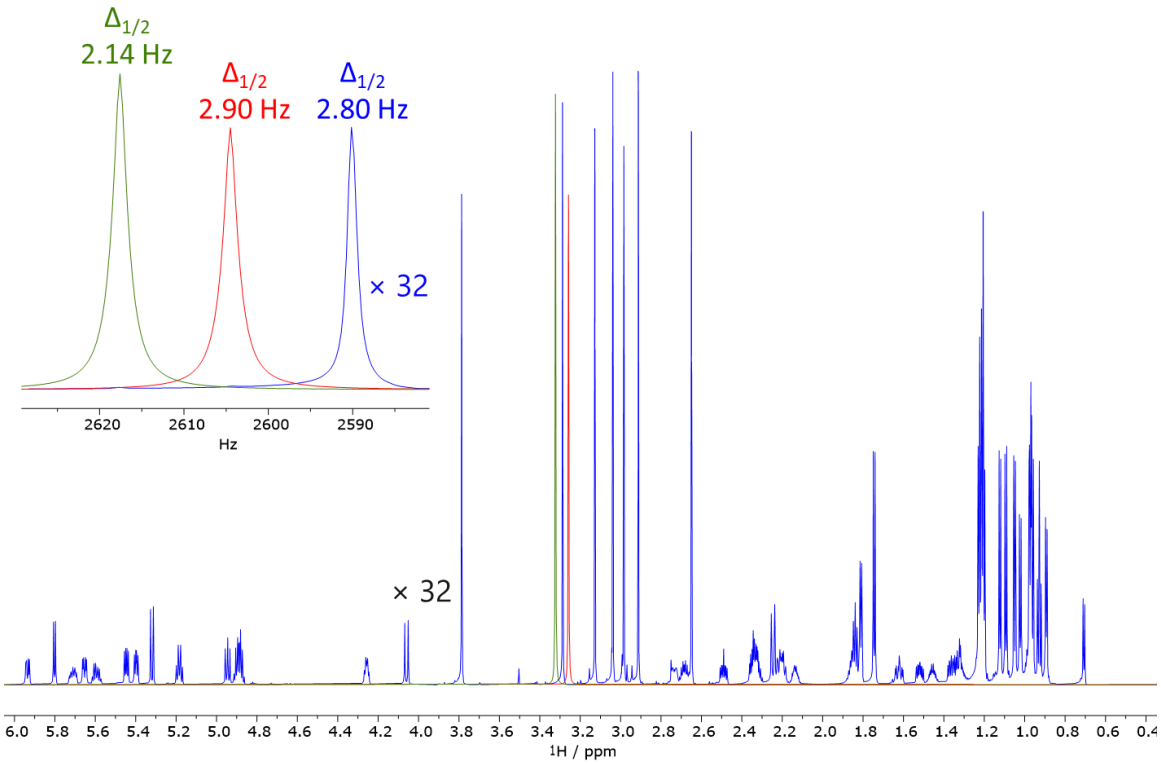

Figure 5.11: Overlay of a BSPE ^{1}H spectrum of cyclosporine (blue) and two BSPE-SHARPER spectra acquired using 90° (green) and 180° (red) ^{1}H spin echo pulses. The height of the BSPE spectrum has been increased by a factor of 32 and the 90° spectrum has been shifted by -50 Hz to aid visibility. The inset shows a comparison of the two SHARPER singlets and the NCH_3 singlet found at 3.72 ppm. All spectra have been processed using matched exponential filters, so the stated $\Delta_{1/2}$ values are double the value of the original linewidth.

The pulse sequence used to produce the BSPE-SHARPER spectra shown in Figure 5.11 is presented below in Figure 5.12. Removal of the SHARPER acquisition block produces the BSPE experiment used to obtain the blue spectrum in Figure 5.11. The requirement for the BSPE spectrum to be scaled up 32 times to enable the N-CH_3 singlets to match the BSPE-SHARPER singlets in intensity shows a 96-fold intensity increase of the SHARPER signal relative to a hypothetical singlet proton signal from the 1D spectrum. The inset in Figure 5.11 shows that the singlet obtained using 90°

pulses is the narrowest and highest which compensates for the greater loss in integral intensity when compared to the 180° peak.

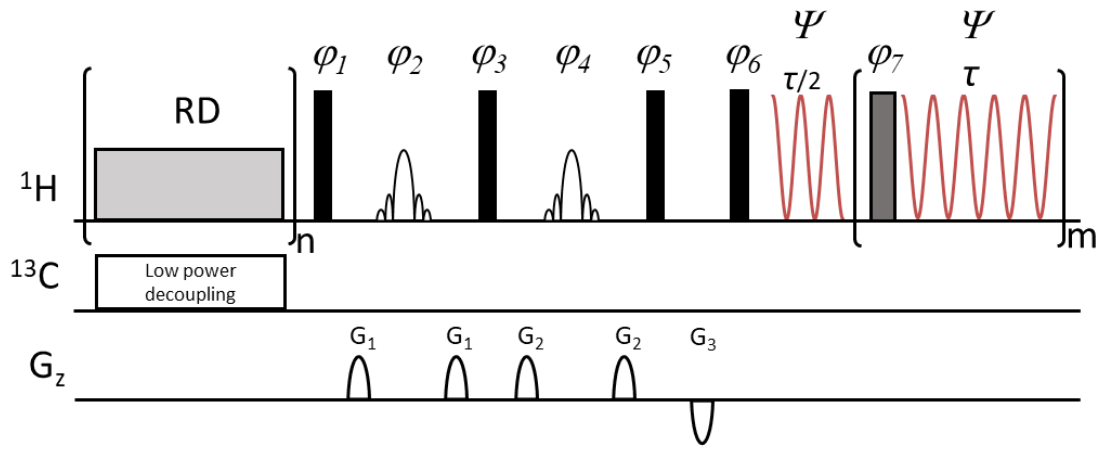

Figure 5.12: Pulse sequence of BSPE-SHARPER with a presaturation module and optional z-filter (pulses φ_5, G_3 and φ_6). Black filled rectangles represent 90° non-selective pulses, while a reduced power grey pulse of the SHARPER module can have arbitrary flip angle (180° or 90° recommended). 180° band selective ReBurp pulses are applied in the middle of the BSPE. The delays between pulses are limited to PFG and the recovery delay. τ is the acquisition chunk time. The phases of the BSPE-SHARPER experiment are: φ_1=4x, 4(-x); φ_2=8y, 8(-y); φ_3=2y, 2(-y); φ_4=8y, 8(-y); φ_5=x φ_6=-x, φ_7=y, -y and Ψ = 4x, 4(-x).

5.3 SHARPER-DOSY

Having shown that the SHARPER acquisition module can be used to collapse spectra and be combined with various selection methods the next step was to add the DOSY module[25,83] between the signal presaturation and BSPE blocks. The resulting sequence is shown below in Figure 5.13.

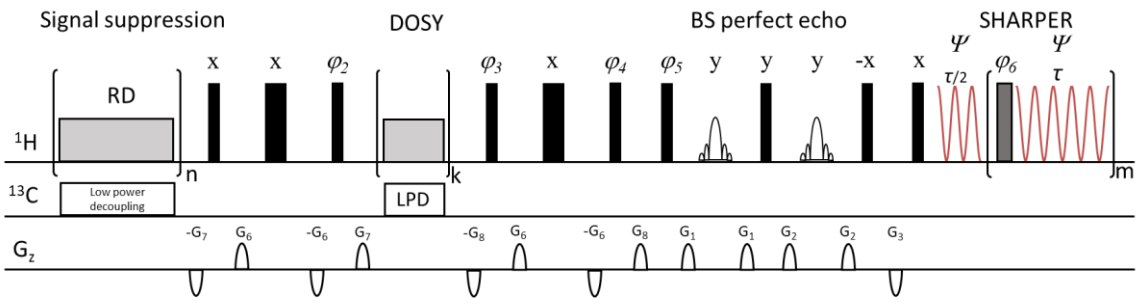

Figure 5.13: Pulse sequence of the SHARPER-DOSY experiment with optional

presaturation module, band-selective perfect echo and a z-filter. Black narrow and wide filled rectangles represent 90° and 180° non-selective pulses, while a reduced power grey pulse of the SHARPER module can have arbitrary flip angle. 180° band selective ReBurp pulses are applied in the middle of the BSPE. The delays between pulses are limited to PFG and the recovery delay. τ is the acquisition chunk time, n,m,k represent the number of loops. The phases are: φ_2=2x, 2(-x); φ_3=4x, 4(-x); φ_4=2(x,-x), 2(-x, x); φ_5=4x, 4(-x); φ_{10}= 8y, 8(-y) Ψ = x, 2(-x), x, -x, 2x,-x.The gradients strength as a % of the total value (66.4 G/cm) are G_1 = 7%, G_2 = 5%, G_3 = -12%, G_6 = 5 to 95%, G_7 = -17.13%, G_8 = -13.17%.

This sequence was initially tested on a sample of cyclosporine with both 90° and 180° pulses then compared to a standard DOSY experiment to determine the accuracy of the diffusion coefficient obtained from the SHARPER singlet. The results from this are shown in Figure 5.14.

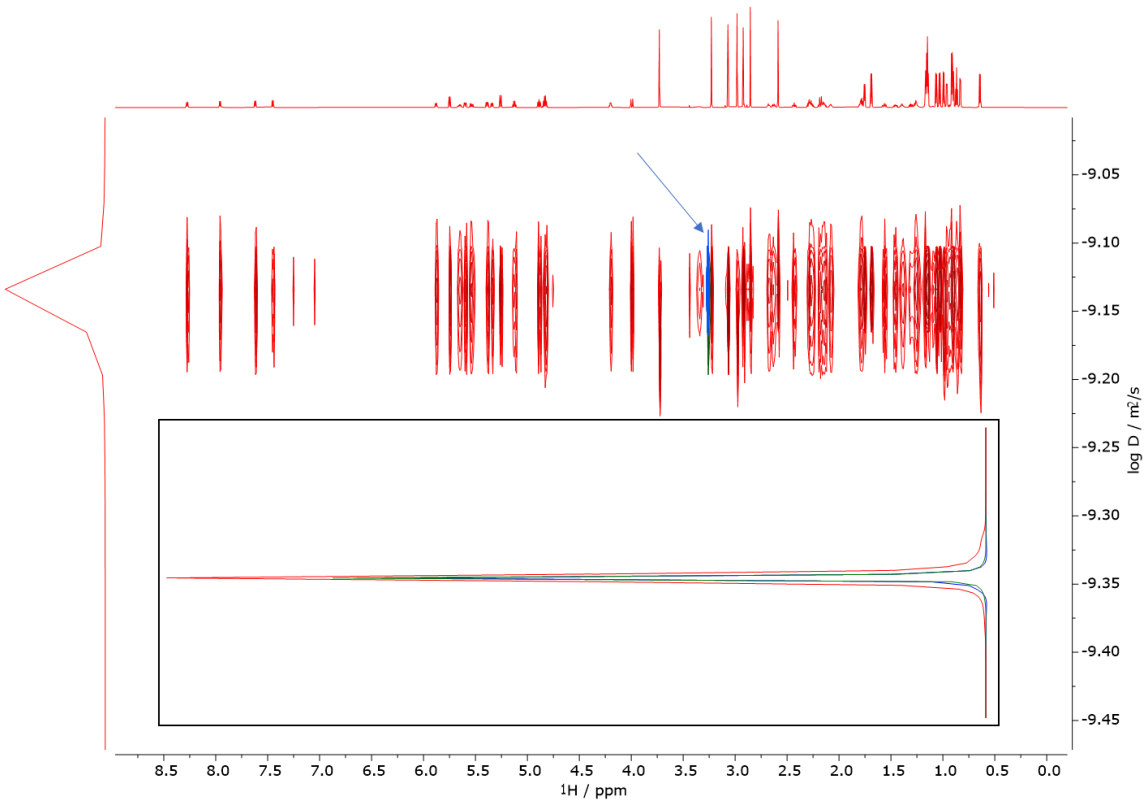

Figure 5.14: DOSY spectrum of cyclosporine (red) overlaid with the BSPE-DOSY-SHARPER spectra of cyclosporine acquired using 90°(green) and 180°(blue) spin-echo pulses. The blue arrow indicates the BSPE-DOSY-SHARPER peaks. The inset box

shows an overlay of the projection of each spectrum in F_1. The DOSY spectra and its projection were both scaled up 32 times to achieve similar signal height for all spectra.

The familiar smearing of signals in the F_1 dimension is observed as is common for DOSY spectra but of note is the narrower profile of the SHARPER-DOSY spectra, this is illustrated more clearly by the inset of Figure 5.14 but the alignment of the F_1 projections from each experiment confirm the accuracy of SHARPER-DOSY for measuring diffusion coefficients.

5.3.1 SHARPER-DOSY using µg quantities of sample.

Based on the incredible signal enhancement observed from DOSY-SHARPER it was theorised that the sequence could be used to determine diffusion coefficients of samples on a micromolar scale. In order to test this, a sample of sodium cholate ($C_{24}H_{39}O_5Na$, M_w = 430.55 g mol^{-1}) was used due to it being a convenient example of a medium size organic molecule. 1.3 µg of the compound was dissolved in 0.55 mL of D_2O producing a sample with a concentration of 5.5 µM. The structure and spectrum of sodium cholate obtained from a 7.7 mM sample are shown below in Figure 5.15 and illustrate another benefit of the compound as a model system.

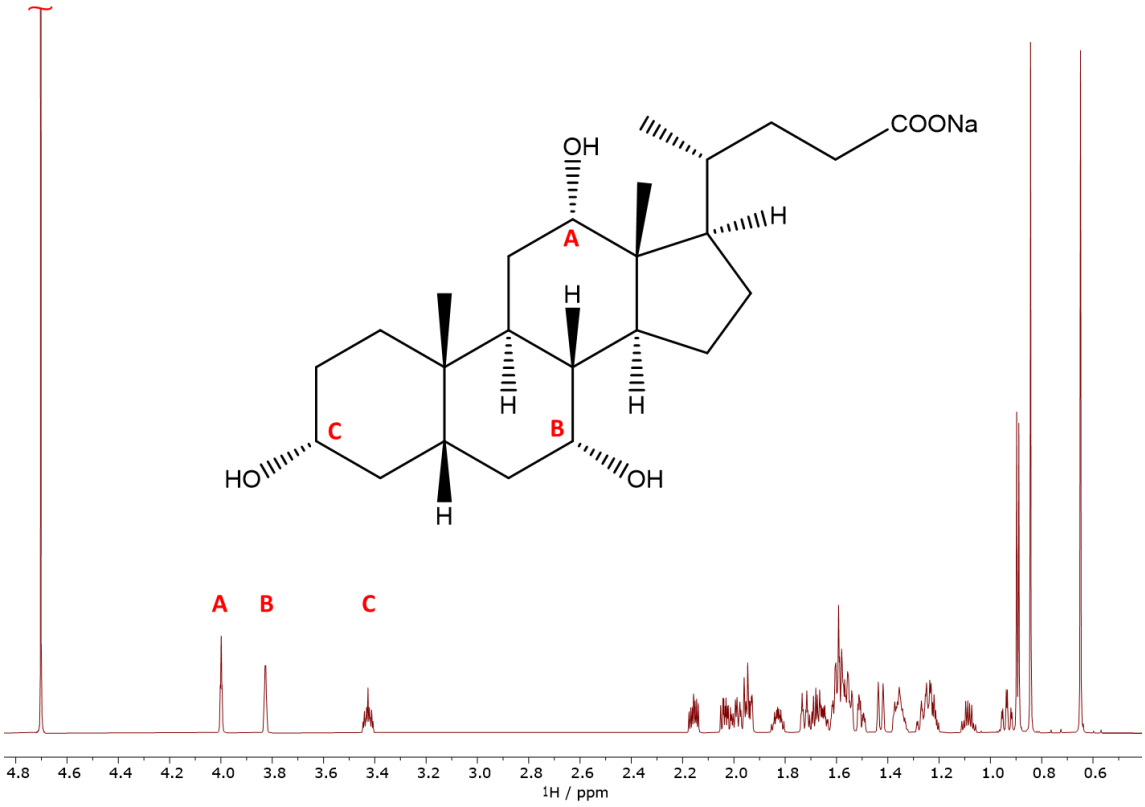

Figure 5.15: Molecular structure and spectra of a 7.7 mM sample of sodium cholate in D_2O. The red letters indicate de-shielded HO-CH protons and the position of their signals in the spectrum. The H_2O solvent peak has been cut off to show the appropriate sodium cholate peaks.

The benefit of sodium cholate demonstrated in Figure 14 is the small range of signals present in the spectrum. Except for three de-shielded HO-CH protons, all the H nuclei in the system resonate in a frequency range of ± 0.75 ppm which means that by using presaturation and BSPE techniques only a very small frequency range needs to be collapsed. This allows longer chunk times to be used which increases the signal recovery of the SHARPER collapse technique. The chunk length used to collapse this region in the 5.5 µM sample was τ = 448 µs achieving > 80% signal recovery from the integral area of the whole region. However, when this spectrum was overlaid with that of a 1D BSPE spectrum and the heights were scaled to account for differing numbers of scales it was observed that the SHARPER signal was more intense than the CH_3 singlets by a factor of 22 times. This is double the increase expected based on the number of protons present in the system and as such cannot fully be accounted for by the narrowing of the SHARPER signal. Upon further examination of the spectra several

signals were identified that were not part of the spectrum of sodium cholate, most prominently a doublet present at 1.28 ppm. Repeating both the SHARPER and BSPE experiments on a blank sample of D_2O it was identified that these signals are present due to solvent impurities that are of a comparable intensity to that of the micromolar sodium cholate. These spectra are shown in Figure 5.16.

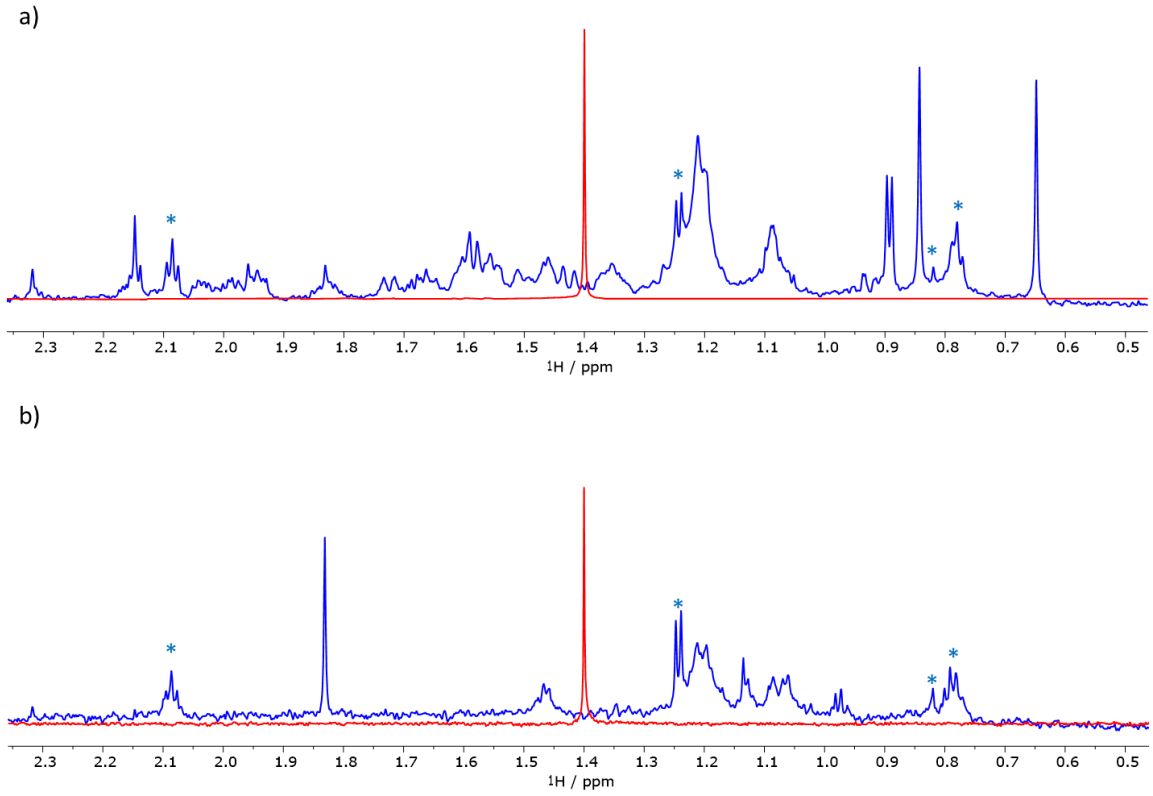

Figure 5.16: Overlay of 128 scan 1D 1H (blue) and 8 scan BSPE-SHARPER spectra (red) of a) 5.5µM sodium cholate and b) D_2O. The peaks present in both spectra are indicated by asterisk. The 1D spectra have been scaled up by a factor of 16.

These solvent impurities also account for the increased intensity of the SHARPER spectrum which prevents accurate determination of the diffusion coefficient from a SHARPER-DOSY spectrum. This is because the solvent impurities will contribute to the SHARPER peak and will spread out the signals in the DOSY dimension giving a significant contribution from compounds with a range of sizes. Figure 5.17 illustrates how these extra signals will be collapsed into a single central peak and the range of diffusion coefficients that would contribute to the final value.

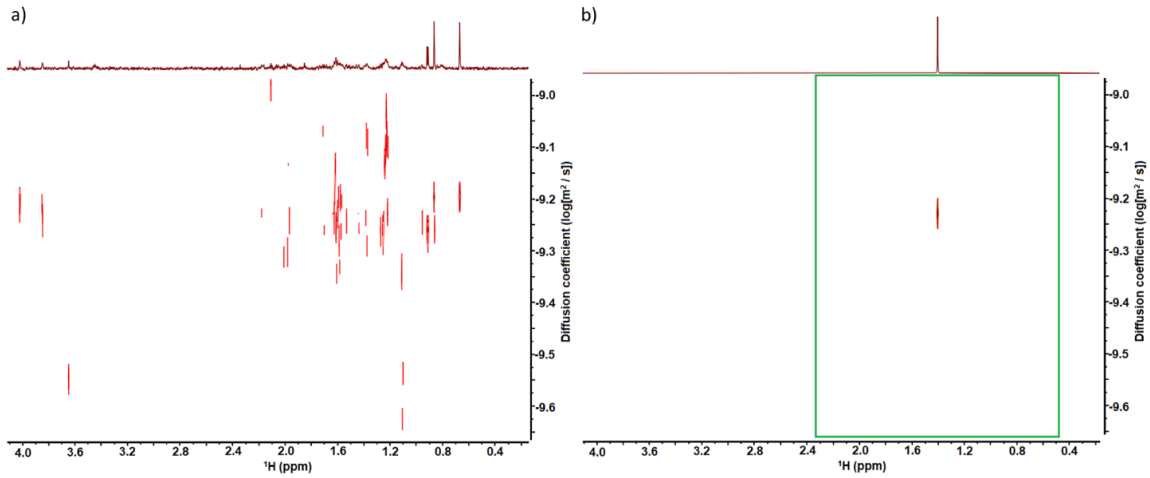

Figure 5.17: a) DOSY spectrum of 5.5 µM sodium cholate in 99.9% D_2O, b) BSPE-DOSY-SHARPER spectrum of the same sample. The green box indicates the region selected by the band selective technique.

The solution used to counter this problem is to simply record two datasets, one on the cholate sample and one on a blank D_2O sample and subtract the D_2O spectra from the original spectrum prior to DOSY processing. This requires the use of the same D_2O, but the processing is simplified by an AU program which has been written to automate the subtraction. However, as the sample was prepared by multiple dilutions, two ampules of D_2O were pooled to produce a single "master" solvent which could be used to accurately record a background spectrum. The result is shown in Figure 5.18 and the overlay of F_1 projections of four DOSY spectra shows the broadness of the original peak and the narrowing effect of subtracting the solvent spectrum.

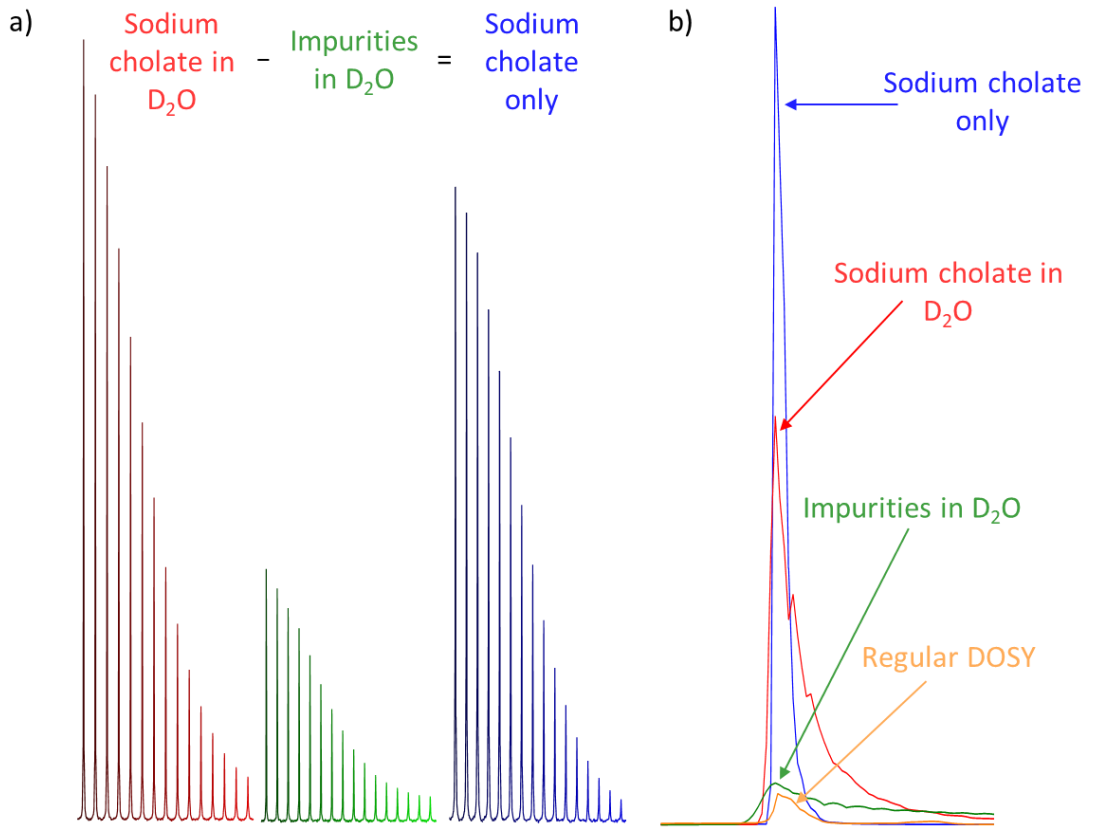

Figure 5.18: a) SHARPER-DOSY signals from 32 scan spectra of 5.5 µM sodium cholate, D_2O and the difference acquired by increasing the strength of the pulsed field gradient. b) Overlay of projections of the SHARPER-DOSY spectrum of 5.5 µM sodium cholate in D_2O, the reference D_2O spectrum and the calculated difference and a standard DOSY spectrum of 5.5 µM sodium cholate in D_2O.

The broadness of the original spectrum is due to the differing sized molecules contributing to the diffusion coefficient whereas the very narrow peak of the difference spectrum is dominated by the three CH_3 sodium cholate signals. Given the recording time of 40 minutes per SHARPER-DOSY spectrum a total time of 80 minutes was required to acquire the spectra to determine the diffusion coefficient of a medium sized molecule at a concentration of 5.5 µM on an 800 MHz cryoprobe spectrometer. The SNR ratio in these SHARPER-DOSY spectra is excellent, meaning that 1.3 µg does not represent the limit of detection, and hundreds of nanograms would be sufficient – a remarkable achievement.

5.3.2 Analysis of diffusion coefficients

Having produced a difference spectrum from which a diffusion coefficient could be obtained the next step was to determine the most accurate method of determining the diffusion coefficient value. The two methods chosen were analysis based on integration of spectra and integration of time domain points.

The spectra of the sodium cholate shown in Figures 17 and 18 are based on the time domain points for two samples of sodium cholate, one at 7.7 mM concentration and the other at 5.5 μM. Note that the time domain points of the dilute sample in Figure 5.19 were produced by using eight scans only.

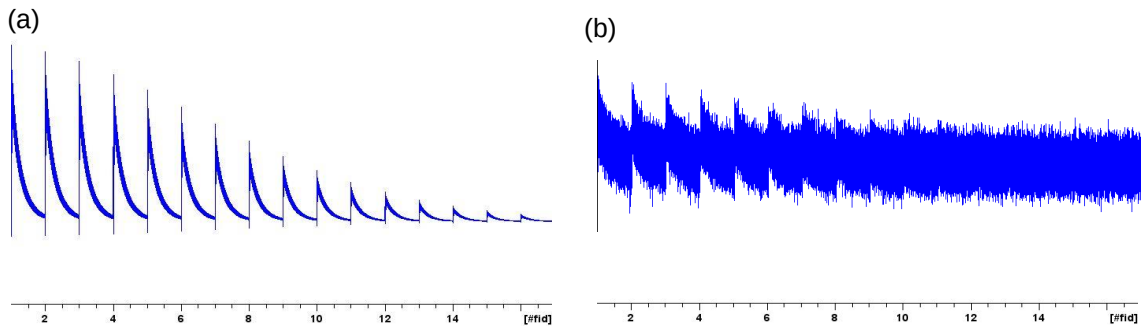

Figure 5.19: Time domain data acquired of 16 DOSY spectra acquired using increasing gradient strength of a) 7.7 mM sodium cholate and b) 5.5 μM sodium cholate after subtraction of the D_2O reference spectrum. The figures are not to scale.

To process the spectra, the 16k real points were zero filled to 128k points and a matched exponential line broadening of 1.1 Hz and 0.78 Hz was applied to the concentrated and dilute sample, respectively. Following this the 15 1D DOSY spectra that had been acquired were fitted using Equation 28 where I is the integral intensity, either of the SHARPER spectra or the time domain points, $\gamma_{^1H}$ is the gyromagnetic ratio of proton, g is the gradient amplitude, δ is the gradient length, Δ is the diffusion delay and D is the diffusion coefficient.

$$\ln(I) = (\gamma_{^1H} g\delta)^2 \left(\Delta - \frac{\delta}{3}\right) D \qquad (28)$$

The spectra from the 7.7 mM sample had SNR ranging from from 149,311:1 (1st spectrum) to 9636:1 (15th spectrum) and were integrated over the region of ± 2400 Hz

to include the base of the SHARPER peak while the spectra from the 5.5 μM sample had SNR ranging from 135:1 (1st spectrum) to 6:1 (15th spectrum) and were integrated over the region of ± 16 Hz to include the base of the SHARPER peak. The 16th spectrum was not included due to poor SNR observed for the dilute sample.

For the time domain data, NMRglue was used to extract the data and up to 16k points of real data that was integrated by summing the total intensity without any pre-processing. The reduced number of data points used for up to 1.26 T_2^S was chosen as this is where the maximum SNR of the time domain data is obtained[84]. This value fell at 6000 and 8000 points for the 7.7 mM and 5.5 μM samples respectively. The resulting diffusion coefficients are presented below in Table 5.1.

Table 5.1: Diffusion coefficient of sodium cholate calculated at two different concentrations and using two methods of evaluation.

Concentration	Diffusion coefficient $D \times 10^9$ /m^{2}s^{-1}		
	Spectra integrated	Time domain integrated	
	Matched exponential line-broadening + FT	0-16,384 real points	Up to 1.26 T_2^S
7.7 mM	0.353 ± 0.001	0.353 ± 0.001	0.354 ± 0.001
5.5 μM	0.407 ± 0.003	0.407 ± 0.003	0.387 ± 0.003

This data shows that for the 7.7 mM sample all methods produced the same diffusion coefficient of 0.353 ± 0.001 × 10^{-9} /m^{2}s^{-1} while the value for the lower concentration 5.5 μM sample varies with the method chosen. Integrating the spectra and all the time domain points gave the same value of 0.407 ± 0.003 × 10^{-9} /m^{2}s^{-1} while only integrating time domain points up to 1.26 T_2^S gave a smaller value of 0.387 ± 0.003 × 10^{-9} /m^{2}s^{-}. To determine the true diffusion coefficient of the sample at each concentration data reported in the literature[85,86] were analysed. The data showed a linear dependency of diffusion coefficient on concentration over a range of 0.96 to 54 mM in H_2O, which

was adjusted to match D_2O used in our experiments using the relationship[87] $D_{D_2O} = \frac{D_{H_2O}}{1.25}$ to give Equation 29.

$$D_A = -(0.0036 \pm 0.002)c + 0.356 \pm 0.006 \quad (29)$$

This equation was used to calculate a diffusion coefficient for each concentration and then was compared to the results from Table 5.1. The outcome is presented in Table 5.2.

Table 5.2: Comparison of experimentally determined diffusion coefficients with those calculated using Equation 29.

Concentration	$D_A \times 10^9$ /m^{2}s^{-1} All time domain points, or spectra	$D_B \times 10^9$ /m^{2}s^{-1} Time domain points up to 1.26 T_2^S	$D_C \times 10^9$ /m^{2}s^{-1} Based on Eqn. 29
7.7 mM	0.353 ± 0.001	0.353 ± 0.001	0.333 ± 0.007
5.5 μM	0.407 ± 0.003	0.387 ± 0.003	0.360 ± 0.006

Upon comparing the literature and experimentally determined diffusion coefficients it is observed that the smallest difference is present for the higher concentration sample with a difference of only 5.9% between our data and literature data. This difference increases to 7% for the truncated time domain data of the lower concentration but rises to 11.4% for the integration of spectra or all time domain points at lower concentrations. The 5.9-7% difference can be attributed to systematic errors present in the NMR technique or the open capillary method used in the literature. However, the variation in discrepancies indicates that processing of the initial time domain points up to 1.26 T_2^S is the most accurate method of determining diffusion coefficients of low concentration samples based on SHARPER-DOSY spectra. This also confirms that SHARPER-DOSY is a suitable technique for calculating diffusion coefficients in general and that the subtraction of a background spectra reliably removes the effect of other molecules on the diffusion coefficient.

5.4 Experimental

The samples used were doped water (0.1 mg $GdCl_3$ / mL D_2O + 1% H_2O + 0.1% $^{13}CH_3OH$), 1-phenylethanol (40 µl in 550 µl of D_2O), cyclosporine (Mw = 1,202.61 g mol^{-1}, 38 mg in 550 µl of benzene-d_6, concentration = 3.67 mM) and sodium cholate (M_w = 430.55 g/mol, 1.4 µg in 550 µL of D_2O, c = 5.5 µM).

The data for doped water and 1-phenylethanol was acquired and processed in TopSpin3.2 on a 400 MHz Bruker AVANCE III spectrometer while the data for cyclosporine and sodium cholate was acquired in TopSpin 4.1 on an 800 MHz BRUKER NEO NMR spectrometer equipped with a TCl cryoprobe. Individual parameters and pulse sequences are listed below.

Doped water data was acquired with the following parameters: 1 s relaxation time (D1), 1.229 s nominal acquisition time (AQ), 2 dummy (DS) and 2 real (NS) scans, 20,000 Hz (49.983 ppm) spectral width (SW), 49152 time domain points (TD), $pw_{90^\circ} = 30\mu s$, $pw_{180^\circ} = 60\mu s$ at 4.46W, acquisition chunk times, τ, of 100, 200 and 400µs, 25µs dwell time (DW) with 4, 8 or 16 points per chunk, 12,228, 6,144 or 3,072 spin echoes, respectively. The T_1 and T_2 relaxation time determined by inversion recovery and a CPMG methods were 230 and 180ms, respectively.

1-phenylethanol used the following parameters: D1=16s, AQ=9.83s, DS=2, NS=2, SW=10,000 Hz (49.983ppm), TD=196608. The 1D SHARPER spectrum was acquired using the sharper_collapse.du pulse sequence and identical common parameters as for the 1D ^1H spectrum. The following specific parameters were used: τ=200µs, $pw_{90^\circ} = 30\mu s$, $pw_{180^\circ} = 60\mu s$ at 4.46 W, DW= 50µs (4 points per chunk, 49152 spin echoes). The actual acquisition time was AQ*(τ+pw_{180°)/τ = 12.78 s.

For all cyclosporine experiments, identical common parameters, as stated for the 1D ^1H spectrum, were used: D1 =3.0 s, AQ=1.652 s, DS=4, NS=8, SW= 39682.54 Hz (49.6384 ppm), TD = 128k. Presaturation parameters: pw = 25764.461 µs, l6 = 117, carrier frequency o1 = 2612.50 Hz, ν(CHD_5) = (o1 + 3105.05) Hz; ν(H_2O) = (o1 - 2173.57) Hz (optimised primarily for the suppression of CHD_5). For ^{13}C decoupling a xy32 super cycle[88] modified to implement composite 180° pulses ($90^o_x 180^o_y 90^o_x$) with

$pw_{90^\circ} = 192\mu s$ was used with the ^{13}C carrier frequency at 128 ppm. For the BSPE spectrum (zgpebs.du) and the BSPE-SHARPER spectra (sharper_collapse.du) the following parameters were used: 1 ms ReBurp pulse, 600 μs PFG, G_1=7%, G_2=5% and G_3=12%. For the BSPE-SHARPER experiments the specific parameters were: τ=100.8 μs, DW = 12.6 μs (8 points per chunk, 16,384 spin echoes), the spin echo pulses, $pw_{90^\circ} = 40\mu s$, $pw_{180^\circ} = 80\mu s$ at 0.33 W resulting in the actual acquisition time = AQ*(τ+pw_{180°)/τ = 2.96 s and = AQ*(τ+pw_{90°)/τ = 2.30 s.

The spectra were processed using matched filters, line broadening LB=1.4 Hz for the 1D and BSPE spectra and LB=1.45 and 1.07 Hz for BSPE-SHARPER with 180° and 90° spin-echo pulses, respectively.

A reference 2D DOSY spectrum (ledbpgp2s.compensated.dn) was acquired using a modified Bruker pulse sequence, *ledbpgp2s*, to include a compensating PFGs before the start of the pulse sequence and off-resonance presaturation. The following DOSY specific parameters were used: diffusion time, d20= 200 ms, diffusion PFGs, p30 = 1 ms, the spoil and compensation PFGs, p19=0.6 ms and the eddy current delay d21=5 ms. All PFGs were sine shaped and applied at the strength specified in the pulse programme. The diffusion gradients were ramped up in 16 increments using 5 to 95 % strength of the PFG coil (66.4 G/cm). Number of scans was 8 per increment, yielding total acquisition time of 11 minutes. The SHARPER-DOSY spectra (ledbpgp2s.sharper_collapse.du) were acquired using the combination of parameters used for the BSPE-SHARPER and DOSY experiments stated above. The overall acquisition time was 14 and 12.5 min for the 180 and 90° spin echo pulses. The spectra were processed using matched filters, line broadening LB=1.56 Hz for the 2D DOSY spectrum and LB=1.39 and 1.02 Hz for SHARPER-DOSY with 180° or 90° spin-echo pulses, respectively. The number of points in the F_1 was 256, linear prediction was not used.

For all experiments on sodium cholate, identical common parameters, as stated for the 1D ^1H spectrum (zgpr_pulse.du), were used: D1 =3.0 s, AQ=1.05 s, DS=4, NS=128, SW= 15625 Hz (19.5451 ppm), TD = 32k. The HOD signal presaturation was performed using the PRESAT_JUMP option with $\gamma B_1/2\pi$=96 Hz. For the BSPE spectrum (zgpebs.du) and the BSPE-SHARPER spectra (sharper_collapse.du) the

following parameters were used: 3 ms ReBurp pulse, 600 μs PFG, G_1=7%, G_2=5% and G_3=12%. For the BSPE-SHARPER experiments the specific parameters were: τ=448 μs, DW = 32 μs (14 points per chunk, 2340 spin echoes), the spin echo pulses, $pw_{90^\circ} = 15.7\mu s$, $pw_{180^\circ} = 31.3\mu s$ at 2.78 W resulting in the actual acquisition time = AQ*(τ+pw_{180°)/τ = 1.12 s.

The spectra were processed using matched exponential filters with broadening, LB=1.5 and 0.8 Hz (BSPE and BSPE-SHARPER spectrum of the 3) and LB=1.25 or 0.53 Hz (BSPE and BSPE-SHARPER spectrum of D_2O impurities).

A reference 2D DOSY spectrum (ledbpgp2s.compensated.dn) was acquired using a modified Bruker pulse sequence, *ledbpgp2s*, to include a compensating PFGs before the start of the pulse sequence and off-resonance presaturation. The following DOSY specific parameters were used: diffusion time, d20= 200 ms, diffusion PFGs, p30 = 1 ms, the spoil and compensation PFGs, p19=0.6 ms and the eddy current delay d21=5 ms. All PFGs were sine shaped and applied at the strength specified in the pulse programme. The diffusion gradients were ramped up in 16 increments using 5 to 95 % strength of the PFG coil (66.4 G/cm). Number of scans was 8 per increment with 16 increments, yielding total acquisition time of 10 minutes. The SHARPER-DOSY spectra (ledbpgp2s.sharper_collapse.du) were acquired using the combination of parameters used for the BSPE-SHARPER and DOSY experiments stated above.

6 CSSF-SHARPER

6.1 Declaration

The work in section 6.3.1 on CSSF baseline elevation and sample preparation was carried out by Patrick Boaler as part of his Postdoctoral project. I carried out experimental design, data acquisition and data analysis.

6.2 Chemical Shift Selective Filter

In contrast to the previous chapter which concerns collapsing entire spin systems into a single SHARPER peak using a CPMG like acquisition scheme, this chapter is concerned with high levels of selectivity and selecting heavily overlapped signals to be transformed into a SHARPER peak. This topic has already been approached with the *sel*-SHARPER variations introduced previously[2,89] however these sequences have been limited by the frequency selection method chosen. The primary method has been to use Gaussian pulses to select a signal; these techniques require signals to be isolated and fail to perform when overlap is encountered. Instead, an alternative selection method called a gradient enhanced Chemical Shift Selective Filter (ge-CSSF)[90] has been chosen and combined with SHARPER in order to give extraordinary selectivity of peaks separated by as little as 1-2 Hz. The ge-CSSF is a selection method that selectively excites in phase magnetisation of an on-resonance spin, while removing off-resonance signals. This is achieved by constructive addition of on resonance signals while variable chemical shift evolution causes the off-resonance signals to change phase and cancel out due to destructive interference. In order to vary the evolution of the off resonance signals several fids are acquired with a gradually incremented chemical shift evolution period using the sequence shown in Figure 6.1.

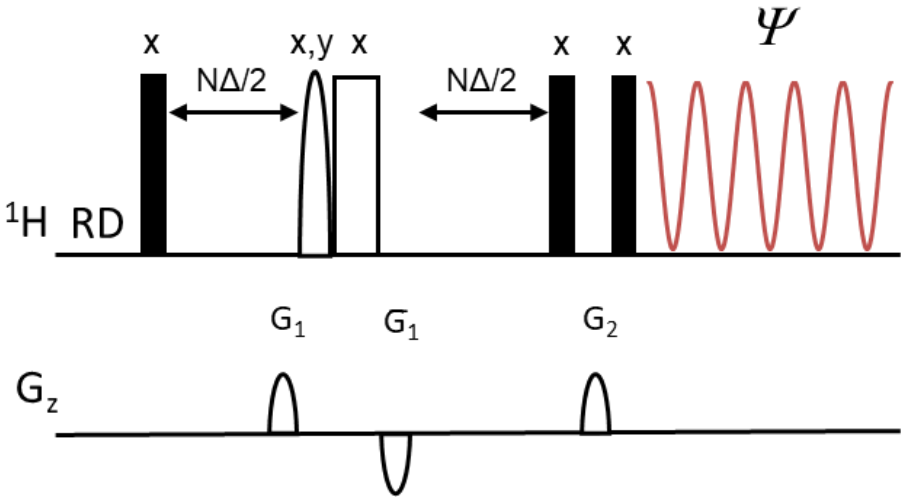

Figure 6.1: Pulse sequence for the ge-CSSF experiment. The black rectangles represent 90° hard pulses, white rectangle is a 180° hard pulse, and the rounded shape is a 180° Gaussian pulse. N = 0, 1, 2,…, n and Δ is the increment of the CSSF.

The selective 180° pulse in Figure 6.1 ensures that signals within the inversion bandwidth effectively experience a 360° rotation while the signals outside of this window experience a 180° rotation. The off-resonance spins that experienced a 360° rotation during $N\Delta$ will therefore only evolve under their chemical shifts, and upon addition of a series of FIDs with increasing $N\Delta$ will experience destructive interference and cancel out leaving only the on-resonance peak of interest. Through use of many increments peaks very close to being on resonance can be caused to destructively interfere resulting in selection of signals that have a 1-2 Hz distance from the nearest neighbour. Signals that only experienced a nonselective 180 pulse will be removed by PFGs. This selection is demonstrated in Figure 6.2, on a sample of 5.2 kDa dextran where each peak has been individually selected using CSSF.

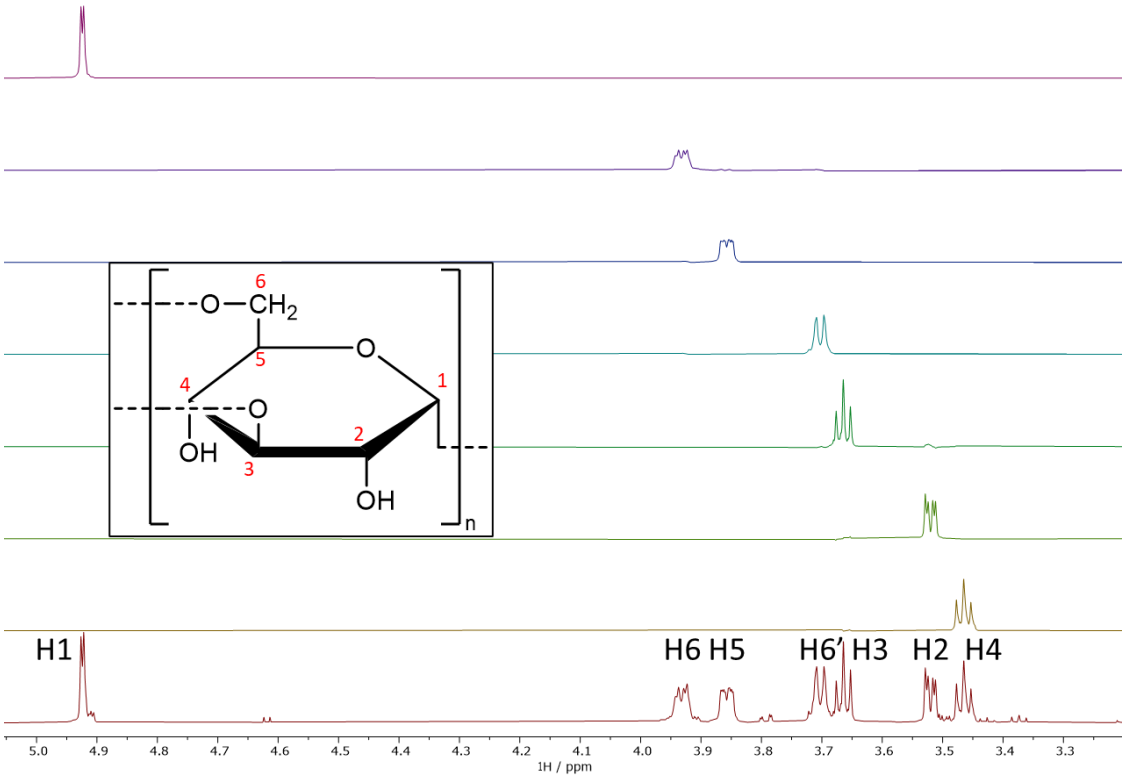

Figure 6.2: ^{1}H spectrum of 5.2 kDa dextran (bottom) with peaks assigned and CSSF spectra of each individual peak. The inset shows the structure of dextran and the peak assignments.

As CSSF is a selection block and has been successfully combined with other pulse program building blocks such as COSY, TOCSY and ROESY[90]. It would be an efficient selection method to place before a SHARPER acquisition block in order to select heavily overlapped signals.

6.3 CSSF-SHARPER

The SHARPER acquisition block was added to the CSSF sequence as shown in Figure 6.3.

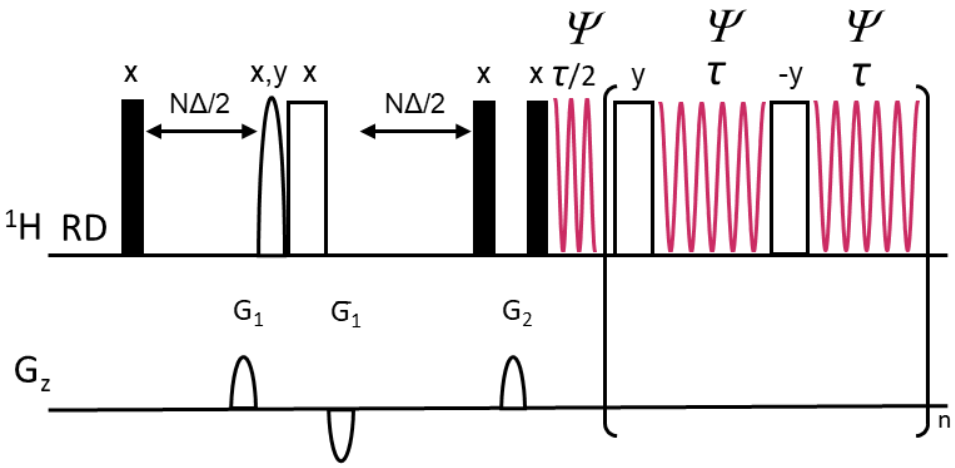

Figure 6.3: Pulse sequence for the CSSF-SHARPER experiment. The black rectangles represent 90° hard pulses, white rectangle is a 180° hard pulse, and the rounded shape is a 180° Gaussian pulse. N = 0, 1, 2,…, n and Δ is the increment of the CSSF. τ = AQ/(2n), where AQ is the total acquisition time and n is the total number of loops.

As CSSF requires multiple increments; the sequence is no longer truly one scan and run time is increased, but this is compensated for by the increased selectivity. To demonstrate this, dextran was again used as a reference and the results of CSSF-SHARPER on each peak are shown in Figure 6.4.

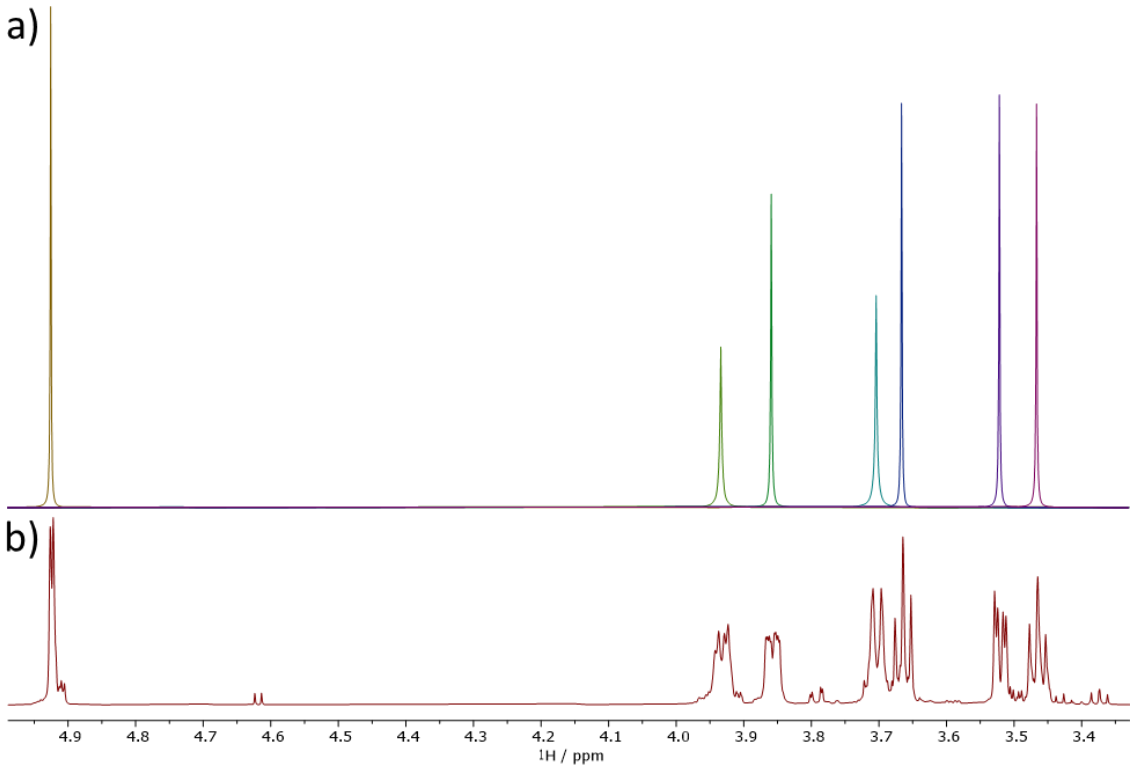

Figure 6.4: Spectra of 5.2 kDa Dextran in D_2O. b) is the normal 1D ^1H spectrum and a) is a superposition of the CSSF-SHARPER peak of each individual dextran signal in b).

In order to determine the signal retention of the CSSF and CSSF-SHARPER techniques the integrals for each peak in a normal ^1H spectrum, CSSF spectrum and CSSF-SHARPER spectrum were measured and are compared in Table 5.1.

Table 6.1: Integral areas of each peak in 5.2 kDa dextran from spectra acquired using CSSF, CSSF-SHARPER, CSSF-SHARPER with 90° refocusing pulses and traditional SPFGSE-SHARPER with a 20 ms gaussian pulse being used to select signal 1, a 40 ms Gaussian pulse being used to select signals 2, 4, 5, 6 and 6' and an 80 ms selective pulse used to select peak 3. The areas are normalised against a 16 scan ^{1}H experiment and the SPFGSE spectrum was acquired with 16 scans while the CSSF spectra were acquired using 2 scans with 8 increments in each scan.

Peak	Integral area / % (normalised relative to 1D ^{1}H spectrum)			
	CSSF	CSSF-SHARPER	CSSF-SHARPER 90° pulse	SPFGSE-*sel*-SHARPER
1	82	77	77	90
2	79	69	65	73
3	70	61	58	46
4	75	66	62	68
5	63	61	60	68
6	53	53	50	63
6'	61	60	62	60

As Table 5.1 shows the addition of SHARPER to a standard CSSF experiment has some impact on the signal retention. However, this only appears to be evident when initial signal retention is high. The greatest differences are seen for peaks 2, 3 and 4 which have CSSF integral areas over 70% and lose about 10% of integral area when SHARPER is added. In contrast peaks 5, 6 and 6' lose little to no signal. These however, are already at lower retention values of around 60%. Peak 1 is the exception due to the isolation of the peak, enabling more efficient constructive addition of signal during the CSSF increments. The key information however is the comparison to the SPFGSE-*sel*-SHARPER data. This shows that the CSSF-SHARPER integral areas broadly match those of the less selective SPFGSE method with the exceptions arising when CSSF itself is losing signal rather than SHARPER. Another key result is that the use of 90° refocusing pulses rather than 180° pulses has a negligible minor impact on the integral

area while reducing the pulse time which shortens the experiment and lowers the risk of damage to the probe.

One additional factor that needs to be considered when looking at the CSSF-SHARPER experiment is the elevation of the baseline that can occur when successive scans are added without perfect cancellation. Work done by Dr Patrick Boaler and presented in section 6.3.1 shows how this can be minimised.

6.3.1 CSSF baseline elevation

When using the chemical shift selective filter to perform challenging signal selections (<5 Hz separation), care must be taken to ensure that the chosen parameters don't cause an elevated baseline, as this will negatively impact the quality of the SHARPER spectrum. The most important parameter for mitigating this is the number of CSSF increments, where larger numbers of increments efficiently suppress the elevation effect in the baseline.

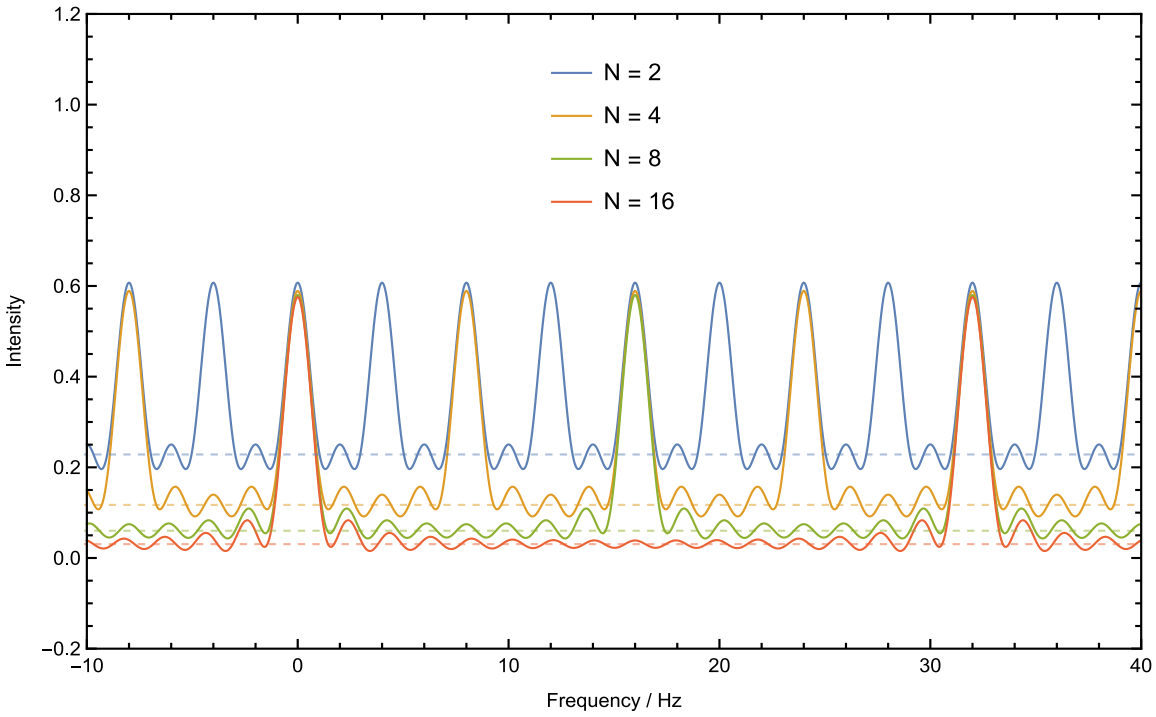

Figure 6.5: Simulated CSSF Intensities (filled lines) as a function of frequency for a signal separation of 1 Hz and T_2 of 0.4 s with different numbers of increments (n). The dashed lines correspond to the baseline level for each of the different simulation conditions.

In Figure 6.5, the CSSF intensities are simulated according to Equation 30. Where N is the total number of CSSF increments, ν is the frequency in Hz, and $\Delta\nu$ is the signal separation in Hz.

$$I_{\Delta\nu}(\nu) = \frac{1}{N+1}\sum_{n=0}^{N}\cos\left(\frac{n\,\pi\,\nu}{\mathrm{N}\,\Delta\nu}\right)e^{\left(\frac{-n}{2\,N\,T_2\,\Delta\nu}\right)} \quad (30)$$

The high-intensity sidebands generated by this function are periodic and occur every $2N\Delta\nu$ Hz from the on-resonance signal. This periodicity was used to approximate the frequency independent baseline elevation for any set of parameters: N, $\Delta\nu$, and T_2. By using the fact that the main contributor to the intensity vs frequency curve has its minimum at the half period length $N\Delta\nu$ from the on-resonance signal, Equation 30 can be further simplified, giving Equation 31.

$$I_{\Delta\nu}(N\Delta\nu) = \frac{1}{N+1}\sum_{n=0}^{N}\cos(n\,\pi)\,e^{\left(\frac{-n}{2\,N\,T_2\,\Delta\nu}\right)} \quad (31)$$

It should be noted that evaluating Equation 31 gives a local minimum when N is odd, and a local maximum when N is even. To extract the average baseline about which the curve oscillates, the average of two separate evaluations is taken, one where $N \to N + \frac{1}{2}$, and the other where $N \to N - \frac{1}{2}$. This baseline elevation is plotted in Figure 6.6 as a function of the number of increments N, and T_2 for a signal separation of 1 Hz.

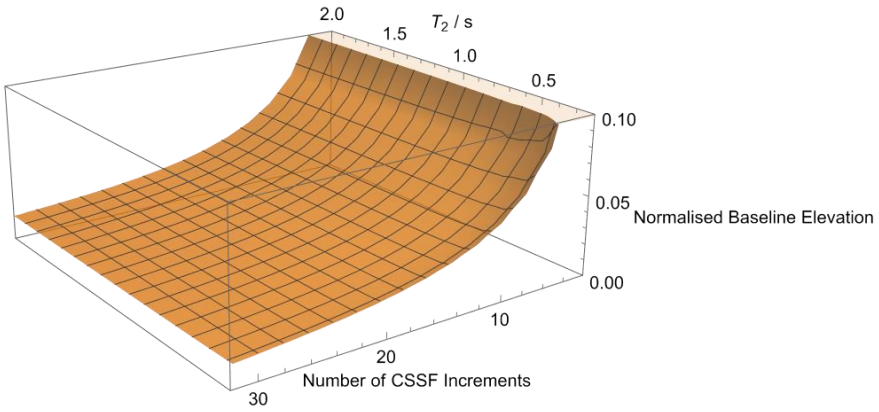

Figure 6.6: Simulated CSSF baseline elevation as a function of N and T_2, where the signal separation ($\Delta\nu$) is 1 Hz.

To keep the normalised baseline elevation under intensity values of 0.1, we recommend that the maximum practical number of CSSF increments be used, and that this parameter never be reduced below 8 increments for a CSSF-SHARPER experiment.

6.4 DOSY-CSSF-SHARPER

While the combination of CSSF and SHARPER presented in the previous section represents a great improvement of the *sel*-SHARPER sequences previously reported[2,89] it has much greater potential when combined with the DOSY building block. As reported in the previous chapter diffusion coefficients are a very useful molecular parameters, their determination using NMR is limited by sample constraints. The previous chapter provided a solution for when a sample is at a very low concentration but is pure, although the solvent may not be, whereas CSSF offers a solution to the problem of the sample being part of a mixture of molecules. In mixtures the overlap of peaks in the 1D spectra may make it difficult to determine the diffusion coefficients of individual molecules. While some solutions to this issue have been determined that involve pure shift techniques[91,92] the techniques are still limited in the case of high degrees of overlap. CSSF-SHARPER's ability to select a single peak with a separation of as few as 1-2 Hz overcomes this problem and allows the diffusion coefficient to be determined accurately with the added bonus of greatly increasing the SNR of the peak.

To combine the different building blocks the DOSY component was placed first, followed by the CSSF and the SHARPER acquisition. The sequence is shown in Figure 6.7.

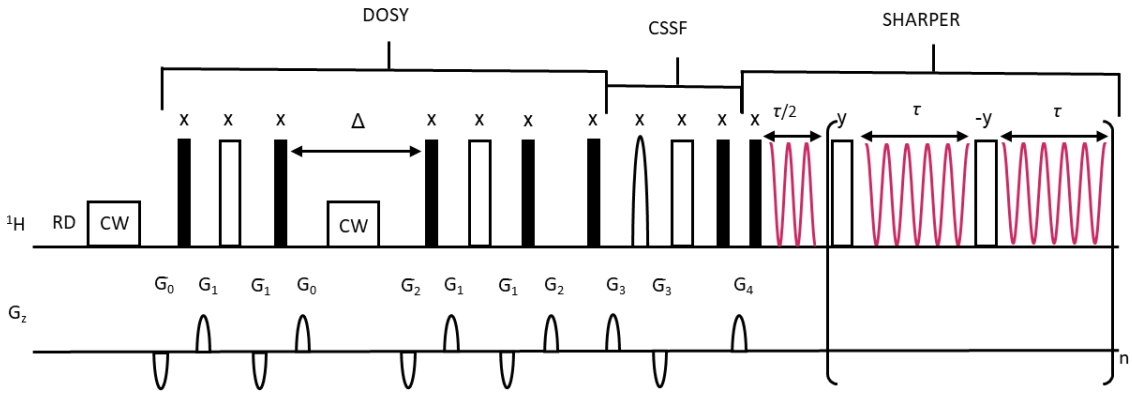

Figure 6.7: Pulse sequence for the DOSY-CSSF-SHARPER experiment with initial phase cycling shown. The black rectangles represent 90° hard pulses, white rectangle is a 180° hard pulse, and the white rounded shape is a 180° Gaussian pulse. N = 0, 1, 2,…, n and Δ is the increment of the DOSY block. τ = AQ/(2n), where AQ is the total acquisition time and n is the total number of loops.

6.4.1 Preparation of a model mixture

Having produced the combined DOSY-CSSF-SHARPER sequence the next step is to test it and this requires a model sample that both has multiple signals with a range of separations from nearest neighbours but also a range of diffusion coefficients. In order to meet these criteria a model sample was prepared containing a monosaccharide, methyl β-D-xylopyranoside, a disaccharide, cellobiose and a pentasaccharide, fondaparinux in the concentration ratio 2:1:1. The structures of these compounds are shown in Figure 6.8. Cellobiose is a mixture of α and β anomeric forms with distinct ^{1}H signals, increasing the overlap further. The other two compounds have a Me group at position 1, selecting only of the two anomeric forms.

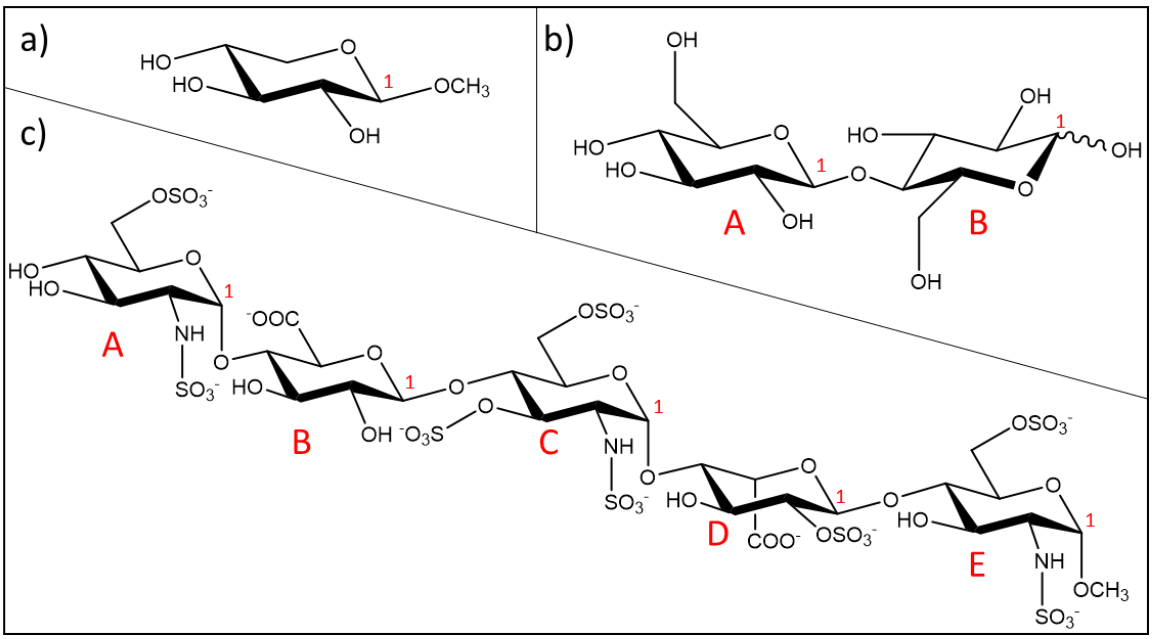

Figure 6.8: Structures of a) methyl β-D-xylopyranoside, b) cellobiose, and c) fondaparinux. The rings of fondaparinux are labelled in red and the position of the anomeric proton is indicated on each ring.

This sample is a good example to demonstrate CSSF-SHARPER-DOSY as the differing number of rings in each carbohydrate provides a range of diffusion coefficients while there is also a high degree of overlap of signals, particularly in the range of 3.2ppm to 4.5 ppm as shown in Figure 6.9.

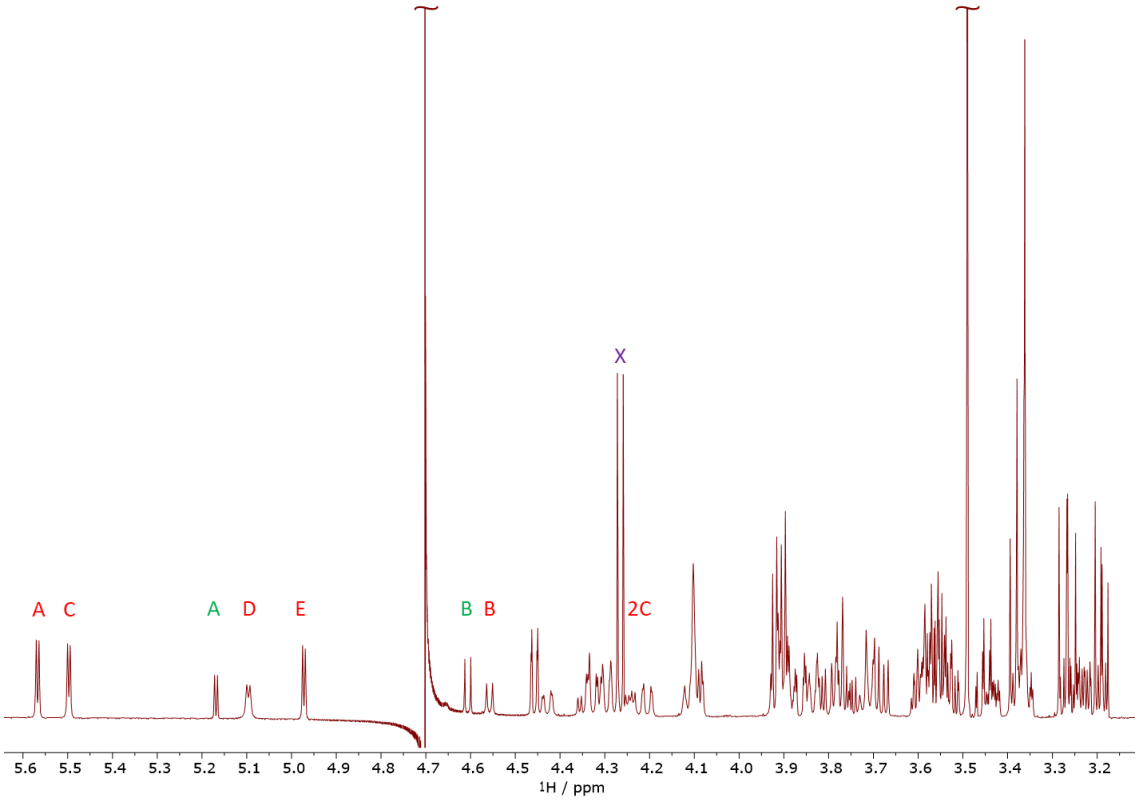

Figure 6.9: 600 MHz ^{1}H NMR spectrum of a 2:1:1 mixture of methyl β-D-xylopyranoside, cellobiose, and fondaparinux, in D_2O recorded with solvent presaturation. The residual solvent peak at 4.7 ppm and OMe signal from methyl β-D-xylopyranoside at 3.5 ppm have been cut off to enable lower intensity peaks to be visible. The anomeric proton signal of each ring has been labelled with a red letter for fondaparinux, green symbol for cellobiose and X for methyl β-D-xylopyranoside along with proton 2C of fondaparinux.

To demonstrate the DOSY-CSSF-SHARPER sequence two peaks were chosen from different compounds that overlap and would not be separable by other, more conventional selection methods. The signals chosen are X in methyl β-D-xylopyranoside, and 2C in fondaparinux, these are present at 2562 Hz (4.26 ppm) and 2548 Hz (4.24 ppm) respectively. As these signals also come from the smallest and largest molecule the diffusion values obtained will be very different so it will be possible to conclusively determine which peak has been selected in a DOSY spectrum and identify if multiple peaks are contributing the SHARPER signal. First though a CSSF spectrum of each signal was acquired and the result of this is shown in Figure 6.10.

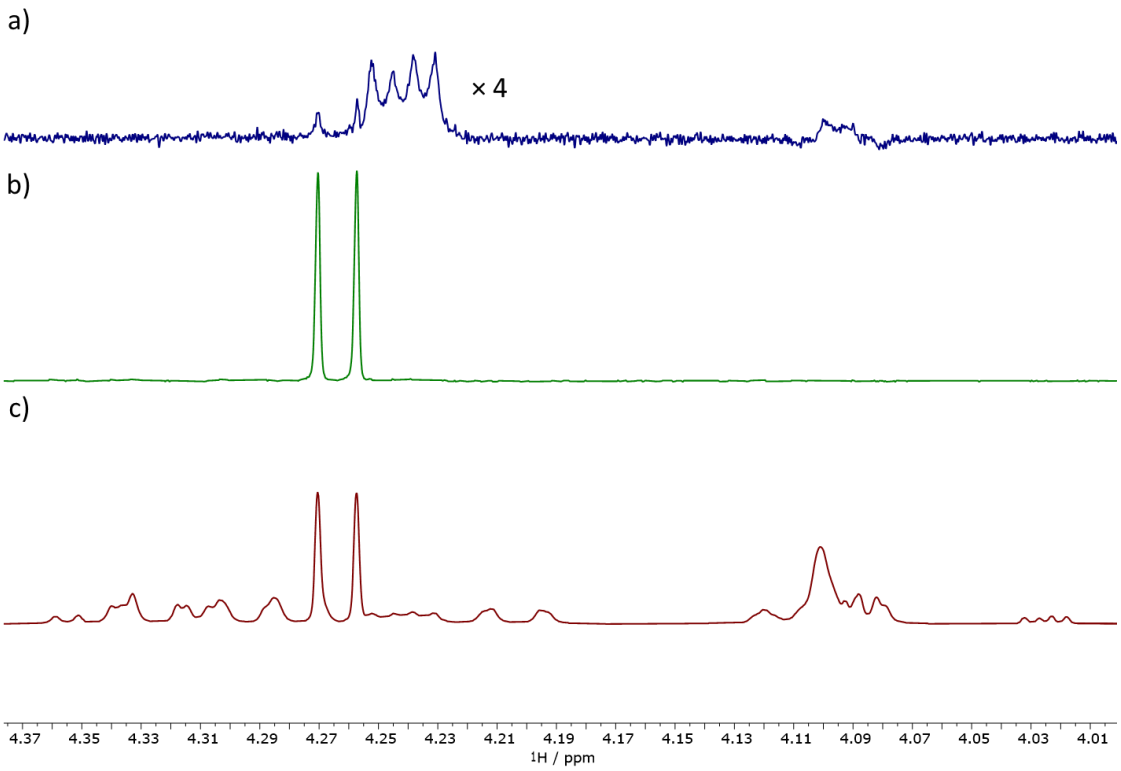

Figure 6.10: CSSF spectra of a) signal 2C from fondaparinux acquired using 1 scan and 16 CSSF increments and multiplied by a factor of 4 to highlight the artefacts, b) signal 1 from methyl β-D-xylopyranoside acquired using 1 scan and 4 CSSF increments and c) A reference 4 scan ^{1}H presat experiment on the carbohydrate mixture.

Figure 6.10 shows that CSSF selection works well on the signal from methyl β-D-xylopyranoside but is not as useful when trying to isolate the signal from fondaparinux. There are still visible artefacts arising from the strongly coupled signals of 3C and 4C. To remove these signals a swept gradient z-filter[18], was added to the sequence which removed the majority of the residual artefact signals. The new sequence is shown in Figure 6.11.

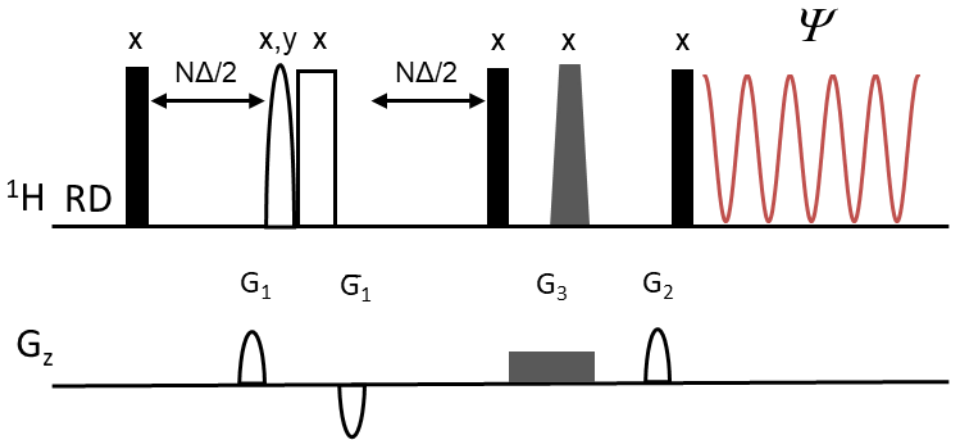

Figure 6.11: Pulse sequence for the CSSF-SHARPER experiment with additional z-filter. The black rectangles represent 90° hard pulses, white rectangle is a 180° hard pulse, and the rounded shape is a 180° Gaussian pulse. The grey rectangle is a block gradient pulse while the grey trapezium is a smoothed adiabatic chirp pulse[93]. N = 0, 1, 2,…, n and Δ is the increment of the CSSF. τ = AQ/(2n), where AQ is the total acquisition time and n is the total number of loops.

A swept gradient z-filter was chosen as the artefacts present arise from some of the strong coupling being transferred into of zero-quantum coherence which isn't suppressed by the standard z filter. The presence of the gradients suppresses zero quantum coherences as well leaving only Z magnetisation which contains the selected signal. The result of adding the z-filter to the CSSF sequence is shown in Figure 6.12.

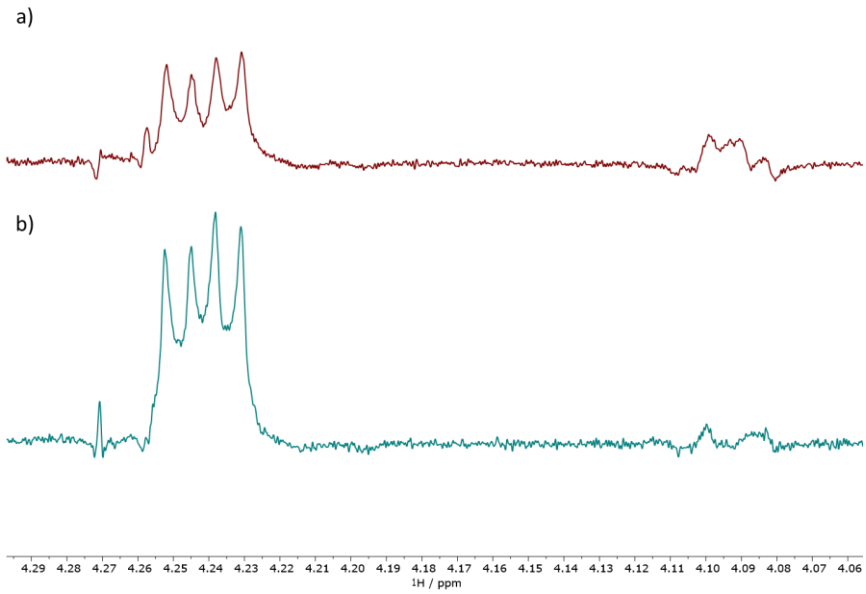

Figure 6.12: Signal 2C of fondaparinux acquired using CSSF a) without addition of a z filter and b) with the addition of a z filter. Both spectra were acquired using 8 scans and 16 CSSF increments.

Having demonstrated the efficacy of the CSSF experiment in selecting these peaks the CSSF-SHARPER experiment was run on both signals to determine the effectiveness of the selection and ensure the lineshapes were as expected for the SHARPER sequence. The results are shown in Figure 6.13 and demonstrate the SNR increase provided by CSSF-SHARPER despite the close proximity of the peaks.

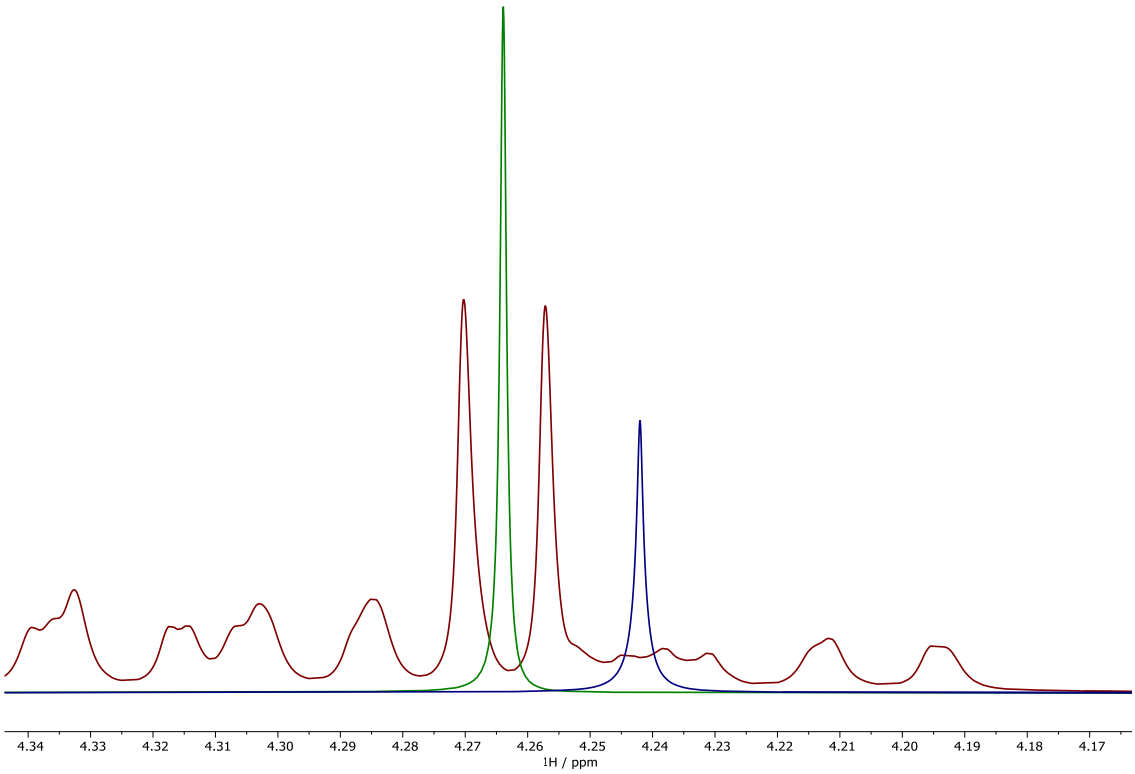

Figure 6.13: CSSF-SHARPER spectra of signal 1 of methyl β-*D*-xylopyranoside (green) and signal 2C of fondaparinux (blue) overlaid with a 16 scan ^{1}H experiment. The green spectrum was recorded with 4 scans and 8 CSSF increments for a total of 32 scans. The blue spectrum was recorded with 6 scans and 16 CSSF increments for a total of 96 scans so has been reduced in height by a factor of three while the red spectrum was recorded with 16 scans so has been scaled up by a factor of 2 in order to present a true comparison of signal intensities.

The integral area of each peak was measured compared relative to the integral of the standard ^{1}H experiment giving a value of 78% for the fondaparinux signal but only 45% signal retention for the methyl β-D-xylopyranoside signal. The value of 78% for the fondaparinux signal matches the value expected from Table 5.1, however, the value of 45% is much lower than expected implying that there is much more signal loss than previously observed. This however isn't the case, due to the high overlap present in the spectrum there are actually small signals from fondaparinux that are hidden beneath the larger monosaccaride peak. These peaks contribute integral area to the value acquired from the 1D spectrum and lower the apparent signal retention of the CSSF-SHARPER experiment. To gain an accurate measure of signal retention, the integrals of the CSSF spectrum and CSSF-SHARPER spectrum for signal 1 were compared to each other and

to the ^{1}H integrals. This gave a result of 80% retention between CSSF and CSSF-SHARPER but only 57% retention between ^{1}H and CSSF. This matches the expected signal loss from introducing SHARPER to CSSF but provides a discrepancy between the ^{1}H and CSSF values which are explained by the presence of additional peaks. When these are removed by CSSF the integral area drops giving a false impression of the signal retention from CSSF-SHARPER.

6.4.2 DOSY-CSSF-SHARPER results

Having identified two suitable signals for demonstrating the use of DOSY-CSSF-SHARPER the next step is to record the data. First a normal DOSY spectrum was recorded for the sample to demonstrate the difficulties in identifying diffusion coefficients from mixtures and to allow comparison with the DOSY-CSSF-SHARPER peaks. This spectrum is shown in Figure 6.14 along with lines indicating approximate diffusion coefficients for each compound based on signal 1C for fondaparinux, 1α for cellobiose and the large OMe signal from methyl β-D-xylopyranoside. Looking at the central section of the spectrum, ranging from 3.1 to 4.4 ppm, it is clear that there are several peaks with greatly differing diffusion coefficients that are difficult to assign to the horizontal projection of the spectrum. This is a situation where the high selection capabilities afforded by DOSY-CSSF-SHARPER would be greatly useful for determining a diffusion coefficient from a known signal in the 1D spectrum.

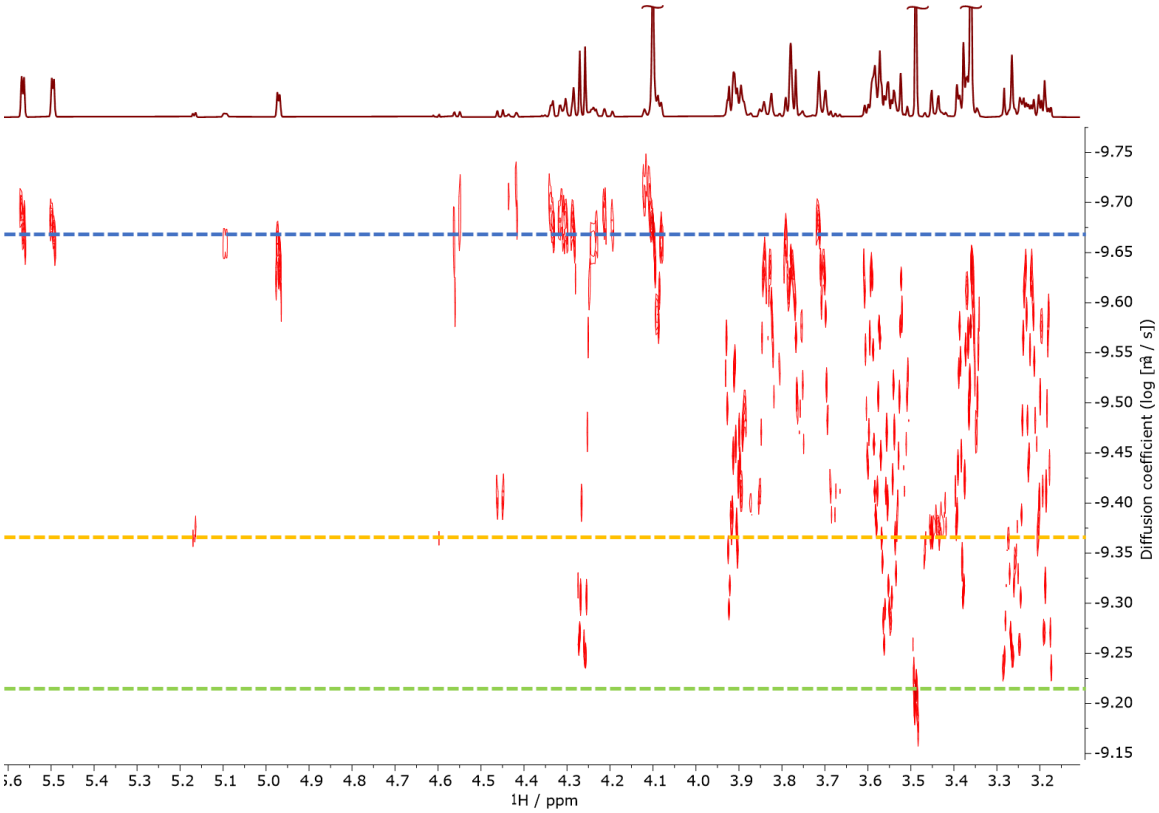

Figure 6.14: DOSY spectrum of the mixed carbohydrate sample. The vertical projection has been scaled up to show the smaller peaks which contribute to the large number of DOSY signals. The blue, yellow and green dashed lines indicate the rough diffusion coefficients of fondaparinux, cellobiose and methyl β-*D*-xylopyranoside respectively and have been placed based on the location of the 1C, 1α and OMe DOSY peaks.

The DOSY-CSSF-SHARPER sequence was then run on the two signals mentioned in section 6.4.1 and the results were overlaid with the original spectrum as shown in Figure 6.15.

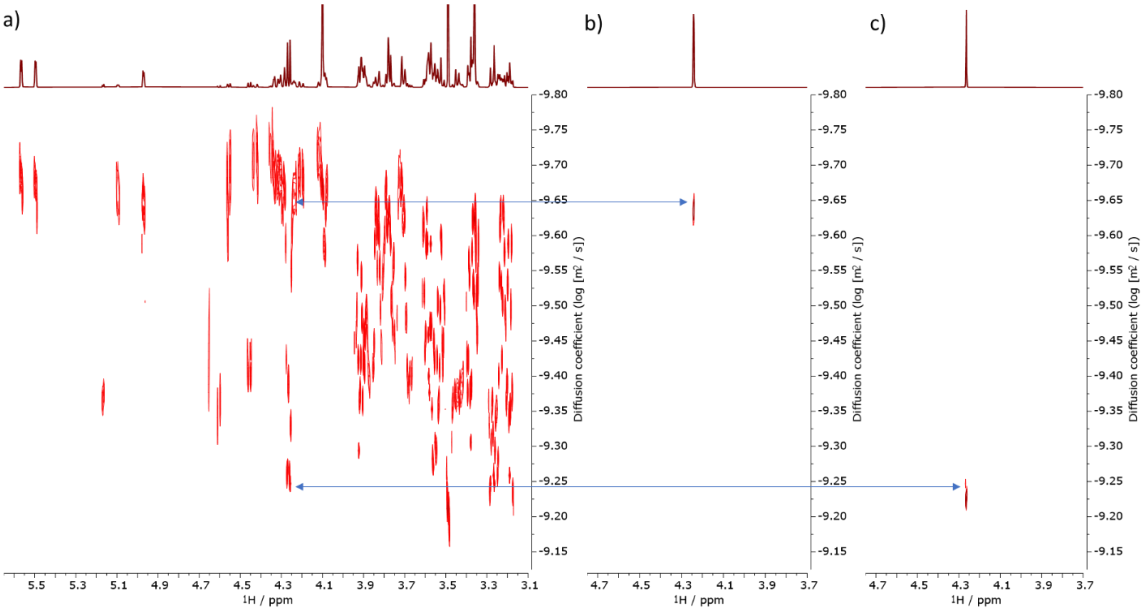

Figure 6.15: a) is the DOSY spectrum of the mixed carbohydrate sample b) is the DOSY-CSSF-SHARPER spectra of signal 2C of fondaparinux and c) is the DOSY-CSSF-SHARPER signal 1 of methyl β-D-xylopyranoside. Arrows indicate the position of the sharpened peaks relative to the signals used to calculate diffusion parameters in Figure 6.14.

Figure 6.15 shows that the diffusion coefficients obtained from each SHARPER peak are very close to the values indicated by the peaks used in Figure 6.14 to identify the diffusion coefficient of each compound. The actual values as obtained from the spectra are tabulated below and show that the DOSY-CSSF-SHARPER sequence can accurately determine diffusion coefficients from a single overlapped peak in a 1D spectrum. This is in addition to the increase in SNR achieved by SHARPER acquisition, which was 14-fold for the methyl β-D-xylopyranoside signal. This is remarkable and shows how the sequence can be used to overcome a common problem encountered when trying to measure diffusion coefficients of samples in mixtures.

Table 6.2: Diffusion coefficients calculated from the spectra shown in Figure 6.15

Sample	Peak	DOSY	Diffusion coefficient D / log(m^2s^{-1})
methyl β-D-xylopyranoside	OMe	Standard	-9.222
	1	CSSF-SHARPER	-9.227
Fondaparinux	1C	Standard	-9.634
	2C	CSSF-SHARPER	-9.632

6.5 Experimental

The samples used were 5.2 kDa dextran (Mw = 5220 g mol^{-1}, 5 mg) dissolved in 550 μL of D_2O and a mixture of methyl β-D-xylopyranoside (Mw = 164.16 g mol^{-1}, 0.85 mg), cellobiose (Mw = 342.30 g mol^{-1}, 0.89 mg) and fondaparinux (Mw = 1728.03 g mol^{-1}, 4.520 mg) in 550 μL of D_2O giving final concentrations of 6.47 mM, 3.25 mM and 3.27 mM respectively.

All data was acquired in TopSpin3.2 on a 600 MHZ Bruker AVANCE III spectrometer equipped with a TCI cryo-probe and then processed in TopSpin 4.1. Individual parameters and pulse sequences are listed below.

The 1D ^1H dextran data was acquired with the following parameters: D1=3s, AQ=1.05s, DS=2, NS=16, SW= 7812.5 Hz (9.7725ppm), TD= 16384. The CSSF spectra used the following specific parameters: NS = 2, 8 CSSF increments and an 80 ms Gaussian pulse, while the CSSF-SHARPER experiments differed with AQ = 2.10s, NS = 16 and acquisition chunk times, τ, 0.5 ms. $pw_{90^\circ} = 15\mu s$, $pw_{180^\circ} = 30\mu s$ was used with Gaussian pulses of 20 and 40 ms

The 1D ^1H spectra of the mixed carbohydrate sample was acquired with the following parameters: D1= 2s, AQ=2.73s, DS=4, NS=16, SW=6009.6 Hz (10.003 ppm) and TD=32768. The CSSF spectra used identical parameters except for NS = 4 and 6, 8, 12

or 16 CSSF increments and an 80 ms Gaussian pulse. The CSSF-SHARPER experiments had identical parameters with a SHARPER acquisition chunk time of 0.5 ms.

The reference 2D DOSY spectrum (ledbpgp2s.compensated.dn) was acquired using a modified Bruker pulse sequence, *ledbpgp2s*, to include compensating PFGs before the start of the pulse sequence and off-resonance presaturation. The following DOSY specific parameters were used: diffusion time, d20= 500 ms, diffusion PFGs, p30 = 0.5 ms, the spoil and compensation PFGs, p19=0.6 ms and the eddy current delay d21=5 ms. All PFGs were sine shaped and applied with powers GP0 = -17.13%, GP1 = 100% and GP2 = -13.17 % for. The diffusion gradients were ramped up in 16 increments using 5 to 95 % strength of the PFG coil (66.4 G/cm). Number of scans was 8 per increment, with 8 increments. The DOSY-CSSF-SHARPER spectra were acquired using the combination of parameters used for the CSSF-SHARPER and DOSY experiments stated above and had a run time of 195 minutes each.

7 Conclusions

Throughout this project, several NMR pulse sequence building blocks have been successfully combined to produce more complex NMR experiments that provide new information or reduce the amount of sample required. These are applicable across a range of research areas.

The first part of the project has successfully combined the DISPEL experiment with both the TOCSY and JRES 2D experiments allowing ^{1}H spectra to be acquired to distinguish ^{1}H signals originating from ^{12}C- or ^{13}C-attached protons. Added to this, further manipulation of DISPEL-TOCSY spectra allowed the isolation of signals arising from transfers between different combinations of ^{12}CH and ^{13}CH protons. The peaks in the DISPEL-TOCSY spectra were used to calculate site specific ^{13}C enrichment levels. The DISPEL-JRES spectra allowed to separate multiplets of ^{12}CH and ^{13}CH protons. The methods have been tested on a series of model compounds as well as an unknown mixture of metabolites. To facilitate the use of these experiments, automated processing scripts have been developed, which allow for easy implementation of the methods on Bruker NMR spectrometers. Future work on this project will focus on applying these experiments to biological samples, as well as on improving the determination of the accuracy of ^{13}C enrichment levels.

The second part of the project focused on the SHARPER acquisition block and is divided into three sub projects. The first of these focused on taking the SHARPER sequence from high field to low field NMR spectrometers and implementing it on a 60 MHz Magritek instrument. The transfer to lower field instruments was carried out in order to capitalise on the capability of SHARPER experiments to effectively compensate for the magnetic field inhomogeneity and to boost the sensitivity of measurements - both of these attributes are particularly important for the lower field, less sensitive spectrometer. These improvements will help to increase the use of benchtop instruments, e.g., in reaction monitoring directly in the synthetic chemistry laboratory. This research produced four different pulse sequences that suit a range of instrument specifications. Signal to noise ratio improvements ranging from 11 to 21-fold have been achieved compared to standard ^{19}F spectra. A further processing step was developed which involves directing all the signal into the real channel of the FID and then removing the imaginary component, resulting in a further 41% increase in

SNR increasing the gains up to 30-fold. Additionally, it has been shown that due to elimination effects of the effects arising from magnetic field inhomogeneity, the linewidth of SHARPER peaks are approaching the theoretical natural linewidths based on T_2 values.

The second area of SHARPER research involved using very short spin-echo to acquire signal to collapse all or selected peaks in a spectrum into a single central SHARPER peak by suppressing both the chemical shift evolution of the resonances as well as the splitting due to *J* couplings. This module was then combined with the DOSY experiment resulting in 10-100 fold sensitivity increases. These levels allow to reduce the time required to acquire a DOSY spectrum 100-10000 times. The sequence was tested on a 1.3 μg sample of sodium cholate and effectively measured the diffusion coefficient in 80 minutes by acquiring two 40-minute spectra, one of the cholate sample and one of a blank D_2O reference sample that was then subtracted to allow accurate determination of the diffusion coefficient of the cholate. SHARPER-DOSY pulse sequences, as well as an automation program to facilitate the processing and subtraction of the DOSY peaks were developed.

Finally, the third SHARPER project focused on increasing the selectivity of the DOSY-SHARPER experiment rather than collapsing an entire spectrum. To this end the chemical shift selective filter was introduced and has been shown to selectively excite overlapping peaks separated by as little as 4 Hz in the chemical shift from their neighbours while retaining up to 80% of the original signal. This has enabled diffusion coefficients to be obtained from a mixture of several oligosaccharides from heavily overlapped peaks with greatly improved SNR compared to the parent peak. Future work on this area will focus on applying the sequence to more complex samples and investigating the possibility of replacing the CSSF experiment with its one-scan equivalent, the Gradient-Enhanced Multiplet-Selective Targeted-Observation NMR Experiment.

8 References

1 P. Moutzouri, P. Kiraly, A. R. Phillips, S. R. Coombes, M. Nilsson and G. A. Morris, *Anal Chem*, 2017, **89**, 11898–11901.

2 A. B. Jones, G. C. Lloyd-Jones and D. Uhrín, *Anal Chem*, 2017, **89**, 10013–10021.

3 F. Bloch, *Physical Review*, 1946, **70**, 460–474.

4 F. Bloch, W. W. Hansen and M. Packard, *The Nuclear Induction Experiment*, 1946, vol. 70.

5 E. M. Purcell, H. C. Torrey and R. V Pound, *Physical Review*, 1945, **69**, 37–38.

6 J. Keeler, *Understanding NMR Spectroscopy* , John Wiley & Sons , 2010.

7 M. Grootveld, B. Percival, M. Gibson, Y. Osman, M. Edgar, M. Molinari, M. L. Mather, F. Casanova and P. B. Wilson, *Anal Chim Acta*, 2019, **1067**, 11–30.

8 S. D. Riegel and G. M. Leskowitz, *Trends in Analytical Chemistry*, 2016, **83**, 27–38.

9 M. V. Silva Elipe and R. R. Milburn, *Magnetic Resonance in Chemistry*, 2016, **54**, 437–443.

10 E. L. Hahn, *Physical Review*, 1950, **80**, 580–594.

11 H. Y. Carr and E. M. Purcell, *Physical Review*, 1954, **94**, 630–638.

12 M. R. Bendall and D. T. Pegg, *Magn Reson Med*, 1985, **2**, 298–306.

13 S. Meiboom and D. Gill, *Review of Scientific Instruments*, 1958, **29**, 688–691.

14 K. Takegoshi, K. Ogura and K. Hikichi, *Journal of Magnetic Resonance*, 1989, **84**, 1–6.

15 A. M. Torres, G. Zheng and W. S. Price, *Magnetic Resonance in Chemistry*, 2010, **48**, 129–133.

16 P. W. A. Howe, *Magnetic Resonance in Chemistry*, 2020, **58**, 77–83.

17 P. W. A. Howe, *Anal Chem*, 2018, **90**, 4316–4319.

18 M. J. Thrippleton and J. Keeler, *Angewandte Chemie - International Edition*, 2003, **42**, 3938–3941.

19 W. P. Aue, E. Bartholdi and R. R. Ernst, *J Chem Phys*, 1976, **64**, 2229–2246.

20 L. Braunschweiler and R. R. Ernst, *Journal of Magnetic Resonance*, 1983, **53**, 521–528.

21 A. Bax, in *Methods in enzymology*, 1989, vol. 176, pp. 151–167.

22 S. P. Rucker and A. J. Shaka, *Mol Phys*, 1989, **68**, 509–517.

23 K. F. Morris and C. S. Johnson, *J Am Chem Soc*, 1992, **114**, 3140–3141.

24 H. Barjat, G. A. Morris, S. Smart, A. G. Swanson and S. C. R. Williams, *J Magn Reson B*, 1995, **108**, 170–172.

25 D. Wu, A. Chen and C. S. Johnson, *J Magn Reson A*, 1995, **115**, 260–264.

26 W. P. Aue, J. Karhan and R. R. Ernst, *J Chem Phys*, 1976, **64**, 4226–4227.

27 C. Ludwig and M. R. Viant, *Phytochemical Analysis*, 2010, **21**, 22–32.

28 Y. Huang, Z. Zhang, H. Chen, J. Feng, S. Cai and Z. Chen, *Sci Rep*, , DOI:10.1038/srep08390.

29 C. M. Thiele and W. Bermel, *Journal of Magnetic Resonance*, 2012, **216**, 134–143.

30 P. Kiraly, M. Foroozandeh, M. Nilsson and G. A. Morris, *Chem Phys Lett*, 2017, **683**, 398–403.

31 A. J. Shaka, J. Keeler and A. Freeman, *Journal of Magnetic Resonance*, 1983, **53**, 13–340.

32 A. J. Shaka and P. B. Barker, *Journal of Magnetic Resonance*, 1985, **64**, 541–552.

33 A. Bax and D. Davis, *Journal of Magnetic Resonance*, 1985, **6**, 355–360.

34 E. Kupce and R. Freeman, *J Magn Reson A*, 1995, **117**, 246–256.

35 E. Kupce and R. Freeman, *J Magn Reson A*, 1995, **115**, 273–276.

36 P. Moutzouri, P. Kiraly, A. R. Phillips, S. R. Coombes, M. Nilsson and G. A. Morris, *Anal Chem*, 2017, **89**, 11898–11901.

37 E. Worgotter, G. Wagner and K. Wüthrich, *Journal of the American Chemical Society* , 1986, **108**, 113–114.

38 R. Freeman and E. Kupče, *NMR Biomed*, 1997, **10**, 372–380.

39 H. Kogler, W. Wrensen, G. Bodenhausen and R. R. Ernst, *Journal of Magnetic Resonance*, 1983, **55**, 157–163.

40 M. J. Thrippleton and J. Keeler, *Angewandte Chemie - International Edition*, 2003, **42**, 3938–3941.

41 P. W. A. Howe, *Anal Chem*, 2018, **90**, 4316–4319.

42 P. Moutzouri, P. Kiraly, M. Foroozandeh, A. R. Phillips, S. R. Coombes, M. Nilsson and G. A. Morris, *Journal of Magnetic Resonance*, 2018, **295**, 6–11.

43 T. E. Walker, R. E. London, T. W. Whaley, R. Barker and N. A. Matwiyoff, *J Am Chem Soc*, 1976, **98**, 5807–5814.

44 S. P. Rucker and A. J. Shaka, *Mol Phys*, 1989, **68**, 509–517.

45 A. Bax, M. Ikura, L. E. Kay and G. Zhu, *Journal of Magnetic Resonance*, 1991, **91**, 174–178.

46 C. Jang, L. Chen and J. D. Rabinowitz, *Cell*, 2018, 173, 822–837.

47 K. E. Hillyer, D. A. Dias, A. Lutz, U. Roessner and S. K. Davy, *New Phytologist*, 2017, **214**, 1551–1562.

48 S. Klein and E. Heinzle, *Wiley Interdiscip Rev Syst Biol Med*, 2012, **4**, 261–272.

49 R. Mi Peyraud, P. Kiefer, P. Christen, S. Massou, J.-C. Portais and J. A. Vorholt, *Proceedings of the National Academy of Sciences*, 2009, **106**, 4846–4851.

50 R. H. De Deken, *The Journal of General Microbiology*, 1966, **44**, 149–156.

51 N. Struyf, E. Van der Maelen, S. Hemdane, J. Verspreet, K. J. Verstrepen and C. M. Courtin, *Compr Rev Food Sci Food Saf*, 2017, **16**, 850–867.

52 T. Zambanini, W. Kleineberg, E. Sarikaya, J. M. Buescher, G. Meurer, N. Wierckx and L. M. Blank, *Biotechnol Biofuels*, 2016, **9**, 135–145.

53 I. A. E. Selvakumari, J. Jayamuthunagai and B. Bharathiraja, *Journal of the Indian Chemical Society*, 2021, **98**, 100075–100085.

54 A. Y. Skorokhodova, A. A. Stasenko, N. V. Krasilnikova, A. Y. Gulevich and V. G. Debabov, *Fermentation*, 2022, **8**, 738–756.

55 P. F. W. Stouten, B. R. Leeflang, B. P. Van Eijck, J. Kroon and J.-R. Mellema, *J Mol Struct*, 1988, **189**, 65–80.

56 D. S. Wishart, C. Knox, A. C. Guo, R. Eisner, N. Young, B. Gautam, D. D. Hau, N. Psychogios, E. Dong, S. Bouatra, R. Mandal, I. Sinelnikov, J. Xia, L. Jia, J. A. Cruz, E. Lim, C. A. Sobsey, S. Shrivastava, P. Huang, P. Liu, L. Fang, J. Peng, R. Fradette, D. Cheng, D. Tzur, M. Clements, A. Lewis, A. de souza, A. Zuniga, M. Dawe, Y. Xiong, D. Clive, R. Greiner, A. Nazyrova, R. Shaykhutdinov, L. Li, H. J. Vogel and I. Forsythei, *Nucleic Acids Res*, 2009, **37**, 603–610.

57 Stryer L, in *Biochemistry*, W.H. Freeman and Company, New York, 4th edn., 1995, pp. 483–508.

58 R. M. Zelle, E. De Hulster, W. A. Van Winden, P. De Waard, C. Dijkema, A. A. Winkler, J. M. A. Geertman, J. P. Van Dijken, J. T. Pronk and A. J. A. Van Maris, *Appl Environ Microbiol*, 2008, **74**, 2766–2777.

59 M. Pathan, S. Akoka and P. Giraudeau, *Journal of Magnetic Resonance*, 2012, **214**, 335–339.

60 K. Zangger, *Prog Nucl Magn Reson Spectrosc*, 2015, **86–87**, 1–20.

61 M. Foroozandeh, R. W. Adams, N. J. Meharry, D. Jeannerat, M. Nilsson and G. A. Morris, *Angewandte Chemie - International Edition*, 2014, **53**, 6990–6992.

62 L. Castañar, P. Nolis, A. Virgili and T. Parella, *Chemistry - A European Journal*, 2013, **19**, 17283–17286.

63 J. A. Aguilar, S. Faulkner, M. Nilsson and G. A. Morris, *Angewandte Chemie - International Edition*, 2010, **49**, 3901–3903.

64 J. R. Garbow, D. P. Weitekamp and A. Pines, *Chem Phys Lett*, 1982, **93**, 504–509.

65 E. O. Stejskal and J. E. Tanner, *J Chem Phys*, 1965, **42**, 288–292.

66 R. Freeman, *Journal of Progress in Nuclear Magnetic Resonance Spectroscopy*, 1998, **32**, 59–106.

67 H. Geen and R. Freeman, *Journal of Magnetic Resonance*, 1991, **93**, 93–141.

68 M. V. Gomez and A. De La Hoz, *Beilstein Journal of Organic Chemistry*, 2017, **13**, 285–300.

69 Y. Ogawa, E. Tokunaga, O. Kobayashi, K. Hirai and N. Shibata, *iScience*, 2020, **23**, 101467.

70 M. Inoue, Y. Sumii and N. Shibata, *ACS Omega*, 2020, **5**, 10633–10640.

71 Y. Ben-Tal, P. J. Boaler, H. J. A. Dale, R. E. Dooley, N. A. Fohn, Y. Gao, A. García-Domínguez, K. M. Grant, A. M. R. Hall, H. L. D. Hayes, M. M. Kucharski, R. Wei and G. C. Lloyd-Jones, *Prog Nucl Magn Reson Spectrosc*, 2022, 129, 28–106.

72 B. Gouilleux, J. Farjon and P. Giraudeau, *Journal of Magnetic Resonance*, 2020, **319**, 106810.

73 L. Emsley and G. Bodenhausen, *Journal of Magnetic resonance*, 1989, **82**, 211–221.

74 G. S. Rule and T. K. Hitchens, *Fundamentals of Protein NMR Spectroscopy*, Springer, 2006, vol. 5.

75 E. D. Becker, J. A. Ferretti and P. N. Gambhir, *Anal Chem*, 1979, **51**, 1413–1421.

76 R. G. Spencer, *Concepts in Magnetic Resonance Part A*, 2010, **36 A**, 255–265.

77 J. C. Lindon and A. G. Ferrige, *Progress in NMR spectroscopy*, 1980, **14**, 27–67.

78 A. Allerhand, *J Chem Phys*, 1966, **44**, 19–22.

79 J. Hennig, *Concepts Magn Reson*, 1991, **3**, 125–143.

80 N. N. Lukzen and A. A. Savelov, *Journal of Magnetic Resonance*, 2007, **185**, 71–76.

81 M. V. Petrova, A. B. Doktorov and N. N. Lukzen, *Journal of Magnetic Resonance*, 2011, **212**, 330–343.

82 W. Kew, N. G. A. Bell, I. Goodall and D. Uhrín, *Magnetic Resonance in Chemistry*, 2017, **55**, 785–796.

83 M. D. Pelta, G. A. Morris, M. J. Stchedroff and S. J. Hammond, *Magnetic Resonance in Chemistry*, 2002, **40**, S147–S152.

84 S. G. Hyberts, S. A. Robson and G. Wagner, *J Biomol NMR*, 2013, **55**, 167–178.

85 B. Lindman, N. Kamenka and B. Brun, *J Colloid Interface Sci*, 1976, **56**, 328–336.

86 J. S. Anderson and K. S. Saddington, *Journal of the Chemical Society (resumed)*, 1949, s381–s386.

87 R. C. Hardy and R. L. Cottington, *J Res Natl Bur Stand (1934)*, 1949, **42**, 573–579.

88 Y. Li and J. N. S. Evans, *Chem Phys Lett*, 1995, **241**, 79–83.

89 C. L. Dickson, G. Peat, M. Rossetto, M. E. Halse and D. Uhrín, *Chemical Communications*, 2022, **58**, 5534–5537.

90 P. T. Robinson, T. N. Pham and D. Uhrín, *Journal of Magnetic Resonance*, 2004, **170**, 97–103.

91 M. Nilsson and G. A. Morris, *Chemical Communications*, 2007, 933–935.

92 M. J. Smith, L. Castañar, R. W. Adams, G. A. Morris and M. Nilsson, *Anal Chem*, 2022, **94**, 12757–12761.

93 J. Bohlen and G. Bodenhausen, *Journal of Magnetic Resonance*, 1993, **102**, 293–301.

A Appendix

A.1 DISPEL

A.1.1 1D interleaved DISPEL sequence.

```
;DISPEL (four stage) with interleaved acquisition

;

;       Pulse sequence for the suppression of one-bond 13C satellites in 1H spectra

;

;       Returns one spectra with 13C satellites and one without

;

;$CLASS=HighRes

;$DIM=1D

;$TYPE=

;$SUBTYPE=

;$COMMENT=

#include <Avance.incl>

#include <Grad.incl>

#include <Delay.incl>

;CHECK SPECTROMETER POWER LIMITS FOR SECOND POWER IN LIST

define list<power> pw1= {Watt 0 79}

"acqt0=-p1*2/3.1416"

"p2=p1*2"

"d2=4050u"

"d3=3200u"

"d4=1100u"

"d5=3950u"

"d6=1560u"

"d12=20u"

"d13=50u"

"l0=0"
```

```
"DELTA =d3-d13-(p3/2)-d16-p16"
"DELTA2=d2-d3-(p3/2)-(p2/2)"
"DELTA3=d2-d3+d4-(p3/2)-(p2/2)-p16-d16"
"DELTA4=d3-d4-(p3/2)-(p1/2)"
"DELTA6=d2-d5-(p3/2)-(p2/2)"
"DELTA7=d2-d5+d6-(p2/2)-(p3/2)-p16-d16"
# ifdef PURGE
"DELTA5=d5-p16-d16-(p1/2)-(p3/2)"
"DELTA8=d5-d6-(p3/2)"
"acqt0=-p1*2/3.1416"
# else
"DELTA5=d5-p16-d16-(p1/2)-(p3/2)-p1*2/3.1416"
"DELTA8=d5-d6-(p3/2)-de"
"acqt0=0"
baseopt_echo
# endif
1 ze
2 20u BLKGRAD
3 d13 pl1:f1 pw1:f2 st0
4 30m
  20u BLKGRAD
# ifdef PRESAT
     d12 pl9:f1
     d1 cw:f1 ph29
     4u do:f1
     d12 pl1:f1
# else
     d1
# endif
```

```
5 (p1 ph1):f1
        d13 UNBLKGRAD
  DELTA1
        p16:gp1
        d16
        (p3 ph5):f2
  DELTA2
        (p2 ph2):f1
        p16:gp1
        d16
  DELTA3
        (p3 ph6):f2
  DELTA4
  (p1 ph3):f1
  DELTA5
        p16:gp2
        d16
  (p3 ph7):f2
        DELTA6
        (p2 ph4):f1
        p16:gp2
        d16
  DELTA7
        (p3 ph8):f2
  DELTA8
# ifdef PURGE
     (p1 ph9):f1
                  10u gron0 pl0:f1
                 (p32:sp29 ph11):f1
```

```
                    20u groff
                        d16 pl1:f1
                        p18:gp3
                    d16
                     (p1 ph10):f1
# endif
  goscnp ph31
  30m pw1.inc
  30m pw1:f2 st
  lo to 4 times nbl
  3m ipp1 ipp2 ipp3 ipp4 ipp5 ipp6 ipp7 ipp8 ipp31
  lo to 4 times ns
  d1 wr #0
  3m rppall
  3m zd
  lo to 4 times l4
  20u BLKGRAD
exit
ph1=0 2
ph2=0 0 0 0 0 0 0 0 1 1 1 1 1 1 1 1 2 2 2 2 2 2 2 2 3 3 3 3 3 3 3 3
ph3=1 3
ph4=2 2 3 3 0 0 1 1
ph5=0 2
ph6=0 0 2 2
ph7=0 0 0 0 2 2 2 2
ph8=0 0 0 0 0 0 0 0 2 2 2 2 2 2 2 2
ph9=0
ph10=0
ph11=0
```

ph29=0

ph31=0 2 2 0 2 0 2 0

;POWER LEVEL

;pl0 : 0W

;pl1 : f1 channel - power level for pulse (default)

;pl2 : f2 channel - power level for pulse (default)

;sp29: f1 channel - power level of adiabatic pulse of ZQF element

;PULSE SHAPE

;spnam29 : f1 channel - file name for the adiabatic shaped pulse using in ZQF [Crp60,20,20.10]

;PULSE DURATION

;p1 : f1 channel - 90 degree high power pulse

;p2 : f1 channel - 180 degree high power pulse

;p3 : f2 channel - 90 degree high power pulse

;p32: f1 channel - 180 degree shaped pulse (adiabatic) [20 msec]

;GRADIENT DURATION

;p16: duration of CTP gradients [1 msec]

;p18: homospoil gradient [1 msec]

;DELAY

;d1 : relaxation delay; 1-5 * T1

;d13: delay for UNBLKGRAD/BLKGRAD

;d16: delay for gradient recovery [500usec]

;CONSTANTS

;cnst7: 0 / 1 (no ZQF / ZQF)

;GRADIENT SHAPE

;gpnam1 : SMSQ10.100

;gpnam2 : SMSQ10.100

;gpnam3 : SMSQ10.100

;GRADIENT STRENGTH

;gpz0 : ZQF gradient [2-4%]

;gpz1 : CTP gradient [43%]

;gpz2 : CTP gradient [37%]

;gpz3 : homospoil gradient [31%]

;OTHER

;ns: 1 * n, total number of scans: NS * TD0

;ds: 2

A.1.2 DISPEL-TOCSY sequence.

;dipsi2gpphzs with DISPEL

;homonuclear Hartman-Hahn transfer using DIPSI2 sequence

; for mixing

;phase sensitive

;with zero quantum suppression

;

;Define BEFORE and AFTER to activate the DISPEL sequences on either side of the mixing

;

;$CLASS=HighRes

;$DIM=2D

;$TYPE=

;$SUBTYPE=

;$COMMENT=

#include <Avance.incl>

#include <Delay.incl>

#include <Grad.incl>

"p2=p1*2"

"p4=p3*2"

"d2=4050u"

"d3=3200u"

"d4=1100u"

"d5=3950u"

"d6=1560u"

"d12=20u"

"d11=30m"

"d13=50u"

"DELTA1=d3-d13-(p3/2)-d16-p16"

"DELTA2=d2-d3-(p3/2)-(p2/2)"

"DELTA3=d2-d3+d4-(p3/2)-(p2/2)-p16-d16"

"DELTA4=d3-d4-(p3/2)-(p1/2)"

"DELTA6=d2-d5-(p3/2)-(p2/2)"

"DELTA7=d2-d5+d6-(p2/2)-(p3/2)-p16-d16"

ifdef PURGE

"DELTA5=d5-p16-d16-(p1/2)-(p3/2)"

"DELTA8=d5-d6-(p3/2)"

"acqt0=-p1*2/3.1416"

else

"DELTA5=d5-p16-d16-(p1/2)-(p3/2)-p1*2/3.1416"

"DELTA8=d5-d6-(p3/2)-de"

"acqt0=0"

baseopt_echo

endif

"in0=0.5*inf1"

"d0=in0/2-p1*2/3.1416-p3"

"FACTOR1=(d9/(p6*115.112))/2"

"l1=FACTOR1*2"

"spoff29=0"

1 ze

  d12 pl1:f1

ifdef C13DEC

ifdef PRESAT

```
2     d11 do:f2
      50u BLKGRAD
      d12 pl9:f1
      d1 cw:f1 ph29
      4u do:f1
      d12 pl1:f1
# else
2     d11 do:f2
      50u BLKGRAD
      d1
# endif
# else

# ifdef PRESAT
2     d11
      50u BLKGRAD
      d12 pl9:f1
      d1 cw:f1 ph29
      4u do:f1
      d12 pl1:f1
# else
2     d11
      50u BLKGRAD
      d1
# endif
# endif
# ifdef START
      d13 pl2:f2
# else
```

```
    d13 pl8:f2
# endif
 (p1 ph1):f1
        d13 UNBLKGRAD
 DELTA1
        p16:gp1
        d16
        (p3 ph1):f2
 DELTA2
        (p2 ph2):f1
        p16:gp1
        d16
 DELTA3
        (p3 ph8):f2
 DELTA4
 (p1 ph3):f1
 DELTA5
        p16:gp2
        d16
 (p3 ph2):f2
        DELTA6
        (p2 ph4):f1
        p16:gp2
        d16
 DELTA7
        (p3 ph2):f2
 DELTA8 pl2:f2
# ifdef PURGE
                        (p1 ph2):f1
```

```
                    10u gron0 pl0:f1
                    (p32*1.1:sp29 ph11):f1
                    20u groff
                        d16 pl1:f1
                        p16:gp3
                    d16
                     (p1 ph10):f1
# endif
  d0
  (p4 ph2):f2
  d0
  p1 ph6
  10u gron0 pl0:f1
  (p32:sp29 ph4):f1
  20u groff
  d16 pl10:f1
                                                    ;begin DIPSI2
4 p6*3.556 ph23
  p6*4.556 ph25
  p6*3.222 ph23
  p6*3.167 ph25
  p6*0.333 ph23
  p6*2.722 ph25
  p6*4.167 ph23
  p6*2.944 ph25
  p6*4.111 ph23
  p6*3.556 ph25
  p6*4.556 ph23
  p6*3.222 ph25
```

p6*3.167 ph23

p6*0.333 ph25

p6*2.722 ph23

p6*4.167 ph25

p6*2.944 ph23

p6*4.111 ph25

p6*3.556 ph25

p6*4.556 ph23

p6*3.222 ph25

p6*3.167 ph23

p6*0.333 ph25

p6*2.722 ph23

p6*4.167 ph25

p6*2.944 ph23

p6*4.111 ph25

p6*3.556 ph23

p6*4.556 ph25

p6*3.222 ph23

p6*3.167 ph25

p6*0.333 ph23

p6*2.722 ph25

p6*4.167 ph23

p6*2.944 ph25

p6*4.111 ph23

lo to 4 times l1

;end DIPSI2

p16:gp4

d16

10u gron0*1.333 pl0:f1

```
  (p32*0.75:sp29 ph4):f1
  20u groff
  d16 pl1:f1
#ifdef END
     d13 pl2:f2
# else
     d13 pl8:f2
# endif
  (p1 ph8):f1
          d13 UNBLKGRAD
  DELTA1
          p16:gp1
          d16
          (p3 ph5):f2
  DELTA2
          (p2 ph29):f1
          p16:gp1
          d16
  DELTA3
          (p3 ph14):f2
  DELTA4
  (p1 ph3):f1
  DELTA5
          p16:gp2
          d16
  (p3 ph2):f2
          DELTA6
          (p2 ph13):f1
          p16:gp2
```

```
        d16
  DELTA7
        (p3 ph29):f2
  DELTA8
# ifdef PURGE
                        (p1 ph2):f1
                   10u gron0 pl0:f1
                  (p32*1.1:sp29 ph11):f1
                  20u groff
                        d16 pl1:f1
                        p16:gp3
# endif
# ifdef C13DEC
    d16 pl12:f2
    p1 ph29
    go=2 ph31 cpd2:f2
    d11 do:f2 mc #0 to 2
    F1PH(calph(ph6, -90), caldel(d0, +in0))
# else
    d16
    p1 ph29
    go=2 ph31
    d11 mc #0 to 2
    F1PH(calph(ph6, -90), caldel(d0, +in0))
# endif
  4u BLKGRAD
exit
ph1=0 2
ph2=0
```

ph3=1 3

ph4=2 2 3 3

ph5=0 2

ph6=0 0 0 0 2 2 2 2

ph7=0 0 0 0 2 2 2 2

ph8=0 0 0 0 0 0 0 0 2 2 2 2 2 2 2 2

ph10=0

ph11=0

ph12=1 1 3 3

ph13=2 2 2 2 2 2 2 2 3 3 3 3 3 3 3 3

ph14=0 0 2 2

ph23=3

ph25=1

ph29=0

ph31=0 2 2 0 2 0 0 2

;POWER LEVEL

;pl0 : 0W

;pl1 : f1 channel - power level for pulse (default)

;pl2 : f2 channel - power level for pulse (default)

;pl8 : f2 channel - 0W for deactivating dispel sequence

;pl10: f1 channel - power level for TOCSY-spinlock

;sp29: f1 channel - shaped pulse (adiabatic)

;PULSE DURATION

;p1 : f1 channel - 90 degree high power pulse

;p2 : f1 channel - 180 degree high power pulse

;p3 : f2 channel - 90 degree high power pulse

;p6 : f1 channel - 90 degree low power pulse

;GRADIENT DURATION

;p16: duration of CTP gradients [1 msec]

;p18: homospoil gradient [1 msec]

;p32: f1 channel - 180 degree shaped pulse (adiabatic) [20 msec]

; smoothed chirp (sweepwidth, 20% smoothing, 10000 points)

;DELAY

;d0 : incremented delay (2D) = in0/2-p1*4/3.1416

;d1 : relaxation delay; 1-5 * T1

;d9 : TOCSY mixing time

;d12: delay for power switching [20 usec]

;d13: delay for UNBLKGRAD/BLKGRAD

;d16: delay for homospoil/gradient recovery [500usec]

;l1: loop for DIPSI cycle: ((p6*115.112) * l1) = mixing time

;inf1: 1/SW = 2 * DW

;in0: 1/(1 * SW) = 2 * DW

;nd0: 1

;ns: 8 * n

;ds: 16

;td1: number of experiments

;FnMODE: States-TPPI, TPPI, States or QSEQ

;CONSTANTS

;cnst7: 0 / 1 (no ZQF / ZQF)

;PULSE SHAPE

;spnam29 : f1 channel - file name for the adiabatic shaped pulse using in ZQF [Crp60,20,20.10]

;for z-only gradients:

;gpz0: ca. 11%

;gpz1: 31%

;GRADIENT SHAPE

;gpnam1: SMSQ10.100

;gpnam2 : SMSQ10.100

;gpnam3 : SMSQ10.100

;GRADIENT STRENGTH

;gpz2 : CTP gradient [37%]

;gpz3 : homospoil gradient [31%]

;gpz0 : ZQF gradient [2-4%]

;gpz1 : CTP gradient [43%]

;gpz4 : CTP gradient [13%]

;OTHER

;ns: 1 * n, total number of scans: NS * TD0

;ds: 2

;for sweepwidth of adiabatic shape and adjusting gpz0

; see supplementary material of M.J. Thrippleton & J. Keeler,

; Angew. Chem. Int. Ed. 42, 3938-3941 (2003)

;Processing

;PHC0(F1): 90

;PHC1(F1): -180

;FCOR(F1): 1

A.1.3 DISPEL-TOCSY interleaved sequence

;dipsi2gpphzs with DISPEL interleaved

;homonuclear Hartman-Hahn transfer using DIPSI2 sequence for mixing

;phase sensitive

;with zero quantum suppression

;4 interleaved experiments wiht DISPEL before/after DIPSI2

;

; Returns in order: all couplings, c12 and c13 to c12, c12 to c12 and c13, c12 to c12

;

;$CLASS=HighRes

;$DIM=2D

```
;$TYPE=
;$SUBTYPE=
;$COMMENT=
#include <Avance.incl>
#include <Delay.incl>
#include <Grad.incl>
"p2=p1*2"
"p4=p3*2"
"d2=4050u"
"d3=3200u"
"d4=1100u"
"d5=3950u"
"d6=1560u"
"d12=20u"
"d11=30m"
"d13=50u"
"DELTA1=d3-d13-(p3/2)-d16-p16"
"DELTA2=d2-d3-(p3/2)-(p2/2)"
"DELTA3=d2-d3+d4-(p3/2)-(p2/2)-p16-d16"
"DELTA4=d3-d4-(p3/2)-(p1/2)"
"DELTA5=d5-p16-d16-(p1/2)-(p3/2)"
"DELTA6=d2-d5-(p3/2)-(p2/2)"
"DELTA7=d2-d5+d6-(p2/2)-(p3/2)-p16-d16"
"DELTA8=d5-d6-(p3/2)"
"in0=0.5*inf1"
"d23=in0*td1+3u"
# ifdef F1180
"d0=in0/2"
"TAU=3u"
```

```
# else
"d0=3u"
"TAU=2*d0"
# endif
"FACTOR1=(d9/(p6*115.112))/2"
"l1=FACTOR1*2"
"acqt0=-p1*2/3.1416"
"spoff29=0"
"l0=0"
1 ze
  d12 pl1:f1
# ifdef C13DEC
# ifdef PRESAT
2     d11 do:f2
# ifdef HEATCOMP
      d23               ; heat compensation delay
# endif
      50u BLKGRAD
      d12 pl9:f1
      d1 cw:f1 ph29
      4u do:f1
      d12 pl1:f1
# else
2     d11 do:f2
# ifdef HEATCOMP
      d23               ; heat compensation delay
# endif
      50u BLKGRAD
      d1
```

```
# endif
# else
# ifdef PRESAT
2     d11
# ifdef HEATCOMP
      d23               ; heat compensation delay
# endif
                                50u BLKGRAD
      d12 pl9:f1
      d1 cw:f1 ph29
      4u do:f1
      d12 pl1:f1
# else
2     d11
# ifdef HEATCOMP
      d23               ; heat compensation delay
# endif
                                50u BLKGRAD
      d1
# endif
# endif
if "l0 %4 == 0"
     {
     d13 pl8:f2
     }
if "l0 %4 == 1"
     {
     d13 pl8:f2
     }
```

```
if "l0 %4 == 2"
    {
    d13 pl2:f2
    }
if "l0 %4 == 3"
    {
    d13 pl2:f2
    }
 (p1 ph1):f1
          d13 UNBLKGRAD
 DELTA1
          p16:gp1
          d16
          (p3 ph5):f2
 DELTA2
          (p2 ph2):f1
          p16:gp1
          d16
 DELTA3
          (p3 ph6):f2
 DELTA4
 (p1 ph3):f1
 DELTA5
          p16:gp2
          d16
 (p3 ph7):f2
 DELTA6
          (p2 ph4):f1
          p16:gp2
```

```
            d16
  DELTA7
            (p3 ph8):f2
  DELTA8 ;pl8:f2
;# ifdef PURGE
            (p1 ph9):f1
            10u gron0 pl0:f1
            (p32*1.1:sp29 ph11):f1
            20u groff
            d16 pl1:f1
            p16:gp3
            d16
            (p1 ph10):f1
;# endif

# ifdef F1180
# ifdef F1C13DEC
  d0
 (p14:sp3 ph29):f2
  d0
 p2 ph16
  (p14:sp3 ph29):f2
# else
  d0
  d0
  TAU
  p2 ph16
  TAU
# endif
```

```
# else
# ifdef F1C13DEC
  d0
 (p14:sp3 ph29):f2
  d0
 p2 ph16
  (p14:sp3 ph29):f2
  TAU
# else
  d0
  d0
  p2 ph16
  TAU
# endif
# endif
  p1 ph12
  10u gron0 pl0:f1
  (p32:sp29 ph13):f1
  20u groff
  d16 pl10:f1
                                                ;begin DIPSI2
4 p6*3.556 ph23
  p6*4.556 ph25
  p6*3.222 ph23
  p6*3.167 ph25
  p6*0.333 ph23
  p6*2.722 ph25
  p6*4.167 ph23
  p6*2.944 ph25
```

p6*4.111 ph23

p6*3.556 ph25

p6*4.556 ph23

p6*3.222 ph25

p6*3.167 ph23

p6*0.333 ph25

p6*2.722 ph23

p6*4.167 ph25

p6*2.944 ph23

p6*4.111 ph25

p6*3.556 ph25

p6*4.556 ph23

p6*3.222 ph25

p6*3.167 ph23

p6*0.333 ph25

p6*2.722 ph23

p6*4.167 ph25

p6*2.944 ph23

p6*4.111 ph25

p6*3.556 ph23

p6*4.556 ph25

p6*3.222 ph23

p6*3.167 ph25

p6*0.333 ph23

p6*2.722 ph25

p6*4.167 ph23

p6*2.944 ph25

p6*4.111 ph23

```
  lo to 4 times l1
                                                    ;end DIPSI2
  p16:gp4
  d16
  10u gron0*1.333 pl0:f1
  (p32*0.75:sp29 ph14):f1
  20u groff
  d12 pl1:f1

if "l0 %4 == 0"
    {
    d13 pl8:f2
    }
if "l0 %4 == 1"
    {
    d13 pl2:f2
    }
if "l0 %4 == 2"
    {
    d13 pl8:f2
    }
if "l0 %4 == 3"
    {
    d13 pl2:f2
    }
  (p1 ph11):f1
          d13
  DELTA1
          p16:gp1*1.1
```

```
        d16
        (p3 ph17):f2
  DELTA2
        (p2 ph2):f1
        p16:gp1*1.1
        d16
  DELTA3
        (p3 ph18):f2
  DELTA4
        (p1 ph3):f1
  DELTA5
        p16:gp2*1.1
        d16
        (p3 ph19):f2
  DELTA6
        (p2 ph4):f1
        p16:gp2*1.1
        d16
  DELTA7
        (p3 ph20):f2
  DELTA8
;# ifdef PURGE
        (p1 ph9):f1
        10u gron0 pl0:f1
        (p32*1.1:sp29 ph14):f1
        20u groff
        d16 pl1:f1
        p16:gp3*1.1
;# endif
```

```
# ifdef C13DEC
    d16 pl12:f2
    p1 ph15
    go=2 ph31 cpd2:f2
    d11 do:f2 mc #0 to 2
    F1I(iu0,4)
    F1PH(calph(ph10, 90), caldel(d0, +in0) & caldel(d23,-in0))
# else
    d16 pl8:f2
    p1 ph15
    go=2 ph31
    d11 mc #0 to 2
    F1I(iu0,4)
    F1PH(calph(ph10, 90), caldel(d0, +in0) & caldel(d23,-in0))
# endif
  4u BLKGRAD
exit
ph1=0 2
ph2=0
ph3=1
ph4=2
ph5=0 0 0 0 2 2 2 2 2 2 2 2 0 0 0 0
ph6=0
ph7=0
ph8=0
ph9=0
ph10=0 0 2 2
ph11=0 0 0 0 0 0 0 0 2 2 2 2 2 2 2 2
ph12=0
```

ph13=0

ph14=0

ph15=0

ph16=0

ph17=1 1 1 1 3 3 3 3

ph18=1

ph19=1

ph20=1

ph23=3

ph25=1

ph29=0

ph31=0 2 2 0 0 2 2 0 2 0 0 2 2 0 0 2

;POWER LEVEL

;pl0 : 0W

;pl1 : f1 channel - power level for pulse (default)

;pl2 : f2 channel - power level for pulse (default)

;pl8 : f2 channel - 0W for deactivating dispel sequence

;pl10: f1 channel - power level for TOCSY-spinlock

;sp29: f1 channel - shaped pulse (adiabatic)

;PULSE DURATION

;p1 : f1 channel - 90 degree high power pulse

;p2 : f1 channel - 180 degree high power pulse

;p3 : f2 channel - 90 degree high power pulse

;p6 : f1 channel - 90 degree low power pulse

;GRADIENT DURATION

;p16: duration of CTP gradients [1 msec]

;p18: homospoil gradient [1 msec]

;p32: f1 channel - 180 degree shaped pulse (adiabatic) [20 msec]

; smoothed chirp (sweepwidth, 20% smoothing, 10000 points)

;DELAY

;d0 : incremented delay (2D) = in0/2-p1*4/3.1416

;d1 : relaxation delay; 1-5 * T1

;d9 : TOCSY mixing time

;d12: delay for power switching [20 usec]

;d13: delay for UNBLKGRAD/BLKGRAD

;d16: delay for homospoil/gradient recovery [500usec]

;l1: loop for DIPSI cycle: ((p6*115.112) * l1) = mixing time

;inf1: 1/SW = 2 * DW

;in0: 1/(1 * SW) = 2 * DW

;nd0: 1

;ns: 8 * n

;ds: 16

;td1: number of experiments

;FnMODE: States-TPPI, TPPI, States or QSEQ

;CONSTANTS

;cnst7: 0 / 1 (no ZQF / ZQF)

;PULSE SHAPE

;spnam29 : f1 channel - file name for the adiabatic shaped pulse using in ZQF [Crp60,20,20.10]

;use gradient files:

;gpnam1: SMSQ10.100

;gpnam2: SMSQ10.100

;gpnam3 : SMSQ10.100

;gpnam4 : SMSQ10.100

;GRADIENT STRENGTH

;gpz0 : ZQF gradient [2-4%]

;gpz1 : CTP gradient [43%]

;gpz2 : CTP gradient [37%]

;gpz3 : homospoil gradient [31%]

;gpz4 : TOCSY gradient [27%]

;OTHER

;ns: 16 * n

;ds: 4

;for sweepwidth of adiabatic shape and adjusting gpz0

; see supplementary material of M.J. Thrippleton & J. Keeler,

; Angew. Chem. Int. Ed. 42, 3938-3941 (2003)

;Processing

;PHC0(F1): 90

;PHC1(F1): -180

;FCOR(F1): 1

A.1.4 DISPEL-TOCSY interleaved processing AU program

```
#include <inc/sysutil>

#include <inc/exptUtil>

//gives 8 spectra, 1=all connections, 2=13-12+12-12,3=12-13+12-12,4=12-12,5=13-12,6=12-13,7=13-12+12-13+13-13,8=13-13

int     first,iexpno;

float f1phc0;

//double  swp;

char buffer[1024]; //this buffer is for the XCMD string for splitting, may need memory optimisation

//get current data

GETCURDATA

//define our new expnos for the split data

first=expno;

iexpno = expno+1000;

GETINT("Enter the EXPNO for the first spectrum, ensure there are 8 empty slots following this number for further spectra. e.g. 1000-1007", iexpno)

if (first==iexpno)

        STOPMSG("program aborted\nYou don't want to split into the original dataset")

//generate and execute the split command. Calls the default bruker AU program "split".
```

```
snprintf(buffer, sizeof(buffer), "split 4 %d", iexpno);
XCMD(buffer);
DATASET(name, iexpno, 1, disk, user)
VIEWDATA_SAMEWIN
XFB;
STOREPAR("ALPHA",1.0);
STOREPAR("GAMMA",-1.0);
WRA(iexpno+6)
WRPA(name, iexpno+6, procno, disk, user)
WRA(iexpno+7)
WRPA(name, iexpno+7, procno, disk, user)
DATASET(name, iexpno+6, procno, disk, user)
VIEWDATA_SAMEWIN
XFB;
STOREPAR("ALPHA",1.0);
STOREPAR("GAMMA",-1.0);
DATASET(name, iexpno+7, procno, disk, user)
VIEWDATA_SAMEWIN
XFB;
STOREPAR("ALPHA",1.0);
STOREPAR("GAMMA",-1.0);
DATASET(name, iexpno+1, procno, disk, user)
VIEWDATA_SAMEWIN
XFB;
STOREPAR("ALPHA",1.0);
STOREPAR("GAMMA",-1.0);
WRA(iexpno+5)
WRPA(name, iexpno+5, procno, disk, user)
DATASET(name, iexpno+5, procno, disk, user)
```

```
VIEWDATA_SAMEWIN

XFB;

STOREPAR("ALPHA",1.0);

STOREPAR("GAMMA",-1.0);

DATASET(name, iexpno+2, procno, disk, user)

VIEWDATA_SAMEWIN

XFB;

STOREPAR("ALPHA",1.0);

STOREPAR("GAMMA",-1.0);

WRA(iexpno+4)

WRPA(name, iexpno+4, procno, disk, user)

DATASET(name, iexpno+4, procno, disk, user)

VIEWDATA_SAMEWIN

XFB;

STOREPAR("ALPHA",1.0);

STOREPAR("GAMMA",-1.0);

DATASET(name, iexpno+3, procno, disk, user)

VIEWDATA_SAMEWIN

XFB;

STOREPAR("ALPHA",1.0);

STOREPAR("GAMMA",-1.0);


DATASET(name, iexpno+4, procno, disk, user)

VIEWDATA_SAMEWIN

DATASET2(name, iexpno+3, procno, disk, user);

ADD2D;

DATASET(name, iexpno+5, procno, disk, user)

VIEWDATA_SAMEWIN

STOREPAR("ALPHA",1.0);
```

```
STOREPAR("GAMMA",-1.0);
DATASET2(name, iexpno+3, procno, disk, user);
ADD2D;
DATASET(name, iexpno+6, procno, disk, user)
VIEWDATA_SAMEWIN
STOREPAR("ALPHA",1.0);
STOREPAR("GAMMA",-1.0);
DATASET2(name, iexpno+3, procno, disk, user);
ADD2D;
DATASET(name, iexpno+7, procno, disk, user)
VIEWDATA_SAMEWIN
STOREPAR("ALPHA",1.0);
STOREPAR("GAMMA",-1.0);
DATASET2(name, iexpno+1, procno, disk, user);
ADD2D;
DATASET(name, iexpno+7, procno, disk, user)
VIEWDATA_SAMEWIN
STOREPAR("ALPHA",1.0);
STOREPAR("GAMMA",-1.0);

DATASET2(name, iexpno+2, procno, disk, user);
ADD2D;
DATASET(name, iexpno+3, procno, disk, user)
VIEWDATA_SAMEWIN
STOREPAR("ALPHA",1.0);
STOREPAR("GAMMA",1.0);
DATASET(name, iexpno+7, procno, disk, user)
VIEWDATA_SAMEWIN
STOREPAR("ALPHA",1.0);
```

STOREPAR("GAMMA",1.0);

DATASET2(name, iexpno+3, procno, disk, user);

ADD2D;

snprintf(buffer, sizeof(buffer), "Processing complete\nSee expnos starting %d for results. You may need to refresh the data directory to show files 5-8", iexpno+1);

QUITMSG(buffer);

A.1.5 *J*-RES-DISPEL sequence

;jresgpprqf and DISPEL

;homonuclear J-resolved 2D correlation

;with presaturation during relaxation delay

;using gradients

;

;$CLASS=HighRes

;$DIM=2D

;$TYPE=

;$SUBTYPE=

;$COMMENT=

#include <Avance.incl>

#include <Grad.incl>

#include <Delay.incl>

"acqt0=-p1*2/3.1416"

"p2=p1*2"

"d2=4050u"

"d3=3200u"

"d4=1100u"

"d5=3950u"

"d6=1560u"

"d11=30m"

```
"d12=20u"
"d13=50u"
"in0=inf1/2"
"d0=3u"
"DELTA1=d3-d13-(p3/2)-d16-p16"
"DELTA2=d2-d3-(p3/2)-(p2/2)"
"DELTA3=d2-d3+d4-(p3/2)-(p2/2)-p16-d16"
"DELTA4=d3-d4-(p3/2)-(p1/2)"
"DELTA6=d2-d5-(p3/2)-(p2/2)"
"DELTA7=d2-d5+d6-(p2/2)-(p3/2)-p16-d16"
# ifdef PURGE
"DELTA5=d5-p16-d16-(p1/2)-(p3/2)"
"DELTA8=d5-d6-(p3/2)"
"acqt0=-p1*2/3.1416"
# else
"DELTA5=d5-p16-d16-(p1/2)-(p3/2)-p1*2/3.1416"
"DELTA8=d5-d6-(p3/2)-de"
"acqt0=0"
baseopt_echo
# endif
1 ze
2 d11 BLKGRAD
3 d12 pl9:f1
  d1 cw:f1 ph29
  4u do:f1
# ifdef DISPEL
     d12 pl1:f1 pl2:f2
#  else
     d12 pl1:f1 pl8:f2
```

```
# endif
  (p1 ph5):f1
        d13 UNBLKGRAD
  DELTA1
        p16:gp1
        d16
        (p3 ph5):f2
  DELTA2
        (p2 ph12):f1
        p16:gp1
        d16
  DELTA3
        (p3 ph6):f2
  DELTA4
  (p1 ph3):f1
  DELTA5
        p16:gp2
        d16
  (p3 ph7):f2
        DELTA6
        (p2 ph4):f1
        p16:gp2
        d16
  DELTA7
        (p3 ph8):f2
  DELTA8
# ifdef PURGE
                        (p1 ph9):f1
                10u gron0 pl0:f1
```

```
                    (p32:sp29 ph11):f1
                    20u groff
                            d16 pl1:f1
                            p18:gp3
                    d16
                     (p1 ph10):f1
# endif
 4u
 d0
 p16:gp1
 d16
 p2 ph2
 4u
 p16:gp2
 d16
 d0 BLKGRAD
 go=2 ph31
 d11 mc #0 to 2 F1QF(caldel(d0, +in0))
exit
ph1=0 0 0 0 1 1 1 1 2 2 2 2 3 3 3 3
ph2=0 2 1 3 1 3 2 0 1 3 2 0 2 0 3 1
ph3=1 3
ph4=2 2 3 3 0 0 1 1
ph5=0 2
ph6=0 0 2 2
ph7=0 0 0 0 2 2 2 2
ph8=0 0 0 0 0 0 0 0 2 2 2 2 2 2 2 2
ph9=0
ph10=0
```

ph11=0

ph12=0 0 0 0 0 0 0 0 1 1 1 1 1 1 1 1 2 2 2 2 2 2 2 2 3 3 3 3 3 3 3 3

ph29=0

ph31=2 0 2 0 0 2 0 2

;pl0 : 0W

;pl1 : f1 channel - power level for pulse (default)

;pl2 : f2 channel - power level for pulse (default)

;pl9 : f1 channel - power level for presaturation

;p1 : f1 channel - 90 degree high power pulse

;p2 : f1 channel - 180 degree high power pulse

;p3 : f2 channel - 90 degree high power pulse

;p16: homospoil/gradient pulse [1 msec]

;p18: homospoil gradient [1 msec]

;sp29: f1 channel - power level of adiabatic pulse of ZQF element

;p32: f1 channel - 180 degree shaped pulse (adiabatic) [20 msec]

;d0 : incremented delay (2D) [3 usec]

;d1 : relaxation delay; 1-5 * T1

;d11: delay for disk I/O [30msec]

;d13: delay for UNBLKGRAD/BLKGRAD

;d12: delay for power switching [20 usec]

;d16: delay for homospoil/gradient recovery [500usec]

;inf1: 1/w, w = max. width of multiplet

;in0: 1/(2 * w), w = max. width of multiplet

;nd0: 2

;ns: 4 * n

;ds: 16

;td1: number of experiments

;FnMODE: QF

;cnst7: 0 / 1 (no ZQF / ZQF)

;use gradient ratio: gp 1 : gp 2

; 10 : 10

;for z-only gradients:

;gpz1: 10%

;gpz2: 10%

;use gradient files:

;gpnam1: SMSQ10.100

;gpnam2: SMSQ10.100

;gpnam3 : SMSQ10.100

;GRADIENT STRENGTH

;gpz0 : ZQF gradient [2-4%]

;gpz1 : CTP gradient [43%]

;gpz2 : CTP gradient [37%]

;gpz3 : homospoil gradient [31%]

;spnam29 : f1 channel - file name for the adiabatic shaped pulse using in ZQF [Crp60,20,20.10]

A.1.6 *J*-RES-DISPEL interleaved sequence

;jresgpprqf with DISPEL

;homonuclear J-resolved 2D correlation

;with presaturation during relaxation delay

;using gradients

;

;$CLASS=HighRes

;$DIM=2D

;$TYPE=

;$SUBTYPE=

;$COMMENT=

#include <Avance.incl>

#include <Grad.incl>

#include <Delay.incl>

"acqt0=-p1*2/3.1416"

"p2=p1*2"

"d2=4050u"

"d3=3200u"

"d4=1100u"

"d5=3950u"

"d6=1560u"

"d11=30m"

"d12=20u"

"d13=50u"

"in0=inf1/2"

"d0=3u"

"DELTA1=d3-d13-(p3/2)-d16-p16"

"DELTA2=d2-d3-(p3/2)-(p2/2)"

"DELTA3=d2-d3+d4-(p3/2)-(p2/2)-p16-d16"

"DELTA4=d3-d4-(p3/2)-(p1/2)"

"DELTA6=d2-d5-(p3/2)-(p2/2)"

"DELTA7=d2-d5+d6-(p2/2)-(p3/2)-p16-d16"

ifdef PURGE

"DELTA5=d5-p16-d16-(p1/2)-(p3/2)"

"DELTA8=d5-d6-(p3/2)"

"acqt0=-p1*2/3.1416"

else

"DELTA5=d5-p16-d16-(p1/2)-(p3/2)-p1*2/3.1416"

"DELTA8=d5-d6-(p3/2)-de"

"acqt0=0"

baseopt_echo

endif

1 ze

```
2 d11 BLKGRAD
3 d12 pl9:f1
  d1 cw:f1 ph29
  4u do:f1
  d12 pl1:f1
if "l0 %2 == 0"
    {
  d12 pl2:f2
    }
else
    {
  d12 pl8:f2
    }
  (p1 ph5):f1
          d13 UNBLKGRAD
  DELTA1
          p16:gp1
          d16
          (p3 ph5):f2
  DELTA2
          (p2 ph12):f1
          p16:gp1
          d16
  DELTA3
          (p3 ph6):f2
  DELTA4
  (p1 ph3):f1
  DELTA5
          p16:gp2
```

```
        d16
  (p3 ph7):f2
        DELTA6
        (p2 ph4):f1
        p16:gp2
        d16
  DELTA7
        (p3 ph8):f2
  DELTA8
# ifdef PURGE
                        (p1 ph9):f1
                   10u gron0 pl0:f1
                  (p32:sp29 ph11):f1
                  20u groff
                        d16 pl1:f1
                        p18:gp3
                  d16
                   (p1 ph10):f1
# endif
  4u
  d0
  p16:gp1
  d16
  p2 ph2
  4u
  p16:gp2
  d16
  d0 BLKGRAD
  go=2 ph31
```

```
 d11 mc #0 to 2
 F1I(iu0,2)
 F1QF(caldel(d0, +in0))
exit
ph1=0 0 0 0 1 1 1 1 2 2 2 2 3 3 3 3
ph2=0 2 1 3 1 3 2 0 1 3 2 0 2 0 3 1
ph3=1 3
ph4=2 2 3 3 0 0 1 1
ph5=0 2
ph6=0 0 2 2
ph7=0 0 0 0 2 2 2 2
ph8=0 0 0 0 0 0 0 0 2 2 2 2 2 2 2 2
ph9=0
ph10=0
ph11=0
ph12=0 0 0 0 0 0 0 0 1 1 1 1 1 1 1 1 2 2 2 2 2 2 2 2 3 3 3 3 3 3 3 3
ph29=0
ph31=2 0 2 0 0 2 0 2
;pl0 : 0W
;pl1 : f1 channel - power level for pulse (default)
;pl2 : f2 channel - power level for pulse (default)
;pl9 : f1 channel - power level for presaturation
;p1 : f1 channel -  90 degree high power pulse
;p2 : f1 channel -  180 degree high power pulse
;p3 : f2 channel -  90 degree high power pulse
;p16: homospoil/gradient pulse                    [1 msec]
;p18: homospoil gradient                                                    [1 msec]
;sp29: f1 channel - power level of adiabatic pulse of ZQF element
;p32: f1 channel - 180 degree shaped pulse (adiabatic)    [20 msec]
```

;d0 : incremented delay (2D) [3 usec]

;d1 : relaxation delay; 1-5 * T1

;d11: delay for disk I/O [30msec]

;d13: delay for UNBLKGRAD/BLKGRAD

;d12: delay for power switching [20 usec]

;d16: delay for homospoil/gradient recovery [500usec]

;inf1: 1/w, w = max. width of multiplet

;in0: 1/(2 * w), w = max. width of multiplet

;nd0: 2

;ns: 4 * n

;ds: 16

;td1: number of experiments

;FnMODE: QF

;cnst7: 0 / 1 (no ZQF / ZQF)

;use gradient ratio: gp 1 : gp 2

; 10 : 10

;for z-only gradients:

;gpz1: 10%

;gpz2: 10%

;use gradient files:

;gpnam1: SMSQ10.100

;gpnam2: SMSQ10.100

;gpnam3 : SMSQ10.100

;GRADIENT STRENGTH

;gpz0 : ZQF gradient [2-4%]

;gpz1 : CTP gradient [43%]

;gpz2 : CTP gradient [37%]

;gpz3 : homospoil gradient [31%]

;spnam29 : f1 channel - file name for the adiabatic shaped pulse using in ZQF [Crp60,20,20.10]

A.2 Benchtop SHARPER

A.2.1 Table of nutation curve parameters

Table 8.1: Table of nutation curve parameters used to calibrate the pulse length for the benchtop spectrometer.

Power (dB)	Initial pulse length (us)	Step size (us)	Power (dB)	Initial pulse length (us)	Step size (us)
0	80	2.5	-9.5	250	6
-0.5	80	4	-10	300	5
-1	100	2.5	-10.5	280	6
-1.5	110	4	-11	320	5
-2	120	2.5	-11.5	320	7
-2.5	110	4	-12	340	6
-3	140	2.5	-12.5	390	7
-3.5	120	4	-13	360	7
-4	160	2.5	-13.5	390	8
-4.5	130	4	-14	450	7
-5	180	2.5	-14.5	460	8
-5.5	130	5	-15	510	7
-6	200	3	-15.5	550	8
-6.5	190	5	-16	570	8
-7	220	3	-16.5	580	9
-7.5	190	5	-17	670	8
-8	250	3	-17.5	630	9
-8.5	210	5	-18	670	8
-9	270	4			

A.2.2 Python script for zeroing imaginary components of Bruker FIDs

'''

Script to remove the imaginary component from Bruker NMR data

Application -> Boost S/N in phase-corrected SHARPER spectra

@author: Patrick Boaler

@email: Patrick.Boaler@ed.ac.uk

Works with TopSpin 3.5, 4.0 and 4.1.

```
Only NMR experiment directories (expnos)can be in the starting directory of this script

'''

import argparse

import os

import shutil

import nmrglue as ng

parser = argparse.ArgumentParser(prog = "zim.py",

                                 description = 'Script to remove the imaginary component from Bruker NMR data
to boost S/N in phase-corrected SHARPER spectra',

                                 epilog = "If no --expno is specified, the script will search the directory for all
experiments whose pulse-programme contains \"sharp\" and complete the operation for all of them,
depositing the output in a new directory, appended with \"-zim\" ")

parser.add_argument('filepath')

parser.add_argument('-e', '--expno', type=int, help="specify an experiment number to remove
imaginary component on a particular experiment (must be an integer)")

args = parser.parse_args()

path = args.filepath

def read_data2(dir):

    try:

        dic,data = ng.bruker.read(dir)

    except ZeroDivisionError:

        try:

            dic,data = ng.bruker.read(dir,'ser')

        except (FileNotFoundError,ZeroDivisionError):

            print('Error on ' + dir)

            return None,None

    return dic,data

if args.expno:

    inpath = os.path.join(path,str(args.expno))

    outpath = os.path.join(path + '-zim',str(args.expno))

        if 'pulseprogram' not in os.listdir(inpath):
```

```
            shutil.copy(os.path.join(inpath,'pulseprogram.precomp'),os.path.join(inpath,'pulseprogram'))
    dic,data = ng.bruker.read(inpath)     # reads bruker data
    newdata = ng.proc_base.di(data) + 0j  # sets imaginary component to 0j for all points in FID
    try:
        shutil.copytree(inpath,outpath)
    except FileExistsError:
        shutil.rmtree(outpath)
        shutil.copytree(inpath,outpath)
    ng.fileio.bruker.write(outpath,dic,newdata,overwrite=True)
else:
    dirs = []
    for subdir in os.listdir(path):
        if 'pulseprogram' not in os.listdir(os.path.join(path,subdir)):

shutil.copy(os.path.join(path,subdir,'pulseprogram.precomp'),os.path.join(path,subdir,'pulseprogram'))
        dic,data = read_data2(os.path.join(path,subdir))
        try:
            if 'sharp' in dic['acqus']['PULPROG'].lower():
                dirs.append(subdir)
        except TypeError:
            pass
    for subdir in dirs:
        inpath = os.path.join(path,subdir)
        outpath = os.path.join(path + '-zim',subdir)
        dic,data = read_data2(inpath)
        newdata = ng.proc_base.di(data) + 0j
        try:
            shutil.copytree(inpath,outpath)
            ng.fileio.bruker.write(outpath,dic,newdata,overwrite=True)
        except FileExistsError:
```

```
        shutil.rmtree(outpath)
        shutil.copytree(inpath,outpath)
    ng.fileio.bruker.write(outpath,dic,newdata,overwrite=True)
```

A.2.3 AU program for zeroing imaginary components of Bruker FIDs

```
/*
George Peat
July 2023
george.peat@ed.ac.uk
 - Making a new folder (name, expno, procno) and coping the current data to it.
 - Opening the FID and making a "rawdata" array for further editing.
 - The imaginary data in "rawdata" is then set to zero.
- Note: both raw (FID) and processed (spectrum) data are copied so the
        FID must be reprocessed to see the result of removing the imaginary channel.
- Notes:
 1. Both raw (FID) and processed (spectrum) data are copied.
 The FID must be reprocessed to see the result.
 2. For Bruker data (NEO console) use double (as below).
 3. For Bruker data (AVIII console) all instances of double should be replaced with float.
 4. Benchtop data has not been tested.
 */
// Initialisation.
#define MAXSIZE 800000
int expno1, procno1, expno2, procno2, td, tdtest, a, b, c;
double rawdata[MAXSIZE];
char oldname[500], newname[500], infile[PATH_MAX], outfile[PATH_MAX];
FILE *fpin, *fpout;
// Get the foreground data set.
GETCURDATA
// Set initial data variables from current dataset.
```

```
expno1 = expno;
procno1 = procno;
strcpy(oldname, name);
strcpy(infile, ACQUPATH("fid"));
// Set new data variables from current dataset.
expno2 = expno;
procno2 = procno;
strcpy(newname, name);
// Print some information.
printf("\tSTART \n\n");
printf("Current dataset: \t%s %d %d \n", name, expno, procno);
printf("Initial dataset: \t%s %d %d \n", oldname, expno1, procno1);
printf("Initial FID file path: \t%s\n", infile);

// Offer user the chance to change one or all of the variables for the new data.
GETSTRING("Enter a file name:", newname)
GETINT("Enter a new experiment file number:", expno2)
GETINT("Enter a processed file number:", procno2)
// Write a copy of the inital dataset to the new location.
WRPA(newname, expno2, procno2, disk, user)
printf("\n\tCopy raw and processed data to new file location. \n");
printf("Current dataset: \t%s %d %d \n", name, expno, procno);
printf("Initial dataset: \t%s %d %d \n", oldname, expno1, procno1);
printf("New dataset: \t\t%s %d %d \n", newname, expno2, procno2);
// Load the new location.
DATASET(newname, expno2, procno2, disk, usr)
strcpy(outfile, ACQUPATH("fid"));
printf("\n\tGo to new file location. \n");
printf("Current dataset: \t%s %d %d \n", name, expno, procno);
```

```
printf("Initial dataset: \t%s %d %d \n", oldname, expno1, procno1);
printf("New dataset: \t\t\t%s %d %d \n", newname, expno2, procno2);
printf("New FID file path: \t%s\n\n", outfile);
// Load in TD (real+imaginary points) from the experiment parameters
FETCHPAR("TD", &td)
// Open the FID for reading using the outfile path, return an error message if it fails.
if((fpin = fopen(outfile,"r")) == NULL){STOPMSG("Open of new FID failed for reading.\n")};
// Read the data in the FID into rawdata
// Data in the FID is 8 bytes, with alternating real and imaginary rows up to TD.
fread(rawdata,sizeof(double),td,fpin);
//Close the FID which is in the outfile path
fclose(fpin);

// Print some of the intial points of the FID
printf("\n\t Check the first five rows of the initial FID. \nRow\t\tReal\t\tImaginary\n");
for(a=0;a<10;a++)
	{
		if (a%2 == 0)
			printf("%d\t\t%f\t\t", a/2, rawdata[a]);
		else
			printf("%f\n", rawdata[a]);
	}
// Set the imaginary points to 0
for(b=0;b<td;b++)
	{
		if (b%2 == 1)
			rawdata[b] = 0;
	}
// Print some of the intial points of the processed FID
```

```
printf("\n\t Check the first five rows of the new FID. \nRow\t\tReal\t\tImaginary\n");

for(a=0;a<10;a++)

        {

                if (a%2 == 0)

                        printf("%d\t\t%f\t\t", a/2, rawdata[a]);

                else

                        printf("%f\n", rawdata[a]);

        }

// Open the FID for writing using the outfile path, return an error message if it fails.

if((fpout = fopen(outfile,"w")) == NULL){STOPMSG("Open of new FID failed for writing.\n")};


// Read the data in the FID into rawdata

// Data in the FID is 8 bytes, with alternating real and imaginary rows up to TD.

fwrite(rawdata,sizeof(double),td,fpout);

//Close the FID which is in the outfile path

fclose(fpout);

QUIT
```

A.3 CPMG-DOSY-SHARPER

A.3.1 CPMG-SHARPER sequence with BSPE

```
;sharper_collapse.du

;avance-version (18/10/2022)

;written for TopSpin 4 and NEO console, for avIII+ the dwl_clk_on/off commands are different; see the acquisition part

;

;pulse sequence to collapse all or some (selected by band selective perfect echo) signals into a singlet

;solvent presaturation using pulsed presat or changing frequencies

;optional 13C decoupling

;

;G. Peat, P.J. Boaler, C.L. Dickson, G.C. Lloyd-Jones & D. Uhrin, Nat. Commun., 2023.

;solvent suppression based on:
```

;Kew, W., Bell, N.G.A. Goodall, I., Uhrin, D., Magn. Reson. Chem. 55, 785-796, (2017)

;

;For mutli-resonance suppression use Multi-reson-suppress.xlsx and PresatOptimise.jl to optimise p23 and o1

;

;optional band selective excitation based on perfect echo

;J. A. Aguilar, M. Nilsson, G. Bodenhausen and G. A. Morris, Chem. Commun., 2012, 48, 811

;

;for SHARRPER papers see

;Jones, A.B., Lloyd-Jones, G.C., Uhrin D, Anal. Chem. 89 10013-10021 (2017)

;Dickson, C.L., Peat, G. Rossetto, M., Halse, M.E. and Uhrin, D. Chem. Commun., 58, 5534-5537 (2022)

;Davy, M., Dickson, C.L., Wei, R., Uhrin, D., Butts, C.P. Analyst, 147, 1702-1708 (2022)

;Silva-Terra, A. I., Rossetto, M., Dickson, C. L., Peat, G., Uhrin D., Halse, M. E. ACS Meas Sci Au. 3, 73-81 (2022).

;$CLASS=HighRes

;$DIM=1D

;$TYPE=

;$SUBTYPE=

;$COMMENT=

#include <Avance.incl>

#include <Grad.incl>

#include <Delay.incl>

#include <De.incl>

#ifdef P90

"p6=p5"

#else

"p6=p5*2"

#endif

"d11=30m"

"d12=20u"

```
"d62=dw*l2"
# ifdef PURGE
"d13=4u"
"d63=(d62/2)-cnst13*dw"
"de=cnst13*dw-p1*2/PI"
# else
"d13=de"
"d63=d62/2"
"d14=d16+p1*2/PI-de"
"acqt0=0"
baseopt_echo
# endif
"l0=(aq/d62-0.5)/2"
"l31=l0+4"
# ifdef PULSED_PRESAT
"FACTOR1=(d1/(p23))+ 0.5"
"l6=FACTOR1"
# endif
"acqt0=0"
 baseopt_echo
dwellmode explicit
1 ze
# ifdef C13_DEC
  d12 pl12:f2
# endif
2 d11
# ifdef BSPE
  50u BLKGRAD
# endif
```

```
# ifdef PRESAT
# ifdef C13_DEC
  d12 cpds2:f2
# endif

# ifdef PULSED_PRESAT
  d12 pl0:f1
3 (p23:sp23 ph29):f1
  2u
  lo to 3 times l6
  d12 pl1:f1
# endif
#ifdef PRESAT_JUMP
  d12  fq=cnst23(bf):f1 ;solvent offset in Hz
  d12 pl9:f1
  d1 cw:f1 ph29
  4u do:f1
  d12 pl1:f1
  d12  fq=cnst24(bf):f1 ; real offset o1 in Hz
#endif
# ifdef C13_DEC
  d12 do:f2
# endif
# else
  d1 pl1:f1
#endif
# ifdef BSPE
  50u UNBLKGRAD
# endif
```

```
  (p1 ph1)


#ifdef BSPE
  d13
  p19:gp1
  d16 pl0:f1
  4u
  (p11:sp1 ph2):f1
  4u
  p19:gp1
  d16
  d13 pl1:f1
  (p1 ph3)
  d13
  p19:gp2
  d16 pl0:f1
  4u
  (p11:sp1 ph4):f1
  4u
  p19:gp2
# ifdef PURGE
  d16 pl1:f1
  d13
# ifdef PURGE1
  p1 ph5
  4u
  p19:gp3
  d16
  p1 ph6
```

```
# endif
# ifdef PURGE2
  p1 ph5
  4u
  10u gron0
  (p32:sp29 ph1):f1
  20u groff
  d16
  p16:gp3
  d16 pl1:f1
  p1 ph6
# endif
# else
  d14
# endif
#endif
            ACQ_START(ph30,ph31)
            0.05u START_NEXT_SCAN  ;Topspin3: leave out
        0.1u REC_UNBLK
            0.05u DWELL_RELEASE  ;Topspin3: replace with DWL_CLK_ON
            d63 pl5:f1
            0.05u DWELL_HOLD  ;Topspin3: replace with DWL_CLK_OFF
            0.1u REC_BLK
4           d10
       (p6 ph7):f1
            d10

            0.1u REC_UNBLK
            0.05u DWELL_RELEASE  ;Topspin3: replace with DWL_CLK_ON
```

```
        d62
        0.05u DWELL_HOLD  ;Topspin3: replace with DWL_CLK_OFF
        0.1u REC_BLK
        d10
        (p6 ph8):f1
        d10
        0.1u REC_UNBLK
        0.05u DWELL_RELEASE  ;Topspin3: replace with DWL_CLK_ON
        d62
        0.05u DWELL_HOLD  ;Topspin3: replace with DWL_CLK_OFF
        0.1u REC_BLK
        lo to 4 times l31
        d63
        rcyc=2
        d11 mc #0 to 2 F0(zd)
# ifdef BSPE
  50u BLKGRAD
# endif
exit
ph1=0 0 0 0 2 2 2 2
ph2=1 1 1 1 1 1 1 3 3 3 3 3 3 3 3
ph3=1 1 3 3
ph4=1 1 1 1 1 1 1 3 3 3 3 3 3 3 3
ph5=2
ph6=0
ph7=1 3
ph8=1 3
ph29=0
ph30=(360) 0 ;set phcor30 to direct signal into one channel
```

ph31=0 0 0 0 2 2 2 2

;for presat set zgoptns -DPRESAT -DPULSED_PRESAT or zgoptns -DPRESAT -DPRESAT_JUMP

;for selective 13C decoupling zgoptns -DC13_DEC

;for band selective perfect echo set zgoptns -DBSPE

;for z-filter set zgoptns -DPURGE -DPURGE1 or zgoptns -DPURGE -DPURGE2

;for 90 deg spin-echo pulses set zgoptns -DP90

;DIGMOD = baseopt

;d1 : relaxation delay [1-5 * T1]

;d11: delay for disk I/O [30 msec]

;d12: delay for power switching [20 usec]

;d16: delay for homospoil/gradient recovery [200 usec]

;d10: ringdown time - microseconds to hudreads of microseconds

;p1 : f1 channel - 90 degree high power pulse

;p5 : f1 channel - 90 degree lower power pulse for spin-echoes

;p6 : f1 channel - 180 degree lower power pulse for spin-echoes

;pl1 : f1 channel - power level for pulse (default)

;pldb1 : f1 channel - high power

;pl5 : f1 channel - power level for spin-echo pulses IMPORTANT! (see SI of the Peat et al paper)

;pldb5 : f1 channel - lower power

;ns: 2 * n, total number of scans: NS * TD0

;ds: 4

;p19: 600us homospoil/gradient pulse

;p16: 1ms homospoil/gradient pulse

;p23 : ~50 ms low power rectangular pulse

;if off-resonance, calculate its exact length, (see SI of the Peat et al paper)

;if only one signal needs to be suppressed:

;SPNAM23 : Squa100.1000

;SPOFFS23 : o1 - resonance frequency of the suppressed signal [Hz]

;spdb23 : use minimum power start with 69dB

;for zgoptns -DPRESAT_JUMP set

;cnst23: signal to be suppressed [Hz]

;cnst24: o1 [Hz]

;for zgoptns -DPULSED_PRESAT set

;p23 : ~50 ms low power rectangular pulse

;if off-resonance, calculate its exact length as desctiben in the Supplementary Information

;if only one signal needs to be suppressed:

;SPNAM23 : Squa100.1000

;SPOFFS23 : resonance frequency of the suppressed signal minus o1 [Hz]

;spdb23 : use minimum power start with 60dB, asses the result

;if multiple signals need to be suppressed use Multi-reson-suppress.xlsx and PresatOptimise.jl to optimise p23 and o1

;create a phase-ramped shape using the calulated pulse length and the distances from o1

;prepare a rectangular shape and place it into the user library, e.g. Squa100.1000 (100us, 1000 points)

;on a topspin command line type:

;st manipulate /opt/topspin4.1/exp/stan/nmr/lists/wave/user/Squa100.1000 offs e 68936 3 565.73 -580.27 -754.27

;this will OVERWRITE the Squa100.1000 shape in /opt/topspin4.1/exp/stan/nmr/lists/wave/user/

;creating a 68936 us shape that will irradiate at 565.73, -580.27 and -754.27Hz away from optimised o1

;Note: for n frequencies replace 3 with n

;spdb23 : use minimum power, start with 60dB, asses the result. For every addtional frequency adjust by subtracting 6dB.

;if zgoptns -DC13_DEC:

;o2p : 13C chemical shift of the suppressed solvent signal

;pldb12 : power level for 13C decoupling

;at least 12dB weaker than regular decoupler power

;pcpd2 : around 200us for selective decoupling

;cpdprg2 : xy32 or garp4

;l0 : number of blocks during acquisition time adjusted to get d62 as required

;l2 : number of points in full chunk [2-16] depending on dw = 1/2*SWH (increase SWH to decrease dw)

;d62: dw*l2 acquisition block between decoupling pulses [< 0.5msec]

;d63: = d62/2, length of initial half chunk if PURGE not used

;d63: d62/2-cnst13*dw if PURGE used

;cnst13: typically 1,increse SWH if negative

;d10: delay around spin-echo pulses [5-20 us]

;for zgoptns -DBSPE

;p11: f1 channel - 180 degree shaped pulse (Reburp.1000) [0.5-3 msec]

;pl9 : f1 channel - power level for presaturation [~55-69dB]

;sp1:f1 channel - 180 degree shaped pulse (Reburp.1000) [0.5-3 msec]

;spnam1: Reburp.1000

;spdb1: power level for sp1

;for zgoptns -DPURGE2 set

;sp29: f1 channel - shaped pulse (adiabatic)

;p32: f1 channel - 180 degree shaped pulse (adiabatic) [20 msec]

; smoothed chirp (sweep width, 20% smoothing, 10000 points)

; Instructions for setting receiver phase, ph30

; 1) Record spectrum with PH30 = (360) 0 and phcor30=0

; 2) Phase the spectrum using PHC0 only

; 3) If PHCO > 0 set phcor30 = 360-PHC0, if PHC0 < 0 set phcor = -PHC0

; 4) Set PHC0=0 PHC1=0

; 5) If the phase changes, rephase, do not store PHC0, set phcor30 = phcor30 - PHC0

;for z-only gradients:

;gpz0: ca 11%

;gpz1: 7%

;gpz2: 5%

;gpz3: -12%

;use gradient files:

;gpnam1: SMSQ10.100 or SINE.100

;gpnam2: SMSQ10.100 or SINE.100

;gpnam3: SMSQ10.100 or SINE.100

A.3.2 CPMG- DOSY-SHARPER sequence with BSPE

;ledbpgp2s.sharper_collapse.du

;avance-version (18/10/22)

;written for TopSpin 4 and NEO console, for avIII+ the dwl_clk_on/off commands are different, see the acquisition part

;

;2D sequence for diffusion measurement using stimulated

; echo and LED based on Bruker's ledbpgp2s

;using 2 spoil gradients and a compensating gradient

;collapsing all or some signals (selected by a band selective perfect echo) into a singlet

;optional solvent presaturation using pulsed presat or changing frequencies

;during relaxation and diffusion delays

;optional 13C decoupling

;

;G. Peat, P.J. Boaler, C.L. Dickson, G.C. Lloyd-Jones & D. Uhrin, Nat. Commun., 2023

;

;diffusion part based on

;D. Wu, A. Chen & C.S. Johnson Jr.,J. Magn. Reson. A 115, 260-264 (1995)

;Pelta, MD, Morris, GA, Stchedroff, MJ and Hammond, SJ. Magn. Reson. Chem. 40:S147-S152 (2002)

;

;solvent suppression based on:

;Kew, W., Bell, N.G.A. Goodall, I., Uhrin, D., Magn. Reson. Chem. 55, 785-796, (2017)

;For mutli-resonance suppression use Multi-reson-suppress.xlsx and PresatOptimise.jl to optimise p23 and o1

;

;optional band selective excitation based on perfect echo

;J. A. Aguilar, M. Nilsson, G. Bodenhausen and G. A. Morris, Chem. Commun., 2012, 48, 811

;

;for SHARRPER papers see:

;Jones, A.B., Lloyd-Jones, G.C., Uhrin D, Anal. Chem. 89 10013-10021 (2017)

;Dickson, C.L., Peat, G. Rossetto, M., Halse, M.E. and Uhrin, D. Chem. Commun., 58, 5534-5537 (2022)

;Davy, M., Dickson, C.L., Wei, R., Uhrin, D., Butts, C.P. Analyst, 147, 1702-1708 (2022)

;Silva-Terra, A. I., Rossetto, M., Dickson, C. L., Peat, G., Uhrin D., Halse, M. E., ACS Meas Sci Au. 3, 73-81 (2022).

;

;$CLASS=HighRes

;$DIM=2D

;$TYPE=

;$SUBTYPE=

;$COMMENT=

#include <Avance.incl>

#include <Grad.incl>

#include <Delay.incl>

#include <De.incl>

define list<gradient> diff=<Difframp>

"p2=p1*2"

ifdef P90

"p6=p5"

else

"p6=p5*2"

endif

"d11=30m"

"d12=20u"

"d62=dw*l2"

ifdef PURGE

"d13=4u"

"d63=(d62/2)-cnst13*dw"

"de=cnst13*dw-p1*2/PI"

else

"d13=de"

"d63=d62/2"

"d14=d16+p1*2/PI-de"

endif

"l0=(aq/d62-0.5)/2"

"l31=l0+4"

ifdef PULSED_PRESAT

"FACTOR1=(d1/(p23))+ 0.5"

"l6=FACTOR1"

endif

ifdef PULSED_PRESAT1

"FACTOR2=(d20/(p24))+ 0.5"

"l7=FACTOR2"

"d22=l7*p24"

endif

ifdef PRESAT1

ifdef PULSED_PRESAT1

"DELTA1=d22-p1*2-p2-p30*2-d16*4-p19*2-2*d12"

endif

ifdef PRESAT_JUMP1

"DELTA1=d20-p1*2-p2-p30*2-d16*4-p19*2-d12*4-4u"

endif

else

"DELTA1=d20-p1*2-p2-p30*2-d16*4-p19*2"

endif

```
"DELTA2=d21-p19-d16-4u"
"acqt0=0"
baseopt_echo
dwellmode explicit
1 ze
# ifdef C13_DEC
  d12 pl12:f2
# endif
2 d11
  50u BLKGRAD
# ifdef PRESAT

# ifdef C13_DEC
  d12 cpds2:f2
# endif
# ifdef PULSED_PRESAT
  d12 pl0:f1
3 (p23:sp23 ph29):f1
  2u
  lo to 3 times l6
  d12 pl1:f1
# endif
# ifdef PRESAT_JUMP
  d12  fq=cnst23(bf):f1 ;solvent offset in Hz
  d12 pl9:f1
  d1 cw:f1 ph29
  4u do:f1
  d12 pl1:f1
  d12  fq=cnst24(bf):f1 ; real offset o1 in Hz
```

```
#endif
# ifdef C13_DEC
  d12 do:f2
# endif
# else
  d1 pl1:f1
#endif
  50u UNBLKGRAD
# ifdef PURGE1
  p19:gp7*-1
# else
  p19:gp4*-1
# endif
  d16
  p1 ph1
  p30:gp6*diff
  d16
  p2 ph1
  p30:gp6*-1*diff
  d16
  p1 ph2
  p19:gp7
  d16
# ifdef PRESAT1
# ifdef C13_DEC
  d12 cpds2:f2
# endif
# ifdef PULSED_PRESAT1
  d12 pl0:f1
```

```
4 (p24:sp24 ph29):f1
  2u
  lo to 4 times l7
  d12 pl1:f1
# endif
# ifdef PRESAT_JUMP1
  d12  fq=cnst23(bf):f1 ;solvent offset in Hz
  d12 pl9:f1
  DELTA1 cw:f1 ph29
  4u do:f1
  d12 pl1:f1
  d12  fq=cnst24(bf):f1 ;o1 offset in Hz
# endif
# ifdef C13_DEC
  d12 do:f2
# endif
# else
  DELTA1 pl1:f1
# endif
  p19:gp8*-1
  d16
  p1 ph3
  p30:gp6*diff
  d16
  p2 ph1
  p30:gp6*-1*diff
  d16
  p1 ph4
  p19:gp8
```

d16

DELTA2

4u

(p1 ph5)

ifdef BSPE

d13

p19:gp1

d16 pl0:f1

4u

(p11:sp1 ph6):f1

4u

p19:gp1

d16

d13 pl1:f1

(p1 ph7)

d13

p19:gp2

d16 pl0:f1

4u

(p11:sp1 ph6):f1

4u

p19:gp2

ifdef PURGE

d16 pl1:f1

d13

ifdef PURGE1

p1 ph8

4u

p19:gp3

```
  d16
  p1 ph9
# endif

# ifdef PURGE2
  p1 ph8
  4u
  10u gron0
  (p32:sp29 ph1):f1
  20u groff
  d16
  p16:gp3
  d16 pl1:f1
  p1 ph9
# endif
# else
  d14
# endif
#endif
        ACQ_START(ph30,ph31)
        0.05u START_NEXT_SCAN  ;Topspin3: leave out
        0.1u REC_UNBLK
            0.05u DWELL_RELEASE             ;Topspin3: replace with DWL_CLK_ON
        d63 pl5:f1
        0.05u DWELL_HOLD  ;Topspin3: replace with DWL_CLK_OFF
        0.1u REC_BLK
5       d10
        (p6 ph10):f1
        d10
```

```
        0.1u REC_UNBLK
        0.05u DWELL_RELEASE  ;Topspin3: replace with DWL_CLK_ON
        d62
        0.05u DWELL_HOLD  ;Topspin3: replace with DWL_CLK_OFF
        0.1u REC_BLK
        d10
        (p6 ph11):f1
        d10
        0.1u REC_UNBLK
        0.05u DWELL_RELEASE  ;Topspin3: replace with DWL_CLK_ON
        d62
        0.05u DWELL_HOLD  ;Topspin3: replace with DWL_CLK_OFF
        0.1u REC_BLK
        lo to 5 times l31
        d63
        rcyc=2
        d11 mc #0 to 2 F1QF(igrad diff)
        4u BLKGRAD
exit
ph1= 0
ph2= 0 0 2 2
ph3= 0 0 0 0 2 2 2 2
ph4= 0 2 0 2 2 0 2 0
ph5= 0 0 0 0 2 2 2 2
ph6= 1
ph7= 1
ph8= 2
ph9= 0
ph10= {1}*8 {3}*8
```

ph11= {1}*8 {3}*8

ph29=0

ph30=(360) 0 ;set phcor30 to direct signal into one channel

ph31=0 2 2 0 2 0 0 2

;for presat during relaxation delay set

;zgoptns -DPRESAT -DPULSED_PRESAT or zgoptns -DPRESAT -DPRESAT_JUMP

;for presat during diffusion delay set

;zgoptns -DPRESAT1 -DPULSED_PRESAT1 or zgoptns -DPRESAT1 -DPRESAT_JUMP1

;for zgoptns -DPRESAT_JUMP or -DPRESAT_JUMP1 set

;cnst23: signal to be suppressed [Hz]

;cnst24: o1 [Hz]

;for zgoptns -DPULSED_PRESAT set

;p23 : ~50 ms low power rectangular pulse

;if off-resonance, calculate its exact length as desctiben in the Supplementary Information

;if only one signal needs to be suppressed:

;SPNAM23 : Squa100.1000

;SPOFFS23 : resonance frequency of the suppressed signal minus o1 [Hz]

;spdb23 : use minimum power start with 60dB, asses the result

;if multiple signals need to be suppressed use Multi-reson-suppress.xlsx and PresatOptimise.jl to optimise p23 and o1

;create a phase-ramped shape using the calulated pulse length and the distances from o1

;prepare a rectangular shape and place it into the user library, e.g. Squa100.1000 (100us, 1000 points)

;on a topspin command line type:

;st manipulate /opt/topspin4.1/exp/stan/nmr/lists/wave/user/Squa100.1000 offs e 68936 3 565.73 -580.27 -754.27

;this will OVERWRITE the Squa100.1000 shape in /opt/topspin4.1/exp/stan/nmr/lists/wave/user/

;creating a 68936 us shape that will irradiate at 565.73, -580.27 and -754.27Hz away from optimised o1

;Note: for n frequencies replace 3 with n

;spdb23 : use minimum power, start with 60dB, asses the result. For every addtional frequency adjust by subtracting 6dB.

;for zgoptns -DPULSED_PRESAT1 repeat the process to set p24, SPNAM24, SPOFFS24 and spdb24, use shorter p24 (~ 10-20ms)

;for selective 13C decoupling zgoptns -DC13_DEC

;for band selective perfect echo set zgoptns -DBSPE

;for z-filter set zgoptns -DPURGE -DPURGE1 or zgoptns -DPURGE -DPURGE2

;for 90 deg spin-echo pulses set zgoptns -DP90

;if zgoptns -DC13_DEC:

;o2p : 13C chemical shift of the suppressed solvent signal

;pldb12 : power level for 13C decoupling

;at least 12dB weaker than regular decoupler power

;pcpd2 : around 200us for selective decoupling

;cpdprg2 : xy32 or garp4

;DIGMOD = baseopt

;p1 : f1 channel - 90 degree high power pulse

;p2 : f1 channel - 180 degree high power pulse

;p5 : f1 channel - 90 degree lower power pulse for spin-echoes

;p6 : f1 channel - 180 degree lower power pulse for spin-echoes

;pl1 : f1 channel - power level for pulse (default)

;pldb1 : f1 channel - high power

;pl5 : f1 channel - power level for spin-echo pulses IMPORTANT! (see SI of the Peat et al paper)

;pldb5 : f1 channel - lower power

;p19: gradient pulse 2 (spoil gradient)

;p30: gradient pulse (little DELTA * 0.5)

;d1 : relaxation delay; 1-5 * T1

;d10: ringdown time - microseconds to hudreads of microseconds

;d11: delay for disk I/O [30 msec]

;d12: delay for power switching [20 usec]

;d16: delay for homospoil/gradient recovery [200 usec]

;d20: diffusion time (big DELTA)

;d21: eddy current delay (Te) [5 ms]

;NS: 8 * n

;DS: 4 * m

;td1: number of experiments

;FnMODE: QF

; use xf2 and DOSY processing

;l0 : number of blocks during acquisition time adjusted to get d62 as required

;l2 : number of points in full chunk [2-16] depending on dw = 1/2*SWH (increase SWH to decrease dw)

;d62: dw*l2 acquisition block between decoupling pulses [< 0.5msec]

;d63: = d62/2, length of initial half chunk if PURGE not used

;d63: d62/2-cnst13*dw if PURGE used

;cnst13: typically 1,increse SWH if negative

;d10: delay around spin-echo pulses [5-20 us]

;for zgoptns -DBSPE

;p11: f1 channel - 180 degree shaped pulse (Reburp.1000) [0.5-3 msec]

;pl9 : f1 channel - power level for presaturation [~55-69dB]

;sp1:f1 channel - 180 degree shaped pulse (Reburp.1000) [0.5-3 msec]

;spnam1: Reburp.1000

;spdb1: power level for sp1

;for zgoptns -DPURGE2 set

;sp29: f1 channel - shaped pulse (adiabatic)

;p32: f1 channel - 180 degree shaped pulse (adiabatic) [20 msec]

; smoothed chirp (sweep width, 20% smoothing, 10000 points)

; Instructions for setting receiver phase, ph30

; 1) Record spectrum with PH30 = (360) 0 and phcor30=0

; 2) Phase the spectrum using PHC0 only

; 3) If PHCO > 0 set phcor30 = 360-PHC0, if PHC0 < 0 set phcor = -PHC0

; 4) Set PHC0=0 PHC1=0

; 5) If the phase changes, rephase, do not store PHC0, set phcor30 = phcor30 - PHC0

;for z-only gradients:

;gpz0: ca. 11%

;gpz1: 7%

;gpz2: 5%

;gpz3: -12%

;gp4: gp7+2*gp1+2*gp2

;gpz6: 100%

;gpz7: -17.13% (spoil)

;gpz8: -13.17% (spoil)

;use gradient files:

;gpnam1: SINE.100

;gpnam2: SINE.100

;gpnam3: SINE.100

;gpnam4: SINE.100

;gpnam6: SINE.100

;gpnam7: SINE.100

;gpnam8: SINE.100

;use AU-program dosy to calculate gradient ramp-file Difframp

A.3.3 AU program to perform subtraction of reference solvent DOSY spectrum from sample spectrum.

/* dosy_adsu.gp

A 2D dataset is produced by subtracting the DOSY-SHARPER spectrum of the solvent from the DOSY-SHARPER of a sample

- start in the EXPNO containing the DOSY data of the sample (A).

- input the EXPNO containing the DOSY data of solvent only (B).

- program asks for the EXPNO for the A-B data set.

- performs xf2 and expect the user to proceed with additional commands manually.

- can take initial data pre or post DOSY transform, before or after the removal of the imaginary component (if applicable).

George Peat

05 October 2022

```
george.peat@ed.ac.uk

*/

#include <inc/sysutil>

#include <inc/exptUtil>

int     first,iexpno;

float f1phc0;

//double  swp;

char buffer[1024]; //this buffer is for the XCMD string for splitting, may need memory optimisation

//get current data

GETCURDATA

//define our new expnos for the split data

first=expno;

iexpno = expno+1000;

expno2 = expno+1;

GETINT("Enter the EXPNO of the solvent dataset to be subtracted", expno2)

GETINT("Enter the EXPNO for the final cleaned spectrum", iexpno)

if (first==iexpno)

        STOPMSG("program aborted\nYou don't want to overwrite the original dataset")


//Open main data set and process

DATASET(name, expno, 1, disk, user)

VIEWDATA_SAMEWIN

XF2;

// store paramters for subtraction

STOREPAR("ALPHA",1.0);

STOREPAR("GAMMA",-1.0);

WRA(iexpno)

WRPA(name, iexpno, procno, disk, user)

DATASET(name, iexpno, 1, disk, user)
```

```
VIEWDATA_SAMEWIN

XF2;

// Perform subtraction and store data in new expno

DATASET2(name, expno2, procno, disk, user);

ADDSER;

DATASET(name, iexpno, 1, disk, user)

VIEWDATA_SAMEWIN

XF2;

snprintf(buffer, sizeof(buffer), "Processing complete\nSee expno  %d for results. ", iexpno);

QUITMSG(buffer);
```

A.3.4 Julia script for optimization of the duration of the selective pulse and carrier offset.

```
"""

@author Patrick Boaler

@email Patric.Boaler@ed.ac.uk

"""

function distanceToInt(num::Float64)

    absValue = abs(num)

    nearestInt = round(absValue)

    abs(nearestInt - absValue)

end

function fracNorm(freqs::Vector{Float64})

    sum(map(distanceToInt,freqs))

end

function PresatOptimise(rawfreqs::Vector{Float64},tauGuess::Float64,rawO1::Float64)

    o1Range = range(rawO1-2.5, step = 0.01, length = 500)

    tauRange = range(0.8*tauGuess, 1.2*tauGuess, length = 10000)

    fracNormMatrix = [fracNorm(t*(rawfreqs .- o)) for o in o1Range, t in tauRange]

    optFracNorm = minimum(fracNormMatrix)

    o1Index, tauIndex = argmin(fracNormMatrix)[1], argmin(fracNormMatrix)[2]
```

```
    println("\nOptimised pulse length is ", tauRange[tauIndex], " s")

    println("Optimised carrier frequency is ", o1Range[o1Index], " Hz")

    println("Optimised DNInorm is ", optFracNorm,"\n")

end

println("\n--Multi-resonance presaturation parameter optimiser--\n")

println("Usage: call the function PresatOptimse( [freq1 , freq2, ... ], pulse-length , carrier freq )\n\nUnits: freq -> Hz, pulse-length -> s, carrier freq -> Hz\n\nEnsure all inputs are floating point numbers")
```

A.4 CSSF-SHARPER

A.4.1 CSSF-SHARPER sequence

```
;cssf_sharper_ts4.gp

;note for avIII+ the dwl_clk_on/off commands are different

;

;multi resonance sharper with CSSF option

;Modifying method of calculating SHARPER loops for compatibility with Bristol scripts

;HF_TESTS_SHARPER.CLD

;1D sequence

;For testing different phase cycles, gradients and receiver phase set-ups

;

;

; Instructions for setting receiver phase, PH30:

;   1) Record spectrum with PH30 = (360) 0

;   2) Phase the spectrum using PH0

;   3) a. Set PH30 as the 360-PH0 phase, set PH0=0 PH1=0

;      b. Set PH30 as the 450-PH0 phase, set PH0=90 PH1=0

;      c. See additional note for ZG Option -Dselex below

;

;

;ZG Options for SHARPER loop using Hard/broadband pulses:

;
```

; Gradients: -Dgrad

; Switches on the gradients flanking the 180deg pulses

; This also works for the selective sequences.

;

; Phase Cycle: -Dalt

; Changes 90x - [180-y - 180-y]n to 90x - [180-y - 180y]n

; This also works for the selective sequences.

;

; Miscalibrated 180deg pulse in SHARPER loop: -Dmiscal

; Set d13 as the percentage [0%-30%] to

; miscalibrate the 180 deg pulse by

; This does not apply to the selective sequences.

;

;

;ZG Options for sel-SHARPER:

;

; Selective excitation: -Dselex

; Using a selective pulse for excitation (either 90 or 270)

; When this is used 180 must be added to PH0 (whether PH0 = 0 or PH0 = 90)

;

; SPFGSE: -DSPFGSE

; Single pulse field gradient spin echo for selection.

; The gradients here cannot be switched off

;

; DPFGSE: -DDPFGSE

; Double pulse field gradient spin echo for selection.

; The gradients here cannot be switched off

;

; Selective refocussing: -Dselre

```
;                   Uses selective 180deg shaped pulses for refocussing in the SHARPER loop
;                   -Dgrad as described above can be used to include gradients
;                   -Dalt as described above can be used to change phase cycle
;
;
; Additional ZG Options:
;
; Presaturation of single signal: -DPresat
;                   Simple 2 second presaturation of single signal power level set with pl9.
;   Placed at the end of D1 and withing the D1 period (D1>2s)
;   Uses offset switching (cnst23 and cnst24) to allow
;   the presaturation to occur before moving back to the signal of interest
;
;Developement of the sequence from:
; SHARPER reaction monitoring: generation of a narrow linewidth NMR
; singlet, without X-pulses, in an inhomogeneous magnetic field.
; A.B.Jones, G.C.Lloyd-Jones, D. Uhrin, Anal. Chem. 2017,
; DOI:10.1021/acs.analchem.7b02437
;$CLASS=HighRes
;$DIM=1D
;$TYPE=
;$SUBTYPE=
;$COMMENT=
#include <Avance.incl>
#include <Grad.incl>
#include <Delay.incl>
#include <De.incl>
#ifdef P90
"p6=p5"
```

```
#else
"p6=p5*2"
#endif"
"p2=p1*2"
"p29=300u"
"d9=2"
"d11=30m"
"d12=20u"
"d13=5u"
"d20=3u"
"d62=dw*l2"
;"d62=aq/(l0*2+0.5)"
"d63=d62/2"
"DELTA=d1-d11"
"in20=1s/(cnst20*td0*2)"
"spoff2=0"
"l0=(aq/d62-0.5)/2"
"l31=l0+4"
"acqt0=-p1*2/PI"
dwellmode explicit
1 ze
2 d11
        4u BLKGRAD
; DELTA
#ifdef PRESAT
  d12  fq=cnst23(bf):f1 ;water offset in Hz
  d12 pl9:f1
  d1 cw:f1 ph29
  4u do:f1
```

```
  d12 pl1:f1
; d12 pl5:f1
  d12  fq=cnst24(bf):f1 ; real offse Hz
# else
 d1 pl1:f1 ;pl5:f1
#endif
            50u UNBLKGRAD
  p1 ph1
  d20 ;pl0:f1
  p16:gp3
  d16
  (p12:sp2 ph2):f1
  2u
  2u pl1:f1
  (p2 ph1)
  p16:gp3*-1
  d16
  4u
  d20
  (p1 ph1)
#ifdef zfilter
  10u gron0
  (p32:sp29 ph1):f1
  20u groff
  d16
  p16:gp4
  d16 pl1:f1
#else
  p16:gp4
```

```
 d16
#endif
 (p1 ph1)
        ACQ_START(ph30,ph31)
        0.1u REC_UNBLK
        0.05u START_NEXT_SCAN
        d63 pl5:f1
        0.05u DWELL_HOLD
        0.1u REC_BLK
4       10u
        p6 ph4
        10u
        0.1u REC_UNBLK
        0.05u DWELL_RELEASE
        d62
        0.05u DWELL_HOLD
        0.1u REC_BLK
5       10u
        p6 ph4
        10u
        0.1u REC_UNBLK
        0.05u DWELL_RELEASE
        d62
        0.05u DWELL_HOLD
        0.1u REC_BLK
        lo to 4 times l31
        d63
 0.05u DWELL_RELEASE
        rcyc=2
```

```
        30m mc #0 to 2 F0(id20 & zd)
        4u BLKGRAD
exit
ph1=0
ph2=0 0 1 1
ph3=0
ph4=1 3
ph5=1 3
ph29=0
ph30=(360) 0 ; 184;234
ph31=0 0 2 2
;pl1 : f1 channel - power level for pulse (default)
;p1 : f1 channel - 90 degree high power pulse
;p2 : f1 channel - 180 degree high power pulse
;p11 : f1 channel - selective excitation shaped pulse (90 or 270 degree)
;p12: f1 channel - 180 degree shaped pulse for CSSF
;p14 : f1 channel - SPFGSE or DPFGSE: selective refocussing shaped pulse (180 degree)
;pl9 : f1 channel - power level for presaturation [~55-65dB for water]
;p29: gradient pulse 0 [300 usec]
;p28: gradient pulses 1 and 2 [300-1000 usec]
;d1 : relaxation delay [1-5 * T1]
;d11: delay for disk I/O [30 msec]
;d9: length of presaturation [2 s]
;d16: delay for homospoil/gradient recovery
;d20: incremented delay                    [3 usec]
;d62: length of block between decoupling pulses : = aq/l0 [< 20-25msec]
;d63: = d62/2, length of initial half chunk
;ns: 2 * n, total number of scans: NS * TD0
;ds: 4
```

;cnst20: distance (in Hz) to next multiplet (to be suppressed)

;in20: 1s/(cnst20*td0*2)

;ns: 2 * n, total number of scans: NS * TD0

;td0: TD0 = number of steps for suppression of undesired signals [8-16]

;sp1 : shaped pulse for selective excitation [Gauss270 or EBURP2]

;sp2: f1 channel - shaped pulse CSSF

;sp4 : shaped pulse for selective refocussing [Gauss180, ReBURP, RSNOB etc]

;sp29: f1 channel - shaped pulse (adiabatic)

;cnst23: water (presat) offset [ppm]

;cnst24: chosen offset [ppm]

;zgoptns: Gradients: -Dgrad, Phase Cycle: -Dalt, Miscalibration: -Dmiscal, Selective excitation: -Dselex, -DSPFGSE or -DDPFGSE, Selective refocussing: -Dselre, Presaturation: -Dpresat

;l0 : number of blocks during acquisition time adjust to get d62 as required

;l1 : percentage miscalibration on 180deg pulse [integer 1-30%]

;l2 : number of points in full chunk from 2 * 1/2 chunk from python scripts

;ns: 1

;ds: 0 (4)

;for z-only gradients:

;gpz0: 1%

;gpz1: 11-30% smaller than gpz2

;gpz2: 11-31% larger than gpz1

;gpz3: 40%

;gpz4: 25%

;use gradient files:

;gpnam0: SMSQ10.100 or SINE.100

;gpnam1: SMSQ10.100 or SINE.100

;gpnam2: SMSQ10.100 or SINE.100

;gpnam3: SMSQ10.100

;gpnam4: SMSQ10.100

A.4.2 CSSF-DOSY-SHARPER sequence

```
;ledbpgp2s.zgpebs_sharp_comp.du

;sharper_ledbpgp2s.comp.du

;avance-version (07/04/03)

;2D sequence for diffusion measurement using stimulated

;   echo and LED

;using bipolar gradient pulses for diffusion

;using 2 spoil gradients

;

;D. Wu, A. Chen & C.S. Johnson Jr.,

;   J. Magn. Reson. A 115, 260-264 (1995).

;

;$CLASS=HighRes

;$DIM=2D

;$TYPE=

;$SUBTYPE=

;$COMMENT=

#include <Avance.incl>

#include <Grad.incl>

#include <Delay.incl>

#include <De.incl>

define list<gradient> diff=<Difframp>

"p2=p1*2"

# ifdef P90

"p6=p5"

# else

"p6=p5*2"

# endif

"d11=30m"
```

"d12=20u"

"d10=5u"

"d23=3u"

"d9=2"

"d62=dw*l2"

"d63=d62/2"

"l0=(aq/d62-0.5)/2"

"l31=l0+4"

"in23=1s/(cnst25*td0*2)"

"spoff2=0"

ifdef PULSED_PRESAT

"p22=1e6/abs(cnst23-cnst24)"

"FACTOR1=0.5*p21/p22+0.5"

"l6=FACTOR1*2"

"p23=l6*p22"

"cnst25=cnst23-cnst24"

endif

ifdef PULSED_PRESAT1

"FACTOR2=0.5*d1/p23+0.5"

"l7=FACTOR2*2"

"DELTA1=d20-p1*2-p2-p30*2-d16*2-p19*2-d16*2-d12*4-4u"

endif

ifdef PRESAT1

"FACTOR2=(d20/(p23))/2-0.5"

"l7=FACTOR2*2"

"DELTA1=d20-p1*2-p2-p30*2-d16*2-p19*2-d16*2-d12*4-4u"

endif

ifdef NOPRESAT1

"DELTA1=d20-p1*2-p2-p30*2-d16*2-p19*2-d16*2"

```
# endif
"d22=(d20-p1*2-p2-p30*2-d16*2-p19*2-d16*2-d12*4-4u-l7*p23)" ; no entirely correct
"DELTA2=d21-p19-d16-4u"
;"DELTA2=d21-p19-d16-4u-p16-d16"
dwellmode explicit
"acqt0=-p1*2/3.1416"
1 ze
2 d11
4u BLKGRAD
# ifdef C13_DEC
  d12 pl12:f2
# endif
# ifdef PULSED_PRESAT
30m
 d12 pl0:f1
3 (p23:sp23 ph29):f1
  4u
  lo to 3 times l7
  d12 pl1:f1
# else
# ifdef PRESAT
  d12  fq=cnst23(bf):f1 ;water offset in Hz
  d12 pl9:f1
  d1 cw:f1 ph29
  4u do:f1
  d12  pl1:f1
  d12  fq=cnst24(bf):f1 ; = o1
# else
  d1
```

```
# endif
# endif
  50u UNBLKGRAD
  p19:gp7*-1
  d16
 ; p16:gp2*-1
  ; d16
  p1 ph1
  p30:gp6*diff
  d16
  p2 ph1
  p30:gp6*-1*diff
  d16
  p1 ph2
  p19:gp7
  d16
# ifdef C13_DEC
  d12 pl12:f2
# endif
# ifdef PULSED_PRESAT1
30m
 d12 pl0:f1
4 (p23:sp23 ph29):f1
  4u
  lo to 3 times l7
  d12 pl1:f1
# else
# ifdef PRESAT1
  d12  fq=cnst23(bf):f1 ;water offset in Hz
```

```
  d12 pl9:f1
  DELTA1 cw:f1 ph29
  4u do:f1
  d12  pl1:f1
  d12  fq=cnst24(bf):f1 ; = o1
# else
  DELTA1
# endif
# endif
  p19:gp8*-1
  d16
  p1 ph3
  p30:gp6*diff
  d16
  p2 ph1
  p30:gp6*-1*diff
  d16
  p1 ph4
  p19:gp8
  d16; pl5:f1
;  p16:gp2*-1 ;new PFG
;  d16
  DELTA2
  4u
;  4u BLKGRAD
# ifdef SPFGSE
  (p1 ph5)
   p16:gp1
   d16 pl0:f1
```

```
  4u
  (p11:sp1 ph6):f1
  4u
  p16:gp1
  d16 pl1:f1
# else
  (p1 ph5)
# endif
# ifdef CSSF
  d23
  p16:gp1
  d16
  (p12:sp2 ph2):f1
  2u
  2u pl1:f1
  (p2 ph1)
  p16:gp1*-1
  d16
  4u
  d23
  (p1 ph1)
  p16:gp2
  d16
  (p1 ph1)
# endif
  ACQ_START(ph30,ph31)
      0.1u REC_UNBLK
      0.05u DWL_CLK_ON ;START_NEXT_SCAN
      d63 pl5:f1
```

```
        0.05u DWL_CLK_OFF ;DWELL_HOLD
        0.1u REC_BLK
5       d10
       (p6 ph10):f1
        d10
        0.1u REC_UNBLK
        0.05u DWL_CLK_ON ;DWELL_RELEASE
        d62
        0.05u DWL_CLK_OFF ;DWELL_HOLD
        0.1u REC_BLK
        d10
       (p6 ph11):f1
        d10
        0.1u REC_UNBLK
        0.05u DWL_CLK_ON ;DWELL_RELEASE
        d62
        0.05u DWL_CLK_OFF ;DWELL_HOLD
        0.1u REC_BLK
        lo to 5 times l31
        d63
;  0.05u DWELL_RELEASE
        rcyc=2
 ;      30m mc #0 to 2 F0(zd)
  d11 mc #0 to 2
                        F0(id23 & zd)
                        F1QF(rd23 igrad diff)
  4u BLKGRAD
exit
ph1= 0
```

ph2= 0 0 2 2

ph3= 0 0 0 0 2 2 2 2 ;1 1 1 1 3 3 3 3

ph4= 0 2 0 2 2 0 2 0 ;1 3 1 3 3 1 3 1

ph5= 0 0 0 0 2 2 2 2 ;1 1 1 1 3 3 3 3

ph6= 1

ph7= 1;3

ph8= 2

ph9= 0

ph10= {1}*8 {3}*8

ph11= {1}*8 {3}*8

ph29=0

ph30=(360) 182

ph31=0 2 2 0 2 0 0 2 ; 3 1 1 3 1 3 3 1

;pl1 : f1 channel - power level for pulse (default)

;pl9 : f1 channel - power level for presaturation

;sp2: f1 channel - shaped pulse

;p1 : f1 channel - 90 degree high power pulse

;p2 : f1 channel - 180 degree high power pulse

;p12: f1 channel - 180 degree shaped pulse

;p16: homospoil/gradient pulse [1 msec]

;p19: gradient pulse 2 (spoil gradient)

;p21: approximate duration of the presaturation pulse

;p22; 1e6/(cnst23-cnst24)

;p23: acutal duration of the presaturation pulse

;p30: gradient pulse (little DELTA * 0.5)

;cnst23: water (presat) offset [Hz]

;cnst24: = o1 [Hz]

;d1 : relaxation delay; 1-5 * T1

;d12: delay for power switching [20 usec]

;d16: delay for gradient recovery

;d20: diffusion time (big DELTA)

;d21: eddy current delay (Te) [5 ms]

;d23: incremented delay [3 usec]

;cnst25: distance (in Hz) to next multiplet (to be suppressed)

;in23: 1s/(cnst25*td0*2)

;ns: 2 * n, total number of scans: NS * TD0

;DS: 4 * m

;td0: TD0 = number of steps for suppression of undesired signals [8-16]

;td1: number of experiments

;FnMODE: QF

; use xf2 and DOSY processing

;use gradient ratio: gp 6 : gp 7 : gp 8

; 100 : -17.13 : -13.17

;for z-only gradients:

;gpz1: 40%

;gpz2: 25%

;gpz6: 100%

;gpz7: -17.13% (spoil)

;gpz8: -13.17% (spoil)

;use gradient files:

;gpnam1: SMSQ10.100

;gpnam2: SMSQ10.100

;gpnam6: SINE.100

;gpnam7: SINE.100

;gpnam8: SINE.100

;use AU-program dosy to calculate gradient ramp-file Difframp

;$Id: ledbpgp2s,v 1.6 2007/04/11 13:34:30 ber Exp $